DEFORMATION AND EROSION OF THE CENTRAL ANDEAN FOLD-THRUST BELT AND PLATEAU

by

Jason Bullard Barnes

A dissertation submitted in partial fulfillment
of the requirements for the degree of
Doctor of Philosophy
(Geology)
in The University of Michigan
2008

Doctoral Committee:

Associate Professor Todd A. Ehlers, Chair
Professor Daniel G. Brown
Professor Larry J. Ruff
Professor Rob Van Der Voo
Associate Professor Christopher J. Poulsen
Assistant Professor Nadine McQuarrie, Princeton University

We take a handful of sand from the endless landscape of awareness around us and call that handful of sand the world.

- Robert Pirsig

To my parents for their enduring support and encouragement and my grandfather Laurel Lewis who also had an interest in geology.

Acknowledgements

My most profound thanks start with my parents, Susan and Sanford Barnes. They have always been enthusiastic and enduring supporters of my educational endeavors.

I deeply thank Todd Ehlers, my advisor, for mentoring me in every aspect of science from proposal and paper writing to conducting research in the lab and the field, presenting results, critically evaluating others work, and teaching and advising other students. I thank Nadine McQuarrie for sharing her detailed knowledge of Bolivian thrust belt geology and kinematics, being patient and appropriately critical of how to best interpret my results within this framework, many enlightening discussions, and hosting me at Princeton University.

I am grateful to my other committee members, Rob Van Der Voo, Chris Poulsen, Larry Ruff, and Dan Brown for their input. Being both a student and GSI under Rob has been a true honor, especially the assignment of writing an NSF proposal in his tectonics of oceans and continents class which ended up funding much of my PhD work. Chris provided important criticisms concerning how to better set up the problems I've addressed. Rob, Chris, and Larry specifically helped me improve the presentation of chapters 1, 5, and 6.

My graduate work would not have been possible without the inspiring work and ideas of Brian Horton that originally got me interested in Bolivia. It was through Brian that I was able to develop collaborations with Sohrab Tawackoli and SERGIOTECMIN, without which none of the logistics of working in Bolivia would have been possible.

I cannot go without mentioning the countless hours trouble-shooting, debating and discussing science, sharing advice, and general support and friendship from my fellow Earth Surface Processes graduate students Dave Whipp, Matt Densmore, and Nadja Insel. Much of my scientific growth happened through interactions with them. Nadja also provided valuable assistance in the field.

This PhD work was supported by a University of Michigan Rackham Graduate School Predoctoral Fellowship, several Scott Turner Awards in Earth Sciences from the Department of Geological Sciences at the University of Michigan, a Sokol International Summer Research Fellowship in the Sciences from Rackham, and NSF – Tectonics grant EAR 0409289 to T. Ehlers.

Finally, I owe much of my sanity, survival, and social life to the ultimate community in Ann Arbor and the Great Lakes region. Richard Eikstadt, in particular, has helped me improve as a player, been an incredible colleague and mentor as a coach, and provides incessant humorous interludes. Craig Frankland is a rock and a truly inspirational defensive player that I admire. Tyler Kinley, Vitaly Volberg, Javier Carey, Eric Geile, JB, Chris Reynolds, Jello, BT, Rook, Ryan Purcell, Dave Fumo, Nick Slovan, Dave Collins, Sam Cohen, Brix, Swigs, Pug, Boone, Branson, James Batey, JZ, Boz, Mundo, Colin McIntyre, Will Neff and additional members of BAT and MagnUM; thanks for helping me balance academics with an athletic outlet that has lead to great times, adventures, and significant success and sometimes failure.

Table of Contents

List of Figures

List of Tables

List of Appendices

Chapter 1

Introduction

Orogenic plateaus contain a significant amount of the high elevation topography on Earth. Today, the Tibetan and Andean Plateaus are the two most prominent orogenic plateaus and are characterized by exceptionally large (≥500,000 km^2) and flat (<~0.5 km in relief) regions at high mean elevation (≥3 km) flanked by steep margins [e.g. Isacks, 1988; Tapponnier et al., 2001; Sobel et al., 2003]. Evidence also suggests orogenic plateaus existed in the geologic past in regions currently occupied by the Western Cordillera of North America (the Nevadaplano) [DeCelles, 2004], southern Europe (the Hercynian Tibetan Plateau) [Menard and Molnar, 1988], and the southern portion of the modern Tibetan Plateau (the Lhasaplano) [Kapp et al., 2007]. The Tibetan Plateau is the largest of the two modern plateaus and the result of continental collision between India and Eurasia over the last ~50 Myrs [e.g. Molnar et al., 1993]. The Andean Plateau is the core of the central Andes and the result of Nazca Plate subduction below South America throughout the Cenozoic [e.g. Isacks, 1988]. These plateaus possess such significant gravitational potential energy that eventually they reach their limit and collapse as one of the penultimate results of orogenesis [Dewey, 1988; Willett and Pope, 2004]. Current motivating questions about plateau evolution include: (1) What is the deformation history associated with plateau development? (2) What is the erosional response to plateau growth? (3) What is the history of elevation gain? (4) Why are they so broad and low in relief? (5) What processes are important in

their evolution? I specifically quantify the first two questions applied to the Andean Plateau (Fig. 1.1) and use the results to comment on the remaining questions.

The basic form, width, and evolution of mountain belts and orogenic plateaus are thought to be the result of the interactions between tectonics and erosion [e.g. Hoffman and Grotzinger, 1993; Masek et al., 1994]. Plateau deformation and uplift is governed by shortening and thickening of the lithosphere driven by tectonic plate interactions. Models of plateau evolution range from broad, uniform uplift as the result of a pre-weakened lithosphere to outward spreading from an initially strong lithosphere capable of supporting a narrow mountain belt [Isacks, 1988; Wdowinski and Bock, 1994; Royden, 1996; Willett and Pope, 2004]. Unfortunately, testing these models is hindered by a significant lack of knowledge of the kinematic and deformation history specific to plateau formation. A principal goal of this dissertation is to constrain the kinematic and deformation history of the Andean Plateau.

Numerical models of orogen growth have demonstrated how the distribution of precipitation and erosion can influence mountain architecture and focus deformation and uplift [e.g. Beaumont et al., 1992; Avouac and Burov, 1996; Willett, 1999; Beaumont et al., 2001; Stolar et al., 2006]. Numerous studies have tried to document this tectonic-erosion coupling at regional scales using predominantly spatial correlations between climate, sediment flux, exhumation, and metamorphic grade [Zeitler and Meltzer, 2001; Finlayson et al., 2002; Dadson et al., 2003; Molnar, 2003; Reiners et al., 2003; Wobus et al., 2003; Thiede et al., 2005]. However, significant questions remain about tectonic-erosion coupling at a regional scale. For example, observations of tectonic-climate decoupling exist [e.g. Burbank et al., 2003] and debate continues about the relative importance of tectonics and climate in forcing erosion over million-year timescales [e.g. Molnar, 2003]. The second main goal of this dissertation is to constrain the regional

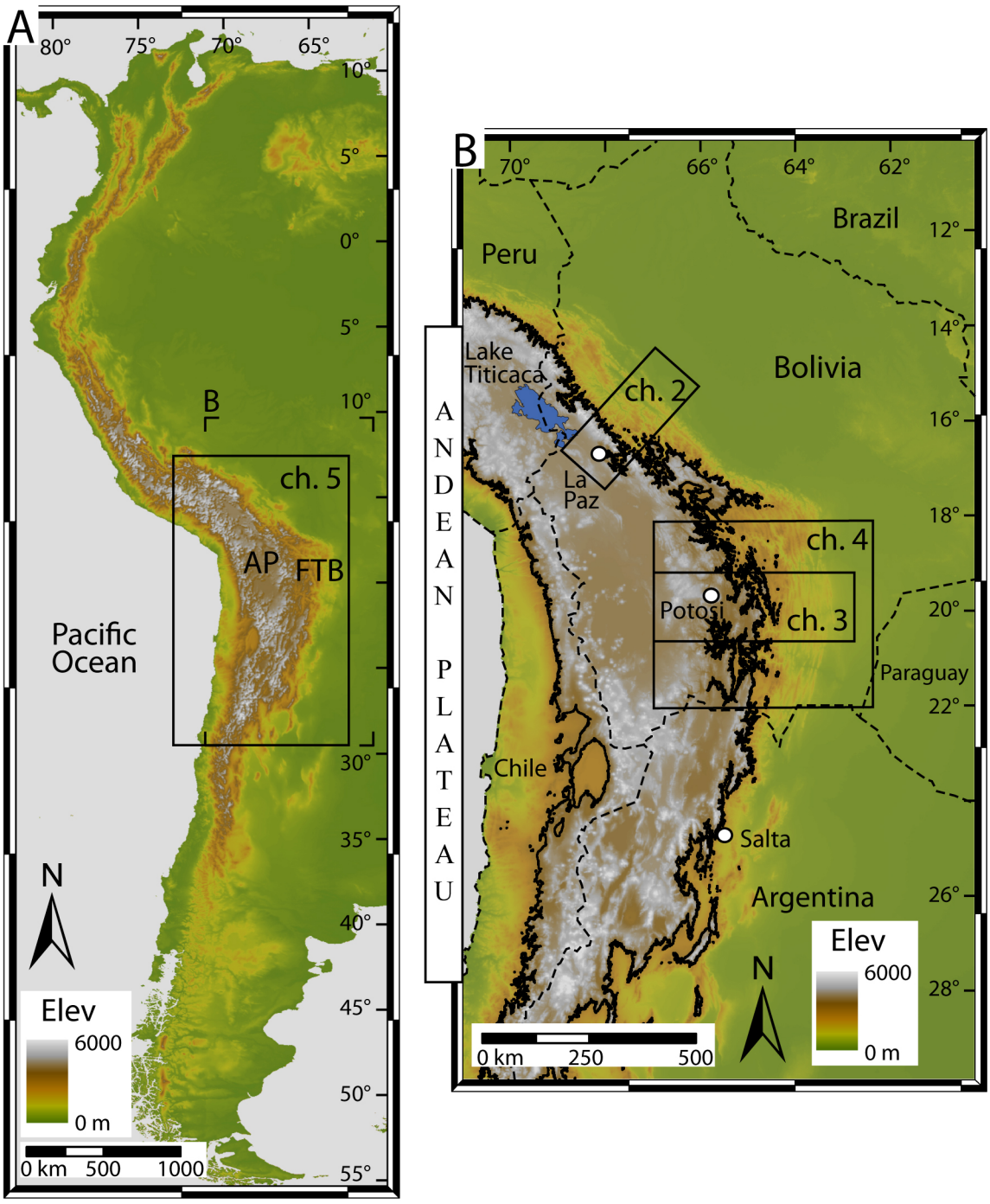

Figure 1.1. The Andes of South America with particular focus on the central Andean fold-thrust belt (FTB) and Andean Plateau (AP). Boxes and labels outline the specific study locations for chapters (ch.) 2-5. Elev = elevation. (A) Topography of the Andes from the GTOPO30 1 km dataset. (B) Topography of the Andean Plateau region from the SRTM 90 m dataset. Extent of the plateau is defined by the 3 km contour (solid irregular black line) after Isacks [1988]. Location is in part A.

exhumation and erosion history associated with Andean Plateau growth and integrate it with the kinematic and deformation history.

The central Andean fold-thrust belt and plateau is an ideal location to focus on the deformation and erosion history associated with plateau growth at a regional scale. First, recent studies have linked the growth of the Andean Plateau with large basement structures that are significant components of the central Andean fold-thrust belt in Bolivia (Fig. 1.1) [Kley, 1996; McQuarrie and DeCelles, 2001; McQuarrie, 2002]. This correlation of thrust belt kinematics with plateau growth allows an unprecedented opportunity to infer the record of plateau development by chronicling thrust belt evolution. Second, along-strike correlations in deformation width, morphology, and climate as well as analogue models suggest erosion has played a fundamental role in the evolution of the central Andean fold-thrust belt in Bolivia [Masek et al., 1994; Mugnier et al., 1997; Horton, 1999; Leturmy et al., 2000; Montgomery et al., 2001]. Despite this importance of erosion, observational constraints on the long-term (>10 Myr) erosion history and its along-strike variations across the entire thrust belt were lacking when this project began [e.g. Barnes and Pelletier, 2006]. The hypotheses that regionally link orogenic plateau growth to thrust belt evolution and that variable erosion has been important in the evolution of the eastern fold-thrust belt margin of the Andean Plateau in Bolivia are what determined the geographic focus of this dissertation. This dissertation demonstrates that questions related to plateau formation and erosion in orogenesis are better addressed by integrating the regional chronology of deformation, kinematics, exhumation, erosion, and sedimentation.

This dissertation constrains the deformation and history across and along strike of the central Andean fold-thrust belt and plateau (Fig. 1.1). Deformation and exhumation are quantified with apatite and zircon fission-track and (U-Th)/He thermochronology combined with inverse thermal modeling [e.g. Reiners and Ehlers,

2005]. Sample cooling histories are then interpreted within their regional stratigraphic, structural, and kinematic contexts [McQuarrie, 2002; McQuarrie et al., 2005; McQuarrie et al., 2008]. The regional-scale exhumation and deformation patterns are also integrated with the documented foreland basin sedimentation history [Horton et al., 2001; Horton et al., 2002; DeCelles and Horton, 2003; Horton, 2005]. Digital topography, erosion surface reconstructions, erosion-rate estimates, and foreland sediment isopachs are used to calculate sediment volumes and production/delivery rates in order to perform a sediment budget analysis in southern Bolivia. Finally, a synoptic view of the evolution of the entire Andean Plateau is developed by synthesizing an even wider variety of geologic observations.

Dissertation outline

This dissertation is composed of 4 main chapters (2-5) proceeded by this introductory chapter 1 and followed by the summary and conclusions chapter 6. Chapter 2 documents the exhumation history along a transect across the entire central Andean fold-thrust belt and eastern plateau margin in northern Bolivia at 15-17°S (ch. 2 box in Fig. 1.1B). An associated paper presents the structural and kinematic history along the same transect and integrates it with the exhumation history outlined in chapter 2 [McQuarrie et al., 2008]. Chapter 3 quantifies the exhumation history along another transect across the central Andean fold-thrust belt where the plateau is at its widest extent in southern Bolivia at ~19.5°S (ch. 3 box in Fig. 1.1B). An associated paper provides an observational test of theoretical calculations that predict erosion is limiting the orogen width by relating the spatial and temporal variations in tectonic shortening (results of chapters 2 and 3) and the modern climate across the central Andean fold-thrust belt in Bolivia [McQuarrie et al., in review]. Chapter 4 quantifies the Plio-Quaternary (~3-0 Ma) sediment budget between central Andean fold-thrust belt erosion

and the record of sedimentation in the adjacent foreland throughout southern Bolivia at ~18-22°S (ch. 4 box in Fig. 1.1B). Chapter 5 is an up-to-date synthesis of studies that use observational constraints to determine the lithospheric structure and history of deformation, sedimentation, uplift, elevation, and fluvial incision across the entire Andean Plateau from southern Peru to northern Argentina (ch. 5 box in Fig. 1.1A).

Publications and abstracts resulting from this dissertation

Publications (peer-reviewed)

Barnes, J. B., T. A. Ehlers, N. McQuarrie, P. B. O'Sullivan, and J. D. Pelletier (2006), Eocene to recent variations in erosion across the central Andean fold-thrust belt, northern Bolivia: Implications for plateau evolution, Earth and Planetary Science Letters, v. 248, 118-133. **(Chapter 2).**

McQuarrie, N., **J. B. Barnes**, and T. A. Ehlers (2008), Geometric, kinematic, and erosional history of the central Andean Plateau, Bolivia (15-17°S), Tectonics, doi:10.1029/2006TC002054, in press.

Barnes, J. B., T. A. Ehlers, N. McQuarrie, P. B. O'Sullivan, and S. Tawackoli (2008), Thermochronometer record of central Andean Plateau growth, Bolivia (19.5°S), Tectonics, doi:10.1029/2007TC002174, in press. **(Chapter 3).**

Barnes, J. B. and W. A. Heins (2008), Plio-Quaternary sediment budget between thrust belt erosion and foreland deposition in the central Andes, southern Bolivia, Basin Research, in press. **(Chapter 4).**

McQuarrie, N., T. A. Ehlers, **J. B. Barnes**, and B. J. Meade (in review), Temporal variation in climate and tectonic coupling in the central Andes. Geology.

Barnes, J. B. and T. A. Ehlers (in prep), Cenozoic deformation, uplift, and evolution of the central Andean Plateau. **(Chapter 5).**

Conference abstracts

Barnes, J. B. and T. A. Ehlers (2007), Deformation and exhumation history of the central Andes, Bolivia: insights from thermochronology and numerical modeling, Eos Trans. AGU, 88(52), Fall Meet. Suppl., Abstract T11G-06.

Ehlers, T. A. and **J. B. Barnes** (2007), Comparison of estimates for Andean plateau formation from thermochronology and stable isotope paleoaltimetry, Goldschmidt Conference Abstracts, p. A250.

McQuarrie, N., T. A. Ehlers, and **J. B. Barnes** (2007), Deformation, precipitation, and the width of the central Andean plateau, GSA Abstracts with Programs, v. 39, n. 6, p. 184.

Barnes, J. B., T. A. Ehlers, and N. McQuarrie, (2006), Eocene to recent exhumation patterns correlated with deformation across 200 km of the central Andean fold-thrust belt, northern Bolivia, Backbone of the Americas, Mendoza, Argentina, April 3-7, 2-17, p. 28-29.

McQuarrie, N., **J. B. Barnes**, and T. A. Ehlers (2006), Geometric, kinematic, and erosional history of the central Andean plateau, northern Bolivia; Eos Trans. AGU, 87(52), Fall Meet. Suppl., Abstract T44A-06.

Barnes, J. B., T. A. Ehlers, N. McQuarrie, O'Sullivan, P.B., and J. D. Pelletier (2005), Erosion, climate and early growth of the central Andean Plateau, northern Bolivia: Insights from low-temperature thermochronology, GSA Abstracts with Programs, v. 37, n. 7, p. 199.

McQuarrie, N., **J. B. Barnes,** and T. A. Ehlers (2005), The relationship between deformation and exhumation in the central Andean Plateau, Bolivia; GSA Abstracts with Programs v. 37, n. 7, p. 271.

Barnes, J. B., T. A. Ehlers, and N. McQuarrie (2004), New constraints on the erosion history of the Andean Plateau inferred from detrital thermochronology across the northern Bolivian thrust belt, Eos Trans. AGU, 85(47), Fall Meet. Suppl., Abstract T53A-0474.

References

Avouac, J. P., and E. B. Burov (1996), Erosion as a driving mechanism of intracontinental mountain growth, Journal of Geophysical Research, v. 101, 17747-17769.

Barnes, J. B., and J. D. Pelletier (2006), Latitudinal variation of denudation in the evolution of the Bolivian Andes, American Journal of Science, v. 306, 1-31.

Beaumont, C., P. Fullsack, and J. Hamilton (1992), Erosional control of active compressional orogens, in Thrust Tectonics, K. McClay (ed.), Chapman & Hall, London, UK, 1-18.

Beaumont, C., R. A. Jamieson, M. H. Nguyen, and B. Lee (2001), Himalayan tectonics explained by extrusion of a low-viscosity crustal channel coupled to focused surface denudation, Nature, v. 414, 738-742.

Burbank, D. W., A. E. Blythe, J. Putkonen, B. Pratt-Sitaula, E. Gabet, M. Oskin, A. Barros, and T. P. Ojha (2003), Decoupling of erosion and precipitation in the Himalayas, Nature, v. 426, 652-655.

Dadson, S. J., N. Hovius, H. Chen, W. B. Dade, M.-L. Hsieh, S. D. Willett, J.-C. Hu, M.-J. Horng, M.-C. Chen, C. P. Stark, D. Lague, and J.-C. Lin (2003), Links between erosion, runoff variability and seismicity in the Taiwan Orogen, Nature, v. 426, 648-651.

DeCelles, P. G. (2004), Late Jurassic to Eocene evolution of the Cordilleran thrust belt and foreland basin system, western U.S.A, American Journal of Science, v. 304, 105-168.

DeCelles, P. G., and B. K. Horton (2003), Early to middle Tertiary foreland basin development and the history of Andean crustal shortening in Bolivia, Geological Society of America Bulletin, v. 115, 58-77.

Dewey, J. F. (1988), Extensional collapse of orogens, Tectonics, v. 7, 1123-1139.

Finlayson, D. P., D. R. Montgomery, and B. Hallet (2002), Spatial coincidence of rapid inferred erosion with young metamorphic massifs in the Himalayas, Geology, v. 30, 219-222.

Hoffman, P. F., and J. P. Grotzinger (1993), Orographic precipitation, erosional unloading, and tectonic style, Geology, v. 21, 195-198.

Horton, B. K. (1999), Erosional control on the geometry and kinematics of thrust belt development in the central Andes, Tectonics, v. 18, 1292-1304.

Horton, B. K. (2005), Revised deformation history of the central Andes: Inferences from Cenozoic foredeep and intermontane basins of the Eastern Cordillera, Bolivia, Tectonics, v. 24, doi:10.1029/2003TC001619.

Horton, B. K., B. A. Hampton, B. N. Lareau, and E. Baldellon (2002), Tertiary provenance history of the northern and central Altiplano (Central Andes, Bolivia); a detrital record of plateau-margin tectonics, Journal of Sedimentary Research, v. 72, 711-726.

Horton, B. K., B. A. Hampton, and G. L. Waanders (2001), Paleogene synorogenic sedimentation in the Altiplano Plateau and implications for initial mountain building in the Central Andes, Geological Society of America Bulletin, v. 113, 1387-1400.

Isacks, B. L. (1988), Uplift of the Central Andean Plateau and bending of the Bolivian Orocline, Journal of Geophysical Research, v. 93, 3211-3231.

Kapp, P., P. G. DeCelles, A. L. Leier, J. M. Fabijanic, S. He, A. Pullen, and G. E. Gehrels (2007), The Gangdese retroarc thrust belt revealed, GSA Today, v. 17, 4-9.

Kley, J. (1996), Transition from basement-involved to thin-skinned thrusting in the Cordillera Oriental of southern Bolivia, Tectonics, v. 15, 763-775.

Leturmy, P., J. L. Mugnier, P. Vinour, P. Baby, B. Colletta, and E. Chabron (2000), Piggyback basin development above a thin-skinned thrust belt with two detachment levels as a function of interactions between tectonic and superficial mass transfer; the case of the Subandean Zone (Bolivia), Tectonophysics, v. 320, 45-67.

Masek, J. G., B. L. Isacks, T. L. Gubbels, and E. J. Fielding (1994), Erosion and tectonics at the margins of continental plateaus, Journal of Geophysical Research, v. 99, 13941-13956.

McQuarrie, N. (2002), The kinematic history of the central Andean fold-thrust belt, Bolivia; implications for building a high plateau, Geological Society of America Bulletin, v. 114, 950-963.

McQuarrie, N., J. B. Barnes, and T. A. Ehlers (2008), Geometric, kinematic, and erosional history of the central Andean Plateau, Bolivia (15-17ºS), Tectonics, doi:10.1029/2006TC002054, in press.

McQuarrie, N., and P. G. DeCelles (2001), Geometry and structural evolution of the central Andean backthrust belt, Bolivia, Tectonics, v. 20, 669-692.

McQuarrie, N., T. A. Ehlers, J. B. Barnes, and B. J. Meade (in review), Temporal variation in climate and tectonic coupling in the central Andes, Geology.

McQuarrie, N., B. K. Horton, G. Zandt, S. Beck, and P. G. DeCelles (2005), Lithospheric evolution of the Andean fold-thrust belt, Bolivia, and the origin of the central Andean plateau, Tectonophysics, v. 399, 15-37.

Menard, G., and P. Molnar (1988), Collapse of a Hercynian Tibetan Plateau into a late Palaeozoic European Basin and Range Province, Nature, v. 334, 235-237.

Molnar, P. (2003), Nature, nurture and landscape, Nature, v. 426, 612-614.

Molnar, P., P. England, and J. Martinod (1993), Mantle dynamics, uplift of the Tibetan Plateau, and the Indian monsoon, Reviews of Geophysics, v. 31, 357-396.

Montgomery, D. R., G. Balco, and S. D. Willett (2001), Climate, tectonics, and the morphology of the Andes, Geology, v. 29, 579-582.

Mugnier, J., P. Baby, B. Colletta, P. Vinour, P. Bale, and P. Leturmy (1997), Thrust geometry controlled by erosion and sedimentation; a view from analogue models, Geology, v. 25, 427-430.

Reiners, P. W., and T. A. Ehlers (ed.) (2005), Low-temperature thermochronology: Techniques, Interpretations, and Applications, 622 pp., Mineralogical Society of America, Chantilly, VA.

Reiners, P. W., T. A. Ehlers, S. G. Mitchell, and D. R. Montgomery (2003), Coupled spatial variations in precipitation and long-term erosion rates across the Washington Cascades, Nature, v. 426, 645-647.

Royden, L. (1996), Coupling and decoupling of crust and mantle in convergent orogens; implications for strain partitioning in the crust, Journal of Geophysical Research, v. 101, 17679-17705.

Sobel, E. R., G. E. Hilley, and M. R. Strecker (2003), Formation of internally drained contractional basins by aridity-limited bedrock incision, Journal of Geophysical Research, v. 108, doi:10.1029/2002JB001883.

Stolar, D. B., S. D. Willett, and G. H. Roe (2006), Climatic and tectonic forcing of a critical orogen, in Tectonics, climate, and landscape evolution, S. D. Willett, N. Hovius, M. T. Brandon and D. M. Fisher (ed.), Geological Society of America Special Paper 398, 241-250.

Tapponnier, P., X. Zhiqin, F. Roger, B. Meyer, N. Arnaud, G. Wittlinger, and Y. Jingsui (2001), Oblique stepwise rise and growth of the Tibetan Plateau, Science, v. 294, 1671-1677.

Thiede, R. C., J. R. Arrowsmith, B. Bookhagen, M. O. McWilliams, E. R. Sobel, and M. R. Strecker (2005), From tectonically to erosionally controlled development of the Himalayan Orogen, Geology, v. 33, 689-692.

Wdowinski, S., and Y. Bock (1994), The evolution of deformation and topography of high elevated plateaus 2. Application to the Central Andes, Journal of Geophysical Research, v. 99, 7121-7130.

Willett, S. D. (1999), Orogeny and orography; the effects of erosion on the structure of mountain belts, Journal of Geophysical Research, v. 104, 28957-28982.

Willett, S. D., and D. C. Pope (2004), Thermo-mechanical models of convergent orogenesis; thermal and rheologic dependence of crustal deformation, in Rheology and deformation of the lithosphere at continental margins, G. D.

Karner, B. Taylor, N. W. Driscoll and D. L. Kohlstedt (ed.), Columbia University Press, New York, NY., 179-222.

Wobus, C. W., K. V. Hodges, and K. X. Whipple (2003), Has focused denudation sustained active thrusting at the Himalayan topographic front?, Geology, v. 31, 861-864.

Zeitler, P., and A. Meltzer (2001), Erosion, Himalayan geodynamics, and the geomorphology of metamorphism, GSA Today, v. 11, 4-9.

Chapter 2

Eocene to recent variations in erosion across the central Andean fold-thrust belt, northern Bolivia: Implications for plateau evolution[1]

Abstract

Quantifying the erosional and kinematic evolution of orogenic plateaus has been limited by insufficient age constraints on their deformation and erosion histories. Palinspastic restorations suggest the central Andean fold-thrust belt and plateau evolved concurrently in Bolivia. We present an analysis that synthesizes 19 new and 32 previous apatite and zircon fission-track and (U-Th)/He mineral cooling ages along a 200 km traverse across the plateau margin and entire thrust belt in northern Bolivia. The new apatite fission-track data are interpreted using a grain-age deconvolution algorithm with inverse thermal modeling of track lengths, grain ages, and mineral composition proxy data. Results suggest: (1) Eo-Oligocene (~40-25 Ma) initial rapid erosion of the plateau margin, (2) accelerated, distributed erosion across the entire thrust belt since the early to mid-Miocene (~15 Ma), and (3) the magnitude of erosion decreases eastward from ~10-4 km. We compare these results with two end-member models of the central Andes that contrast in duration and magnitude of deformation. The rapid Eo-Oligocene

---

[1]**Official citation:**

Barnes, J. B., T. A. Ehlers, N. McQuarrie, P. B. O'Sullivan, and J. D. Pelletier (2006), Eocene to recent variations in erosion across the central Andean fold-thrust belt, northern Bolivia: Implications for plateau evolution, Earth and Planetary Science Letters, v. 248, 118-133.

(~40-25 Ma) erosion is only consistent with the end-member that emphasizes the long duration and large magnitude deformation controlled by the sequential stacking of basement thrust sheets. However, the distributed Miocene (~15 Ma) to recent erosion is consistent with both end-members because the recorded cooling could have resulted from active deformation, protracted erosion, or both. If the long duration model is correct, the time between the two phases of accelerated cooling brackets the cessation of the first basement thrust sheet and implies the early development of the Andean plateau analogous to its modern width, but unknown elevation by the early Miocene (~20 Ma).

Introduction

Many active mountain ranges are characterized by fold-thrust belts that exhibit significant relief, deformation, and erosion. In the central Andes and the Himalayas, the hinterland portions of the thrust belts are occupied by high elevated plateaus characterized by unusually low relief and internal drainage [Isacks, 1988; Tapponnier et al., 2001; Sobel et al., 2003]. The Andean and Tibetan plateaus are invoked to force global climate, Cenozoic climate change, terrestrial sediment flux, and even ocean chemistry [Richter et al., 1992; Royden, 1996; Ruddiman et al., 1997]. Despite their significance, observational constraints on plateau formation mechanisms across the entire width of their marginal thrust belts are lacking. Nevertheless, proposed mechanisms for plateau formation prescribe a wide range of kinematic predictions from uniform plateau uplift to outward growth from a narrow orogenic belt [Wdowinski and Bock, 1994; Royden, 1996].

The timing of formation of these large plateaus also remains unresolved [e.g. Murphy et al., 1997; McQuarrie et al., 2005]. In particular, estimates on timing and rate of Andean plateau (AP) formation are based on a wide variety of proxies for plateau

formation and elevation. These estimates are highly varied and range from ~40-5 Ma [Benjamin et al., 1987; Isacks, 1988; Sempere et al., 1990; Gubbels et al., 1993; Allmendinger et al., 1997; Kennan et al., 1997; Lamb and Hoke, 1997; Gregory-Wodzicki, 2000; DeCelles and Horton, 2003; Horton, 2005; McQuarrie et al., 2005; Garzione et al., 2006]. Thus, quantifying the timing and mechanisms of plateau development necessitates detailed regional knowledge of their deformation and erosion histories.

Erosion is the primary mechanism of exhumation in fold-thrust belts. In active tectonic settings such as the central Andes, the initial stages of accelerated erosion can also be a signature of deformation. For example, the relief generated by deformation is often what begins to drive the erosion process [Coughlin et al., 1998; Willett, 1999; Willett and Brandon, 2002; Sobel and Strecker, 2003; Carrapa et al., 2005; Clark et al., 2005]. Low-temperature thermochronometers quantify rock exhumation in the shallow (upper 2-10 km) crust [e.g. Ehlers and Farley, 2003]. In this study, we (1) quantify the spatial and temporal patterns of erosion across a 200 km transect through the entire northern Bolivian thrust belt by integrating new apatite fission-track (AFT) and zircon (U-Th)/He (ZHe) data with previous AFT and zircon fission-track (ZFT) data (Fig. 2.1), and (2) evaluate how these erosion patterns correlate with two models for the timing and kinematics of AP formation.

Geologic setting

The central Andean fold-thrust belt is divided into four physiographic regions (Fig. 2.1). These regions [after Kley, 1999] are: The Altiplano, Eastern Cordillera, Interandean zone, and Subandes (Fig. 2.1A). The AP occupies the hinterland portion of the thrust belt and is defined as the broad region of low relief above 3 km elevation that encompasses both the Altiplano and the westernmost Eastern Cordillera [e.g. Isacks,

1988]. The physiographic regions are defined by large structural steps that correlate with an eastward down-stepping in average topographic elevation (Fig. 2.1A) [McQuarrie, 2002]. The structural steps are basement highs that define the regional boundaries and play fundamental roles in the thrust belt structure [Kley, 1996; Kley, 1999; McQuarrie, 2002]. The exposed rocks involved in the deformation range from Paleozoic marine siliciclastics to Mesozoic non-marine clastics and Tertiary synorogenic deposits (Fig. 2.1B) [Guarachi et al., 2001; e.g. McQuarrie, 2002]. Although the regional structure is important, correlations between along-strike variations in topography, climate, and thrust belt geometry have been used to propose that the latitudinal erosion gradient also exerts a first-order control on the evolution of the plateau margin [Horton, 1999; Montgomery et al., 2001; Lamb and Davis, 2003].

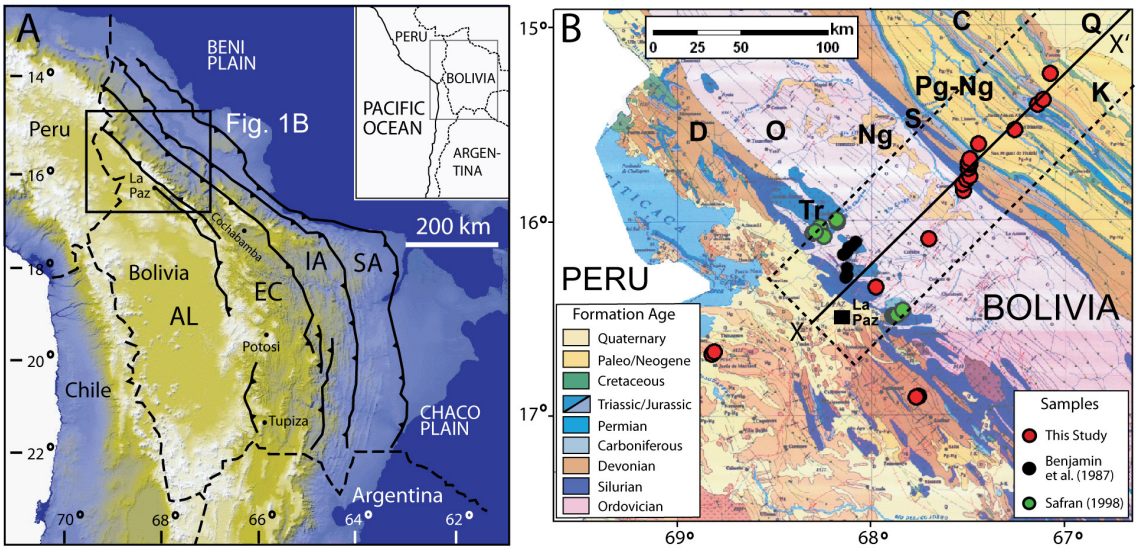

Figure 2.1. The central Andean fold-thrust belt and plateau in Bolivia. (A) Major zones: AL = Altiplano, EC = Eastern Cordillera, IA = Interandean zone, SA = Subandes. Zone-bounding faults from McQuarrie (2002). (B) Regional geologic map [from Guarachi et al., 2001] with thermochronometer sample locations. Age of rock units are D = Devonian, O = Ordovician, S = Silurian, C = Carboniferous, Tr = Triassic, K = Cretaceous, Pg = Paleogene, Ng = Neogene, Q = Quaternary. X-X' is transect line in Figures 2.2, 2.4, and 2.5. Dashed rectangle is the extent of the swath-averaged topography plotted in Figures 2.2 & 2.4A.

Previous work

In northern Bolivia, previous fission-track studies targeted predominantly Triassic plutons of the Eastern Cordillera which are limited to a narrow region of the plateau margin (Figs. 2.1 & 2.2) [Crough, 1983; Benjamin et al., 1987; Safran, 1998; Guarachi et al., 2001]. More recently, combined U-Pb, $^{40}Ar/^{39}Ar$, AFT and ZFT data of some of the same and adjacent plutons shows erosion-related exhumation with two rapid phases in the Eo-Oligocene and late Miocene to present totaling ~10 km in magnitude [Gillis et al., 2006]. These aforementioned cooling histories have been used to indicate that shortening began ~40 Ma in the northern Eastern Cordillera [McQuarrie, 2002; McQuarrie et al., 2005]. Northern Subandes deformation is inferred to be Neogene from limited ages constraints on the foreland basin chronostratigraphy and structure [Roeder, 1988; Sempere et al., 1990; Roeder and Chamberlain, 1995]. Unfortunately, no constraints exist on the timing and amount of long-term exhumation for most of the northern thrust belt that extends ~150 km eastward from the plateau margin [Barnes and Pelletier, 2006]. This study presents new thermochronometer data from across the entire northern Bolivian thrust belt at 15-16°S (Fig. 2.1).

Methods

Apatite and zircon fission-track thermochronology utilizes the thermally-sensitive retention of ^{238}U fission-generated damage trails in those minerals to constrain sample thermal histories [Donelick et al., 2005; Tagami, 2005; Tagami and O'Sullivan, 2005]. Zircon (U-Th)/He thermochronology uses the accumulation of ^{4}He from the alpha decay of ^{238}U, ^{235}U, and ^{232}Th in zircon crystals [Farley, 2002]. Although cooling rate and composition dependant, fission tracks in apatite generally become stable and record time since cooling through ~110ºC [Gallagher et al., 1998] which is commonly referred to as the closure temperature [Dobson, 1973]. The closure temperature for ZHe is ~180ºC

[Reiners et al., 2004] and ~240ºC for ZFT [Brandon et al., 1998]. Additionally, fission tracks experience length reduction (annealing), and ^{4}He can be lost by diffusion through temperatures significantly lower than their closure temperature (i.e. ~110-50ºC for AFT). This temperature region where the tracks are annealed or ^{4}He is lost is known as the partial annealing/retention zone [Hodges, 2003 and references therein].

AFT analytical results from sedimentary rock samples can exhibit significant variance because individual apatite grains possess non-uniform sources and cooling histories (see further discussion in Appendix 2.2). We interpret the AFT data using the chi-square (χ^2) test [Galbraith, 1981; Green, 1981], a statistical deconvolution of sample grain-age distributions [Brandon, 1992, 2002; Ehlers et al., 2005], and inverse thermal modeling of the age, track lengths, and mineral composition proxy data [Ketcham et al., 2000]. In brief, we (1) use the χ^2 test and grain-age distribution analysis results to identify the significant pooled or component age(s) in each sample grain-age distribution, and (2) use the results to guide placement of thermal constraints on the inverse modeling of each samples AFT data (see Appendix 2.2). These two tools are combined to constrain the full range of possible onset times for the most recent rapid cooling history of each sample.

We use the following terminology to discuss sample AFT grain-age distribution analysis and interpretation. The χ^2 test classifies a grain-age distribution as either concordant ($P(\chi^2) > 5\%$) or discordant ($P(\chi^2) < 5\%$) [Galbraith, 1981; Green, 1981]. Concordant samples have one significant component age that is geologically relevant and equivalent to the pooled age. Discordant samples have more than one significant component age and the pooled age is considered geologically meaningless [Brandon et al., 1998]. In the discordant case, one must use the central age [Galbraith and Laslett,

1993] or better yet identify (1) the minimum component age which not only constrains the most recent cooling, but is also the most easily resolved [Brandon et al., 1998], and

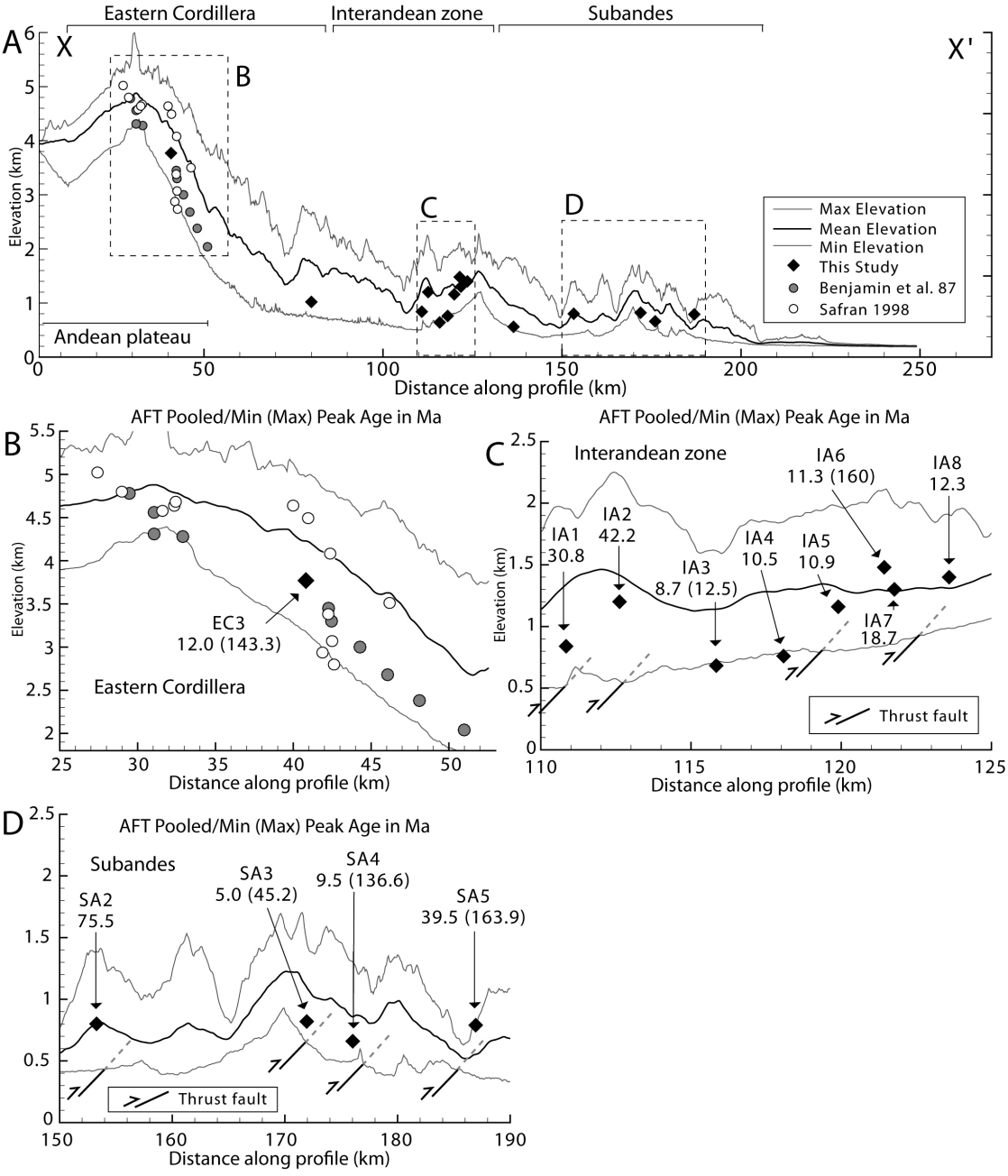

Figure 2.2. Topography, structure, and new apatite fission-track cooling ages across the fold-thrust belt. (A) 70-km wide swath-averaged minimum, mean, and maximum topography profiles with projected sample locations. Topography from 90m SRTM data. Profile location in Figure 2.1B. Enlargements of the Eastern Cordillera (B), Interandean zone (C), and Subandes (D) show sample locations, IDs, and AFT pooled age or Min (Max) component ages in Ma relative to mapped structures.

(2) the older component age(s) as it (or they) may signify cooling associated with either a more thermally resistant apatite composition end-member (i.e. Cl-apatite) and/or the source region [Brandon et al., 1998; Carlson et al., 1999]. Once component age(s) have been identified, their age(s) relative to the sample depositional age allows the sample to be categorized [after Brandon et al., 1998] as follows: Reset samples contain one age component that is younger than the depositional age, and hence the grains have been reset to a younger age. Mixed reset samples contain multiple age components younger than the depositional age that have all been reset since deposition. Partially reset samples contain age components that are both younger and older than the depositional age such that only some of the grain ages were reset. Detrital samples have component ages older than deposition and hence have ages inherited from the source region.

ZHe analytical results can similarly exhibit significant variance because individual zircon grains can possess non-uniform sources and cooling histories as well as variable U & Th zonation, degrees of radiation damage, and abrasion during transport [Reiners, 2005 and references therein]. Regardless, in general, ZHe grain ages similarly represent either the age of rock cooling if it is younger than the depositional age, or the age of source region cooling if the age is older than the depositional age.

Results and interpretations

We present 19 new AFT samples paired with 4 ZHe results from samples across the central Andean fold-thrust belt in northern Bolivia (Fig. 2.1). Samples were collected from a wide range in elevation from Precambrian to Tertiary quartzites and sandstones (Fig. 2.2). Table 2.1 lists essential sample information, Table 2.2 the AFT results, Table 2.3 the ZHe results, and Appendix 2.1 details the analytical procedures.

Interpretations of sample grain-age distributions assume the central or minimum age (or pooled age if only one component) represents the youngest apparent cooling

age or event [following Brandon et al., 1998]. Furthermore, we bracket the onset time of the most recent accelerated cooling by (1) quantifying the range of acceptable or better fits of thermal histories resolved with modeling, and (2) identifying the portion of resolved cooling histories where the particular sample cooled below AFT-sensitive temperatures (detailed in Appendix 2.2). Figure 2.3 shows representative examples of the component age analysis and thermal modeling results. Figure 2.4 illustrates the distribution of all reliable cooling ages along the thrust belt transect. We group observations and interpretations by physiographic region, moving eastward from the Altiplano.

Table 2.1. Sample data

Sample Zone/ID	Sample #	S Lat (WGS84)	W Long (WGS84)	Elev (m)	Fm Age	Dist (m)
AL1	B811-1	-16.682	-68.818	3900	Pe	NA
AL2	B811-4	-16.668	-68.807	4450	Tert	NA
EC1	B721-5	-16.902	-67.766	2320	Sil	NA
EC2	B721-2	-16.896	-67.752	2240	Lwr Dv	NA
EC3	725-13	-16.333	-67.974	3770	Ord	40.8
EC4	JB01-K3	-16.087	-67.701	1020	Ord	80.0
IA1	JB01-L3	-15.840	-67.521	840	Ord	110.8
IA2	JB01-M1	-15.803	-67.525	1200	Ord	112.6
IA3	JB01-M4	-15.783	-67.503	600	Sil	115.8
IA4	JB01-M7	-15.766	-67.489	760	Upr Sil	118.1
IA5	JB01-M8	-15.723	-67.497	1160	Upr Sil	119.9
IA6	JB01-N1	-15.697	-67.497	1480	Upr Dv	121.6
IA7	722-20	-15.704	-67.489	1301	Lwr Dv	121.8
IA8	JB01-N2	-15.676	-67.487	1400	Upr Dv	123.7
SA1	JB01-N3	-15.596	-67.441	522	Tert	136.5
SA2	721-14	-15.526	-67.257	801	Jr	153.3
SA3	JB01-04	-15.395	-67.137	820	Upr Dv	171.9
SA4	JB01-06	-15.370	-67.108	640	Jr	176.0
SA5	JB01-09	-15.235	-67.072	790	Jr	186.9

Elev = Elevation; **Fm age** = Formation age; Pe = Precambrian, Tert = Tertiary, Sil = Silurian, Dv = Devonian, Ord = Ordovician, Jr = Jurassic, Lwr = Lower, Upr = Upper, **Zone** = major zones, see Figure 2.1; AL = Altiplano, EC = Eastern Cordillera, IA = Interandean zone, SA = Subandes; Dist = distance along profile in Figures 2.2 and 2.4, NA = not applicable

Altiplano

Two AFT samples (AL1-2) were collected in the Altiplano ~85 km west of La Paz, Bolivia (Fig. 2.1B). The pooled AFT ages are 9.87 Ma and 37.2 Ma with mean track lengths (MTLs) of 14.09 and 11.82 μm, respectively. Sample AL1 from Precambrian sandstone is interpreted as mixed reset with AFT component ages of 11.4 and 4.2 Ma (Table 2.2). Sample AL2 from Tertiary sandstone is interpreted as partially reset with AFT component ages of 58.6 and 8.7 Ma. Collectively, these two samples show accelerated cooling from ~18-2 Ma which includes the 2σ error of the component ages from sample AL1.

Eastern Cordillera

We report four new AFT samples (EC1-4) from the Eastern Cordillera. Pooled AFT ages range from 101-2.6 Ma with MTLs of 11.81-8.95 μm. Component and central ages range from 143.3 to 2.0 Ma. The AFT samples are interpreted as partially reset, mixed reset, and reset (Table 2.2).

Two samples were collected to the southeast of La Paz significantly separated from the main transect in Devonian and Silurian sandstones exposed within the La Paz river basin (Fig. 2.1B). Sample EC1 is reset with irresolvable component ages, so we report the central age (2.8 Ma) which is nearly identical to the pooled age (2.6 Ma) (Table 2.2). Sample EC2 is mixed reset with component ages of 40.0 and 2.0 Ma with the majority of the grains contributing to the minimum age component.

Along the main transect, sample EC3 (km 40.8, Fig. 2.2B) is consistent with protracted cooling from as early as ~40 Ma (Fig. 2.3A & 2.4C), though a minimum component age of 12 Ma implies more rapid cooling since <25 Ma. Sample EC4 (km 80.0, Fig. 2.2A) has a pooled age of 101 Ma, but <10 measured grain ages and track

lengths. This precludes proper resolving of any component age populations (see Appendix 2.2) and provides very limited modeling constraint on its recent cooling history (Fig. 2.3B). In summary, most of the reset AFT component ages record accelerated cooling from ~20-5 Ma. Additionally, previous work reported twenty-five AFT samples from the Eastern Cordillera (Figs. 2.1, 2.2A,B & 2.4C) [Benjamin et al., 1987; Safran, 1998]. The AFT ages range from 20-4.9 Ma (Fig. 2.4C). Unfortunately, neither χ^2 test results nor track length measurements were reported for these samples [Benjamin, 1986; Safran, 1998]. In summary, AFT ages from the Eastern Cordillera are 25-2 Ma indicating accelerating cooling at this time (Fig. 2.4C) and are consistent with new AFT ages reported by [Gillis et al., 2006]. At 1σ uncertainty, the Eastern Cordillera samples indicate accelerated cooling from ~21-3 Ma (Fig. 2.5). One ZHe sample, EC3 (km 40.8, Fig. 2.4B), has relatively young (33-16 Ma) grain ages that we consider reset and roughly Oligo-Miocene or younger (Table 2.3). The large age range in the zircons insinuates they were either zoned or experienced partial ^{4}He loss. The same sample AFT component ages show a dominant young component at 12 Ma and a minor old component at 143 Ma (Table 2.2). A strong correlation between grain age (but not track length) and Dpar (2.9-2.7 μm for the old peak grains vs. <1.7 μm for the young peak grains) implies resetting of the only the less resistant apatites [Burtner et al., 1994] and thus time spent in the partial annealing zone, consistent with a short MTL of 8.95 μm.

We conclude that the 33-16 Ma ZHe grain ages either (1) must be circumspect since they have a higher closure temperature, but have younger ages than the older component AFT age, or perhaps (2) the measured apatites were of the mixed F/OH Tiago variety [Reiners and Brandon, 2006] that overlaps in partial annealing/retention zone temperatures with ZHe [Reiners et al., 2004]. A more detailed interpretation of the ZHe ages is not possible without additional analyses to characterize the grain-age variability.

Table 2.2. Apatite fission-track data

Sample ID	r_s (10^6 tracks/cm^2)	N_s (tracks)	r_i (10^6 tracks/cm^2)	N_i (tracks)	r_d (10^6 tracks/cm^2)	N_d (tracks)	n	Dpar (µm)	Dper (µm)	P (χ^2) (%)	Pooled Age (Ma ± 2σ)	Component Ages (N_g) (Ma)	MTL ± 1σ (N_t) (µm) (tracks)	Desig
AL1	0.162	162	3.960	3949	4.233	4040	25	1.65	0.45	10.0	9.87±1.68	4.2 (4) , 11.4 (21)	14.09±0.13 (115)	MR
AL2	0.141	169	0.907	1088	4.225	4040	40	2.20	0.61	0.0	37.2±6.6	8.7 (16) , 58.6 (24)	11.82±0.21 (200)	PR
EC1	0.055	26	5.057	2382	4.242	4040	38	1.65	0.48	2.7	2.63±1.06	2.8±1.3#	11.81±0.35 (69)	MR
EC2	0.038	7	1.897	346	4.250	4040	15	1.60	0.47	0.3	4.89±3.74	2.0 (13) , 40.0 (2)	10.83±0.7 (14)	MR
EC3	0.352	60	0.792	135	3.720	4188	13	1.40	0.36	0.0	85.8±27	12.0 (11) , 143.3 (2)	8.95±3.07 (24)	MR
*EC4**	*0.385*	*16*	*0.601*	*25*	*2.783*	*4117*	*5*	*1.74*	*0.39*	*70.3*	*101±64*	*100.6 (5)*	*11.45±2.41 (3)*	*R*
*IA1**	*0.074*	*7*	*0.380*	*36*	*2.794*	*4117*	*7*	*1.63*	*0.47*	*52.8*	*30.8±25.6*	*30.8 (7)*	*14.27±0.93 (2)*	*R*
*IA2**	*0.244*	*30*	*0.920*	*113*	*2.805*	*4117*	*6*	*1.79*	*0.37*	*78.0*	*42.2±17.6*	*42.2 (6)*	*11.23 (1)*	*R*
IA3	0.292	113	3.334	1291	2.816	4117	39	1.76	0.48	39.5	14.0±2.8	8.7 (14) , 12.5 (25)	12.94±2.34 (79)	MR
IA4	0.29	66	4.420	1007	2.827	4117	32	1.78	0.45	92.5	10.5±2.8	10.5 (32)	13.32±1.78 (109)	R
IA5	0.262	109	3.877	1613	2.838	4117	40	1.80	0.41	64.5	10.9±2.2	10.9 (40)	13.46±2.03 (104)	R
IA6	0.308	166	4.355	2344	2.860	4117	40	1.83	0.43	17.1	11.5±2.0	11.3 (39), 160.3 (1)	14.09±1.65 (116)	MR
*IA7**	*0.246*	*17*	*2.127*	*147*	*2.849*	*4117*	*4*	*1.84*	*0.51*	*1.0*	*18.7±9.6*	*18.7 (4)*	*15.33±0.50 (3)*	*R*
IA8	0.301	166	4.007	2208	2.871	4117	39	1.79	0.47	40.2	12.3±2.2	12.3 (39)	13.64±1.75 (120)	R
SA1	0.841	555	1.181	779	2.882	4117	34	2.25	0.60	0.0	116±14	30.9 (14), 181.0 (20)	11.93±1.90 (202)	D/PR
*SA2**	*0.436*	*24*	*0.945*	*52*	*2.893*	*4117*	*4*	*1.89*	*0.66*	*18.1*	*75.5±37.6*	*75.5 (4)*	*11.97±3.04 (3)*	*R*
SA3	0.175	254	5.183	7531	3.759	4188	40	1.43	0.31	0.0	6.62±0.92	5.0 (38), 45.2 (2)	13.02±2.74 (173)	MR
SA4	0.716	596	2.710	2256	3.746	4188	40	1.42	0.34	0.0	51.5±5.6	9.5 (31) , 136.6 (9)	11.79±2.56 (202)	MR
SA5	1.308	841	2.773	1783	3.733	4188	40	1.51	0.36	0.0	91.4±9.4	39.5 (19) , 163.9 (21)	10.69±2.05 (202)	PR

Notes: ρ_s = density (cm^{-2}) of spontaneous tracks; N_s = number of spontaneous tracks counted; ρ_i = density (cm^{-2}) of induced tracks; ρ_d = density (cm^{-2}) of tracks on the neutron fluence monitor (CN-1 glass); N_d = number of tracks counted in the dosimeter; **n** = number of grains counted; **Dpar** = is the mean maximum diameter of fission-track etch figures parallel to the c-axis; **Dper** = is the mean maximum diameter of fission-track etch figures perpendicular to the c-axis; **P(χ2) =** probability (%) of greater chi- squared; **MTL** = mean track length; N_t = number of track lengths measured, **Ng** = number of grains contributing to that peak age, **Desig** = designation after Brandon et al. (1998), R = reset, MR = mixed reset, PR = partially reset, D = detrital

* excluded from Figures 4 & 5 due to less than 10 measured grain ages and track lengths.

central age reported because component ages were unresolvable

Table 2.3. Zircon (U-Th)/He data

Sample ID*	Raw Age (Ma)	Error (2σ)	Corrected (Ma)	Error (2σ)	U (ppm)	Th (ppm)	He (ncc/mg)	Ft
EC3a	11.84	0.44	15.72	0.59	445.10	413.07	781.93	0.75
EC3b	15.24	0.73	20.62	0.99	351.12	125.69	707.27	0.74
EC3c	25.40	6.17	33.35	8.10	54.17	18.14	181.09	0.76
SA3a	316.15	7.26	367.51	8.44	276.06	194.45	12783.77	0.86
SA3b	231.54	5.86	274.98	6.96	201.92	106.55	6548.73	0.84
SA3c	285.39	6.92	349.19	8.47	478.03	187.84	18695.17	0.82
SA4a	500.17	19.83	660.12	26.17	393.37	203.08	28383.85	0.76
SA4c	160.32	7.65	219.79	10.49	367.34	411.95	9189.97	0.73
SA5b	211.68	72.83	296.79	102.11	70.90	38.04	2101.56	0.71
SA5c	222.41	67.05	333.14	100.42	112.72	127.12	3940.26	0.67

Notes: σ = sigma, **ppm** = parts per million, **ncc/mg** = nano cubic centimeters per milligram, **Ft** = Ft correction factor

*2-3 grains, labeled a, b, and/or c were measured for each sample

Additionally, previous work reported seven ZFT ages ranging from 101-24.8 Ma with rapid exhumation interpreted to start ~40 Ma (Fig. 2.4B) [Benjamin, 1986; Benjamin et al., 1987]. The ZFT ages are older than the ZHe ages in the Eastern Cordillera, as would be expected due to its sensitivity to higher temperatures (Fig. 2.4B). The three oldest (101-68 Ma) ZFT ages were interpreted to result from significant time spent in the zircon partial annealing zone before rapid cooling began at ~40 Ma as recorded by the younger (~50-29 Ma) ZFT ages (Fig. 2.4B) [Benjamin et al., 1987].

Interandean zone

Eight samples (IA1-8) were collected from four different thrust sheets in the Interandean zone (Fig. 2.2C). Pooled AFT ages range from 42.2-10.5 Ma and MTLs from 14.27-11.23 μm. Minimum and old component ages range from 11.3-8.7 Ma and 160.3-12.5 Ma, respectively. All samples are designated as reset and mixed reset (Table 2.2).

Low grain yields from samples IA1 and IA2 (km 110.8 and 112.6, Fig. 2.2C) have limited model-constrained recent cooling from between 31-10 Ma and 52-3 Ma, respectively. Sample IA3 (km 115.8, Fig. 2.4C) shows constrained accelerated cooling

from >~100ºC temperatures from as early as ~20 Ma (Fig. 2.4C) consistent with its pooled age of 14 Ma and its component ages of 12 and 9 Ma (Fig. 2.3C). Samples IA4 (km 118.1), IA5 (km 119.9), and IA8 (km 123.7) all passed the χ^2 test and show constrained cooling associated with their pooled ages ranging from 12.3-10.5 Ma (Figs. 2.3D & 2.4C). Sample IA6 has two component ages of 160.3 and 11.3 Ma, but the minimum age is nearly identical to the pooled age of 11.5 ± 2.0 Ma. Modeling shows the acceptable cooling histories within the error associated with the minimum component age estimate (Fig. 2.4C). Sample IA7 (km 121.8, Fig. 2.2C) possesses a low number of grain ages and track lengths measured and modeling does not further constrain its recent cooling history beyond its pooled age of 18.7 ± 9.6 Ma. In summary, the good quality data have young component ages from ~18-3 Ma, and indicate rapid cooling starting from ~15-5 Ma at the 1σ uncertainty (Figs. 2.4C & 2.5).

Subandes

Five samples (SA1-5) were collected from four different thrust sheets in the Subandes (Fig. 2.2A & C). Pooled AFT ages range from 116-6.6 Ma with MTLs of 13.02-10.69 μm. Minimum component ages range from 39.5-5 Ma, and old component ages range from 181-45.2 Ma. These samples are designated as reset, mixed reset, partially reset, and detrital (Table 2.2).

We interpret sample SA1 (km 136.5, Fig. 2.2A) as either detrital or partially reset because it is from Tertiary sandstone and has component ages of 181 and 30.9 Ma. Without further depositional age control, we can't discern if the young age component is older or younger than the depositional age. However, the larger grain contribution to the Mesozoic age component shows that there is a significant detrital cooling signal in this sample (Table 2.2). Note the acceptably-fit recent cooling from ~100ºC since ~41-11 Ma

Figure 2.3. Representative grain-age distributions and modeled thermal histories from the thrust belt transect apatite fission-track data. (I) BinomFit [Brandon, 2002] results showing grain-age histogram (bars), probability density function fit to the grain-age distribution (line), and binomially best-fit component age(s) (thick lines labeled with age). Abbreviations are the same as in Figure 2.1 and Table 2.2. AFTSolve [Ketcham et al., 2000] results showing permissible thermal histories (II) and measured versus modeled track length distributions (III). Thermal histories shown are acceptable (light gray), good (dark gray), and the best (black line), with imposed model constraints (vertical bars). Numbers are the pooled ages (Age) and mean track lengths (MTL) with 1σ, number of grain ages or track lengths measured (N), and goodness of fit (G.O.F) between the model results and the data for both the age and MTL data [Ketcham and Donelick, 2001]. Histograms in (III) show measured (in binned bars) and best-fit model (solid line) track length distributions.

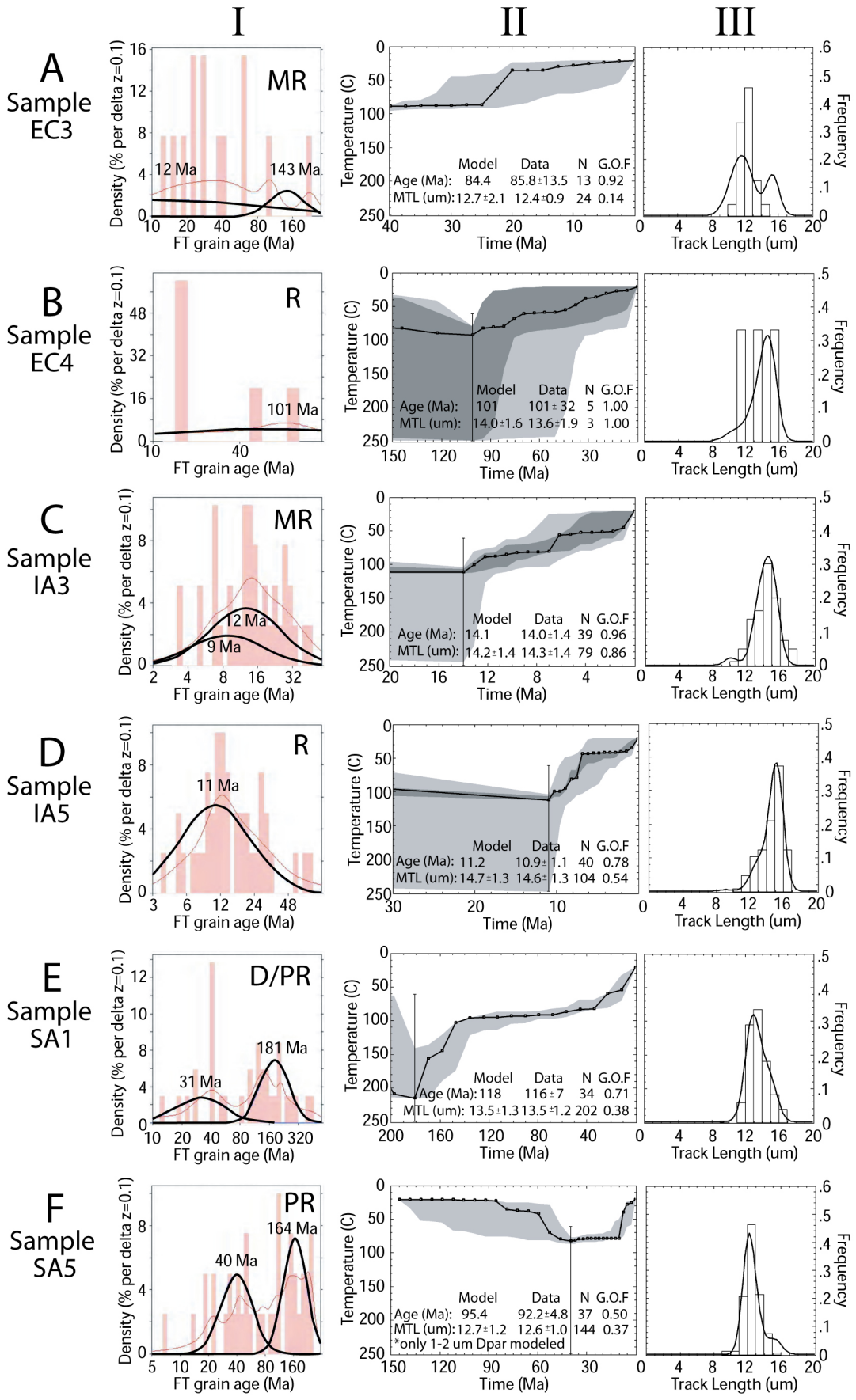
I
II
III
A
Sample
EC3
MR
12 Ma
143 Ma
Density (% per delta z=0.1)
FT grain age (Ma)
Temperature (C)
Time (Ma)
Model Data N G.O.F
Age (Ma): 84.4 85.8±13.5 13 0.92
MTL (um): 12.7±2.1 12.4±0.9 24 0.14
Track Length (um)
Frequency
B
Sample
EC4
R
101 Ma
Age (Ma): 101 101 ± 32 5 1.00
MTL (um): 14.0±1.6 13.6±1.9 3 1.00
C
Sample
IA3
MR
12 Ma
9 Ma
Age (Ma): 14.1 14.0±1.4 39 0.96
MTL (um): 14.2±1.4 14.3±1.4 79 0.86
D
Sample
IA5
R
11 Ma
Age (Ma): 11.2 10.9± 1.1 40 0.78
MTL (um): 14.7±1.3 14.6± 1.3 104 0.54
E
Sample
SA1
D/PR
181 Ma
31 Ma
Age (Ma): 118 116 ± 7 34 0.71
MTL (um): 13.5±1.3 13.5 ±1.2 202 0.38
F
Sample
SA5
PR
164 Ma
40 Ma
Age (Ma): 95.4 92.2±4.8 37 0.50
MTL (um): 12.7±1.2 12.6±1.0 144 0.37
*only 1-2 um Dpar modeled

as recorded by the minimum component age and modeling (Fig. 2.3E). This recent cooling follows significant time in the apatite partial annealing zone from ~140-40 Ma (Fig. 2.3E) as corroborated by a short MTL of 11.93 μm. Sample SA2 (km 153.3, Fig. 2.2D) has a pooled age of 75.5 Ma and poorly constrained model results with cooling commencing as early as ~110 Ma. This may reflect a lower magnitude of cooling on this structure compared to others, or a poorly resolved cooling history due to the low number of grains (<10 grains) analyzed. Samples SA3 and SA4 (km 171.9, 176.0, Fig. 2.2D) are mixed reset with minimum component ages and modeling indicating recent rapid cooling from ~19-4 Ma (Fig. 2.4C).

Sample SA5 (km 186.9, Fig. 2.4C) is Jurassic sandstone and considered partially reset because it has component ages of 163.9 and 39.5 Ma. The minimum component age, though reset, is unusually old considering that it is from the easternmost structure of the Subandes which is believed to have been active for only the last ~10 Ma [e.g. Gubbels et al., 1993]. Unfortunately, no acceptable modeled cooling histories fit the data when either both component ages or only the minimum age are used as a constraint for the cooling history and no correlation exists between Dpar and grain age. Furthermore, there are no acceptable cooling histories when the grains are grouped into generic fluorapatite (2-1 μm Dpar) and chlorapatite (3-2 μm Dpar) kinetic apatite populations with their respective track length distributions [Burtner et al., 1994; Ketcham and Donelick, 2001]. The only way to achieve any acceptable thermal histories is to model only the most thermally sensitive population of fluorapatite (2-1 μm Dpar, MTL 12.6 μm) grains using a thermal event at 40 Ma, as constrained by the minimum component age [Brandon et al., 1998; Ketcham and Donelick, 2001]. This result suggests accelerated cooling from apatite partial annealing zone temperatures of ~80ºC or more from between ~19-4 Ma (Figs. 2.3F & 2.4C). The protracted time this sample spent in the partial annealing zone prior to rapid cooling is corroborated by a short MTL

of 10.69 μm (Table 2.2). In summary, most of the Subandes samples have young component ages from 30-5 Ma that record accelerated cooling starting from ~19-4 Ma (Fig. 2.4C). At 1σ uncertainty level, it appears rapid cooling began ~12-5 Ma (Fig. 2.5).

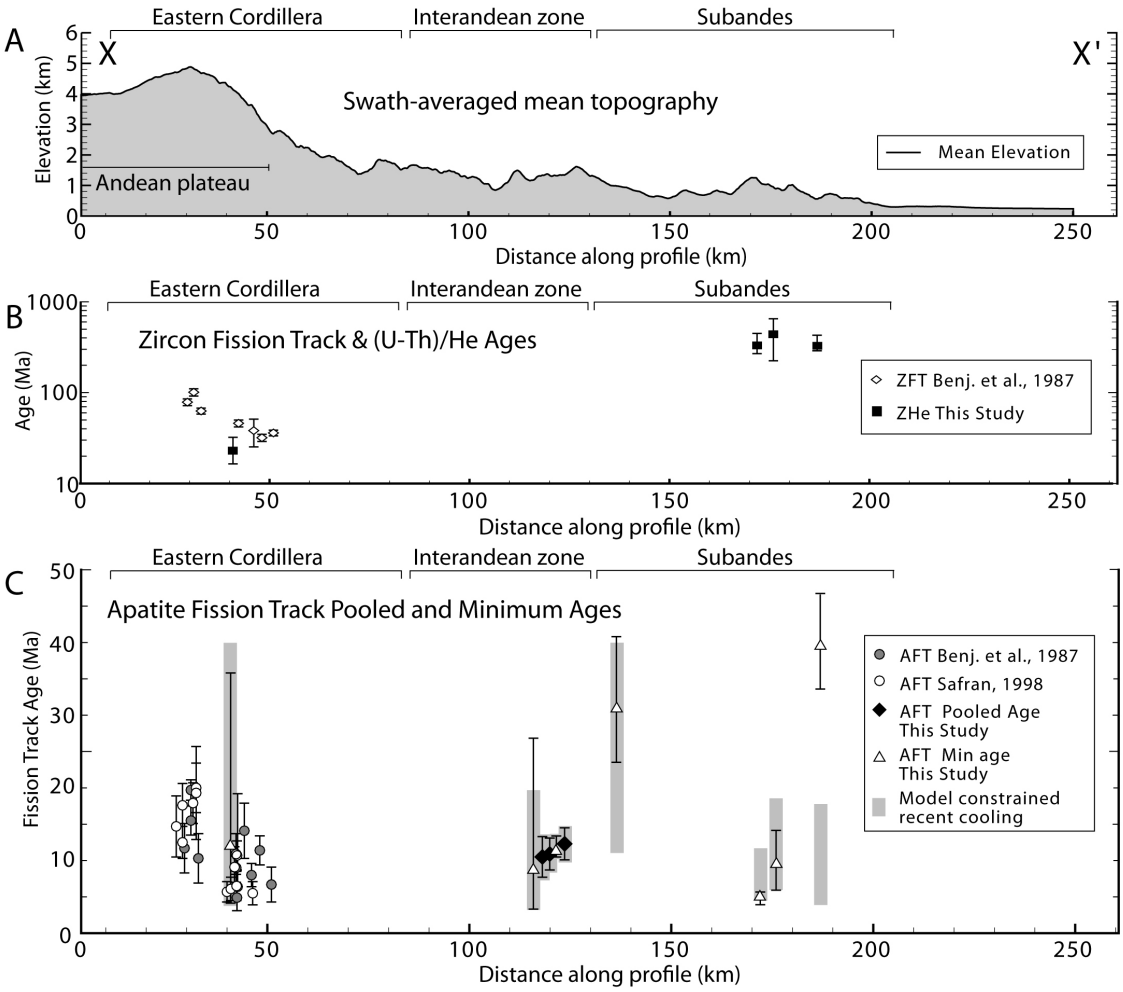

Figure 2.4. Mean topography and robust thermochronometer cooling ages across the fold-thrust belt. See Figure 2.1B for location. (A) 70-km wide swath-averaged mean elevation. (B) ZFT and ZHe ages. Error bars are 2σ for the ZFT. ZHe symbols are plotted on the sample average age (bars show range of grain ages). Note the semi-log scale. (C) AFT pooled or minimum component ages for samples with >10 measured grains and/or track lengths. Error bars are 2σ. Gray bars are the age range for the onset of the most recent cooling constrained by modeling.

From west to east, three Subandes samples with ZHe analyses have ages of 368-275 Ma, 660-220 Ma, and 333-297 Ma, respectively (Fig. 2.4B). We simply interpret these ZHe ages as partially reset for sample SA3 from Upper Devonian rocks and detrital for samples SA4 and SA5 from Jurassic units (Table 2.3). A more detailed interpretation of these sample ZHe ages is not possible without additional analyses to characterize the nature of the range in the ages.

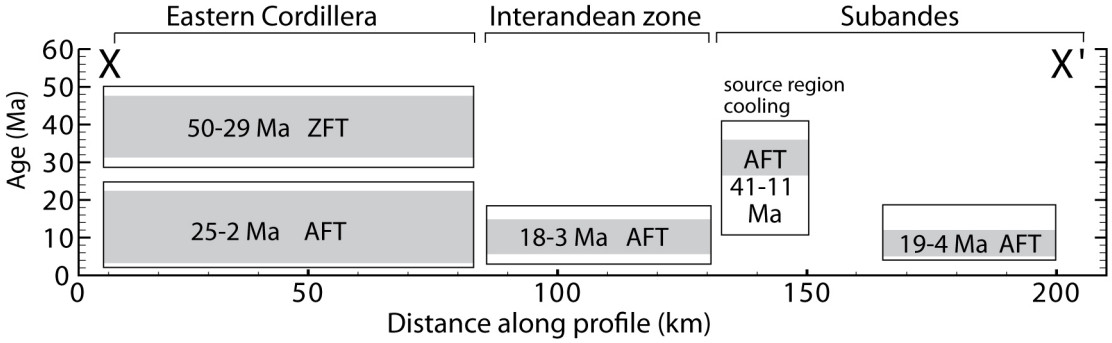

Figure 2.5. Spatial and temporal variations in erosion recorded by thermochronometer ages across the fold-thrust belt. Boxes and labels are the robust cooling age ranges (2σ) further constrained by modeling after Figure 2.4. ZFT = zircon fission track, AFT = apatite fission track. Sample EC3 95%CI range for the young age component excluded due to extremely large error. Gray regions show 1σ range in ages.

Discussion and implications

Thermochronometer ages represent the time since cooling below closure. Combined with additional information, such as track length distributions and kinetic parameters in apatite, cooling histories can be constrained with modeling. Thermochronometer cooling can result from either igneous activity, tectonic exhumation (i.e. normal faulting) or erosion [Ring et al., 1999; Hodges, 2003]. According to the latest mapping, lack of evidence for proximal (<~50 km) Tertiary intrusions/volcanism near the samples in northern Bolivia, as well as significant normal faulting allows the inference

that recorded cooling was the result of erosional exhumation [Sergiomin, 1997; Gillis et al., 2006]. Similar to other studies (see, for example [Coughlin et al., 1998; Willett, 1999; Willett and Brandon, 2002; Sobel and Strecker, 2003; Carrapa et al., 2005; Clark et al., 2005]), we assume that the early stages of erosion-driven exhumation are the result of deformation because thrust faulting facilitates erosion by generating topography and relief. This assumption still recognizes that erosion-related cooling can continue long after deformation has ceased. Thus, thermochronometer data from thrust belts can be sensitive to the onset time of deformation, but poorly constrain when deformation terminates due to protracted erosional exhumation. This highlights the need for future work to address how erosion rates and magnitudes change across structures during and after deformation.

We first highlight the spatial and temporal variations in cooling due to erosion across the thrust belt and compare them with two end-member deformation models. We next estimate the spatial and temporal distribution of erosion magnitudes using constraints on the subsurface thermal field from borehole data. Finally, we briefly compare thermochronologic results from across the entire AP from Peru to Argentina.

Erosion and plateau development

The observed erosion patterns tend to be broad and most easily defined by the various physiographic zones. Figure 2.5 summarizes the regional spatial and temporal trends in cooling ages and the onset of accelerated ZFT-and-AFT-recorded cooling across the thrust belt. The Altiplano and Eastern Cordillera has ZFT ages from 50-29 Ma and AFT ages from 25-2 Ma that record accelerated erosion from ~40-25 Ma and from ~15 Ma (or younger) to the present [Benjamin et al., 1987; Gillis et al., 2006]. The Interandean zone has AFT ages from 18-3 Ma that record accelerated erosion since ~15 Ma. The westernmost Subandes have AFT ages that record erosion from 41-11 Ma

related to the Eastern Cordillera to the west, whereas most of the Subandes experienced accelerated erosion from ~19-4 Ma that could be as recent as ~5 Ma. The distribution of erosion documented by the thermochronometer data across the thrust belt highlights two major trends: (1) initial onset of accelerated erosion ~40 Ma in the Eastern Cordillera, followed by (2) synchronous rapid erosion across the entire plateau and thrust belt since ~15 Ma.

As outlined in McQuarrie et al. [2005], there are two end-member deformation models for the evolution of the central Andes. A short duration and low-magnitude shortening characterizes one end-member that describes predominately Neogene deformation occurring in two stages [Isacks, 1988; Sempere et al., 1990; Gubbels et al., 1993; Allmendinger et al., 1997; Jordan et al., 1997]: (1) distributed deformation in the Altiplano and Eastern Cordillera began at ~27 Ma, followed by (2) deformation concentrated exclusively in the Subandes since ~10 Ma. A long duration and large-magnitude shortening characterizes the other end-member that emphasizes higher magnitudes of shortening and the role of basement-involved deformation [McQuarrie and DeCelles, 2001; McQuarrie, 2002; Horton, 2005; McQuarrie et al., 2005]. Although the exact geometry of the basement deformation is unknown [compare McQuarrie, 2002; and Müller et al., 2002], the deformation chronologies are similar [see also Elger et al., 2005]. This model describes Eocene deformation in the Eastern Cordillera propagated by bi-vergent deformation moving west towards the Altiplano and eastward to the Subandes where it has been concentrated since the early to late Miocene.

If the first end-member model is applicable, we would expect erosion from ~27-10 Ma or less in the Altiplano and Eastern Cordillera (which includes the Interandean zone in this model) followed by erosion from ≤~10 Ma in the Subandes. The ZFT cooling in the Eastern Cordillera from ~40-25 Ma reveals earlier Eocene pre-27 Ma deformation, uplift, and erosion. Furthermore, the model-constrained AFT-cooling from

as early as 19 Ma in the Subandes suggests deformation and erosion began in the region before 10 Ma (Fig. 2.5). However, the fact that accelerated cooling in the Subandes could be as recent as ~12-5 Ma is consistent with this model.

If the second end-member model is applicable, we would expect erosion beginning in the Eastern Cordillera in the Eocene followed by more recent erosion both westwards and eastwards to the present. The Eocene erosion ~40-25 Ma is consistent with the eastward propagation of an upper-basement thrust over a ramp beneath the Eastern Cordillera [Kley, 1996; McQuarrie, 2002]. Additional evidence corroborates this model by limiting deformation in this region from post mid-Paleocene to pre late-Oligocene [Lamb and Hoke, 1997; Horton, 2005; Gillis et al., 2006]. The distributed erosion since ~15 Ma is consistent with the emplacement of a second, lower-basement thrust that began ≤~20 Ma [Kley, 1996; see also Allmendinger and Zapata, 2000; McQuarrie, 2002]. This lower-basement thrusting is responsible for uplifting the Interandean zone with respect to the foreland, transferring slip eastward into the Subandes, and possibly deforming the Altiplano through basement duplexing. In other words, the young accelerated erosion (<~15 Ma) in the Eastern Cordillera was not contemporaneous with deformation on surface structures in this region [Gillis et al., 2006]. Instead, the ~15-2 Ma accelerated cooling must be erosionally-driven while early to late Miocene deformation in the Altiplano [Lamb and Hoke, 1997] and Subandes initially drove the ~15 Ma erosion in those regions. We note that the ~15-5 Ma cooling in the Interandean zone is equally consistent with both end-member models signifying deformation and erosion began in this region at this time.

Shortening associated with the upper-basement thrust is recognized to be responsible for most of the present crustal thickness and presumably some of the AP elevation [McQuarrie, 2002]. The accelerated erosion ~40-25 Ma in the Eastern Cordillera probably records movement of the upper-basement thrust sheet. If the

distributed erosion since ~15 Ma records motion of the lower basement shortening, then it follows that the upper-basement thrust sheet must have ceased between 25 and 15 Ma. Therefore, we infer the early development of the AP analogous to its modern width and near present day crustal thickness at ~20 Ma. However, evidence from leaf physiognomy and paleoerosion surface remnants imply that much of the modern elevation of the AP came later in the late Miocene [Gubbels et al., 1993; Gregory-Wodzicki, 2000]. The protracted cooling since ~15 Ma in the Altiplano and Eastern Cordillera is also consistent with late Miocene rapid surface uplift [Garzione et al., 2006].

In summary, the two regional cooling events suggested by the thermochronometer data have the following implications for the contending deformation models of the central Andes: (1) The onset of erosion from ~40-25 Ma in the Eastern Cordillera is consistent with the longer duration model [McQuarrie, 2002], (2) Synchronous erosion across the entire plateau and thrust belt since ~15 Ma is consistent with both models [Isacks, 1988; Gubbels et al., 1993; McQuarrie, 2002].

Spatial distribution of erosion magnitude

We estimated erosion magnitudes across the thrust belt using measured thermal gradients and effective closure temperatures [Reiners and Brandon, 2006] for each thermochronometer system to calculate the depth to closure. This effectively allows quantification of the amount of material removed since the samples cooled below their closure temperatures (Fig. 2.6). We assume average closure temperatures of 110ºC for AFT, 180ºC for ZHe, and 240ºC for ZFT, and average surface temperatures of 10ºC for the Altiplano and Eastern Cordillera, 15ºC for the Interandean zone, and 23ºC for the Subandes [Brandon et al., 1998; Gallagher et al., 1998; Springer and Forster, 1998; Instituto Geografico Militar, 2000; Reiners et al., 2004]. Proximal borehole-measured geothermal gradients and estimates of mean surface temperatures combine to represent

the best-available proxy for the thermal field through which the samples cooled. Our selection criteria for borehole-estimated thermal gradients include: (1) measurement reliability, (2) location within the same physiographic province as the samples, (3) application of a topographic correction, and (4) location within one crustal thickness distance (~55-45 km [Beck et al., 1996]) of sample locations to minimize regional variations in basal heat flux that might alter near surface thermal gradients. However, in some cases the measurements we use are not as proximal because the borehole data are sparse and sometimes unreliable.

In the Altiplano, we use a thermal gradient of 27ºC/km ± 20% error. This value comes from the only reliable measurement located at Chacarilla, ~115 km from our two samples [Henry and Pollack, 1988]. We estimate ~3.7 km of erosion in the Altiplano since ~18-2 Ma from the AFT component ages (Fig. 2.6). In the Eastern Cordillera, we use a gradient of 22ºC ± 10% at Chojilla. Chojilla is at most ~50 km from our samples and ~75 km from all previously reported Eastern Cordillera samples [Henry and Pollack, 1988]. The Eastern Cordillera thermal gradient could be less than that observed in the Altiplano due to the large topographic effect from the high relief (> 2 km) (Fig. 2.2A). We estimate ~10.6 km erosion since ~40-25 Ma from the ZFT data and ~4.6 km since ~15-5 Ma from the AFT data (Fig. 2.6). These estimates are a refinement of previous work that assumed a generic thermal gradient of 30ºC/km [Benjamin et al., 1987; Masek et al., 1994; Gillis et al., 2006]. We assume the same gradient for the Interandean zone. The Chojilla station is at most ~90 km from all Interandean samples. We estimate ~4.6 km of erosion since ~15-5 Ma from the AFT data (Fig. 2.6). No proximal thermal gradient measurements exist for our samples in the northern Subandes. However, a large compilation of over 1500 measurements from the southern Subandes and adjacent Chaco basin yields a mean gradient of 22.4 ºC ± ~35% with a mean surface temperature of 23ºC ± 10% from robust linear regression [Springer and Forster, 1998]. Assuming

these values for the northern Subandes, the erosion magnitude is limited to ≤~7.0 km from the mostly detrital ZHe ages since at least ~220 Ma, and estimated to be ~3.9 km since ~15-5 Ma from the AFT data (Fig. 2.6).

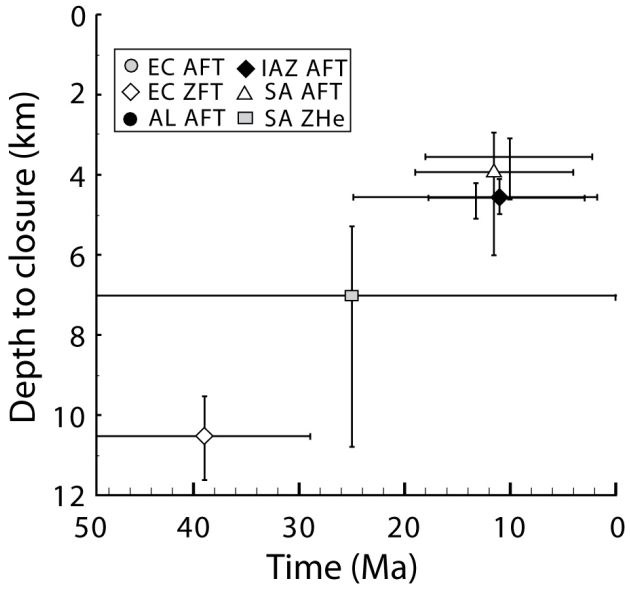

Figure 2.6. Estimated erosion magnitudes across the fold-thrust belt. Symbols are located at the median cooling age for each region and horizontal error bars represent the range in regional cooling ages after Figure 2.5. Vertical bars represent the range in erosion magnitude due to the percent error in the heat flow measured thermal gradients. See Figures 2.1 and 2.4 for abbreviations.

Estimated erosion magnitudes decrease eastward across the thrust belt (Fig. 2.6). The Eastern Cordillera ZFT and ZHe ages are young in contrast to the ZHe ages of the Subandes. The Subandes ZHe ages consist of a dominantly detrital signal inherited from Paleozoic to early Mesozoic times and are presumably not associated with Andean orogenesis. The detrital to partially reset Subandes ZHe ages combined with the reset AFT components from the same samples bracket the magnitude of erosion in the Subandes. The Subandes structures have been eroded from AFT-

sensitive temperatures (~110ºC), but not from ZHe-sensitive temperatures (~180ºC). The mostly detrital Tertiary foreland basin sample from the western Subandes (km 136.5, Fig. 2.4C) suggests the local amount of erosion since deposition and burial has been limited to less than AFT-sensitive temperatures. The modeling constrained cooling from 41-11 Ma (Fig. 2.5) is therefore presumably associated with deformation and erosion of the hinterland structures in the Eastern Cordillera.

One additional observation is the extremely young AFT central and component ages (2.8-2.0 Ma) collected from low elevations within the high relief La Paz basin just south of our transect (Fig. 2.1B). The late Pliocene ages suggests that the basin has experienced rapid recent fluvial incision by the La Paz River in conjunction with its headward erosion into the Altiplano.

Along-strike variation in Andean plateau erosion

Along-strike exhumation of the Andean plateau suggests non-uniform deformation and erosion from as early as the late Eocene to as recent as the late Miocene. North of this study, K-Ar and $^{40}Ar/^{39}Ar$ AFT ages record late Eocene exhumation with continued Oligo-Miocene exhumation recorded by AFT ages in Peru [Kontak et al., 1990]. As summarized in this paper, AFT ages in northern Bolivia show Eocene to late Oligocene accelerated erosion in the Eastern Cordillera followed by widespread Miocene (~15 Ma) to recent accelerated erosion. In southern Bolivia, AFT ages in the AP are Oligocene (~30 Ma), mid-Miocene (17-9 Ma) in the Interandean zone, and late Mio-Pliocene in the Subandes [Ege et al., 2003]. Farther south in Argentina, AFT-recorded exhumation of the Puna plateau is Oligo-Miocene [Coughlin et al., 1998; Carrapa et al., 2005].

Conclusions

Low-temperature thermochronology across the central Andean fold-thrust belt in northern Bolivia reveal a two-phased erosion history. Accelerated erosion began in the Eastern Cordillera in the Eo-Oligocene (~40-25 Ma), followed by distributed, accelerated erosion since the early-mid Miocene (~15 Ma). The magnitude of erosion decreases eastward from ~10.6 km in the Eastern Cordillera, to ~4.6 km in the Interandean zone and to between ~3.9 and ~7.0 km in the Subandes. Models for the kinematic evolution of the central Andean plateau must be consistent with these spatial and temporal trends in erosion, their magnitudes, and associated and inferred deformation. Assessment of two end-member models for central Andean deformation show the following; the earlier Eo-Oligocene phase of erosion is consistent with one model that highlights earlier deformation controlled by the sequential stacking of basement thrusts. However, the distributed erosion since ~15 Ma is equally consistent with both end-member models of deformation that predict deformation and erosion in the Interandean zone and Subandes in the early to late Miocene. If the basement-involved deformation model is correct, the time between the two phases of accelerated cooling brackets the cessation of the first basement thrust and implies establishment of the AP analogous to its modern width, but unknown elevation by the early Miocene (~20 Ma).

Acknowledgements

We thank Sergiotecmin of La Paz, Bolivia and especially Sohrab Tawackoli for logistical support. We thank Ken Farley for access to his lab for the ZHe analyses. J. Barnes recognizes advice by Andy Carter in interpreting the AFT data. Mark Brandon helped with the BinomFit analyses as well as reviewed an earlier version of the manuscript. Reviews by J. Garver and S. Thomson improved this paper. Support was provided to T. A. Ehlers by NSF grant EAR 0409289.

Appendix 2.1. AFT and ZHe analytical procedures

AFT data

Apatite grains were separated using conventional heavy-liquid and magnetic separation techniques, etched and irradiated by Apatite to Zircon, Inc. using the external detector method and irradiation facilities at the Nuclear Radiation Center, Washington State University. For standardization, a mica sheet was attached to a ^{235}U-doped CN-1 glass and the reactor operated at 1 MW power output yielding a thermal-neutron fluence of approximately 10^{16} neutrons/cm^2. Apatite grain mounts were polished following immersion in epoxy resin cured at 90°C for 1 hour. Apatite mounts were immersed in 5.5N HNO_3 at 21°C (± 1°C) for 20.0 seconds (± 0.5 seconds), whereas the mica sheets were immersed in 48% HF for 15 minutes (± 15 seconds) at 20°C (± 1°C). Additional apatite mounts were irradiated by a ^{252}Cf source in a vacuum to enhance the measurability of natural fission tracks [Donelick and Miller, 1991]. Only natural, horizontal, and confined tracks were measured for both length (±0.2 μm) and the angle to the c-axis (±2°). The FT analyses were performed at 2000x magnification under un-polarized light. We conducted age calculations for samples JB01-04, JB01-06, JB01-09, and 725-13 (Table 2.1) from apatite standards of the Fish Canyon Tuff, U.S.A, and Cerro de Mercado, Durango, Mexico with a personal zeta calibration factor of 104.5 ± 2.6 (1σ) (for PBO). For all other samples, a zeta calibration factor of 113.8 ± 2.9 (1σ) (for RAD) was used from the same apatite standards. Table 2.2 details the AFT analytical results.

Age and track-length measured apatite grains were classified for annealing kinetics with the parameter Dpar. Dpar is defined as the fission-track etch pit diameter parallel to the c-axis of the apatite crystal at the polished and etched surface of the

analyzed grain [Burtner et al., 1994]. For each grain measured for age or track length, we recorded between 1 and 4 Dpar values and determined a mean Dpar.

ZHe data

Zircon separates from some of the samples were sieved to 100-150 μm minimum dimensions. Grains were hand-picked under a 120x binocular microscope, measured to determine the α-emission correction [Farley et al., 1996] for the crystallographic a and b axes, loaded into Pt capsules, and out gassed under a Nd-YAG laser at ~1350°C for 15 minutes. Evolved helium was spiked with ^{3}He, cryogenically concentrated and purified, and the $^{4}He/^{3}He$ ratio measured on a quadrupole mass spectrometer. Laser re-extracts of grains yielded no measureable ^{4}He. After outgassing, grains were retrieved, digested, spiked with ^{235}U and ^{230}Th, and the U and Th isotope ratios analyzed by ICP-MS. The propagated 1σ analytical uncertainty on these He ages is ~2% [Farley, 2000]. Table 2.3 details the ZHe data.

Appendix 2.2. AFT data interpretation methodology

In this Appendix, we summarize the relevant principals to sedimentary sample AFT grain-age distribution analysis, and detail our thermal modeling methodology.

Sedimentary AFT grain-age distribution analysis

AFT analytical results from sedimentary units often exhibit significant variance because individual apatites are more likely to have experienced different thermal histories before being incorporated into the sampled depositional unit. In other words, if the sedimentary unit has not been completely reset since deposition, the inherited, variable thermal histories of the individual apatite grains may contribute to a large range in measured AFT cooling ages and track lengths [e.g. Burtner et al., 1994].

Furthermore, individual apatite grains are likely to have different sources and hence different compositions. Composition influences the annealing behavior of apatite [e.g. Carlson et al., 1999]. Therefore, the post-depositional, shared cooling history experienced by all grains in a sample will result in different measured grain ages and track lengths among the grains.

The chi-square (χ^2) test evaluates the variance of a sample grain-age distribution [Galbraith, 1981; Green, 1981]. Unfortunately, statistical reliability of the χ^2 test breaks down with a low number of measured spontaneous and induced fission tracks (N_s, N_i < 5) [Brandon et al., 1998]. Therefore, if a particular sample has very few tracks measured, it could have an inflated chi-square value and pass the P(χ^2) test appearing to be concordant when, in fact, it is discordant.

The AFT grain-age distributions can be analyzed using a deconvolution algorithm that identifies the statistically significant populations and their component ages within each sample [Brandon, 1992]. If only one component age is identified, it is equivalent to the pooled age. We used BinomFit [Brandon, 1992, 2002; Ehlers et al., 2005] to identify the significant component ages in our samples. BinomFit calculates the individual grain ages and their uncertainties, and combines a binomial peak-fitting scheme with an iterative search to optimize the number of significant component ages in a sample [Brandon, 2002].

Thermal modeling of AFT data

The grain-age distribution and component ages, track length distribution, and grain composition proxy data all combine to provide valuable information that can be used to constrain a samples thermal history with inverse modeling. We modeled the fission-track data with AFTSolve [Ketcham et al., 2000] which incorporates track length,

grain age, and composition proxy data. Fundamentally, AFTSolve uses various search methods to quantify the range of statistically acceptable and better thermal histories for a single sample that (1) adheres to user-defined constraints, and (2) matches the measured data.

Overall, our modeling strategy started with an open-ended model with minimal constraints. We incrementally imposed restrictions directed by the successive modeling results and relevant geologic data, such as depositional age of the sampled formation and the sample pooled or component AFT age(s) [Ketcham et al., 2000]. We used a multi-kinetic annealing model which allows for modeling of multiple kinetic apatite populations with Dpar [Ketcham et al., 1999].

For the initial general model, we ran 15,000 simulations with a controlled random search (CRS) technique for each sample. All age and track length data were modeled as one kinetic population projected to the c-axis in order to effectively remove the problems of anisotropic track-length reduction [Donelick et al., 1999]. We imposed two main constraints [Ketcham and Donelick, 2001]: (1) a starting temperature of 200ºC at an age equal to 1.5 times the pooled or maximum component age of the sample, and (2) 20ºC at the present time. Both non-monotonic and monotonic heating/cooling was explored with a rate not allowed to exceed 20-40ºC/My [Ketcham and Donelick, 2001]. Any insights gained on the more recent portion of the sample cooling history were successively explored using a Monte Carlo search technique with additional constraints imposed on the recent portion of the sample cooling history as directed from the previous results. Only the monotonic cooling results are reported in this paper because in most cases the onset of recent cooling was not significantly different from the non-monotonic cases.

Refined modeling involved imposing additional constraints from the sample formation age and the component grain-age analysis results. 15 000 simulations were

first run with all age and length data as one kinetic population using a Monte Carlo search. The constraints on each sample thermal history included: (1) the starting temperature was set to 20ºC at the approximate deposition age of the sample, (2) a temperature of 20ºC at the present time, as well as (3) a 60-250ºC temperature constraint at the pooled or youngest component age (this is a conservative temperature range that AFT data might be sensitive to at a potentially high rate of cooling during thrust sheet emplacement and hanging wall erosion). This setup was explored for the range of 1σ uncertainties in the pooled age or 68% CI (confidence interval) values (very similar to 1σ) in the youngest component age calculated by BinomFit. If the sample had a second age component, then that age was subsequently set as an additional 60-250ºC temperature constraint and similarly explored.

Even though many samples have discordant grain-age distributions, very few samples exhibited even moderate correlations between Dpar and grain age or track length. However, in all samples with two component ages, the kinetic populations were delineated and modeled together to identify the acceptable cooling histories for the sample. Additionally, the lower Dpar population (< 2 μm) was modeled independently since it represents the most thermally sensitive group of grains [Brandon et al., 1998]. These component age modeling efforts followed the methodology above. See [Ketcham and Donelick, 2001] for additional discussion of the methodology for separating kinetic populations.

References

Allmendinger, R. W., T. E. Jordan, S. M. Kay, and B. L. Isacks (1997), The evolution of the Altiplano-Puna Plateau of the Central Andes, Annual Review of Earth and Planetary Sciences, v. 25, 139-174.

Allmendinger, R. W., and T. R. Zapata (2000), The footwall ramp of the Subandean decollement, northernmost Argentina, from extended correlation of seismic reflection data, Tectonophysics, v. 321, 37-55.

Barnes, J. B., and J. D. Pelletier (2006), Latitudinal variation of denudation in the evolution of the Bolivian Andes, American Journal of Science, v. 306, 1-31.

Beck, S. L., G. Zandt, S. C. Myers, T. C. Wallace, P. G. Silver, and L. Drake (1996), Crustal-thickness variations in the central Andes, Geology, v. 24, 407-410.

Benjamin, M. T. (1986), Fission track ages on some Bolivian plutonic rocks; implications for the Tertiary uplift and erosion history of the Altiplano-Cordillera Real, MS thesis, 58 pp, Dartmouth College, Hanover.

Benjamin, M. T., N. M. Johnson, and C. W. Naeser (1987), Recent rapid uplift in the Bolivian Andes; evidence from fission-track dating, Geology, v. 15, 680-683.

Brandon, M. T. (1992), Decomposition of fission-track grain-age distributions, American Journal of Science, v. 292, 535-564.

Brandon, M. T. (2002), Decomposition of mixed grain age distributions using BinomFit, On Track, v. 24, 13-18.

Brandon, M. T., M. K. Roden-Tice, and J. I. Garver (1998), Late Cenozoic exhumation of the Cascadia accretionary wedge in the Olympic Mountains, Northwest Washington State, Geological Society of America Bulletin, v. 110, 985-1009.

Burtner, R. L., A. Nigrini, and R. A. Donelick (1994), Thermochronology of Lower Cretaceous source rocks in the Idaho-Wyoming thrust belt, American Association of Petroleum Geologists Bulletin, v. 78, 1613-1636.

Carlson, W. D., R. A. Donelick, and R. A. Ketcham (1999), Variability of apatite fission-track annealing kinetics; I, Experimental results, American Mineralogist, v. 84, 1213-1223.

Carrapa, B., D. Adelmann, G. E. Hilley, E. Mortimer, E. R. Sobel, and M. R. Strecker (2005), Oligocene range uplift and development of plateau morphology in the southern central Andes, Tectonics, v. 24, doi:10.1029/2004TC001762.

Clark, M. K., M. A. House, L. H. Royden, K. X. Whipple, B. C. Burchfiel, X. Zhang, and W. Tang (2005), Late Cenozoic uplift of southeastern Tibet, Geology, v. 33, 525-528.

Coughlin, T. J., P. B. O'Sullivan, B. P. Kohn, and R. J. Holcombe (1998), Apatite fission-track thermochronology of the Sierras Pampeanas, central western Argentina;

implications for the mechanism of plateau uplift in the Andes, Geology, v. 26, 999-1002.

Crough, S. T. (1983), Apatite fission-track dating of erosion in the eastern Andes, Bolivia, Earth and Planetary Science Letters, v. 64, 396-397.

DeCelles, P. G., and B. K. Horton (2003), Early to middle Tertiary foreland basin development and the history of Andean crustal shortening in Bolivia, Geological Society of America Bulletin, v. 115, 58-77.

Dobson, M. H. (1973), Closure temperature in cooling geochronological and petrological systems, Contributions to Mineralogy and Petrology, v. 40, 259-274.

Donelick, R. A., R. A. Ketcham, and W. D. Carlson (1999), Variability of apatite fission-track annealing kinetics; II, Crystallographic orientation effects, American Mineralogist, v. 84, 1224-1234.

Donelick, R. A., and D. S. Miller (1991), Enhanced TINT fission track densities in low spontaneous track density apatites using ^{252}Cf-derived fission fragment tracks: A model and experimental observations, Nuclear Tracks and Radiation Measurements, v. 18, 301-307.

Donelick, R. A., P. B. O'Sullivan, and R. A. Ketcham (2005), Apatite Fission-Track Analysis, in Low-Temperature Thermochronology: Techniques, Interpretations, and Applications, P. W. Reiners and T. A. Ehlers (ed.), Mineralogical Society of America, Chantilly, VA, 49-94.

Ege, H., E. R. Sobel, V. Jacobshagen, E. Scheuber, and D. Mertmann (2003), Exhumation history of the central Andes of southern Bolivia by apatite fission track dating, Revista Tecnica de Yacimientos Petroliferos Fiscales Bolivianos, v. 21, 165-172.

Ehlers, T. A., T. Chaudhri, S. Kumar, C. W. Fuller, S. D. Willett, R. A. Ketcham, M. T. Brandon, D. X. Belton, B. P. Kohn, A. J. W. Gleadow, T. J. Dunai, and F. Q. Fu (2005), Computational tools for low-temperature thermochronometer interpretation, in Low-Temperature Thermochronology: Techniques, Interpretations, and Applications, P. W. Reiners and T. A. Ehlers (ed.), Mineralogical Society of America, Chantilly, VA, 589-622.

Ehlers, T. A., and K. A. Farley (2003), Apatite (U-Th)/He thermochronometry; methods and applications to problems in tectonic and surface processes, Earth and Planetary Science Letters, v. 206, 1-14.

Elger, K., O. Oncken, and J. Glodny (2005), Plateau-style accumulation of deformation: Southern Altiplano, Tectonics, v. 24, doi:10/1029/2004TC001675.

Farley, K., R. Wolf, and L. Silver (1996), The effects of long alpha-stopping distances on (U-Th)/He ages, Geochimica et Cosmochimica Acta, v. 60, 4223-4229.

Farley, K. A. (2000), Helium diffusion from apatite; general behavior as illustrated by Durango fluorapatite, Journal of Geophysical Research, v. 105, 2903-2914.

Farley, K. A. (2002), (U-Th)/He Dating: Techniques, Calibrations, and Applications, in Noble Gases in Geochemistry and Cosmochemistry, D. Portcelli, C. J. Ballentine and R. Wieler (ed.), Minerological Society of America, Washington, DC., 819-843.

Galbraith, R. F. (1981), On statistical models for fission track counts, Journal of the International Association for Mathematical Geology, v. 13, 471-478.

Galbraith, R. F., and G. M. Laslett (1993), Statistical models for mixed fission track ages, Nuclear Tracks and Radiation Measurements, v. 21, 459-470.

Gallagher, K., R. Brown, and C. Johnson (1998), Fission track analysis and its applications to geological problems, Annual Review of Earth and Planetary Sciences, v. 26, 519-572.

Garzione, C. N., P. Molnar, J. Libarkin, and B. MacFadden (2006), Rapid late Miocene rise of the Bolivian Altiplano: Evidence for removal of mantle lithosphere, Earth and Planetary Science Letters, v. 241, 543-556.

Gillis, R. J., B. K. Horton, and M. Grove (2006), Thermochronology, geochronology, and upper crustal structure of the Cordillera Real: Implications for Cenozoic exhumation of the central Andean plateau, Tectonics, v. 25, doi:10.1029/2005TC001887.

Green, P. F. (1981), A new look at statistics in fission-track dating, Nuclear Tracks and Radiation Measurements, v. 5, 77-86.

Gregory-Wodzicki, K. M. (2000), Uplift history of the Central and Northern Andes; a review, Geological Society of America Bulletin, v. 112, 1091-1105.

Guarachi, H. P., S. Tawackoli, W. A. Salinas, and H. M. Gonzales (2001), Mapa Geologico de Bolivia, Servicio Geologico de Bolivia/YPFB, La Paz, Bolivia, scale 1:1,000,000.

Gubbels, T. L., B. L. Isacks, and E. Farrar (1993), High-level surfaces, plateau uplift, and foreland development, Bolivian central Andes, Geology, v. 21, 695-698.

Henry, S. G., and H. N. Pollack (1988), Terrestrial heat flow above the Andean subduction zone in Bolivia and Peru, Journal of Geophysical Research, v. 93, 15153-15162.

Hodges, K. V. (2003), Geochronology and Thermochronology in Orogenic Systems, in Treatise on Geochemistry, R. L. Rudnick (ed.), Elsevier, 263-292.

Horton, B. K. (1999), Erosional control on the geometry and kinematics of thrust belt development in the central Andes, Tectonics, v. 18, 1292-1304.

Horton, B. K. (2005), Revised deformation history of the central Andes: Inferences from Cenozoic foredeep and intermontane basins of the Eastern Cordillera, Bolivia, Tectonics, v. 24, doi:10.1029/2003TC001619.

Instituto Geografico Militar (2000), Digital Atlas of Bolivia, La Paz, Bolivia, CDROM.

Isacks, B. L. (1988), Uplift of the Central Andean Plateau and bending of the Bolivian Orocline, Journal of Geophysical Research, v. 93, 3211-3231.

Jordan, T. E., J. H. Reynolds, III, and J. P. Erikson (1997), Variability in age of initial shortening and uplift in the Central Andes, in Tectonic uplift and climate change, W. F. Ruddiman (ed.), Plenum Press, New York, 41-61.

Kennan, L., S. H. Lamb, and L. Hoke (1997), High-altitude palaeosurfaces in the Bolivian Andes; evidence for late Cenozoic surface uplift, in Palaeosurfaces; recognition, reconstruction and palaeoenvironmental interpretation, M. Widdowson (ed.), Special Publication of the Geological Society 120, London, 307-323.

Ketcham, R. A., and R. A. Donelick (2001), AFTSolve version 1.3.0, Donelick Analytical, Inc and Richard A. Ketcham.

Ketcham, R. A., R. A. Donelick, and W. D. Carlson (1999), Variability of apatite fission-track annealing kinetics; III, Extrapolation to geological time scales, American Mineralogist, v. 84, 1235-1255.

Ketcham, R. A., R. A. Donelick, and M. B. Donelick (2000), AFTSolve; a program for multi-kinetic modeling of apatite fission-track data, Geological Materials Research, v. 2, 1-32.

Kley, J. (1996), Transition from basement-involved to thin-skinned thrusting in the Cordillera Oriental of southern Bolivia, Tectonics, v. 15, 763-775.

Kley, J. (1999), Geologic and geometric constraints on a kinematic model of the Bolivian Orocline, Journal of South American Earth Sciences, v. 12, 221-235.

Kontak, D. J., E. A. Farrar, A. H. Clark, and D. A. Archibald (1990), Eocene tectono-thermal rejuvenation of an upper Paleozoic-lower Mesozoic terrane in the Cordillera de Carabaya, Puno, southeastern Peru, revealed by K-Ar and $^{40}Ar/^{39}Ar$ dating, Journal of South American Earth Sciences, v. 3, 231-246.

Lamb, S., and P. Davis (2003), Cenozoic climate change as a possible cause for the rise of the Andes, Nature, v. 425, 792-797.

Lamb, S., and L. Hoke (1997), Origin of the high plateau in the Central Andes, Bolivia, South America, Tectonics, v. 16, 623-649.

Masek, J. G., B. L. Isacks, T. L. Gubbels, and E. J. Fielding (1994), Erosion and tectonics at the margins of continental plateaus, Journal of Geophysical Research, v. 99, 13941-13956.

McQuarrie, N. (2002), The kinematic history of the central Andean fold-thrust belt, Bolivia; implications for building a high plateau, Geological Society of America Bulletin, v. 114, 950-963.

McQuarrie, N., and P. G. DeCelles (2001), Geometry and structural evolution of the central Andean backthrust belt, Bolivia, Tectonics, v. 20, 669-692.

McQuarrie, N., B. K. Horton, G. Zandt, S. Beck, and P. G. DeCelles (2005), Lithospheric evolution of the Andean fold-thrust belt, Bolivia, and the origin of the central Andean plateau, Tectonophysics, v. 399, 15-37.

Montgomery, D. R., G. Balco, and S. D. Willett (2001), Climate, tectonics, and the morphology of the Andes, Geology, v. 29, 579-582.

Müller, J. P., J. Kley, and V. Jacobshagen (2002), Structure and Cenozoic kinematics of the Eastern Cordillera, southern Bolivia (21ºS), Tectonics, v. 21, doi: 10.1029/2001TC001340.

Murphy, M. A., A. Yin, T. M. Harrison, S. B. Duerr, Z. Chen, F. J. Ryerson, W. S. F. Kidd, X. Wang, and X. Zhou (1997), Did the Indo-Asian collision alone create the Tibetan Plateau?, Geology, v. 25, 719-722.

Reiners, P. W. (2005), Zircon (U-Th)/He Thermochronometry, in Low-temperature thermochronology : Techniques, Interpretations, and Applications, P. W. Reiners and T. A. Ehlers (ed.), Mineralogical Society of America, Chantilly, VA, 151-179.

Reiners, P. W., and M. T. Brandon (2006), Using Thermochronology to Understand Orogenic Erosion, Annual Reviews of Earth and Planetary Sciences, v. 34, 419-466.

Reiners, P. W., T. L. Spell, S. Nicolescu, and K. A. Zanetti (2004), Zircon (U-Th)/He thermochronometry: He diffusion and comparisons with 40Ar/39Ar dating, Geochimica et Cosmochimica Acta, v. 68, 1857-1887.

Richter, F. M., D. B. Rowley, and D. J. DePaolo (1992), Sr isotope evolution of seawater: The role of tectonics, Earth and Planetary Science Letters, v. 109, 11-23.

Ring, U., M. T. Brandon, S. D. Willett, and G. S. Lister (1999), Exhumation processes, in Exhumation processes; Normal Faulting, Ductile Flow and Erosion, U. Ring, M. T. Brandon, G. S. Lister and S. D. Willett (ed.), Geological Society of London Special Publications, London, 1-27.

Roeder, D. (1988), Andean-age structure of Eastern Cordillera (Province of La Paz, Bolivia), Tectonics, v. 7, 23-39.

Roeder, D., and R. L. Chamberlain (1995), Structural geology of sub-Andean fold and thrust belt in northwestern Bolivia, in Petroleum basins of South America, A. J. Tankard, R. Suarez and H. J. Welsink (ed.), American Association of Petroleum Geologists Memoir 62, 459-479.

Royden, L. (1996), Coupling and decoupling of crust and mantle in convergent orogens; implications for strain partitioning in the crust, Journal of Geophysical Research, v. 101, 17679-17705.

Ruddiman, W. F., M. E. Raymo, W. L. Prell, and J. E. Kutzbach (1997), The uplift-climate connection; a synthesis, in Tectonic uplift and climate change, W. F. Ruddiman (ed.), Plenum Press, New York, 471-515.

Safran, E. B. (1998), Channel network incision and patterns of mountain geomorphology, PhD thesis, 326 pp, University of California, Santa Barbara, CA.

Sempere, T., G. Herail, J. Oller, and M. G. Bonhomme (1990), Late Oligocene-early Miocene major tectonic crisis and related basins in Bolivia, Geology, v. 18, 946-949.

Sergiomin (1997), Mapas Tematicos de Recursos Minerales de Bolivia, Hojas La Paz y Copacabana, Geobol, La Paz, Bolivia, scale 1:250,000.

Sobel, E. R., G. E. Hilley, and M. R. Strecker (2003), Formation of internally drained contractional basins by aridity-limited bedrock incision, Journal of Geophysical Research, v. 108, doi:10.1029/2002JB001883.

Sobel, E. R., and M. R. Strecker (2003), Uplift, exhumation and precipitation: tectonic and climatic control of Late Cenozoic landscape evolution in the northern Sierras Pampeanas, Argentina, Basin Research, v. 15, 431-451.

Springer, M., and A. Forster (1998), Heat-flow density across the Central Andean subduction zone, Tectonophysics, v. 291, 123-139.

Tagami, T. (2005), Zircon Fission-Track Thermochronology and Application to Fault Studies, in Low-Temperature Thermochronology: Techniques, Interpretations, and Applications, P. W. Reiners and T. A. Ehlers (ed.), Mineralogical Society of America, Chantilly, VA, 95-122.

Tagami, T., and P. B. O'Sullivan (2005), Fundamentals of Fission-Track Thermochronology, in Low-Temperature Thermochronology: Techniques, Interpretations, and Applications, P. W. Reiners and T. A. Ehlers (ed.), Mineralogical Society of America, 19-47.

Tapponnier, P., X. Zhiqin, F. Roger, B. Meyer, N. Arnaud, G. Wittlinger, and Y. Jingsui (2001), Oblique stepwise rise and growth of the Tibetan Plateau, Science, v. 294, 1671-1677.

Wdowinski, S., and Y. Bock (1994), The evolution of deformation and topography of high elevated plateaus 2. Application to the Central Andes, Journal of Geophysical Research, v. 99, 7121-7130.

Willett, S. D. (1999), Orogeny and orography; the effects of erosion on the structure of mountain belts, Journal of Geophysical Research, v. 104, 28957-28982.

Willett, S. D., and M. T. Brandon (2002), On steady states in mountain belts, Geology, v. 30, 175-178.

Chapter 3

Thermochronometer record of central Andean Plateau growth, Bolivia (19.5°S)[1]

Abstract

Quantifying the timing, magnitude, and rates of exhumation and deformation across the central Andes is a prerequisite for understanding the history of plateau rise. We present 23 new apatite and zircon fission-track thermochronometer samples to chronicle the exhumation and deformation across the entire (~500 km) Andean fold-thrust belt at ~19.5ºS in Bolivia. Exhumation and deformation are constrained with inverse thermal modeling of the thermochronometer data, regional stratigraphy, geothermal gradients, and mass deficits inferred from a balanced section. Results suggest: (1) initial exhumation of the Eastern Cordillera (EC) fore-thrust and back-thrust belts began in the late Eocene to early Oligocene (27-36 Ma) and continued in a distributed manner in the late Oligocene to early Miocene (19-25 Ma). Interandean zone (IA) exhumation began 19-22 Ma, followed by a third pulse of exhumation (11-16 Ma) in the EC back-thrust belt and initial cooling in the westernmost Subandes (SA) 8-20 Ma. Finally, exhumation propagated eastward across the SA during the late Mio-Pliocene (2-8 Ma). (2) Exhumation magnitudes are spatially variable and range from maximums of

---

[1]**Official citation:**

Barnes, J. B., T. A. Ehlers, N. McQuarrie, P. B. O'Sullivan, and S. Tawackoli (2008), Thermochronometer record of central Andean Plateau growth, Bolivia (19.5ºS), Tectonics, doi:10.1029/2007TC002174**,** in press.

<8 km in the EC fore-thrust belt to average values of ~4-7 km across the EC, ~2.5-3 km in the Altiplano, ~4-6 km in the IA, and ~3 km in the SA. (3) Exhumation rates range from ~0.1-0.2 mm/yr in the EC, from ~0.1-0.6 mm/yr in the IA, and from ~0.1-0.4 mm/yr to locally 1.4 mm/yr or more in the eastern SA. We synthesize similar constraints with sediments throughout Bolivia and characterize plateau development by (A) distributed deformation throughout the Altiplano and EC regions from ~20-40 Ma with minor deformation continuing until ~10 Ma, (B) contemporaneous cessation of most EC deformation and exhumation of the IA ~20 Ma implying establishment of the modern plateau width with significant, but unknown crustal thickness and elevation shortly thereafter by ~15-20 Ma, and (C) dominantly eastward propagation of deformation from the IA since ~20 Ma with minor out-of-sequence deformation in the central-to-eastern SA.

Introduction

Orogenic plateaus are important because of their influence on mantle dynamics, orographic precipitation, physical weathering rates, and their ability to trap large sediment volumes in their protected interiors [e.g. Isacks, 1988; Molnar et al., 1993; Masek et al., 1994; Ruddiman et al., 1997; Beaumont et al., 2001; Sobel et al., 2003]. Although models can simulate plateau growth by temperature-dependent viscosity variations in a shortening and thickening crust, they are limited by incomplete knowledge of the kinematic histories of plateau formation [Wdowinski and Bock, 1994; Royden, 1996; Willett and Pope, 2004]. Constraining the kinematics, timing, and rates of plateau erosion and deformation is necessary to understand both the processes involved in plateau formation as well as the conditions under which they develop [e.g. Oncken et al., 2006]. It is also important to quantify the along-strike variations in the kinematic and erosion history of the central Andean plateau to evaluate the mechanisms that determine

plateau width. In this study, we present new data and interpretations that chronicle the exhumation and deformation across the eastern flank of the central Andean plateau at its widest extent.

The central Andean plateau occupies the core of the Andes, rests ~3 km in average elevation, encompasses over 350,000 km², and straddles humid to semi-arid latitudes from southern Peru to northern Argentina (Fig. 3.1) [e.g. Isacks, 1988]. Numerous processes have been proposed to influence Andean plateau evolution such as; crustal shortening/thickening [e.g. Lamb and Hoke, 1997; Kley and Monaldi, 1998; Elger et al., 2005], plate kinematics [e.g. Pardo-Casas and Molnar, 1987; Oncken et al., 2006], topography and subduction geometry [Gephart, 1994; Iaffaldano et al., 2006], inherited structure and stratigraphy [Allmendinger and Gubbels, 1996; Kley et al., 1999], thermal weakening [Isacks, 1988; Wdowinski and Bock, 1994; Allmendinger et al., 1997; Lamb and Hoke, 1997], and variable erosion resulting from latitudinal precipitation gradients [Masek et al., 1994; Horton, 1999; Montgomery et al., 2001; Lamb and Davis, 2003; Sobel et al., 2003; Gillis et al., 2006].

Observations of the lithospheric structure, sedimentary record, and various proxies have been used to deduce the chronology and mode of Andean plateau uplift. Deformation was initially assumed to begin in the late Oligocene (~27 Ma) [Isacks, 1988; Sempere et al., 1990] and characterized by distributed shortening (pure shear) until ~10 Ma when it shifted to simple shear focused in the easternmost thin-skinned thrust belt of the Subandes where it continues today [Gubbels et al., 1993; Allmendinger and Gubbels, 1996]. However, earlier Eo-Oligocene (~30-40 Ma) deformation has now been well-documented with mapping and seismic profiles [e.g. Elger et al., 2005], Cenozoic basin sediments [e.g. DeCelles and Horton, 2003; Horton, 2005] and thermochronometer-derived exhumation [e.g. Benjamin et al., 1987; Gillis et al., 2006; Ege et al., 2007]. These studies have argued that the Eocene to recent deformation has

accumulated both broadly within the plateau region and propagated eastward towards the foreland. Perhaps most interestingly, mounting evidence inferred from erosion surface remnants [Kennan et al., 1997; Barke and Lamb, 2006], valley incision [Schildgen et al., 2007], and soil carbonate isotopes [Garzione et al., 2006; Ghosh et al., 2006] has lead to the postulation that 2-3+ km of rapid plateau surface uplift occurred ~6-10 Ma by lithospheric mantle delamination or lower crustal flow.

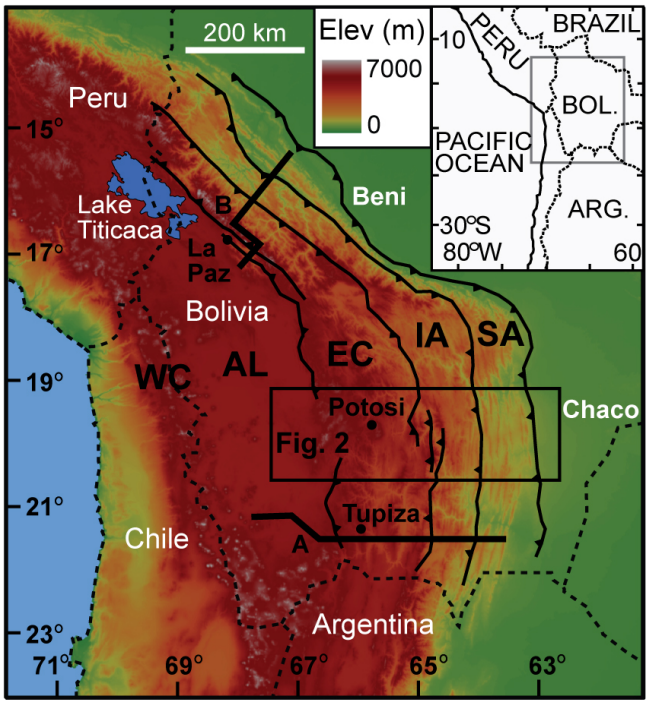

Figure 3.1. The central Andean fold-thrust belt and plateau in Bolivia. Topography is from the SRTM 90 m data set. Elev = elevation. Zone-bounding faults modified from McQuarrie [2002]. Major zones: WC = Western Cordillera, AL = Altiplano, EC = Eastern Cordillera, IA = Interandean zone, SA = Subandes. Inset shows location in western-central South America and box outlines the study area in Figure 3.2. Solid lines are locations of two major additional thermochronometer data transects in the south (A; Scheuber et al. [2006]; Ege et al. [2007]) and north (B; e.g. Barnes et al. [2006]) discussed in the text.

In the Bolivian Andes (~15-20°S), plateau development is coupled to the central Andean fold-thrust belt where the kinematic history has been documented by sequential

kinematic restorations of balanced cross sections [McQuarrie, 2002]. This kinematic linkage provides an opportunity to correlate the kinematics and timing of plateau deformation with its eastern flanking thrust belt. Unfortunately, imprecise age and exhumation constraints still exist on many of the structures in the thrust belt making it difficult to (a) detail a deformation chronology in order to test the sequential reconstructions, (b) estimate the variations in the associated erosional response to the deformation, and (c) use these constraints to improve our understanding of plateau growth. To address these shortcomings, we present a transect of new thermochronometer data at ~19.5ºS in southern Bolivia where both a kinematic reconstruction and a preliminary chronology of the deformation has already been proposed [McQuarrie et al., 2005]. This paper is a companion to McQuarrie et al. [2008] which integrates similar datasets across the central Andean fold-thrust belt ~500 km to the north at 15-17ºS (transect B in Figure 1).

At ~19.5°S, the central Andean fold-thrust belt and plateau are broad, the climate is semi-arid, and the topographic relief is subdued relative to northern Bolivia (Fig. 3.1) [Isacks, 1988; Masek et al., 1994; Horton, 1999]. In this paper, we (1) present apatite and zircon fission-track (AFT & ZFT) thermochronology results from 23 samples to quantify the long-term deformation and exhumation history across the entire thrust belt at ~19.5ºS (Figs. 3.1 & 3.2), (2) quantify sample cooling histories with inverse thermal modeling of the AFT data, (3) incorporate the results within the regional stratigraphy and structure, (4) refine the timing of deformation inferred from the cooling histories, and (5) estimate the spatial variability of exhumation magnitudes with multiple methods. Finally, we compare our results to those in southern Bolivia-northernmost Argentina (19-23ºS) and then throughout Bolivia (15-21.5ºS). The combination of new and previous thermochronometer, sedimentary, and geomorphic records allows an analysis of spatial

and temporal variations in deformation in southern Bolivia, and finally a more complete and generalized history of central Andean plateau growth throughout Bolivia.

Geologic setting

Central Andean fold-thrust belt and plateau

The Andes reach their greatest west-east width of 500 km in southern Bolivia (Fig. 3.1). The central Andean fold-thrust belt is commonly divided into the Western Cordillera, the Altiplano, the Eastern Cordillera (EC), the Interandean zone (IA), and the Subandes (SA). The Western Cordillera is the modern volcanic arc that marks the Pacific-Altiplano drainage divide. The Altiplano is a low-relief, internally-drained basin filled with Tertiary sediments and volcanics. The EC is the highest relief region consisting of deformed, predominantly Paleozoic sedimentary rocks with overlying Tertiary volcanism that mark the eastern drainage divide of the Altiplano. The IA and SA zones step progressively downwards in topographic elevation and upwards in structural depth eastward exposing mostly Devonian and Carboniferous through Mesozoic and Tertiary rocks, respectively (Fig. 3.2) [McQuarrie, 2002]. Large basement structures are thought to be a principal cause for these various structural levels of exposure that differentiate the Altiplano through SA (Fig. 3.2B) [Kley, 1996; Kley, 1999; McQuarrie, 2002; Müller et al., 2002]. The Andean plateau is the high elevation landmass commonly defined by >3 km average elevation that includes the entire Altiplano and a significant portion of the EC (Fig. 3.2C) [after Isacks, 1988].

The central Andean fold-thrust belt encompasses the eastern Altiplano to SA and is an east-vergent, thick to thin-skinned retroarc fold belt that is the result of strain accumulation from the South American plate overriding the Nazca plate (Fig. 3.1) [e.g. Isacks, 1988; Allmendinger et al., 1997; Jordan et al., 1997]. The EC is somewhat unique because it has accommodated the strain with both a west-vergent back-thrust

belt and an east-vergent fore-thrust belt [e.g. Roeder, 1988; McQuarrie and DeCelles, 2001]. In the central Andes (~14-24ºS), structural and stratigraphic data have constrained the deformation in the EC from late Eo-Oligocene (~25-40 Ma) to early-late Miocene (~8-20 Ma) at which point it migrated eastward into the SA [e.g. Sempere et al., 1990; Kley, 1996; Kennan et al., 1997; Kley et al., 1997; Lamb and Hoke, 1997; Elger et al., 2005; Horton, 2005]. To date, two major transects of thermochronometer data exist across the thrust belt in Bolivia; in the far north near Peru at 15-17°S and in the far south near Argentina at ~21.5ºS (Fig. 3.1; lines A & B). In the north, initial late Eo-Oligocene (~25-40 Ma) rapid exhumation began in the EC followed by wide-spread middle to late Miocene to present (~0-15 Ma) exhumation across the entire thrust belt from the eastern Altiplano to SA [Benjamin et al., 1987; Barnes et al., 2006; Gillis et al., 2006; McQuarrie et al., 2008]. In the south, initial late Eocene (36-40 Ma) exhumation began in the central EC, more distributed early Oligocene (27-33 Ma) exhumation throughout the EC and Altiplano continued until ~20 Ma, IA exhumation occurred during the early-to-late Miocene (~9-18 Ma), and finally exhumation in the SA began in the late Miocene (~8 Ma) [Ege et al., 2003; Scheuber et al., 2006; Ege et al., 2007].

Thrust belt stratigraphy

The Paleozoic to Tertiary stratigraphy of the thrust belt including local thickness variations has been well documented throughout southern Bolivia and is synthesized in Figure 3.3. The Paleozoic section is locally thick in the EC and tapers towards the foreland [Sempere, 1995; Welsink et al., 1995]. A continuous succession of Ordovician through Devonian marine siliciclastic rocks is overlain by a discontinuous succession of nonmarine Carboniferous to Cretaceous rocks [Sempere, 1995; McQuarrie, 2002]. Compared to central and northern Bolivia, much greater pre-Jurassic erosion and much less Andean-age erosion in this region has resulted in large exposures of Mesozoic

rocks in the EC that rest directly and unconformably on the Silurian units (Fig. 3.2) [McQuarrie and DeCelles, 2001]. Tertiary synorogenic sedimentary rocks reach local thicknesses of ~12 km in the Altiplano, ~2.5-5+ km in the EC, and ~3-4 km in the SA [Sempere et al., 1990; Dunn et al., 1995; Kennan et al., 1995; Lamb and Hoke, 1997; McQuarrie and DeCelles, 2001; Horton, 2005; Uba et al., 2006].

Thrust belt structure and shortening

McQuarrie [2002] used field and geophysical observations to construct a balanced section across the fold-thrust belt at ~19.5ºS (Fig. 3.2). Dominant structures exposed at the surface are ~1-10 km thick thrust sheets deforming the cover rocks. Individual thrust sheets in both the EC and IA are tightly folded and have minor offsets (~1-5 km). The SA has multiple levels of detachments allowing for thrust sheets with larger (~5-15 km) offsets that are less folded and hence more widely spaced. The balanced section indicates a total shortening of 326 km or 37% [McQuarrie, 2002]. More specifically, the EC has the highest magnitude of shortening of 122 km or 37%, followed by the IA with 96 km or 63%, and the SA with 67 km or 33%.

Although the geometry of the subsurface basement deformation is contentious, there is general agreement that large basement thrusts underlie the entire thrust belt except the SA which feed deformation into the overlying cover rocks [Kley, 1999; McQuarrie, 2002; Müller et al., 2002]. These large basement features, combined with small (1-5 km) offsets along individual surface faults, may provide a structural mechanism for potentially broad and uniform uplift and exhumation in the Altiplano, EC, and IA. In contrast, the SA have more widely-spaced thrust sheets with larger individual offsets that are confined to the cover rocks thereby precluding such a structural mechanism for broad uplift.

Figure 3.2. Geology, balanced cross section, topography, and thermochronology data across the central Andean fold-thrust belt at ~19.5ºS. The geology and cross section is simplified from [McQuarrie, 2002] and location is in Figure 3.1. BTB = back-thrust belt, FTB = fore-thrust belt. (A) Regional geology and sample locations. (B) Balanced cross section (location in A) with samples projected onto the appropriate structures. (C) Transect profile of 80-km-wide swath-averaged mean topography with apatite (black dots) fission track pooled ages. Note the log scale for the ages. Error bars are 2σ. Zircon fission track ages (stars) are off the scale (shown by arrows) with actual values adjacent to the symbol.

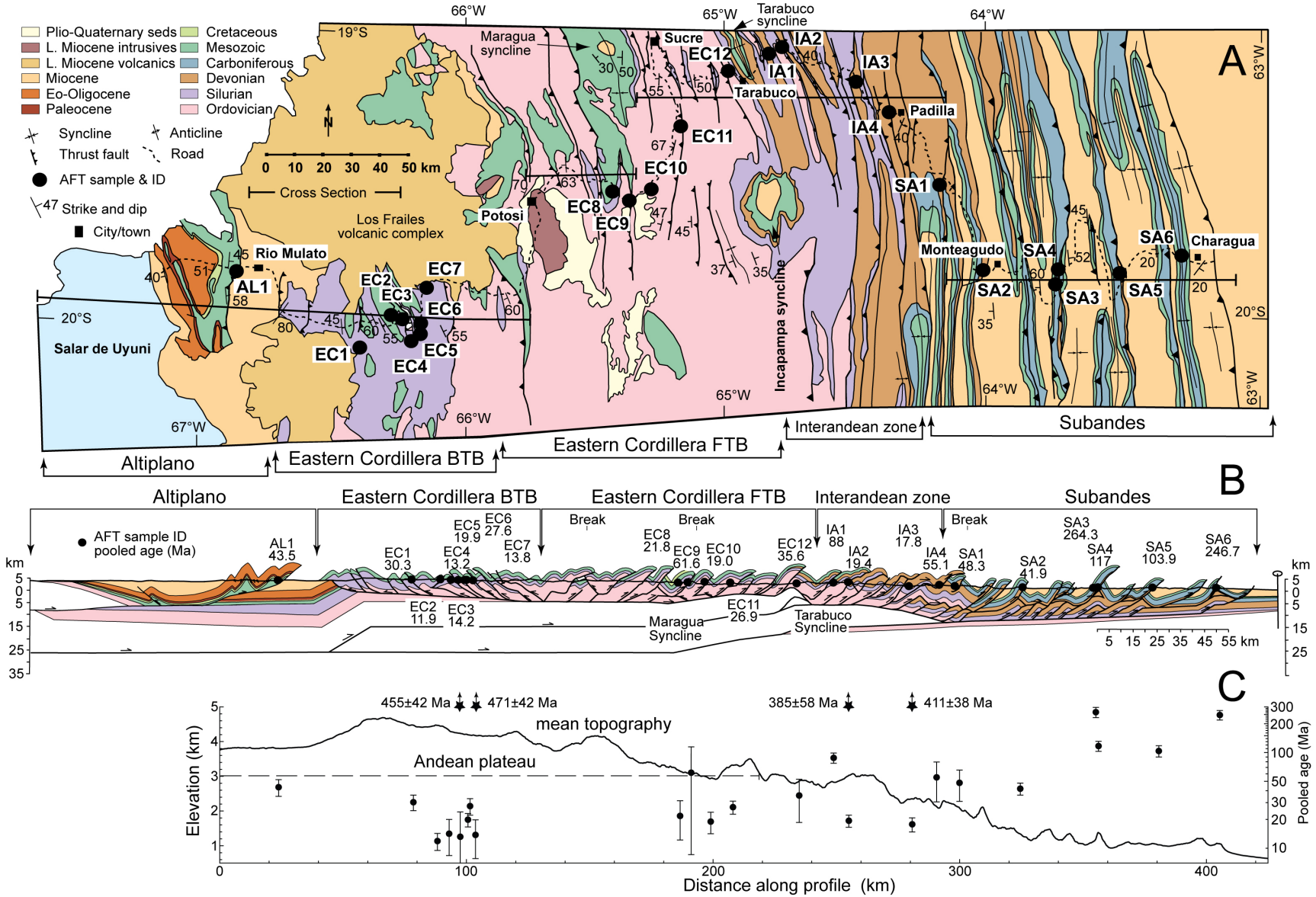
A
Plio-Quaternary seds
L. Miocene intrusives
L. Miocene volcanics
Miocene
Eo-Oligocene
Paleocene
Cretaceous
Mesozoic
Carboniferous
Devonian
Silurian
Ordovician
Syncline
Anticline
Thrust fault
Road
AFT sample & ID
Strike and dip
City/town
0 10 20 30 40 50 km
Cross Section
Maragua syncline
Tarabuco syncline
Incapampa syncline
Los Frailes volcanic complex
Salar de Uyuni
Sucre
Tarabuco
Padilla
Potosi
Rio Mulato
Monteagudo
Charagua
EC1
EC2
EC3
EC4
EC5
EC6
EC7
EC8
EC9
EC10
EC11
EC12
IA1
IA2
IA3
IA4
SA1
SA2
SA3
SA4
SA5
SA6
AL1
19°S
20°S
63°W
64°W
65°W
66°W
67°W
Altiplano
Eastern Cordillera BTB
Eastern Cordillera FTB
Interandean zone
Subandes
B
AFT sample ID
pooled age (Ma)
AL1 43.5
EC1 30.3
EC2 11.9
EC3 14.2
EC4 13.2
EC5 19.9
EC6 27.6
EC7 13.8
EC8 21.8
EC9 61.6
EC10 19.0
EC11 26.9
EC12 35.6
IA1 88
IA2 19.4
IA3 17.8
IA4 55.1
SA1 48.3
SA2 41.9
SA3 264.3
SA4 117
SA5 103.9
SA6 246.7
Break
Maragua Syncline
Tarabuco Syncline
km
C
455±42 Ma
471±42 Ma
385±58 Ma
411±38 Ma
mean topography
Andean plateau
Elevation (km)
Pooled age (Ma)
Distance along profile (km)

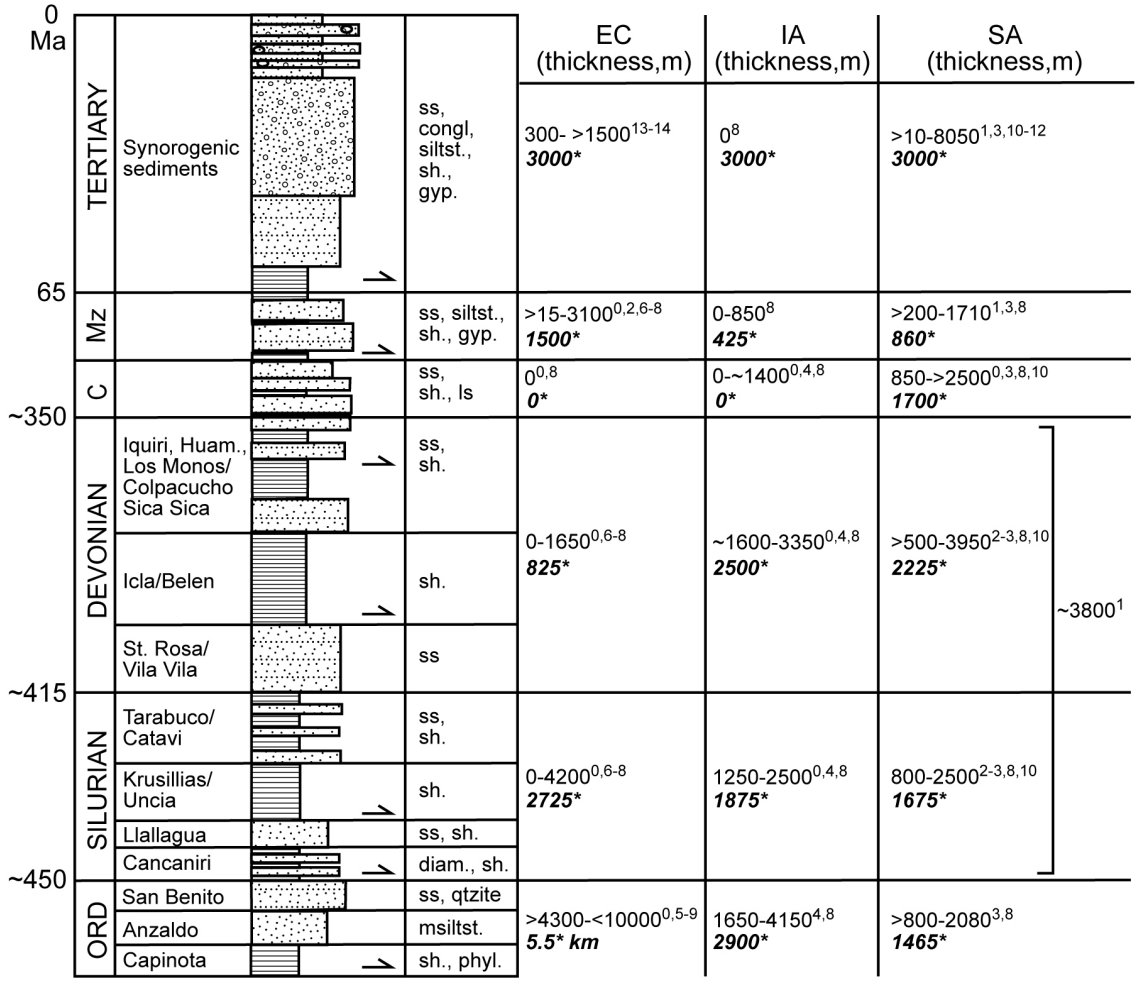

Figure 3.3. Regional stratigraphy and thickness variations of the central Andean fold-thrust belt in southern Bolivia (modified from Figure 2 of McQuarrie [2002]). Slashes delimit formation name changes from east to west and arrows indicate major detachment horizons. Mz = Mesozoic, C = Carboniferous, Ord = Ordovician, Huam. = Huamampampa, ss = sandstone, congl = conglomerate, siltst = siltstone, sh = shale, gyp = gypsum, ls = limestone, diam = diamictite, qtzite = quartzite, msiltst = metasiltstone, phyl = phyllite. Thickness constraints span from ~18-23ºS; 0 = [Kley and Reinhardt, 1994], 1 = [Dunn et al., 1995], 2 = [Sempere, 1995], 3 = [Moretti et al., 1996], 4 = [Kley, 1996], 5 = [Kley et al., 1997], 6 = [McQuarrie and DeCelles, 2001], 7 = [McQuarrie and Davis, 2002], 8 = balanced/restored section from [McQuarrie, 2002], 9 = [Müller et al., 2002], 10 = [Echavarria et al., 2003], 11 = [Uba et al., 2006], 12 = [Coudert et al., 1995], 13 = [Horton, 2005], 14 = [Sempere et al., 1997]. Asterisk indicates the average thickness used in Figure 3.4 (see Appendix 3.1 for details).

Methods

In this study, we integrate new apatite fission-track samples from across the eastern Andean plateau flank at ~19.5ºS with the regional stratigraphy and a balanced cross section. Methods used in the regional stratigraphic compilations and fission-track analyses are outlined below and detailed in the Appendices.

Regional stratigraphy

We compiled regional stratigraphic sections across southern Bolivia (~18-23ºS) to independently estimate the magnitude of exhumation by restoring the thermochronometer samples to original stratigraphic depth (Fig. 3.3) (see details in Appendix 3.1). Specifically, we constructed representative, regional sections measured from the range of thicknesses used in the balanced and restored section of McQuarrie [2002] because (1) it is the most proximal estimate that spans the entire study area, (2) its regional scale is most appropriate, and (3) the thickness variations themselves are derived from local field observations and supported by some of the compiled sections themselves [Dunn et al., 1995; Sempere, 1995; Gagnier et al., 1996; Kley, 1996; Kley et al., 1997; Sempere et al., 1997; Horton et al., 2001; McQuarrie and DeCelles, 2001]. Our calculated average thicknesses are almost always within the compiled bounds (Fig. 3.3). Figure 3.4 schematically shows these representative sections along with approximate sample locations.

Stratigraphic thickness variations in the central Andean fold-thrust belt are large, but systematic (Fig. 3.3). For example, the Ordovician thickens significantly southward along strike [McQuarrie and DeCelles, 2001; McQuarrie and Davis, 2002; Müller et al., 2002] and the Paleozoic section generally thins eastward from a local maximum in the central EC [Roeder and Chamberlain, 1995; Sempere, 1995; Welsink et al., 1995]. Despite these variations, it is useful to generalize the regional stratigraphy so that

samples collected on numerous structures in a region can be interpreted together by evaluating them in the context of stratigraphic depth as a proxy for original depth prior to exhumation.

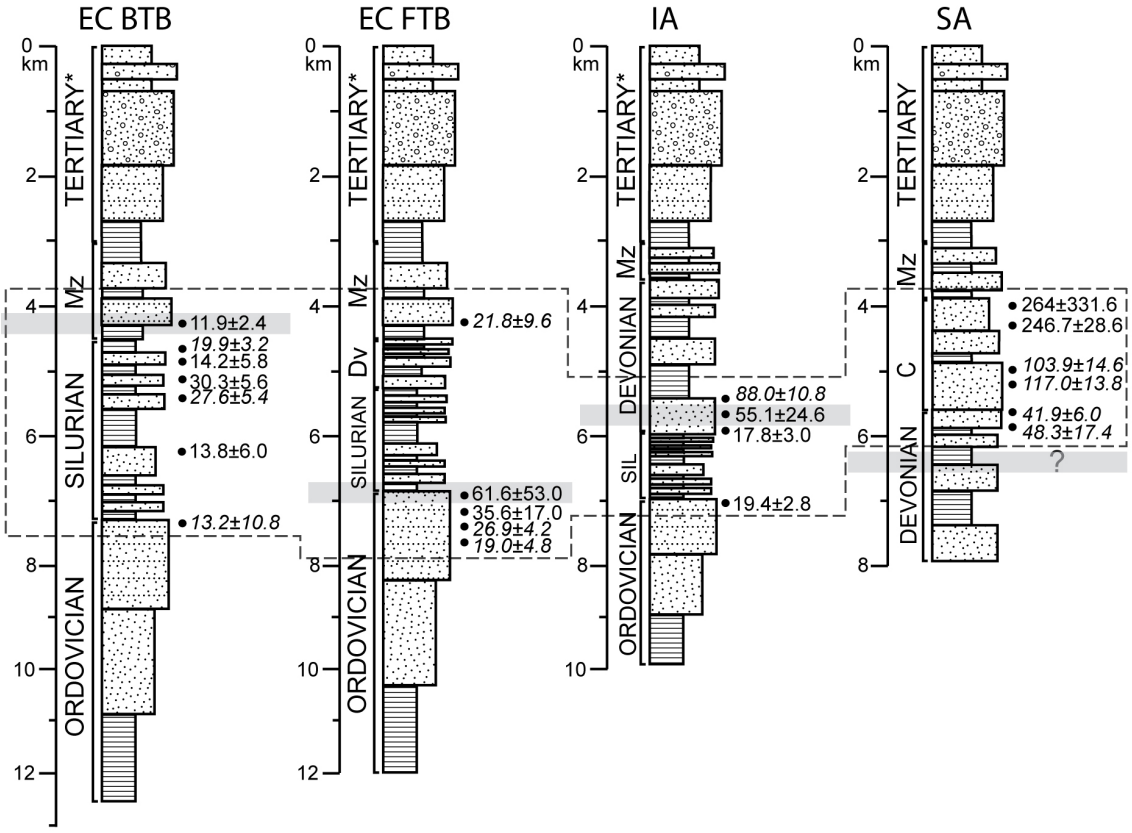

Figure 3.4. Apatite fission-track (AFT) ages integrated within representative stratigraphy across the central Andean fold-thrust belt at ~19.5ºS. Error associated with stratigraphic thickness and sample location is estimated to be ~0.5 km. Asterisk indicates that the Tertiary is assumed to have been there after [DeCelles and Horton, 2003]. Dv = Devonian, Sil = Silurian, additional abbreviations after Figures 3.1-3.3. Discordant samples in italics. Gray regions are estimated depth to full resetting of AFT samples as defined by the shallowest concordant AFT pooled age. Question-marked gray region is the inferred depth to fully reset and concordant AFT samples in the Subandes (see text for discussion). Dashed lines bracket the range of stratigraphic depths sampled in each zone. Lithologic thicknesses are schematic only after Figure 3.3.

Fission-track thermochronology

General background

Fission-track thermochronology uses the accumulation of damage trails (fission tracks) that form from the spontaneous fission of ^{238}U in minerals to constrain sample thermal histories [e.g. Gallagher et al., 1998; Tagami and O'Sullivan, 2005]. Fission-track ages are determined by measuring the parent (^{238}U)/daughter (tracks) ratios and determining the age from the rate of ^{238}U fission decay. Measured ages are cooling ages because the tracks are only quantitatively preserved above a particular closure temperature [Dobson, 1973], which is a function of mineral type, composition, and cooling rate. Fission tracks subsequently shorten (anneal) over a range of temperatures below the closure temperature. This temperature range is called the partial annealing zone (PAZ) [e.g. Hodges, 2003]. For common apatite, the closure temperature is ~110±10ºC and the PAZ spans from ~60-110ºC [e.g. Gallagher et al., 1998]. For common zircon, the closure temperature is ~240±10ºC and the PAZ spans from ~180-240ºC [Brandon et al., 1998].

Cooling ages are commonly determined on ~20-40 individual grains resulting in a sample grain-age distribution. The sample pooled age is determined by the daughter/parent ratio of all the grains summed ("pooled") together [e.g. Brandon, 1992]. A conventional χ^2 test is applied to the sample grain-age distribution to determine its degree of variance. Concordant ($P(\chi^2)>5\%$) samples have low age variance and their pooled age is considered geologically relevant [Galbraith, 1981; Green, 1981; Brandon et al., 1998]. Conversely, discordant ($P(\chi^2)<5\%$) samples, common for sedimentary rocks, have significant age variance suggesting that (a) other mechanisms such as inhomogeneous uranium concentration and variable grain-etching sensitivity are at work, and/or (b) multiple component ages and variable thermal annealing from compositionally

diverse grains exist that render the pooled age less meaningful [Green, 1981; Tagami and O'Sullivan, 2005]. Regardless of the age variance, measured ages and track length distributions are inverted for using empirically-derived annealing algorithms [Ketcham, 2005 and references therein] to constrain permissible thermal histories.

Analytical procedures

The mineral separations and fission-track analysis were performed using standard techniques (see Appendix 3.2 for details). In this study, most fission track ages reported were determined by the new laser ablation method (LA-ICPMS; [Hasebe et al., 2004; Donelick et al., 2005]) with only a few ages determined by the more common external detector method [e.g. Gallagher et al., 1998]. Following age analysis, the apatites were classified for annealing kinetics using the parameter Dpar [e.g. Burtner et al., 1994].

Data analysis and thermal modeling

Methods for determining fission track component age populations within a discordant sample have been developed for data collected with the external detector method. BinomFit uses a deconvolution algorithm to identify statistically significant populations ages from a population of grain ages measured from a sample [Brandon, 2002].

Inverse thermal modeling of the AFT data was performed with HeFTy [Ehlers et al., 2005; Ketcham, 2005] using the multi-kinetic annealing model of [Ketcham et al., 1999] with c-axis projected track lengths [Ketcham, 2003] (see details in Appendix 3.3). We report the commonly used probability of a worse fit designations good (0.5) and acceptable (0.05) for the thermal history envelopes calculated with a Kuiper's statistical test [Press et al., 1992; Ketcham et al., 2000; Ketcham, 2005].

Results

Overview

Twenty-three samples were analyzed from Cretaceous through Ordovician sandstones and quartzites exposed over ~4 km in mean topographic relief from the eastern Altiplano through the Subandes at ~19.5°S (Fig. 3.2). Sample grain age and track length yields ranged from the maximum (40 ages & 200 track lengths/sample) to poor (<10 ages and/or track lengths/sample) with most (17 of 23) samples yielding robust results (>10 ages & track lengths/sample) (Table 3.1). The robust AFT pooled ages are Oligo-Miocene (14-30 Ma) in the EC, mostly early Miocene (18-20 Ma) in the IA, and mid Eocene to Mesozoic (42-265 Ma) in the SA (Fig. 3.2C & Table 3.1). Cooling histories inverted from this data are consistent with Eocene to recent cooling from temperatures of ~65ºC or greater. Consistently old, Paleozoic (385-471 Ma) ZFT pooled ages from the EC and IA indicate that the Tertiary cooling experienced by both regions has been limited to temperatures significantly <240ºC (Table 3.2). Representative stratigraphic sections independently suggest all samples were exhumed from variable depths of ~3-8 km across the study region (Fig. 3.4).

All of the AFT pooled ages are younger than the sample depositional age and considered reset whereas the ZFT pooled ages range from reset to mostly detrital [after Brandon et al., 1998]. In detail, 100% of the individual AFT grain ages in the EC and IA samples are reset and 53-100% of the grain ages in the SA samples are reset. Mean track lengths are short to long (9.97-14.89 μm) with uni-model, bimodal, and/or skewed length distributions suggesting a wide range of cooling histories. AFT grain age and fission-track Dpar values span 0.96-2.96 μm. However, the majority of grains analyzed have Dpar values of 1-1.75 μm suggesting dominantly fast-annealing calcian-fluorapatite compositions [Donelick et al., 2005]. Despite the majority of grains lacking significant compositional variation, only 10 of the 23 sample pooled ages are concordant. The

Table 3.1. Apatite fission-track data

Sample #	ID	Lat	Long	Elev (m)	Fm Age	n	Dpar (mm)	Dper (mm)	N_s (trks)	Area (cm^2)	Σ(PΩ) (cm^2)	1σ Σ(PΩ) (cm^2)	ξ_{MS}	1σ ξ_{MS}	P (χ^2) (%)	Pooled Age (Ma ± 2σ)	MTL ± 1σ (N_t) (μm) (tracks)
Altiplano																	
05JBBL042	*AL1*	*-19.70*	*-66.88*	*3706*	*K*	*36*	*1.57*	*0.36*	*244*	*3.76E-04*	*3.74E-05*	*2.65E-06*	*13.378*	*0.304*	*0.0*	*43.5± 8.6*	*12.06±2.03 (48)*
Eastern Cordillera																	
05JBBL037	EC1	-20.09	-66.39	3668	Sil	27	1.57	0.3	268	4.03E-04	5.94E-05	3.99E-06	13.476	0.306	60.9	30.3± 5.6	12.89±2.02 (123)
05JBBL036	*EC4**	*-20.07*	*-66.21*	*3450*	*Ord*	*2*	*1.43*	*0.28*	*8*	*1.36E-05*	*4.09E-06*	*8.53E-07*	*13.528*	*0.307*	*0.3*	*13.2± 10.8*	*14.07±0.94 (7)*
05JBBL035	*EC5*	*-20.04*	*-66.17*	*3290*	*Sil*	*39*	*1.48*	*0.31*	*254*	*9.40E-04*	*8.65E-05*	*4.23E-06*	*13.580*	*0.308*	*0.0*	*19.9± 3.2*	*13.16±1.92 (162)*
05JBBL034	*EC6*	*-20.00*	*-66.17*	*3311*	*Sil*	*31*	*1.51*	*0.27*	*248*	*5.47E-04*	*6.13E-05*	*4.33E-06*	*13.678*	*0.310*	*0.0*	*27.6± 5.4*	*12.75±1.99 (80)*
05JBBL033	EC7	-19.86	-66.14	3747	Sil	11	1.19	0.21	22	1.48E-04	1.33E-04	3.57E-07	16.712	0.413	88.5	13.8± 6.0	14.89±0.88 (13)
05JBBL031	*EC8**	*-19.58*	*-65.42*	*3156*	*Jr*	*8*	*1.43*	*0.29*	*34*	*1.10E-04*	*1.07E-05*	*1.44E-06*	*13.737*	*0.312*	*3.9*	*21.8± 9.6*	*14.47±2.25 (9)*
05JBBL030	EC9*	-19.62	-65.36	3253	Ord	4	1.9	0.47	6	3.40E-05	6.66E-07	8.95E-08	13.751	0.312	96.8	61.6± 53.0	11.64±1.27 (10)
05JBBL029	*EC10*	*-19.58*	*-65.27*	*3222*	*Ord*	*18*	*1.42*	*0.26*	*109*	*3.47E-04*	*3.94E-05*	*2.97E-06*	*13.780*	*0.313*	*0.7*	*19.0± 4.8*	*13.95±1.37 (31)*
05JBBL026	*EC11*	*-19.34*	*-65.16*	*2255*	*Ord*	*36*	*2.02*	*0.57*	*380*	*1.18E-03*	*9.77E-05*	*5.30E-06*	*13.852*	*0.314*	*0.0*	*26.9± 4.2*	*13.49±1.77 (195)*
05JBBL022	EC12*	-19.15	-64.99	3065	Ord	7	1.56	0.29	22	7.28E-05	4.29E-06	4.47E-07	13.910	0.316	16.9	35.6± 17.0	12.83±1.09 (6)
Interandean zone																	
05JBBL021	*IA1*	*-19.08*	*-64.82*	*2670*	*Dv*	*40*	*1.67*	*0.32*	*1844*	*1.06E-03*	*1.45E-04*	*7.55E-06*	*13.967*	*0.317*	*0.1*	*88.0± 10.8*	*12.32±2.12 (202)*
05JBBL019	IA2	-19.06	-64.77	2371	Ord	39	1.42	0.27	375	8.85E-04	1.36E-04	6.20E-06	14.066	0.319	83.9	19.4± 2.8	13.12±1.88 (136)
05JBBL018	IA3	-19.18	-64.47	2051	Dv	39	1.31	0.26	298	8.45E-04	1.19E-04	6.61E-06	14.164	0.321	61.6	17.8± 3.0	13.82±1.44 (161)
05JBBL017	IA4*	-19.30	-64.34	2125	Dv	8	1.27	0.23	26	6.16E-05	3.34E-06	3.47E-07	14.226	0.323	27.4	55.1± 24.6	11.16±1.64 (22)
Subandes																	
05JBBL013	*SA1**	*-19.51*	*-64.17*	*1825*	*Dv*	*6*	*1.32*	*0.27*	*51*	*4.61E-05*	*7.50E-06*	*8.41E-07*	*14.252*	*0.323*	*2.0*	*48.3± 17.4*	*11.64±2.15 (11)*
05JBBL010	*SA2*	*-19.80*	*-64.02*	*1236*	*Dv*	*39*	*1.39*	*0.29*	*645*	*6.28E-04*	*1.10E-04*	*6.22E-06*	*14.314*	*0.325*	*0.0*	*41.9± 6.0*	*11.50±2.60 (169)*
05JBBL008	SA3	-19.85	-63.73	1367	Cb	40	1.49	0.29	3403	1.33E-03	9.09E-05	4.76E-06	14.412	0.327	74.3	264.3± 31.6	11.14±1.58 (167)
05JBBL006	*SA4*	*-19.81*	*-63.72*	*1260*	*Cb*	*40*	*1.37*	*0.25*	*1332*	*7.09E-04*	*8.18E-05*	*3.81E-06*	*14.510*	*0.329*	*0.0*	*117.0± 13.8*	*10.62±2.33 (164)*
05JBBL003	*SA5*	*-19.84*	*-63.48*	*1137*	*Cb*	*34*	*1.3*	*0.25*	*862*	*5.50E-04*	*6.01E-05*	*3.46E-06*	*14.602*	*0.331*	*0.0*	*103.9± 14.6*	*9.97±1.87 (159)*
05JBBL002	SA6	-19.78	-63.25	844	Cb	40	1.38	0.28	2466	7.79E-04	7.20E-05	3.55E-06	14.694	0.333	9.9	246.7± 28.6	10.79±1.53 (159)

SA = Subandes; **IA** = Interandean zone; **EC** = Eastern Cordillera; **AL** = Altiplano; **Elev =** Elevation; **Fm age** = Formation age; **Cb** = Carboniferous, **Ord** = Ordovician, **Sil** = Silurian, **Dv =** Devonian, **Jr =** Jurassic, **K** = Cretaceous; **n = #** of grains measured; **Dpar** = is the mean maximum diameter of fission-track etch figures parallel to the c-axis; **Dper** = is the mean diameter perpendicular to the c-axis; Ns = number of spontaneous tracks (t/trks) counted; **Area** = grain area analyzed; **Σ(PΩ) =** area weighted $^{238}U/^{43}Ca$, summed over n grains in a sample**; σ =** standard deviation**;** ξ_{MS} **=** mass spectrometer zeta calibration factor; **P(χ2)** = probability (%) of greater chi- squared; MTL = mean track length; N_t **=** number of track lengths measured; *= less than 10 measured grain ages and track lengths; discordant (P(χ2) <5) samples in italics

Sample #	ID	Lat	Long	Elev (m)	Fm Age	n	Dpar (mm)	Dper (mm)	N_s (trks)	ρ_s (10^6 t/cm^{-2})	ρ_i (10^6 t/cm^{-2})	N_i (trks)	ρ_d (10^6 t/cm^{-2})	N_d (trks)	P (χ^2) (%)	Pooled Age (Ma ± 2σ)	MTL ± 1σ (N_t) (μm) (tracks)	C. Ages Ma (N_g)
Eastern Cordillera																		
714-1B	*EC2*	*-19.94*	*-66.29*	*3900*	*Jr*	*29*	*1.69*	*0.46*	*123*	*0.224*	*4.564*	*2503*	*4.258*	*4040*	*3.0*	*11.9± 2.4*	*13.61±1.67 (61)*	*10.8(25),33.6(4)*
713-5B	EC3	-19.95	-66.25	3550	Sil	13	1.59	0.39	27	0.162	2.754	460	4.267	4040	5.4	14.2± 5.8	13.23±1.79 (31)	--

ρ_s = density (cm^{-2}) of spontaneous tracks; ρ_i = density (cm^{-2}) of induced tracks; ρ_d = density (cm^{-2}) of tracks on the neutron fluence monitor (CN-1 glass); N_d = number of tracks counted in the dosimeter; **C. Ages** = component ages & number of contributing grains (N_g)

over-dispersion of grain ages in the discordant samples is not conventionally attributable to composition [Carlson et al., 1999] because none of the samples exhibit correlations between Dpar and grain age or track length.

Below, we detail (a) the modeling results of the AFT data from west to east across each zone mostly highlighting the good-fit cooling histories with representative cooling envelopes shown in Figures 3.5-3.8, and (b) the ZFT pooled ages with ± 2σ errors and associated interpretations.

Table 3.2. Zircon fission-track data

Sample #	ID	Lat	Long	Elev (m)	Fm Age	n	N_s (trks)	Area (cm^2)	Σ(PΩ) (cm^2)	1σ Σ(PΩ) (cm^2)	ξ_{MS}	1σ ξ_{MS}	P (χ^2) (%)	Pooled Age (Ma ± 2σ)
Eastern Cordillera														
05JBBL036	*EC4*	*-20.07*	*-66.21*	*3450*	*Ord*	*20*	*2306*	*6.46E-05*	*1.40E-05*	*1.86E-07*	*5.736*	*0.222*	*0.0*	*455+/- 42*
05JBBL033	*EC7*	*-19.86*	*-66.14*	*3747*	*Sil*	*20*	*2941*	*8.64E-05*	*1.71E-05*	*2.37E-07*	*5.692*	*0.220*	*0.0*	*471+/- 42*
Interandean zone														
05JBBL019	*IA2**	*-19.06*	*-64.77*	*2371*	*Ord*	*6*	*645*	*2.04E-05*	*4.67E-06*	*2.33E-07*	*5.751*	*0.223*	*0.0*	*385+/- 58*
05JBBL018	*IA3*	*-19.18*	*-64.47*	*2051*	*Dv*	*20*	*2947*	*9.08E-05*	*2.00E-05*	*2.89E-07*	*5.765*	*0.224*	*0.0*	*411+/- 38*

abbreviations and symbols same as in Table 3.1.

Altiplano

Our Altiplano sample (AL1) is from the Cretaceous El Molino formation west of Rio Mulato in the east-vergent Rio Mulato fold belt (Fig. 3.2 & Table 3.1) [McQuarrie and DeCelles, 2001]. Local age control for the El Molino is Maastrichtian to Danian (60-~73 Ma) based on marine fossils and tuffs near the base [Sempere et al., 1997; Horton et al., 2001]. Given this, we assumed a depositional age of 60-80 Ma for the thermal history modeling. Sample AL1 acceptable fits suggest post-depositional burial to ≥80ºC 40-60 Ma, followed by >10 Myrs at PAZ temperatures of ~70-85ºC prior to rapid exhumation to the surface broadly constrained to start between 3-30 Ma and end 0-15 Ma.

Eastern Cordillera (EC) back-thrust belt

We report seven samples (EC1-7) of Ordovician to Jurassic rocks exhumed from 4-7 km stratigraphic depths across four different thrust sheets in the EC back-thrust belt (Fig. 3.5). Concordant sample EC1 modeling constrains good-fit cooling from ≥~100ºC 32-35 Ma, followed by slow cooling through the PAZ until ~15 Ma, and ultimately more rapid cooling until ~0-10 Ma (Fig. 3.5C). Discordant sample EC2 has two deconvolved component ages of 10.8 and 33.6 Ma (Table 3.1). Good-fit model results show EC3 cooling began most recently ~13 Ma from ≥~105ºC (Fig. 3.5C). We note these results are nearly identical to those obtained with only a fixed 50-180ºC constraint equal in age to between deposition and 1 Ma as most discordant samples are reported in this study. Model results of concordant sample EC3 demarcate acceptable cooling beginning 10-15 Ma from ≥~90ºC with good fits refining initial cooling to ~15 Ma from ≥~105ºC.

Samples EC4-EC6 project onto the same structure implying their cooling histories should be related (Fig. 3.5). However, they overlie a blind thrust that may have imparted different kinematic histories and thus we report their cooling histories independently. Sample EC4 has poor data quality with acceptable rapid cooling from ≥90ºC at >5 Ma with good fits constraining rapid cooling from ≥105ºC 11-16 Ma. Good-fit modeling results for discordant sample EC5 suggests rapid cooling started from ≥105ºC at 20-25 Ma (Fig. 3.5C). For sample EC6, model results define acceptable rapid cooling from ≥100ºC 29-39 Ma with good fits constraining initial cooling from ≥105ºC 34-36 Ma. Finally, concordant sample EC7 modeling delimits rapid cooling from ≥105ºC 10-20 Ma.

We also report two ZFT results from samples EC4 and EC7 (Fig. 3.5A & Table 3.2). EC4 was exhumed from the greatest stratigraphic depths in the EC of >7 km and has a discordant ZFT pooled age of 455±42 Ma which is equivalent to the Devonian depositional age (Fig. 3.5A). We consider this ZFT sample unreset and probably

Figure 3.5. Eastern Cordillera (EC) back-thrust belt thermochronology data integrated with the regional structure and stratigraphy at ~19.5ºS. (A) Cross section from [McQuarrie, 2002] with samples projected onto the appropriate structures. AFT = apatite fission track, ZFT = zircon fission-track pooled age and 2σ (Ma) where available. V.E. = vertical exaggeration. Discordant samples in italics. Summary table of selected AFT data is directly below (see Table 3.1 for all data & abbreviations). (B) AFT pooled age (Ma) and track-length data in their regional stratigraphic context from Figure 3.4. Track-length distribution histograms uncorrected to c-axis parallel; F = frequency, N = number of tracks measured, and mean track length (dashed line). (C) Selected thermal modeling results showing acceptable (light gray), good (dark), and best (thick line) fit cooling histories inverted from the AFT data. Boxes are modeling constraints. Old Cmpt = old age component, Yg Cmpt = young component age. Track length (TL) distribution (c-axis parallel) shown for the data (bars) and best-fit (line) model.

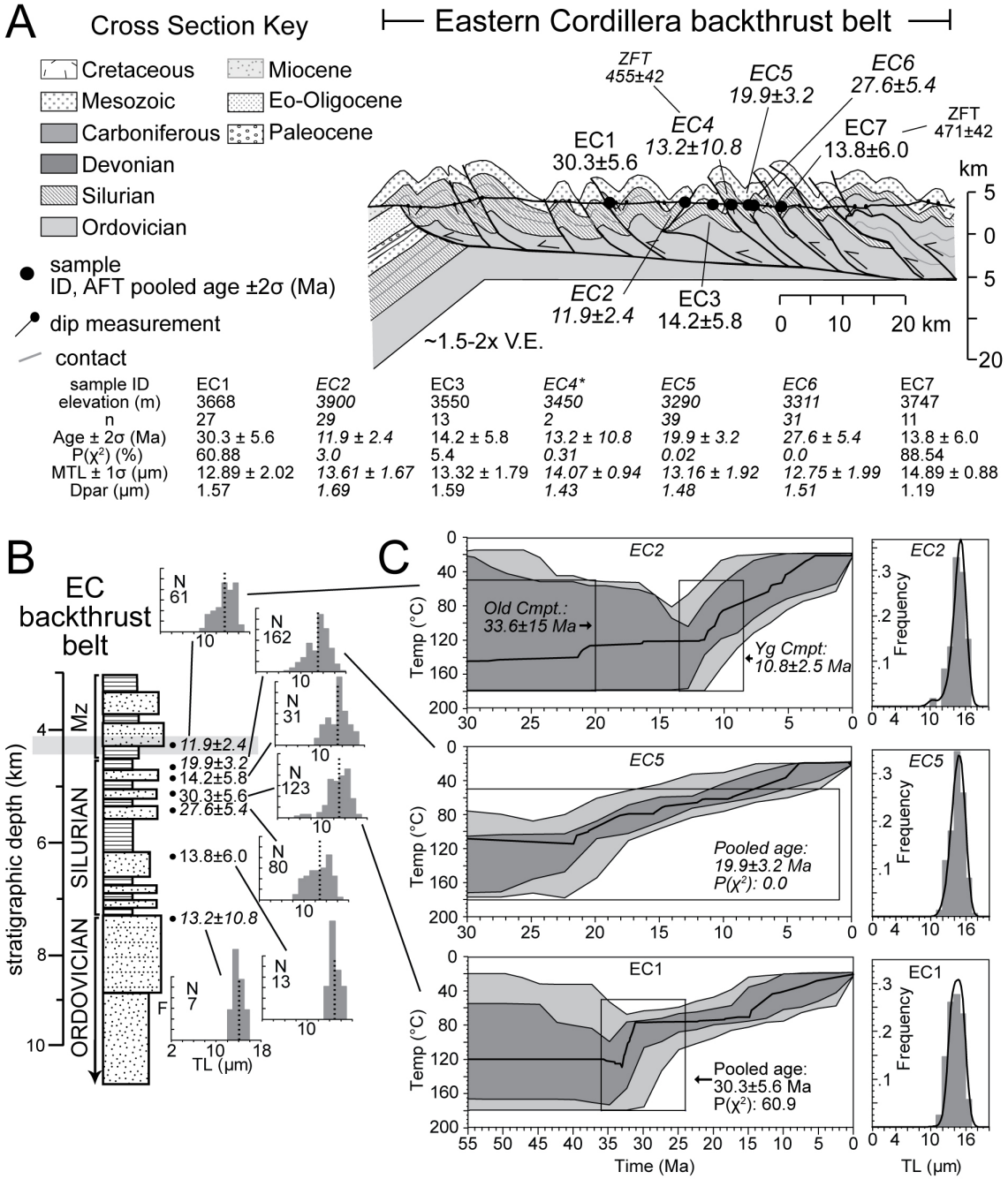

sample ID	EC1	*EC2*	EC3	*EC4**	*EC5*	*EC6*	EC7
elevation (m)	3668	*3900*	3550	*3450*	*3290*	*3311*	3747
n	27	*29*	13	*2*	*39*	*31*	11
Age ± 2σ (Ma)	30.3 ± 5.6	*11.9 ± 2.4*	14.2 ± 5.8	*13.2 ± 10.8*	*19.9 ± 3.2*	*27.6 ± 5.4*	13.8 ± 6.0
P(χ²) (%)	60.88	*3.0*	5.4	*0.31*	*0.02*	*0.0*	88.54
MTL ± 1σ (μm)	12.89 ± 2.02	*13.61 ± 1.67*	13.32 ± 1.79	*14.07 ± 0.94*	*13.16 ± 1.92*	*12.75 ± 1.99*	14.89 ± 0.88
Dpar (μm)	1.57	*1.69*	1.59	*1.43*	*1.48*	*1.51*	1.19

detrital. EC7 has a discordant ZFT pooled age of 471±42 Ma which is older than the Silurian depositional age and considered detrital.

Collectively, the EC back-thrust belt samples were exhumed from 4-7 km stratigraphic depths and record three phases of rapid AFT cooling that started in the; (1) late Eocene (32-36 Ma; EC1 & EC6), (2) late-Oligocene to early Miocene (20-25 Ma; EC5), and (3) mid-late Miocene (~11-16 Ma; EC2-4 & EC7). Two detrital Paleozoic ZFT pooled ages indicate regional Tertiary cooling has been limited to temperatures significantly <240ºC.

Eastern Cordillera (EC) fore-thrust belt

We report five samples (EC8-12) of Ordovician to Jurassic rocks exhumed from 4-8 km stratigraphic depths across four different thrust sheets in the EC fore-thrust belt (Fig. 3.6). Acceptable modeling results for discordant sample EC8 suggest recent cooling began >14 Ma from ≥~100ºC with good fits constraining initial cooling from 21-25 Ma. Concordant sample EC9 good-fit modeling results define cooling from PAZ temperatures of 65-80ºC 4-40 Ma. The most likely cooling history for samples EC8 and EC9 must be defined by where the sample cooling envelopes overlap because they are structurally linked. In this case, EC9 probably cooled rapidly from ~21-25 Ma as did EC8. Discordant sample EC10 good-fit modeling results constrain recent cooling from ≥100ºC 19-22 Ma (Fig. 3.6C). Acceptable modeling fits for sample EC11 constrain rapid cooling at 27-30 Ma from ≥75ºC with good fits refining cooling from ≥125ºC 27-30 Ma (Fig. 3.6C). Sample EC12 acceptable modeling fits suggest recent cooling by >20 Ma from ≥85ºC with good fits refining cooling from ≥95ºC more than 22 Ma.

Collectively, the EC fore-thrust belt samples were exhumed from the greatest stratigraphic depths of mostly ≥7 km and record two phases of rapid AFT cooling that

started in the; (1) early Oligocene (27-30 Ma; EC11; maybe EC12) and (2) early Miocene (19-25 Ma; EC8-10, maybe EC12).

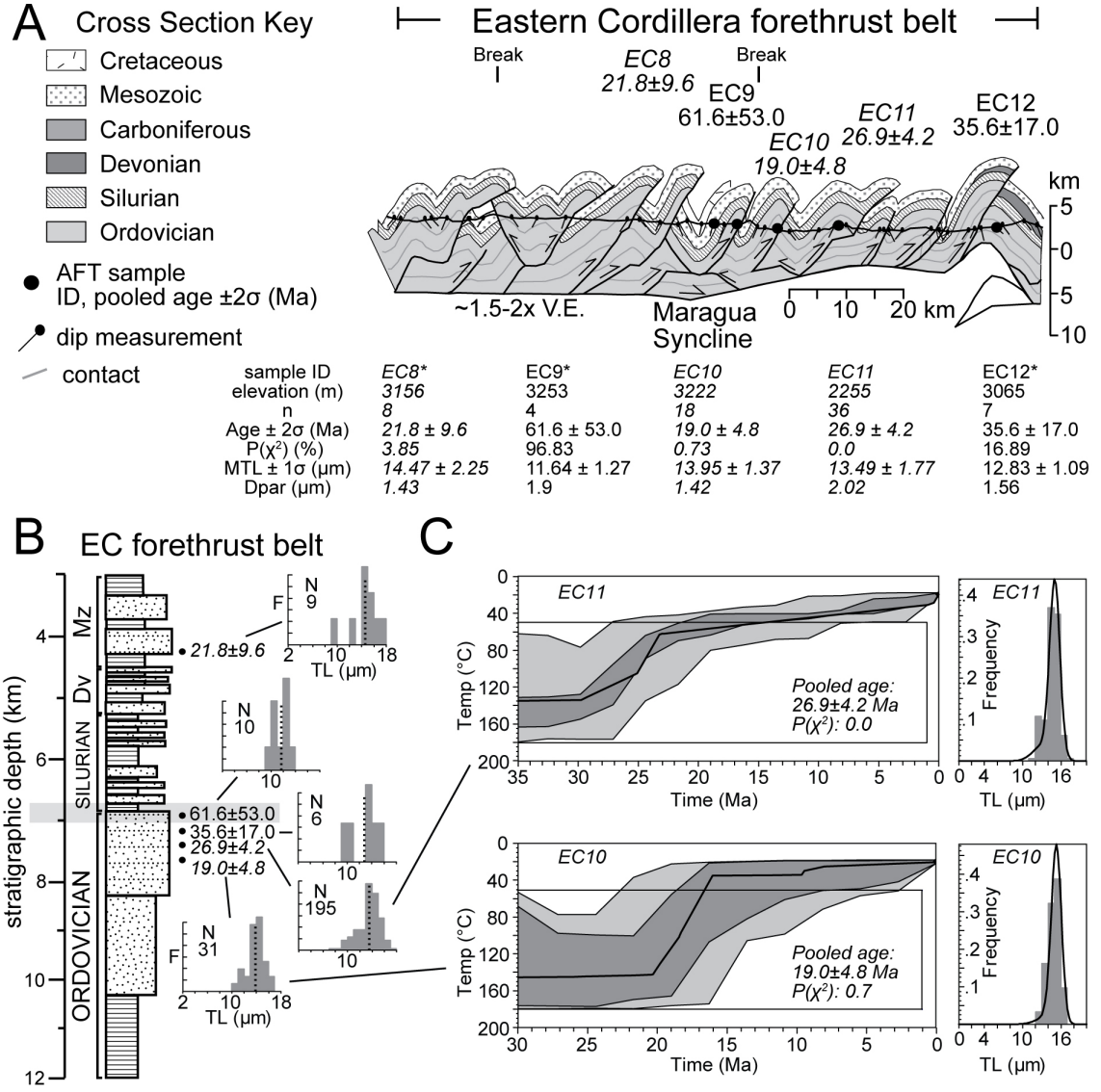

Figure 3.6. Eastern Cordillera (EC) fore-thrust belt thermochronology data integrated with the regional structure and stratigraphy at ~19.5ºS. See Figure 3.5 caption for details.

Interandean zone (IA)

We report four samples (IA1-4) from Ordovician to Devonian rocks exhumed from 5-7 km stratigraphic depths across two different thrust sheets in the IA (Fig. 3.7).

Sample IA1 modeling results infer initial cooling began ~100 Ma from ≥~80ºC, followed by residence in the PAZ until a final episode of more rapid cooling to the present from at most ~40 Ma (Fig. 3.7C). Sample IA2 modeling results delimit recent cooling beginning 20-22 Ma from ≥~100ºC (Fig. 3.7C). Taken together, these two samples are consistent with rapid cooling starting 20-22 Ma and best represented by the results from IA2. Good-fit thermal envelopes for sample IA3 demarcate cooling from temperatures ≥~90ºC beginning 19-21 Ma (Fig. 3.7C). For sample IA4, modeling results imply initial cooling began ≥~40 Ma from ≥~100ºC, followed by residence in PAZ temperatures of 55-80ºC until a final episode of more rapid acceptable cooling initiated from 3-20 Ma with good fits limiting final rapid cooling from 3-10 Ma.

We also report two ZFT results from samples IA2 and IA3 (Fig. 3.7A & Table 3.2). IA2 was exhumed from the greatest stratigraphic depths in the IA of ~7 km and has a discordant ZFT pooled age of 385±58 Ma, but low grain yield. The ZFT pooled age is younger than the Ordovician depositional age and hence considered reset, but not by the Cenozoic Andean orogeny. IA3 has a discordant ZFT pooled age of 411±38 Ma which is equivalent to the Devonian depositional age. We consider this ZFT sample unreset and probably detrital.

Collectively, the IA samples were exhumed from 5-7 km stratigraphic depths and record mostly rapid AFT cooling starting in the early Miocene (19-22 Ma; IA1-3). This early Miocene cooling is roughly uniform across most of the IA. Sample IA4 shows late Miocene or younger (3-10 Ma) initial cooling from the PAZ. Two reset and unreset Paleozoic ZFT ages indicate local Tertiary cooling has been limited to temperatures significantly <240ºC in the IA.

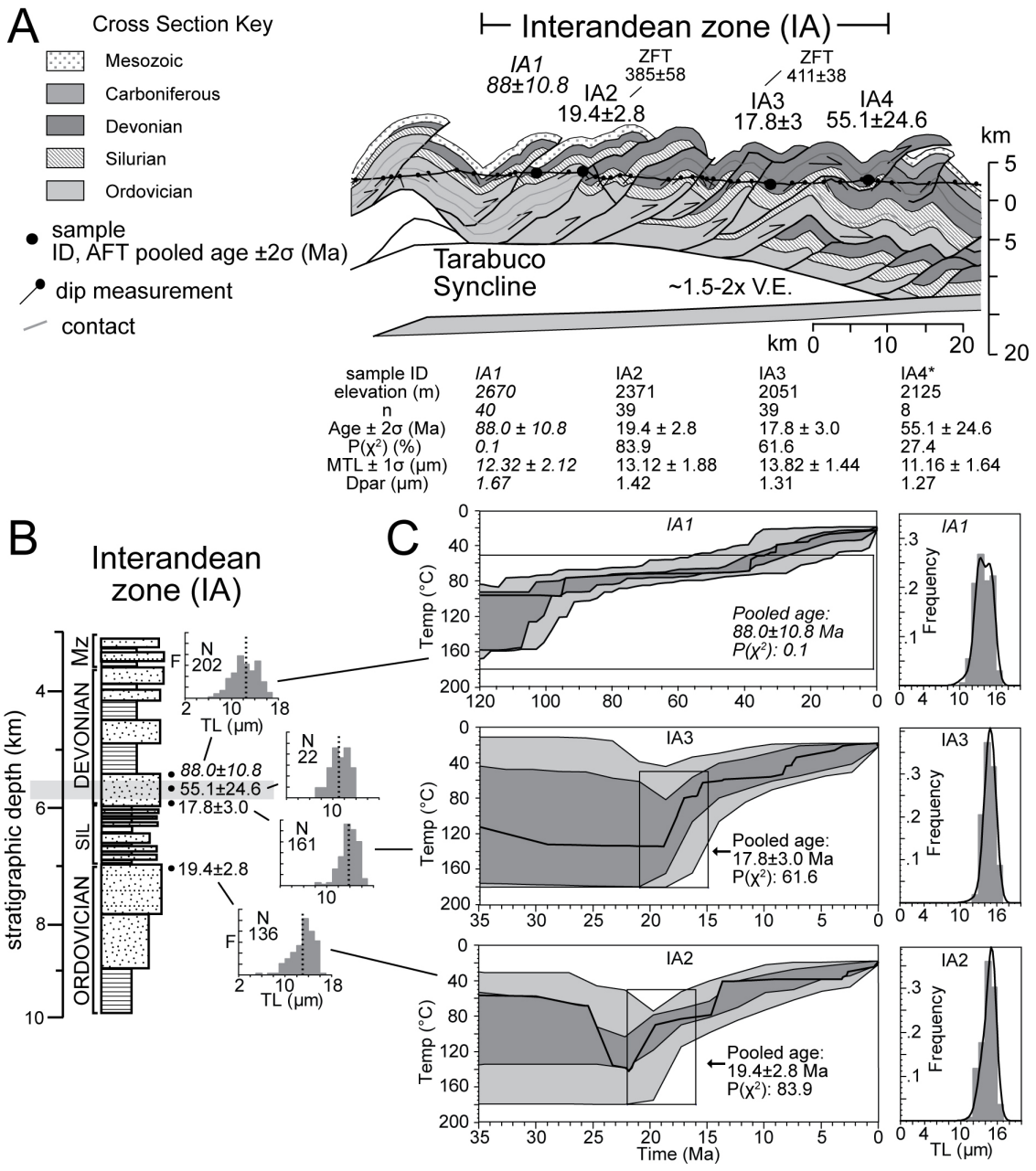

Figure 3.7. Interandean zone (IA) thermochronology data integrated with the regional structure and stratigraphy at ~19.5ºS. See Figure 3.5 caption for details.

Subandes (SA)

We report six samples (SA1-6) from Devonian to Carboniferous rocks exhumed from 4-6 km stratigraphic depths across five different thrust sheets in the SA (Fig. 3.8).

Acceptable modeling results for sample SA1 suggest recent cooling began from PAZ temperatures of <90ºC 3-30 Ma with good fits refining cooling from 60-85ºC 3-30 Ma. Discordant sample SA2 modeling implies cooling began ~50 Ma from ≥~100ºC, followed by residence in the PAZ until more recent cooling began ~8-20 Ma from ~80ºC (Fig. 3.8C). Concordant sample SA3 good fits imply significant residence in PAZ temperatures of ~75ºC until recent, rapid cooling began ~3-8 Ma (Fig. 3.8C). For sample SA4, modeling suggests significant residence in PAZ temperatures of ~70-75ºC until recent, rapid cooling began 4-23 Ma (acceptable fits) or 7-13 Ma (good fits) from 75ºC. As part of the same thrust sheet, samples SA3 and SA4 probably cooled beginning 4-20 Ma (overlapping acceptable fits) or 7-8 Ma (overlapping good fits). Unfortunately, modeling did not produce any acceptable cooling histories for sample SA5. Based on similarities in stratigraphic position, lithology, and AFT data, we assume a cooling history similar to SA4. Finally, modeling of sample SA6 suggests significant residence in PAZ temperatures of ~65ºC until acceptable recent, rapid cooling began 2-19 Ma with good-fits refining that to 2-8 Ma.

Collectively, the SA samples were exhumed from 4-6 km stratigraphic depths and record Miocene to Pliocene initial cooling (~3-20 Ma; SA1-6). Oligo-Miocene cooling (~10-30 Ma; SA1-2) began in the west, stepping eastward to late Miocene (~7-8 Ma; SA3-4) and eventually as young as Pliocene (2-8 Ma; SA6) in the easternmost structure (Fig. 3.8). One additional observation is that the SA samples show a systematic decrease in age with stratigraphic depth from concordant late Paleozoic to earliest Mesozoic pooled ages exhumed from ~4 km depths to discordant mid-Eocene ages exhumed from ~5.5 km depths (Fig. 3.8). Several Devonian to Tertiary exposures previously analyzed along this transect also have Mesozoic to early Tertiary AFT ages [Moretti et al., 1996].

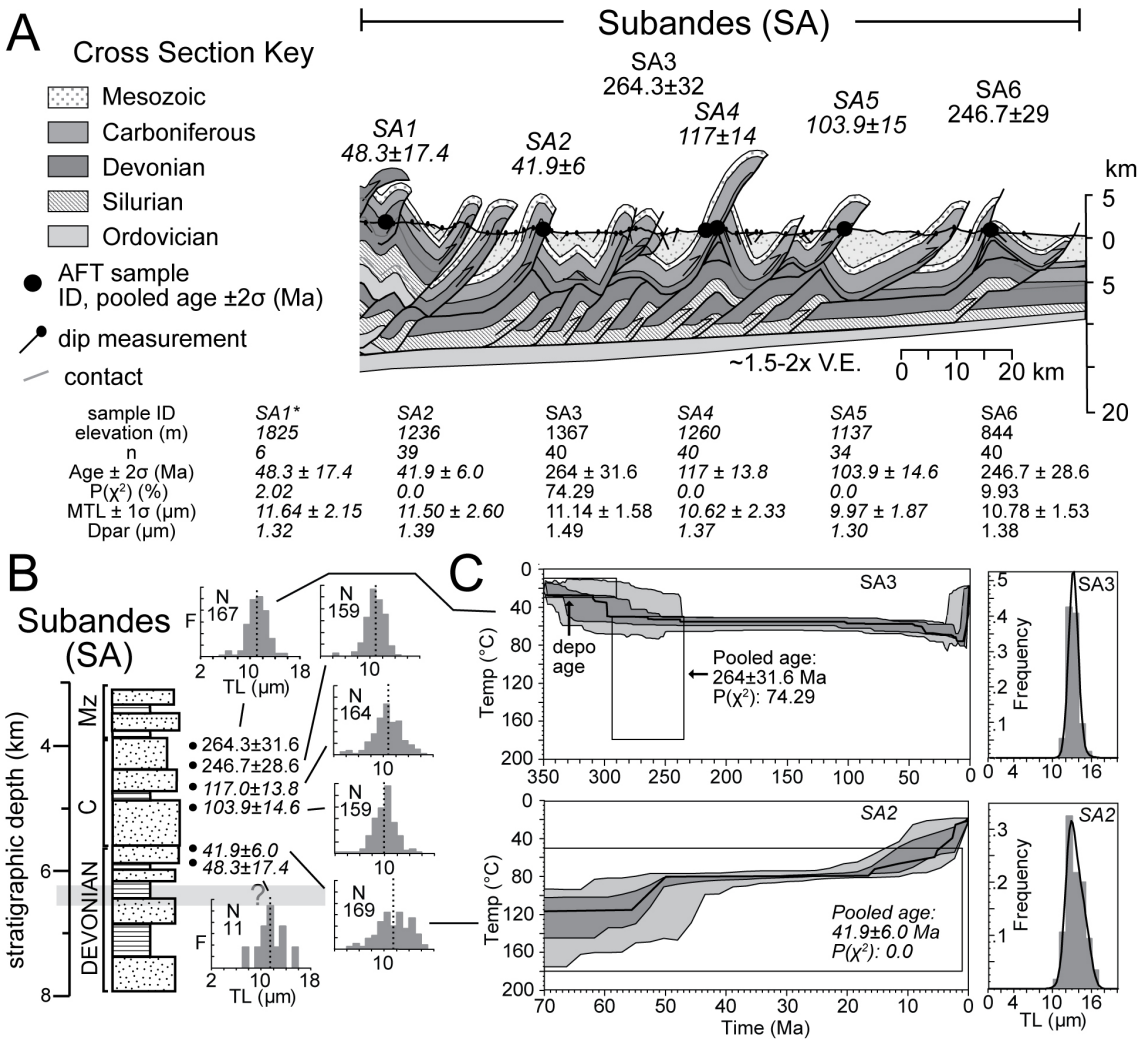

Figure 3.8. Subandes (SA) thermochronology data integrated with the regional structure and stratigraphy at ~19.5ºS. See Figure 3.5 caption for details. Depo age = deposition age.

Discussion

Erosional cooling of thermochronometer data

In active orogens, thermochronometer cooling can result from erosional exhumation, tectonic exhumation along normal faults, magmatism, and/or fluid flow [Ring et al., 1999; Ehlers, 2005]. Erosional exhumation is a common mechanism for sample

cooling in fold-thrust belts. In our study area (Fig. 3.2), a lack of extensional structures, insignificant Mesozoic rifting [e.g. Sempere et al., 2002], and volcanism spatially-limited to the EC back-thrust belt supports that erosional exhumation was responsible for the cooling histories reported. Therefore, we assume that the initiation of deformation generates topography with erosion causing the onset of rapid (>~10ºC/M.y) exhumation recorded by the thermochronometer data [after e.g. Coughlin et al., 1998; Sobel and Strecker, 2003; Barnes et al., 2006; Ege et al., 2007].

Samples EC1-7 in the EC back-thrust belt are proximal (~4-25 km) to Tertiary volcanism suggesting their cooling histories could be associated with magmatism rather than erosional exhumation (Fig. 3.2A). For the following two reasons, we conclude that magmatic heating was insufficient to overprint the erosion-related cooling signal in the sample data. First, the AFT data display no correlation of age or track length distribution with respect to distance to the nearest volcanic outcrop (Figs. 3.2A & 3.5, Table 3.1). Second, we applied a step change in heating [after Ehlers, 2005] to compute the potential thermal disturbance caused by the Miocene to recent (~<1-25 Ma) Los Frailes ignimbrite flows nearby [Riera-Kilibarda et al., 1994; Barke et al., 2007]. We assumed an initial intrusion temperature of 800ºC, a 50ºC country rock temperature, a 300 m thick deposit [Riera-Kilibarda et al., 1994], and 32-64 km²/Ma thermal diffusivities based on average and measured values of conductivity, density, and heat capacity from southern EC rocks [Henry and Pollack, 1988; Ehlers, 2005]. The results predict a minor ~10-13ºC temperature change 4 km (our most proximal sample distance) from the intrusion center.

Timing of deformation at ~19.5ºS

Previous work constraining the deformation history at ~19.5ºS suggests the EC fore-thrust belt deformation initiated in the mid-late Eocene (~35-40 Ma) followed by distributed deformation moving both west and east reaching the Altiplano and SA by the

mid-Miocene (~15 Ma) (Figs. 3.9 & 3.10) [McQuarrie et al., 2005]. Late Eocene to earliest Oligocene (27-36 Ma) rapid erosion in the EC back-thrust and fore-thrust belts suggests distributed deformation at this time (Fig. 3.9B&C). Two samples (EC1 & EC6) record the earliest cooling with robust grain/track yields documenting erosion and deformation in the back-thrust belt 32-36 Ma (Figs. 3.5C & 3.9C). Sample EC11 recorded the earliest cooling in the EC fore-thrust belt suggesting erosion and deformation started slightly later from 27-30 Ma (Figs. 3.6C & 3.9C). However, two additional poor quality samples (EC9 & EC12) are consistent with this early Oligocene or even earlier erosion. Our chronology implies either (a) the EC back-thrust belt started deforming first or (b) the earliest (~35-40 Ma) EC fore-thrust belt deformation was not recorded by our samples because they are limited to the younger, eastern portion as predicted by in-sequence deformation (Figs. 3.2 & 3.9). Regardless, the results attest to near contemporaneous deformation in both directions ~27-36 Ma (Fig. 3.9B&C). Sediments shed by this exhumation were transported eastward into the adjacent foredeep deposits of the Incapampa syncline (Figs. 3.2A & 3.9A&B) [Horton, 2005; McQuarrie et al., 2005].

Late Oligocene to early Miocene (19-25 Ma) cooling suggests deformation across structures in the EC as well as initial deformation of the IA at 19-22 Ma (Fig. 3.9D). Although rapid erosion of samples EC8-10 is consistent with in-sequence deformation, they are all west of earlier exhumation recorded by EC11 indicating the opposite. Sample EC5 erosion is younger in age and intermediate in across-strike distance suggesting out-of-sequence deformation in the EC back-thrust belt. During this time (19-25 Ma), a change from foredeep to intermontane basin sedimentation suggests EC deformation waned while active deformation stepped eastward into the IA [Horton, 2005]. The extensive and contemporaneous rapid erosion portrays distributed deformation localizing sedimentation in the EC, which waned shortly thereafter, and

eventually ceased by ~15 Ma [McQuarrie et al., 2005] or 21-25 Ma [Horton, 2005]. This history is supported by only minor resolved acceptable cooling in the EC back-thrust belt younger than 19 Ma.

The 19-36 Ma deformation in the EC is associated with upper basement shortening (Fig. 3.9A-D) [McQuarrie, 2002; McQuarrie et al., 2005]. Similar magnitudes of shortening in the basement and cover rocks accounts for most of the present-day crustal thickness of the EC and presumably some of the elevation of the Andean plateau (Fig. 3.9D) [McQuarrie, 2002]. This upper basement structure eventually feeds slip in the IA causing early deformation in the IA cover rocks (Fig. 3.9D). The recorded uniform exhumation of the IA at 19-22 Ma can be explained in two ways; a) by contemporaneous thrusting and exhumation in the IA cover rocks fed by upper basement deformation or b) by more passive uplift above the leading edge of a subsequently lower basement structure as it began to migrate eastward feeding slip into the SA (Fig. 3.9D&E). We prefer the latter explanation and suggest that the spatially uniform IA exhumation 19-22 Ma signifies the initiation age for lower basement shortening which begins after cessation of the upper structure [McQuarrie, 2002]. Since it is the older, upper-basement structure that is responsible for a proto-Andean plateau of modern width we infer this to been achieved by ~15-20 Ma (between D & E in Fig. 3.9) [McQuarrie, 2002; see also Barnes et al., 2006].

Mid-to-late Miocene rapid cooling occurred in the EC back-thrust belt (11-16 Ma), easternmost IA (IA4; 3-10 Ma), and initiated in the western SA (8-20 Ma) (Fig. 3.9E). Cooling in the EC back-thrust belt may be the result of (a) strain accumulation from ~12-20 Ma evident by the locally deformed early-to-mid Miocene Mondragon Formation 20-30 km northwest of Potosi [Kennan et al., 1995] or (b) simply enhanced protracted erosion after deformation had already ceased. No record of rapid exhumation and the

Figure 3.9. Chronology of deformation and exhumation across the eastern flank of the central Andean plateau at ~19.5ºS. Previous chronologic estimates (Ma*) and sequential kinematic reconstruction with foreland basin deposits are from McQuarrie et al. [2005]. This previous chronology is based on an integration of published structural, stratigraphic and thermochronologic data in Bolivia. Grey boxes indicate a revised chronology based on the thermochronometer data presented in this paper. Grey box text indicates sample ID(s) (top row) and the age of initial rapid cooling (in Ma) from good (1) and acceptable (2) thermal modeling results. Black dots are samples with ID number. Major exhumation and deformation episodes are highlighted with italicized text. NF = no fits. Arrow is eastern edge of the Andean plateau/Tarabuco & Incapampa syclines (see Fig. 3.2 for location) and jagged line is the western edge of the Brazilian shield.

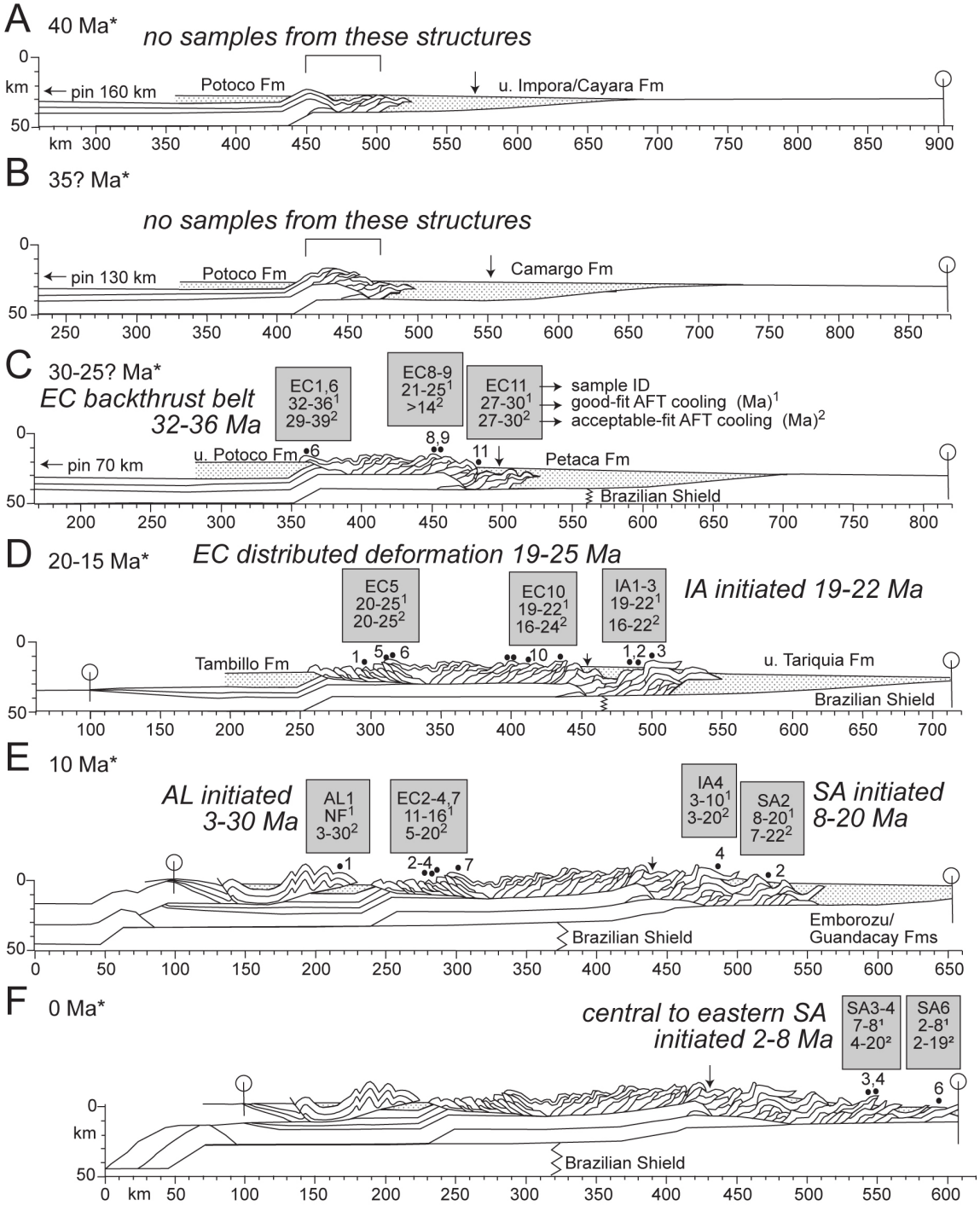
A 40 Ma*
no samples from these structures
0
km
50
pin 160 km
Potoco Fm
u. Impora/Cayara Fm
km 300 350 400 450 500 550 600 650 700 750 800 850 900
B 35? Ma*
no samples from these structures
0
50
pin 130 km
Potoco Fm
Camargo Fm
250 300 350 400 450 500 550 600 650 700 750 800 850
C 30-25? Ma*
EC backthrust belt
32-36 Ma
EC1,6
32-36[1]
29-39[2]
EC8-9
21-25[1]
>14[2]
EC11
27-30[1]
27-30[2]
sample ID
good-fit AFT cooling (Ma)[1]
acceptable-fit AFT cooling (Ma)[2]
0
50
pin 70 km
u. Potoco Fm
6
8,9
11
Petaca Fm
Brazilian Shield
200 250 300 350 400 450 500 550 600 650 700 750 800
D 20-15 Ma*
EC distributed deformation 19-25 Ma
EC5
20-25[1]
20-25[2]
EC10
19-22[1]
16-24[2]
IA1-3
19-22[1]
16-22[2]
IA initiated 19-22 Ma
0
50
Tambillo Fm
1 5 6
10
1,2 3
u. Tariquia Fm
Brazilian Shield
100 150 200 250 300 350 400 450 500 550 600 650 700
E 10 Ma*
AL initiated
3-30 Ma
AL1
NF[1]
3-30[2]
EC2-4,7
11-16[1]
5-20[2]
IA4
3-10[1]
3-20[2]
SA2
8-20[1]
7-22[2]
SA initiated
8-20 Ma
1
2-4
7
4
2
0
50
Brazilian Shield
Emborozu/
Guandacay Fms
0 50 100 150 200 250 300 350 400 450 500 550 600 650
F 0 Ma*
central to eastern SA
initiated 2-8 Ma
SA3-4
7-8[1]
4-20[2]
SA6
2-8[1]
2-19[2]
3,4
6
0
km
50
Brazilian Shield
0 km 50 100 150 200 250 300 350 400 450 500 550 600

existence of the undeformed, regional San Juan del Oro erosion surface [e.g. Gubbels et al., 1993] implies deformation in the EC fore-thrust belt ceased by ~10 Ma. The late Miocene exhumation (from PAZ temperatures) of the eastern IA can be explained by continued migration of the lower basement structure as it advanced farther east [McQuarrie et al., 2005]. Limited thermo-geochronology on Tertiary basin deposits and our recorded exhumation show deformation in the SA began ~8-20 Ma [Moretti et al., 1996; Jordan et al., 1997; Barke, 2004; Uba et al., 2006]. At about the same time, to the west, erosion and deformation of the Rio Mulato fold belt in the Altiplano is broadly constrained between 3 and 30 Ma. The unconformably overlying and folded Miocene Tambillo Formation sediments indicate both pre-Miocene and late Miocene (~10-14 Ma) Altiplano deformation locally [Kennan et al., 1995; Lamb and Hoke, 1997].

Late Miocene to Pliocene (2-8 Ma) rapid exhumation and deformation occurred throughout the central-to-eastern SA (Fig. 3.9F). Local deposition of shallow marine rocks in the Yecua Formation [e.g. Hulka et al., 2006; Uba et al., 2006] place a maximum age of deformation on the SA structures sampled by SA3-6 of ~8 Ma. Late Miocene exhumation is recorded by deposition of the Guandacay Formation (2.1-6 Ma) in the Chaco (Fig. 3.1) to the east that indicates a proximal foredeep outboard this deformation [Uba et al., 2006]. Overlapping good modeling fits of samples SA3-4 from the west-limb of the Sararenda anticline [McQuarrie, 2002] in the central SA record thrusting and exhumation starting 7-8 Ma. A dated tuff from fluvial terraces on the Caipipendi thrust hanging wall (second easternmost SA structure in Fig. 8A) suggests inactivity for the last 1 Ma [Barke, 2004]. The model-constrained cooling envelopes are consistent with in-sequence deformation propagating east with time as proposed [McQuarrie, 2002; McQuarrie et al., 2005]. However, others have suggested out-of-sequence deformation of the central and eastern SA structures over ≤6 Ma [Fig. 11 of Moretti et al., 1996; Barke, 2004 pgs. 148-151].

Revised shortening rates

Previous shortening rates for the EC and IA were ~9-11 mm/yr from ~20-40 Ma reducing to ~4-5 mm/yr in the SA over the last 15-20 Myr (Table 3.3) [see also Ramos et al., 2004]. We revise these rates by assuming the EC started deforming 40 Ma and the SA started either 8 or 20 Ma as suggested by the minimum and maximum good-fit exhumation histories of sample SA2 (Table 3.3). Two hundred-eighteen km of shortening across the EC and IA from 40 to 10-20 Ma translates to a rate of ~7-11 mm/yr. Sixty-seven km of shortening across the SA since 8 or 20 Ma produces shortening rates of ~9 or ~4 mm/yr, respectively. Our revised shortening rates presented here suggest Miocene to recent rates either decreased by half from a long-term average of ~8 mm/yr or remained about the same to slightly increasing depending on the age of initial SA deformation and the end of EC deformation.

Exhumation estimates

Geothermal gradients and depth to closure

The thermal structure across the thrust belt in southern Bolivia varies by a factor of two and has been well-constrained by borehole measurements [Henry and Pollack, 1988; Hamza and Muñoz, 1996; Springer and Forster, 1998; Hamza et al., 2005]. We quantify exhumation magnitudes from AFT and ZFT effective closure depths using measured thermal gradients (Fig. 3.10B) [Reiners and Brandon, 2006]. We assumed average closure temperatures of 110ºC for AFT [e.g. Gallagher et al., 1998] and 240ºC for ZFT [Brandon et al., 1998], and average surface temperatures of 10ºC for the Altiplano and EC, 15ºC for the IA, and 23ºC for the SA [Springer and Forster, 1998; Instituto Geografico Militar, 2000]. Mean surface temperatures and proximal borehole measurements of the thermal gradient combine to represent the best-available proxy for

the thermal field through which the samples cooled. Our selection criteria for thermal gradient estimates include: (1) measurement reliability, (2) location within the same physiographic province as the samples, (3) reported gradient has been corrected for near surface topographic perturbations, and (4) location of measurement is within one crustal thickness distance (~60-75 km in the Altiplano/EC, ~50-60 km in the IA, and ~40 km in the SA [Beck and Zandt, 2002]) of the samples to minimize regional variations in basal heat flux biasing our calculation.

Table 3.3. Shortening rates for the central Andean fold-thrust belt (~19.5ºS), southern Bolivia.

Location	Amount (km)	Time Interval* (Ma)	Rate (mm/yr)	Time Interval (Ma)	Rate (mm/yr)
WC to EC	200-250*	45-70	8-10*	--	--
EC & IA	218^	40-15/20	8.5-11*	40 to 10-20	7.3-11
SA	67^	15/20-0?	3.5-4.5	20-0 (1)	3.5 (1)
SA	67^	--	--	8-0 (2)	8.5 (2)
Total	550*	70-0	7.8 mm/yr*	--	--

* = from *McQuarrie et al.* [2005]; ^ = from *McQuarrie* [2002]
(1) assuming oldest modeling good fit of sample SA2 represents initiation of deformation
(2) assuming youngest modeling good fit of sample SA2 represents initiation of deformation

Five measurements in the Bolivian Altiplano estimate a mean thermal gradient of 38±10 (1σ)ºC/km [Henry and Pollack, 1988]. The high gradient is attributed to the position of a shallow (~70 km) asthenospheric mantle wedge, partial melts in the mid-crust, and proximity to the volcanic arc to the west [Springer, 1999]. This high geothermal gradient suggests an erosion magnitude of ~2.5 km (range ~2-3.5 km) for reset AFT samples. More specifically, the only measurement proximal to our Altiplano

Figure 3.10. Thermochronologic constraints on the exhumation history across the central Andean fold-thrust belt at 19.5-21.5ºS. AL = Altiplano, BTB = back-thrust belt, FTB = fore-thrust belt. (A) Distribution of recorded rapid cooling episodes inferred from apatite fission-track (AFT) data compiled from this study and others. See legend for appropriate references. Range of acceptable (open boxes) and good (gray boxes) fits from inverse modeling of the AFT data for the onset of rapid cooling for this study as well as summary results (dashed boxes) from Figure 12 of Ege et al. [2007], Figure 2 of Ege et al. [2003], and page 24 of Moretti et al. [1996]. (B) Estimated exhumation magnitudes. Assumed surface temperature (Ts) and geothermal gradients necessary to quantify these estimates are listed at the top of each region. Assumed closure temperatures (Tc) for the different thermochronometer systems are listed in the bottom left corner. Abbreviations and references are the same as in A. Black deltas are from Figure 13 of Ege et al. [2007]. ZFT = zircon fission track. Vertical arrows indicate an upper limit due to not fully reset cooling ages. Dashed lines are estimated from the representative stratigraphy with gray bars as estimated (or inferred with question marks) depth to fully reset and concordant AFT samples from Figure 3.4. Dotted box in the SA is the most-likely estimate from the cross section for the SA where depth to AFT closure represents a maximum because the cooling ages are not fully reset. (C) Cross section is the same as in Figure 3.2B.

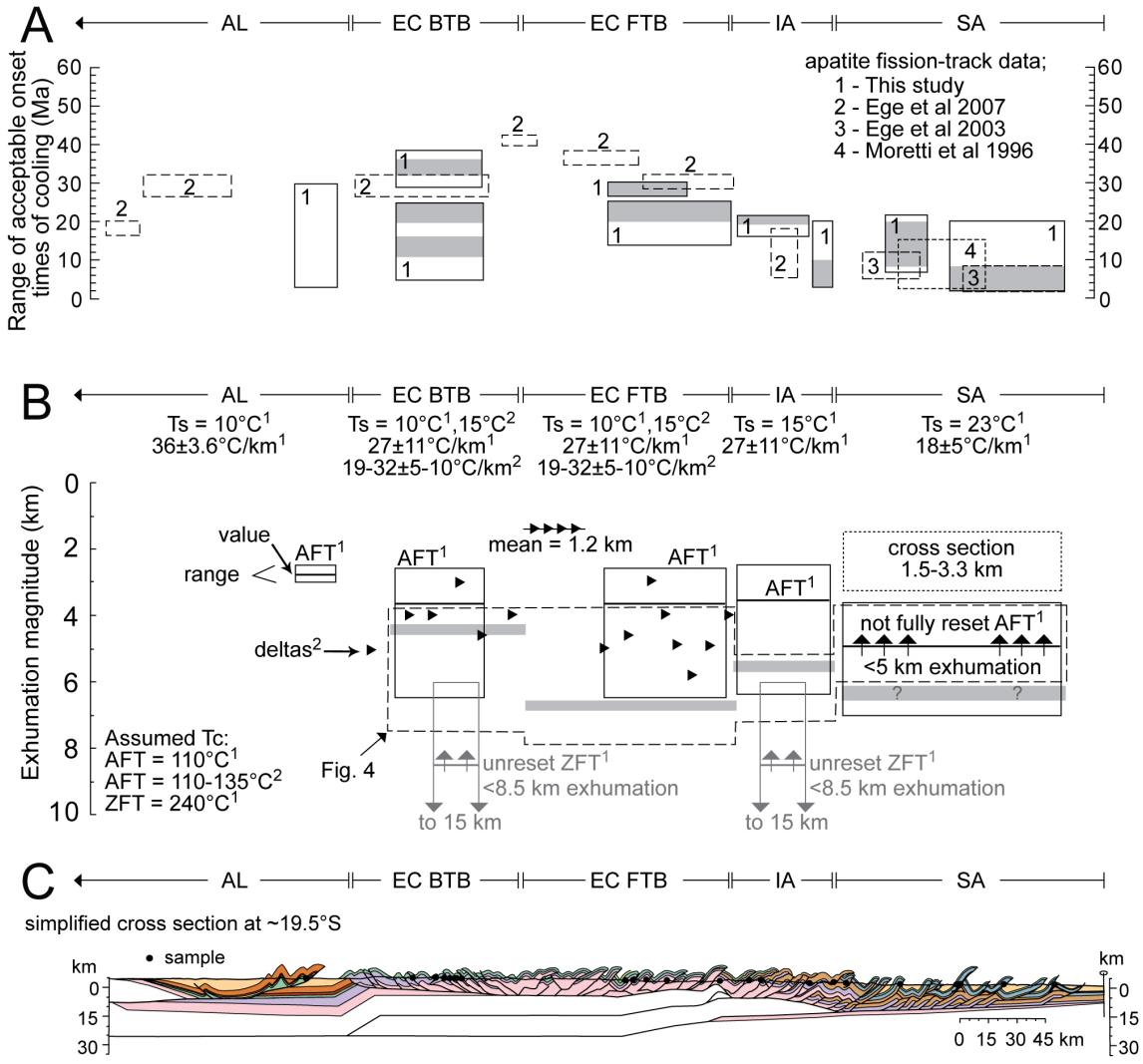
A
AL
EC BTB
EC FTB
IA
SA
Range of acceptable onset times of cooling (Ma)
apatite fission-track data;
1 - This study
2 - Ege et al 2007
3 - Ege et al 2003
4 - Moretti et al 1996
B
Ts = 10°C[1]
36±3.6°C/km[1]
Ts = 10°C[1],15°C[2]
27±11°C/km[1]
19-32±5-10°C/km[2]
Ts = 10°C[1],15°C[2]
27±11°C/km[1]
19-32±5-10°C/km[2]
Ts = 15°C[1]
27±11°C/km[1]
Ts = 23°C[1]
18±5°C/km[1]
Exhumation magnitude (km)
value
range
AFT[1]
mean = 1.2 km
cross section
1.5-3.3 km
not fully reset AFT[1]
<5 km exhumation
deltas[2]
Assumed Tc:
AFT = 110°C[1]
AFT = 110-135°C[2]
ZFT = 240°C[1]
Fig. 4
unreset ZFT[1]
<8.5 km exhumation
to 15 km
C
simplified cross section at ~19.5°S
sample
km
0 15 30 45 km

sample is located ~50 km away at Nasama and has a gradient of 36ºC/km ± 10% heat flow error [Henry and Pollack, 1988]. From this value, we estimate an exhumation magnitude of ~2.8 km ranging from ~2.5-3 km (Fig. 3.10B). In comparison, previously estimated Oligocene paleo-geothermal gradients in the Altiplano to the south range from 26-32ºC/km±~20% [Ege et al., 2007] suggesting this exhumation magnitude estimate is a minimum.

In the Bolivian Eastern Cordillera, twelve measurements constrain a mean thermal gradient of 26±8 (1σ)ºC/km [Henry and Pollack, 1988]. The lower EC thermal gradient relative to the Altiplano is probably due to the large topographic effect from the higher relief (Fig. 3.1). The 26±8 (1σ) ºC/km gradient suggests an erosion magnitude of 3.9 km (range 3-~5.5 km) for reset AFT samples and 9 km (range 7-13 km) if any of the ZFT samples had been reset. More specifically, three most proximal measurements to our EC samples are located ~100-150 km to the south and estimate a similar mean gradient of 27±11ºC/km, but larger uncertainty (stations Choroloque, Tatasi, and Chilcobija from Henry and Pollack [1988]). This decreases the erosion magnitude estimate to 3.7 km and the range from 2.6-6.5 km for AFT and ~8.5 km with a range of 6-15 km for ZFT (Fig. 3.10B). Estimated EC Oligocene paleo-geothermal gradients to the south are similar, ranging from 19-32ºC/km±~20% [Ege et al., 2007].

Unfortunately, no thermal gradient measurements exist for the IA. Therefore, we assume the gradient is the same as the EC at 27±11ºC/km with equivalent estimated erosion magnitudes (Fig. 3.10B). The estimated IA Oligocene paleo-geothermal gradient to the south is nearly identical at 26ºC/km±~35% [Ege et al., 2007]. Regional heat flow studies treat the IA as part of the EC further justifying the assumption of similar gradients between the EC and IA [Springer and Forster, 1998; Springer, 1999].

SA sample cooling ages are not reset by the Miocene to recent deformation allowing us to estimate a depth to AFT closure as a maximum limit on SA exhumation.

Over 1500 measurements from the southern Bolivia SA and adjacent Chaco plain yield a mean geothermal gradient of 22.4ºC/km ± ~35% (Fig. 3.1) [Springer and Forster, 1998]. The low gradient is attributed to the SA being both the locus of substantial late Tertiary sedimentation and proximal to the cold, Brazilian shield to the east [Springer, 1999]. The 22.4ºC/km ± ~35% gradient suggests the SA erosion magnitude is less than ~4 km (range ~3-6 km). Locally, three measurements (stations Monteagudo, Camiri, and Guairay [Springer and Forster, 1998]) within ~50 km of our samples suggest a lower mean gradient of 18±5ºC/km indicating an average maximum exhumation magnitude of ~5 km with a range of <3.8-7 km (Fig. 3.10B).

A systematic decrease in SA sample cooling age with depth allows us to semi-quantitatively test the validity of using modern geothermal gradients to estimate erosion magnitude. We estimate the paleo-thermal gradient through which the SA samples were exhumed by assuming the reconstructed sample stratigraphic depths are correct (Fig. 3.8B), AFT closure is 110ºC, and the surface temperature is 23ºC. As we outline here, the AFT data imply the SA samples were exhumed from within a fossil AFT PAZ [e.g. Fitzgerald et al., 1995]. First, mean track lengths are shortened, range from 9.97-11.64 μm, and their variance generally increases with original stratigraphic depth. Second, the percentage of reset individual grain ages within each sample (from ~55-60% (SA3 and 6) to 100% (SA1)) increases with depth. Third, there is a systematic decrease in pooled age with depth; two shallow, late Paleozoic to early Mesozoic, concordant ages overlie two intermediate-depth samples of much younger, and more significantly reset Cretaceous age, which in turn overlie two mid-Eocene discordant ages (Fig. 3.4). Fourth, sample cooling histories indicate residence in AFT PAZ temperatures that increase with depth from ~65-90ºC (Fig. 3.8C; see also section 4.6). Finally, the youngest pooled ages (mid-Eocene) are discordant and substantially older than the maximum age of deformation in the SA (~20 Ma; [e.g. Barke, 2004; McQuarrie et al.,

2005], suggesting none of the samples were exhumed from above AFT closure by the Miocene deformation. Based on the sample depth profile, full closure must have occurred below the deepest sample at ≥6 km (grey zone in SA; Figs. 3.4 & 3.8). This suggests the SA samples resided in a paleo-PAZ with a minimum depth of 6 km to the 110ºC isotherm corresponding to a paleo-gradient of <~15ºC/km. This is within the lower bound of the modern mean gradient (18±5ºC/km) used to estimate the exhumation magnitude above.

Exhumation magnitude from the balanced section

Balanced cross sections and their restorations provide an independent method for estimating the first-order spatial variations in erosion magnitude across the thrust belt [Barnes and Pelletier, 2006; McQuarrie et al., 2008]. In brief, the balancing of rock area can be used to reconstruct the amount of material eroded by projecting the stratigraphy and structures above the present-day topography in the balanced section (Fig. 3.2). Although a simplification, dividing the estimated area removed by erosion by the modern length of the thrust belt provides an average, regional thickness of denudation. The eroded area estimates at ~19.5ºS in Table 3.4 both exclude (lower range) and include (upper range) a 3 km thick Tertiary section (similar to the modern estimate; [Horton and DeCelles, 1997]) based on preserved deposits throughout the EC that document the eastward migration of the foreland basin during the early to mid-Tertiary [DeCelles and Horton, 2003]. Estimates are 725-1285 km^2 of material removed from the 194 km-wide EC, 347-640 km^2 from the 56 km-wide IA, and 192-432 km^2 from the 130 km-wide SA (Table 3.4). Total magnitude of removed material is estimated to be 1264-2357 km^2.

Synthesis of exhumation magnitudes and rates at ~19.5ºS

Table 3.4 shows a comparison between denudation estimates derived from both the thermochronology and the cross section. Both methods produce denudation estimates for the EC that range from ~3-7 km. Although exhumation is variable across

the different EC structures, ~4-7 km is most consistent amongst the various estimates (Table 3.4 & Fig. 3.10B). Maximum exhumation of the EC is <~8.5 km constrained by several Paleozoic ZFT ages. The IA is unique in that the cross section estimate of erosion is greater than that given by the thermochronology (~3-6.5 vs. ~6-11 km) with the representative stratigraphy suggesting an intermediate value of ~5-7 km. Significant structural overlap (3-5 km) recorded in the IA may have never been expressed as burial if erosion kept pace with faulting. Thus removal of material was lateral verses vertical making the integrated "vertical" amount of exhumation an overestimate. Exhumation estimates across the IA are most likely ~4-6 km. Maximum exhumation of the IA is also <~8.5 km as constrained by two Paleozoic ZFT ages. In the SA, the cross section, closure depth, and the stratigraphy combine to both estimate and limit the exhumation magnitude. The average SA thermal gradient estimate (~5 km) is a maximum because it represents a depth to full AFT closure and none of the sample ages were fully reset by the Miocene to recent erosion and deformation. The stratigraphy estimates (4-6 km) probably represent maximums because a) sample-specific reconstructed depths are up to ~0.5 km less than these regionally averaged stratigraphic thicknesses and b) the assumption of a 3-km thick Tertiary fill might be too large. Give these considerations, we think the cross section-derived magnitude of ~3 km (1.5-3.3 km) is the best average estimate of the SA exhumation magnitude.

We estimated exhumation rates from the cross section and thermochronology-derived magnitudes assuming simplistic timescales for the duration of exhumation across each zone (Table 3.4). Rates for the EC range from ~0.1-0.2 mm/yr with a maximum of ~0.4 mm/yr averaged over the last 40 Myr. IA rates are higher ranging from ~0.1-0.6 mm/yr with a maximum of ~0.8 mm/yr averaged over the last 20 Myr. Rates for the SA range from ~0.1-0.2 mm/yr up to ~0.4 mm/yr averaged over the last 20 Myr or ~0.2-0.4 mm/yr up to ~0.9 mm/yr averaged over the last 8 Myr. However, rates on

Table 3.4. Exhumation estimates for the central Andean fold-thrust belt (~19.5°S), southern Bolivia.

	X-sect. est. (km^2)	X-sect. length (km)	X-sect. est. (km)	thermochron est. (km)	X-sect. est.# (mm/yr)	time scale from	X-sect. est. (mm/yr)	thermochron est. (mm/yr)	Ege et al^ (mm/yr)
EC	725-1285*	194	3.7-6.6	2.6-6.5, (<6-15;zft)	--	40 Ma-0	0.09-0.17	0.07-0.16, (<0.15-0.38;zft)	0.1-0.3
IA	347-640*	56	6.2-11.4	2.6-6.5, (<6-15;zft)	--	20 Ma-0	0.31-0.57	0.13-.33, (<0.30-0.75;zft)	0.4
SA	192-432#	130#	1.5-3.3	<3.8-7.0	0.08-0.17 (20-0 Ma)	20 Ma-0	0.08-0.17	<0.19-0.35	0.9-1.6
SA	192-432#	130#	1.5-3.3	<3.8-7.0	0.10-0.22 (15-0 Ma)	8 Ma - 0	0.19-0.41	<0.48-0.88	0.9-1.6
total	1264-2357#	380#	3.33-6.20	3.0-6.7 (1)	0.08-0.16 (40-0 Ma)	40 Ma-0	0.08-0.16	.08-0.17	

= from *Barnes & Pelletier* [2006]; * = from *McQuarrie et al.* [2008]; X-sect = cross section; thermochrology (thermochron) estimates (est.) from the AFT data unless noted otherwise; zft = zircon fission track; ^ derived by AFT data from *Ege et al.* [2007] and [2003] for ~21.5°S; (1) weighted average exhumation relative to each zones length as % of the total thrust belt length

individual structures could be much higher, especially the eastern SA thrust sheets if they were exhumed as recently as the Pliocene (i.e. ~5 Ma; ~0.8-1.4 mm/yr).

In summary, exhumation magnitudes generally decrease both eastward and westward from local maximums of ~6-8 km in the EC fore-thrust belt to 1.5-3.3 km in the SA and Altiplano (Fig. 3.10B). Exhumation rates range from ~0.1-0.2 mm/yr in the EC, ~0.1-0.6 mm/yr in the IA, and from ~0.1-0.4 mm/yr to 1.4 mm/yr or more in the eastern SA.

Along-strike variations in southern Bolivia/northern Argentina (19-23ºS)

The chronology of exhumation and deformation in the central Andean fold-thrust belt is generally similar, but differs in detail within an along-strike distance of ~400 km from our study area southward to northernmost Argentina (Figs. 3.1 & 3.10A). At ~21.5ºS, AFT began in the central EC during the late Eocene (36-40 Ma) followed by distributed EC deformation [Ege et al., 2007]. We document younger late Eocene to earliest Oligocene (27-36 Ma) distributed exhumation in the EC, to the east and west of the oldest cooling recorded at ~21.5ºS (Fig. 3.10A), also suggesting distributed deformation. Wedgetop basin deposits near Tupiza (~21.5ºS) suggest the EC back-thrust belt began ~34 Ma consistent with our earliest documented exhumation [Horton, 1998; Horton et al., 2002; McQuarrie et al., 2005]. Distributed exhumation existed across the entire EC at 21.5ºS during the early Oligocene (27-33 Ma) [Ege et al., 2007], whereas we document distributed exhumation throughout the late Oligocene to earliest Miocene (19-30 Ma). In both transects (19.5º & 21.5ºS), erosional cooling during these times is generally consistent with (a) mostly eastward propagation of deformation from the central EC, and (b) out-of-sequence exhumation and deformation across the EC back-thrust belt that almost completely ceased by ~20 Ma [Ege et al., 2007]. A late pulse of late Miocene (~11-16 Ma) exhumation in the EC back-thrust belt at ~19.5ºS and

10-18 Ma growth structures in the western Tupiza basin at ~21.5ºS [Horton, 1998] suggest limited deformation continued in the EC until ~10 Ma. Additionally, thermal histories from the Uyuni-Khenayani Fault zone in the central Altiplano (21.5ºS) show exhumation began ~30 Ma [Ege et al., 2007] consistent with our Altiplano sample in the Rio Mulato fold belt, the along-strike equivalent structure to the north.

During the early Miocene (18-22 Ma), the IA became active as exhumation and deformation continued uniformly along strike from 19.5-21.5ºS (Fig. 3.10A) [Ege et al., 2007]. Mid-to-late Miocene (~8-20 Ma) erosion and deformation continued into the eastern IA and western SA (Fig. 3.10A) [Moretti et al., 1996; Echavarria et al., 2003; Ege et al., 2003; Uba et al., 2006]. Unfortunately, we can only say that model-constrained cooling of sample AL1 is consistent with initial cooling anytime between the early Oligocene and Pliocene (3-30 Ma). Several lines of evidence suggest deformation in the EC and Altiplano completely ceased by 7-13 Ma, including: minor folding of late Miocene (~10-14 Ma) sediments in the Rio Mulato fold belt in the Altiplano [Kennan et al., 1995; Lamb and Hoke, 1997], elimination of growth structure evidence near Tupiza (21.5ºS) [Horton, 1998], the undeformed San Juan del Oro erosion surface (18-22+ºS) [Gubbels et al., 1993], exhumation histories in the Uyuni-Khenayani Fault zone (21.5ºS) [Ege et al., 2007], and flat-lying ignimbrites. Finally, late Miocene to Pliocene (2-8 Ma) initial exhumation and deformation occurred in the central to eastern SA and continues today (Fig. 3.10A) [see also Echavarria et al., 2003; Ege et al., 2003; Scheuber et al., 2006].

Estimated magnitudes of exhumation across the thrust belt are remarkably similar between ~19.5 and 21.5ºS (Fig. 3.10B). A variety of methods have been used to estimate exhumation magnitudes across the southern Bolivia portion of the thrust belt: vitrinite reflectance and illite crystallinity (at ~21.5ºS) [Kley and Reinhardt, 1994], representative stratigraphy (this study), mass deficits inferred from a balanced section (this study), and thermochronology (~19.5-21.5ºS) [Ege et al., 2007 and this study]. In

summary, exhumation magnitudes generally range from ~4-7 km in the EC (but may exceed that locally up to <~8.5 km) with the vitrinite and illite data suggesting, in particular, the Ordovician rocks were buried to great depths (~5-7 km) ~350 Ma, and subsequently exhumed either (a) at a constant rate to the surface or (b) to ~2-3 km depths by ~300 Ma, followed by recent rapid exhumation to the surface in the Tertiary [Kley and Reinhardt, 1994]. In the IA, exhumation estimates range from ~4-6 km (and <~8.5 km) with the Devonian rocks supposedly first buried by ~4-6 km of sediments that were later eroded by the end of the Carboniferous, and subsequently followed a similar thermal history to the SA to the present [Kley and Reinhardt, 1994]. Finally, estimates range from ~2-<5 km in the SA (Fig. 3.10B & Table 3.4) [see also Kley and Reinhardt, 1994; Ege et al., 2007]. Estimated rates of exhumation in southern Bolivia range from ~0.1-0.3 mm/yr in the EC, from ~0.1-0.6 mm/yr in the IA, and ~0.1-1.6 mm/yr in the SA (Table 3.4) [Ege et al., 2007].

Along-strike variations in Bolivia (15-21.5ºS)

Comparison of exhumation and deformation in Bolivia (15-21.5ºS) suggests a relatively cohesive evolution with some distinctive differences. For this comparison we focus on 'good-fit' thermal histories reported in the literature. In general, the Bolivia EC experienced several phases of rapid exhumation since the Eocene. Initial deformation and exhumation began in the EC during the late Eocene to earliest Oligocene (~30-40 Ma) [e.g. Gillis et al., 2006; Ege et al., 2007 and this study]. Next, the southern Altiplano and EC (19.5-21.5ºS) experienced extensive erosion and deformation throughout the Oligocene and into the earliest Miocene (~20-33 Ma) distinguished by out-of-sequence strain in the EC as demonstrated by this study and Ege et al. [2007]. Unfortunately, extreme exhumation of the northern EC fore-thrust belt has exposed the lowest Ordovician phyllites and slates [see cross section and sampling gap in Barnes et al.,

2006; McQuarrie et al., 2008] which are poorly amenable to AFT analysis (e.g. sample EC4 in Barnes et al. [2006]) and hence to date, preclude any noteworthy local constraint on the Eo-Oligocene exhumation history. Limited exhumation began in the northern IA by at least the late Oligocene (>~25 Ma), followed by substantial exhumation of the IA all along strike since the early to mid-Miocene (~15-22 Ma) [see also Ege et al., 2007; McQuarrie et al., 2008].

Latest Oligocene to earliest Miocene (~15-25 Ma) is a crucial time period in plateau development throughout Bolivia. Sediment provenance indicates eastern and western highlands suggestive of an internally drained proto-Altiplano by ~25 Ma [Horton et al., 2002]. Transition from foredeep to intermontane sedimentation ~21-25 Ma is immediately followed by a severe reduction (but not complete cessation) of upper-crustal deformation throughout the EC [Horton, 2005]. And finally, kinematic reconstructions suggest IA exhumation (and potentially the onset of SA exhumation as well) both across and along strike ~15-20 Ma is associated with the onset of lower basement deformation signifying the modern width of the plateau was established by this time [McQuarrie, 2002; Barnes et al., 2006].

The northern EC experienced a second exhumation phase during the mid-to-late Miocene (~11-15 Ma) to present [Benjamin et al., 1987; Barnes et al., 2006; Gillis et al., 2006; Safran et al., 2006; McQuarrie et al., 2008]. This young (<~28 Ma) exhumation is unrelated to deformation as constrained by the maximum age of growth structures in the local synorogenic sediments of the Luribay and Salla Formations [McFadden et al., 1985; Sempere et al., 1990; Lamb and Hoke, 1997; Kay et al., 1998; Gillis et al., 2006; McQuarrie et al., 2008]. SA exhumation began in the west ~8-20 Ma all along strike [Moretti et al., 1996; Ege et al., 2003; Barnes et al., 2006; Scheuber et al., 2006], perhaps contemporaneous with a third exhumation pulse (11-16 Ma) in the southern EC back-thrust belt (19.5ºS) related to deformation or post-deformation erosion. The

northern Altiplano experienced late Miocene exhumation and deformation between ~5-11 Ma constrained by mapping, thermochronology, sedimentology of neotectonic strata, and geochronology of volcanic rocks [Lamb and Hoke, 1997; Barnes et al., 2006; McQuarrie et al., 2008]. In contrast, the last gasps of shortening in the southern Altiplano and EC ceased by ~7-13 Ma [Gubbels et al., 1993; Kennan et al., 1995; Lamb and Hoke, 1997; Horton, 1998; Müller et al., 2002; Ege et al., 2007]. Finally, exhumation is consistent with an eastward migration through the central and eastern SA during the Mio-Pliocene (~2-8 Ma) in the south (19.5-21.5ºS) [Ege et al., 2003; Scheuber et al., 2006], but maybe more spatially uniform and somewhat earlier (~5-12 Ma at 1σ uncertainty; ~4-19 Ma at 2 σ) in the north [Barnes et al., 2006]. However, detailed analyses of structural geometries and isolated geochronology suggest some out-of-sequence deformation in the SA [Baby et al., 1995; Roeder and Chamberlain, 1995; Moretti et al., 1996; Barke, 2004].

Comparison of exhumation magnitudes along strike (15-21.5ºS) suggests most significant variations in the EC with only minor differences in the Altiplano, IA, and SA. Exhumation magnitudes for the Altiplano range from ~2-4 km [see also Barnes et al., 2006]. Reset biotite and muscovite $^{40}Ar/^{39}Ar$ and ZFT ages in the northern EC fore-thrust belt suggest ~9-11 km of Tertiary erosion [e.g. Gillis et al., 2006] whereas local maximums from the southern portion range from ~6-8 km (Fig. 3.10B) [see also Ege et al., 2007]. However, neither $^{40}Ar/^{39}Ar$ nor ZFT ages have been measured in the southern EC fore-thrust belt. Estimates for the EC back-thrust belt are ~3-6 km with unreset ZFT ages limiting the maximum to <~8.5 km (Fig. 3.10B) [McQuarrie et al., 2008]. Best estimates for the IA are ~5-9 km in the north and from ~4-6 km in the south with Paleozoic ZFT ages limiting the maximum to <~8 km in the south [see also McQuarrie et al., 2008]. Finally, estimates for the SA in the north are ~3-4 km (from reset young component AFT ages) with an upper limit of <~7 km from unreset zircon (U-

Th)/He ages [Barnes et al., 2006]. The best southern SA estimates are ~3 km by AFT samples exhumed from PAZ temperatures.

Estimated rates of deformation in Bolivia (15-19.5ºS) are similar. The EC and IA regions shortened at rates of ~7-11 mm/yr from ~25-40 Ma (Figs. 3.9 & 3.10) [see also McQuarrie et al., 2008]. The SA shortened at rates of ~4 or 8 mm/yr depending on initiation of deformation either ~15-20 Ma or ~8 Ma [McQuarrie et al., 2008]. Average shortening rates at 21.5ºS are 0-8 mm/yr 30-46 Ma, 5-10 mm/yr 10-30 Ma, and 6-14 mm/yr since 10 Ma [Elger et al., 2005; Oncken et al., 2006].

Implications for plateau growth models

The integrated exhumation and deformation record discussed above provides important constraints on central Andean plateau growth and allows associated insights into proposed models of plateau evolution. First, lithospheric weakening is commonly considered a precondition of the Eocene through Oligocene distributed deformation in the plateau region because of shortening and magmatism [e.g. Isacks, 1988; Francis and Hawkesworth, 1994; Wdowinski and Bock, 1994]. However, deformation generally precedes magmatism [e.g. Elger et al., 2005; Ege et al., 2007 and this study] and the regional time-space distribution of deformation and magmatism precludes a direct connection between the two because they vary independently [Trumbull et al., 2006]. Second, the proposal that mantle delamination caused 2-3+ km of rapid Andean plateau surface uplift ~6-10 Ma also implies concomitant eastward propagation of accelerated deformation into the SA [Garzione et al., 2006; Ghosh et al., 2006]. The SA exhumation and deformation history is certainly consistent with activation ~8 Ma [Echavarria et al., 2003; Ege et al., 2003; Barnes et al., 2006; Scheuber et al., 2006]. However, several western SA thermochronometer samples are also consistent with earlier initial cooling ~10-20 Ma [Barnes et al., 2006 and this study] implying a more gradual eastward

migration of deformation from the IA starting ~20 Ma which may not be consistent with the delamination model.

We interpret the central Andean fold-thrust belt to be deforming as a Coulomb wedge which seeks to maintain taper by both eastward propagation and out-of-sequence deformation [Dahlen and Suppe, 1988; Dahlen, 1990; Willett, 1992]. The early Eo-Oligocene distributed plateau region deformation could represent episodes of alternating wedge conditions leading to both propagation and significant internal deformation, whereas the eastward propagation since ~20 Ma could represent a more stable condition promoting advance at a potentially reduced rate (Table 3.4). Evidence of out-of-sequence SA deformation ≤6 Ma [Moretti et al., 1996; Barke, 2004] suggests some relatively recent readjustments of the wedge to rebuilt taper. The history and changing modes of deformation of a central Andes ancient analogue, the Nevadaplano and Sevier fold-thrust belt in the western US [e.g. DeCelles, 2004], has been previously interpreted this way [DeCelles and Mitra, 1995]. The latitudinal contrast in erosion, which is believed to have existed since potentially as early as the late Miocene [Horton, 1999; Barnes and Pelletier, 2006], is probably effecting the wedge as suggested by (a) a larger magnitude of concentrated exhumation in the northern EC (~9-11 km) compared to more distributed and limited exhumation in the south (<~8.5 km) constrained by ZFT and $^{40}Ar/^{39}Ar$ thermochronometers [Benjamin et al., 1987; Gillis et al., 2006] and (b) younger and mixed reset AFT cooling ages in the northern SA [Barnes et al., 2006] compared to the unreset and discordant Mesozoic AFT cooling ages in the southern SA [Scheuber et al., 2006 and this study].

Summary and conclusions

This study presents 23 new apatite and zircon fission-track (AFT & ZFT) analyses spanning the entire central Andean fold-thrust belt at its widest extent in Bolivia

at ~19.5ºS. Exhumation histories were quantified with thermal modeling, interpreted in the context of the regional geology, stratigraphy, geothermal gradients, and mass deficits inferred from a balanced section, and then integrated with previous kinematic reconstructions and associated foreland basin deposits to refine the chronology and rate of deformation. Primary conclusions of this study are:

1. Cooling histories inverted from the AFT data are consistent with Eocene to recent rapid cooling: (a) Distributed exhumation of the Eastern Cordillera (EC) occurred in the late Eocene to earliest Oligocene (27-36 Ma) and continued during the late Oligocene to early Miocene (19-25 Ma), (b) Exhumation of the eastern Altiplano began anytime from 3-30 Ma, (c) Exhumation across most of the Interandean zone (IA) began 19-22 Ma, (d) Exhumation of the western Subandes (SA) began 8-20 Ma, perhaps contemporaneous with a third exhumation pulse (11-16 Ma) in the EC back-thrust belt, and (e) Exhumation of the central-to-eastern SA propagated eastward during the late Mio-Pliocene (2-8 Ma).

2. The exhumation chronologies characterize EC deformation as distributed, as opposed to previous kinematic reconstructions that assumed in-sequence deformation in the direction of transport. However, Miocene to recent (~0-20 Ma) exhumation of the IA and SA is consistent with in-sequence deformation progressing eastward towards the Chaco foreland. We propose that the propagation of deformation from the EC towards the SA, marked by uniform IA exhumation 19-22 Ma, indicates a switch from a higher to lower basement structure. The cessation of most EC exhumation signifies establishment of the modern Andean plateau width and substantial crustal thickness briefly thereafter by ~15-20 Ma.

3. Exhumation magnitudes decrease laterally from local maximums of <8 km in the EC fore-thrust belt to average values of ~4-7 km. Magnitudes are ~2.5-3 km in the Altiplano, ~4-6 km in the IA, and ~3 km in the SA. Paleozoic ZFT ages constrain maximum exhumation of the EC back-thrust belt and IA to <~8.5 km.

4. Shortening rates across the EC and IA from 40 to 10-20 Ma range from ~7-11 mm/yr. Shortening rates across the SA since 8 or 20 Ma range from ~9 to ~4 mm/yr. These rates suggest the Miocene to recent rates either decreased by half from the long-term average of ~8 mm/yr or remained about the same or slightly increased depending on the age of initial SA deformation and the end of EC deformation.

Finally, we draw three important generalizations from the integrated record of central Andean fold-thrust belt exhumation, deformation, and sedimentation throughout Bolivia: (A) Deformation began in the EC ~35-40 Ma and continued in a distributed manner throughout the Altiplano and EC regions until ~20-25 Ma with minor, isolated deformation continuing until ~10 Ma. (B) Uniform exhumation in the southern IA ~18-22 Ma signifies establishment of the modern width of the Andean plateau with unknown, but significant crustal thickness shortly thereafter by ~15-20 Ma. (C) From ~20 Ma to present, deformation mostly propagated eastward from the IA with evidence for minor out-of-sequence deformation in the central- to-eastern SA.

Acknowledgements

We thank SERGEOTECMIN of La Paz, Bolivia and especially Jaime Tito for logistical support. Nadja Insel assisted in the field. Financial support was provided to T. Ehlers by NSF grant EAR 0409289 and by a University of Michigan Scott Turner Award in the Earth Sciences to J. Barnes. Discussions with B. Horton were also helpful.

Reviews by J. Spotila, V. Ramos, and associate editor M. Rushmore greatly improved the manuscript.

Appendix 3.1. Representative stratigraphy

Representative stratigraphic sections were constructed from measurements of the balanced and restored section of McQuarrie [2002] (Figs. 3.2 & 3.4). We describe the methodology proceeding from west to east and upsection from the Ordovician through the Tertiary. Stratigraphic thicknesses and sample location errors are estimated to be ±~20% arbitrarily, but are not included for brevity.

We estimate the average thickness of the Ordovician at 5.5 km in the EC. The Silurian thins eastward from 4.2-1.2 km with averages of 2725 m and 1500 m for the back-thrust and fore-thrust zones, respectively. The Devonian is absent in most of the EC except for the eastern margin where it thickens rapidly to a maximum of 1650 m at the EC-IA boundary for an average of 825 m in the EC fore-thrust belt. Presumably, the EC Devonian rocks were eroded in pre-Mesozoic time [McQuarrie and DeCelles, 2001]. The Carboniferous section is missing, the Mesozoic rocks are ~1500 m thick, and Tertiary rocks are only present locally [e.g. Horton, 2005].

The Ordovician thins eastward (4.15-1.65 km) with an average thickness of 2.9 km in the IA. The Silurian thins eastward from 2.5-1.25 km for an average of 1875 m. The average Devonian thickness is 2.5 km because it thickens eastward from 1.65 to 3.35 km. The Carboniferous is absent here. The Mesozoic rocks range from 850 m thick to absent from east to west for an average of 425 m. Tertiary rocks are not present regionally.

Minimal Devonian is exposed in the SA, but it supposedly thins from 3950-500 m for an average of 2225 m. The average Carboniferous thickness is 1700 because it ranges from 1150-2250 m. Mesozoic units range from 520-1200 m thick for an average

of 860 m. Finally, Tertiary sediment thicknesses vary greatly among the constraints, but average 3 km with a range from 2-4 km.

Studies tracked the early-mid Tertiary migration of the central Andean foreland basin system as a proxy of the hinterland thrust belt evolution [DeCelles and Horton, 2003; Horton, 2005; McQuarrie et al., 2005]. This suggests that Tertiary foreland deposits existed outboard the thrust belt to the east which was subsequently uplifted and mostly eroded from the EC and IA. Consequently, we assume a uniform 3 km-thick Tertiary foreland section from the EC through the SA in our representative sections [after Barnes and Pelletier, 2006].

Appendix 3.2. Analytical procedures

Mineral separations and fission-track analyses were performed using standard techniques by Apatite to Zircon, Inc. Apatite and zircon concentrates were created using standard heavy-liquid techniques [see Appendix 1 of Donelick et al., 2005]. Apatite grains were immersed in an epoxy resin that was cured at 90°C for 1 hour. The cured mounts were polished to expose grain surfaces, followed by etching in 5.5N HNO_3 for 20.0 seconds (± 0.5 seconds) at 21°C (± 1°C) to reveal all natural fission tracks. Zircon grains were mounted in FEP Teflon. The zircon mounts were also polished followed by immersion in a eutectic melt of NaOH + KOH at ~210°C (± 10°C) for ~37 hours and 10 minutes to adequately reveal the naturally occurring tracks.

Most AFT analyses and all ZFT analyses presented here used the laser ablation (LA-ICPMS) method of Donelick et al. [2005]. Age standards used to calculate the LA-ICPMS zeta calibration factor were (1) Durango apatite (30.6±0.3 Ma) from Cerro de Mercado, Mexico, and (2) Fish Canyon zircon (27.9±0.7 Ma) from the San Juan Mountains, Colorado. AFT sample 713-5B and 714-1B analyses used the external

detector method [e.g. Gallagher et al., 1998]. The age standard used to calculate the traditional zeta factor was the same Durango apatite. A zeta calibration factor of 113.8 ± 2.9 (1σ) (for RAD) was used.

Following age analysis, grain mounts were irradiated by a ^{252}Cf source in a vacuum to enhance the measurability of the natural tracks [Donelick and Miller, 1991]. The irradiated grain mounts were re-immersed in 5.5N HNO_3 for 20.0 seconds (± 0.5 seconds) at 21°C (± 1°C) to reveal any horizontal, confined tracks. Both the track lengths and their angle relative to the crystallographic c-axis were recorded. For each apatite grain age and track length, a mean Dpar value was determined from 1-4 measurements.

Appendix 3.3. AFT data analysis and thermal modeling

We used BinomFit to deconvolve the component ages for sample 714-1B because it is both discordant and was analyzed with the external detector method. The new LA-ICPMS-derived data is not compatible with BinomFit because a non-Poissonian counting process is used in the measurement of the U, Ca, and Si isotopes, and thus the same statistical techniques can not be applied. Consequently, we conservatively modeled all the remaining sample AFT data as one kinetic population.

We conducted inverse thermal modeling of the AFT data with HeFTy beta version 6 [Ehlers et al., 2005; Ketcham, 2005] with the ^{252}Cf irradiation option activated. We used 2σ uncertainty, included Dpar values, and both the traditional zeta and LA-ICPMS ratio methods as appropriate with the age and length data.

For each sample, an initial, open-ended model was performed with all sample data as one kinetic population with (a) a starting temperature of 200ºC at a time that is 50 Myrs older than deposition and (b) 20ºC at present. This model was run to assess how distinct the recent cooling history is without bias from multiple user-defined

constraints. Next, a more refined model was run by imposing additional geologic constraints such as a fixed 10-30ºC temperature equal to the deposition age and a fixed 50-180ºC temperature equal in age to either (a) the 2σ range in the concordant pooled age or the 2σ range in discordant component age(s) (if available), or (b) between the sample depositional age and 1 Ma for discordant samples to allow for the maximum flexibility in attempted thermal history paths explored. These models defined the envelope of permissible thermal histories given the samples' local geologic context. Since we cannot delineate component ages and kinetic populations for discordant samples, we followed this conservative approach and report the refined model results. This approach allows for identification of the full range of sample cooling histories permitted by all measured ages and track lengths.

Modeled thermal history segments were designated as episodic style, monotonic, and random spacing with halved 5 times (5E) to provide the most simple, yet flexible ("allowed complexity") style of cooling paths between constraints [Ketcham, 2005]. A 40ºC/My maximum cooling/heating rate was imposed on all segments. Inversions were run with a Monte Carlo search and 50,000 attempted paths.

References

Allmendinger, R. W., and T. L. Gubbels (1996), Pure and simple shear plateau uplift, Altiplano-Puna, Argentina and Bolivia, Tectonophysics, v. 259, 1-13.

Allmendinger, R. W., T. E. Jordan, S. M. Kay, and B. L. Isacks (1997), The evolution of the Altiplano-Puna Plateau of the Central Andes, Annual Review of Earth and Planetary Sciences, v. 25, 139-174.

Baby, P., R. Limachi, I. Moretti, E. Mendez, J. Oller, B. Guiller, and M. Specht (1995), Petroleum system of the northern and central Bolivian sub-Andean zone, in Petroleum basins of South America, A. J. Tankard, R. Suarez and H. J. Welsink (ed.), American Association of Petroleum Geologists Memoir 62, 445-458.

Barke, R. (2004), Late Cenozoic tectonic and topographic evolution of the Bolivian Andes, PhD thesis, 380 pp, University of Oxford, Oxford, England.

Barke, R., and S. Lamb (2006), Late Cenozoic uplift of the Eastern Cordillera, Bolivian Andes, Earth and Planetary Science Letters, v. 249, 350-367.

Barke, R., S. Lamb, and C. MacNiocaill (2007), Late Cenozoic bending of the Bolivian Andes: New paleomagnetic and kinematic constraints, Journal of Geophysical Research, v. 112, doi:10.1029/2006JB004372.

Barnes, J. B., T. A. Ehlers, N. McQuarrie, P. B. O'Sullivan, and J. D. Pelletier (2006), Variations in Eocene to recent erosion across the central Andean fold-thrust belt, northern Bolivia: Implications for plateau evolution, Earth and Planetary Science Letters, v. 248, 118-133.

Barnes, J. B., and J. D. Pelletier (2006), Latitudinal variation of denudation in the evolution of the Bolivian Andes, American Journal of Science, v. 306, 1-31.

Beaumont, C., R. A. Jamieson, M. H. Nguyen, and B. Lee (2001), Himalayan tectonics explained by extrusion of a low-viscosity crustal channel coupled to focused surface denudation, Nature, v. 414, 738-742.

Beck, S. L., and G. Zandt (2002), The nature of orogenic crust in the central Andes, Journal of Geophysical Research, v. 107, doi:10.1029/2000JB000124.

Benjamin, M. T., N. M. Johnson, and C. W. Naeser (1987), Recent rapid uplift in the Bolivian Andes; evidence from fission-track dating, Geology, v. 15, 680-683.

Brandon, M. T. (1992), Decomposition of fission-track grain-age distributions, American Journal of Science, v. 292, 535-564.

Brandon, M. T. (2002), Decomposition of mixed grain age distributions using BinomFit, On Track, v. 24, 13-18.

Brandon, M. T., M. K. Roden-Tice, and J. I. Garver (1998), Late Cenozoic exhumation of the Cascadia accretionary wedge in the Olympic Mountains, Northwest Washington State, Geological Society of America Bulletin, v. 110, 985-1009.

Burtner, R. L., A. Nigrini, and R. A. Donelick (1994), Thermochronology of Lower Cretaceous source rocks in the Idaho-Wyoming thrust belt, American Association of Petroleum Geologists Bulletin, v. 78, 1613-1636.

Carlson, W. D., R. A. Donelick, and R. A. Ketcham (1999), Variability of apatite fission-track annealing kinetics; I, Experimental results, American Mineralogist, v. 84, 1213-1223.

Coudert, L., M. Frappa, C. Viguier, and R. Arias (1995), Tectonic subsidence and crustal flexure in the Neogene Chaco Basin of Bolivia, Tectonophysics, v. 243, 277-292.

Coughlin, T. J., P. B. O'Sullivan, B. P. Kohn, and R. J. Holcombe (1998), Apatite fission-track thermochronology of the Sierras Pampeanas, central western Argentina; implications for the mechanism of plateau uplift in the Andes, Geology, v. 26, 999-1002.

Dahlen, F. A. (1990), Critical taper model of fold-and-thrust belts and accretionary wedges, Annual Review of Earth and Planetary Sciences, v. 18, 55-99.

Dahlen, F. A., and J. Suppe (1988), Mechanics, growth, and erosion of mountain belts, in Processes in continental lithospheric deformation, S. P. Clark, Jr., B. C. Burchfiel and J. Suppe (ed.), Geological Society of America Special Paper, 161-178.

DeCelles, P. G. (2004), Late Jurassic to Eocene evolution of the Cordilleran thrust belt and foreland basin system, western U.S.A, American Journal of Science, v. 304, 105-168.

DeCelles, P. G., and B. K. Horton (2003), Early to middle Tertiary foreland basin development and the history of Andean crustal shortening in Bolivia, Geological Society of America Bulletin, v. 115, 58-77.

DeCelles, P. G., and G. Mitra (1995), History of the Sevier orogenic wedge in terms of critical taper models, Northeast Utah and Southwest Wyoming, Geological Society of America Bulletin, v. 107, 454-462.

Dobson, M. H. (1973), Closure temperature in cooling geochronological and petrological systems, Contributions to Mineralogy and Petrology, v. 40, 259-274.

Donelick, R. A., and D. S. Miller (1991), Enhanced TINT fission track densities in low spontaneous track density apatites using ^{252}Cf-derived fission fragment tracks: A model and experimental observations, Nuclear Tracks and Radiation Measurements, v. 18, 301-307.

Donelick, R. A., P. B. O'Sullivan, and R. A. Ketcham (2005), Apatite Fission-Track Analysis, in Low-Temperature Thermochronology: Techniques, Interpretations, and Applications, P. W. Reiners and T. A. Ehlers (ed.), Mineralogical Society of America, Chantilly, VA, 49-94.

Dunn, J. F., K. G. Hartshorn, and P. W. Hartshorn (1995), Structural styles and hydrocarbon potential of the sub-Andean thrust belt of southern Bolivia, in Petroleum basins of South America, A. J. Tankard, R. Suarez and H. J. Welsink (ed.), American Association of Petroleum Geologists Memoir 62, 523-543.

Echavarria, L., R. Hernandez, R. Allmendinger, and J. Reynolds (2003), Subandean thrust and fold belt of northwestern Argentina; geometry and timing of the Andean evolution, American Association of Petroleum Geologists Bulletin, v. 87, 965-985.

Ege, H., E. R. Sobel, V. Jacobshagen, E. Scheuber, and D. Mertmann (2003), Exhumation history of the central Andes of southern Bolivia by apatite fission track dating, Revista Tecnica de Yacimientos Petroliferos Fiscales Bolivianos, v. 21, 165-172.

Ege, H., E. R. Sobel, E. Scheuber, and V. Jacobshagen (2007), Exhumation history of the southern Altiplano plateau (southern Bolivia) constrained by apatite fission-track thermochronology, Tectonics, v. 26, doi:10.1029/2005TC001869.

Ehlers, T. A. (2005), Crustal thermal processes and the interpretation of thermochronometer data, in Low-Temperature Thermochronology: Techniques, Interpretations, and Applications, P. W. Reiners and T. A. Ehlers (ed.), Mineralogical Society of America, Chantilly, VA, 315-350.

Ehlers, T. A., T. Chaudhri, S. Kumar, C. W. Fuller, S. D. Willett, R. A. Ketcham, M. T. Brandon, D. X. Belton, B. P. Kohn, A. J. W. Gleadow, T. J. Dunai, and F. Q. Fu (2005), Computational tools for low-temperature thermochronometer interpretation, in Low-Temperature Thermochronology: Techniques, Interpretations, and Applications, P. W. Reiners and T. A. Ehlers (ed.), Mineralogical Society of America, Chantilly, VA, 589-622.

Elger, K., O. Oncken, and J. Glodny (2005), Plateau-style accumulation of deformation: Southern Altiplano, Tectonics, v. 24, doi:10/1029/2004TC001675.

Fitzgerald, P. G., R. B. Sorkhabi, T. F. Redfield, and E. Stump (1995), Uplift and denudation of the central Alaska Range; a case study in the use of apatite fission track thermochronology to determine absolute uplift parameters, Journal of Geophysical Research, v. 100, 20175-20191.

Francis, P. W., and C. J. Hawkesworth (1994), Late Cenozoic rates of magmatic activity in the Central Andes and their relationships to continental crust formation and thickening, Journal of the Geological Society of London, v. 151, 845-854.

Gagnier, P. Y., A. Blieck, C. C. Emig, T. Sempere, D. Vachard, and M. Vanguestaine (1996), New paleontological and geological data on the Ordovician and Silurian of Bolivia, Journal of South American Earth Sciences, v. 9, 329-347.

Galbraith, R. F. (1981), On statistical models for fission track counts, Journal of the International Association for Mathematical Geology, v. 13, 471-478.

Gallagher, K., R. Brown, and C. Johnson (1998), Fission track analysis and its applications to geological problems, Annual Review of Earth and Planetary Sciences, v. 26, 519-572.

Garzione, C. N., P. Molnar, J. Libarkin, and B. MacFadden (2006), Rapid late Miocene rise of the Bolivian Altiplano: Evidence for removal of mantle lithosphere, Earth and Planetary Science Letters, v. 241, 543-556.

Gephart, J. (1994), Topography and subduction geometry in the central Andes; clues to the mechanics of a noncollisional orogen, Journal of Geophysical Research, v. 99, 12279-12288.

Ghosh, P., C. N. Garzione, and J. M. Eiler (2006), Rapid uplift of the Altiplano revealed through ^{13}C-^{18}O bonds in paleosol carbonates, Science, v. 311, 511-515.

Gillis, R. J., B. K. Horton, and M. Grove (2006), Thermochronology, geochronology, and upper crustal structure of the Cordillera Real: Implications for Cenozoic exhumation of the central Andean plateau, Tectonics, v. 25, doi:10.1029/2005TC001887.

Green, P. F. (1981), A new look at statistics in fission-track dating, Nuclear Tracks and Radiation Measurements, v. 5, 77-86.

Gubbels, T. L., B. L. Isacks, and E. Farrar (1993), High-level surfaces, plateau uplift, and foreland development, Bolivian central Andes, Geology, v. 21, 695-698.

Hamza, V. M., F. J. S. S. Dias, A. J. L. Gomes, and Z. G. D. Terceros (2005), Numerical and functional representations of regional heat flow in South America, Physics of the Earth and Planetary Interiors, v. 152, 223-256.

Hamza, V. M., and M. Muñoz (1996), Heat flow map of South America, Geothermics, v. 25, 599-646.

Hasebe, N., A. Carter, A. J. Hurford, J. Barbarand, and K. Jarvis (2004), Apatite fission-track chronometry using laser ablation ICP-MS, Chemical Geology, v. 207, 135-145.

Henry, S. G., and H. N. Pollack (1988), Terrestrial heat flow above the Andean subduction zone in Bolivia and Peru, Journal of Geophysical Research, v. 93, 15153-15162.

Hodges, K. V. (2003), Geochronology and Thermochronology in Orogenic Systems, in Treatise on Geochemistry, R. L. Rudnick (ed.), Elsevier, 263-292.

Horton, B. K. (1998), Sediment accumulation on top of the Andean orogenic wedge; Oligocene to late Miocene basins of the Eastern Cordillera, southern Bolivia, Geological Society of America Bulletin, v. 110, 1174-1192.

Horton, B. K. (1999), Erosional control on the geometry and kinematics of thrust belt development in the central Andes, Tectonics, v. 18, 1292-1304.

Horton, B. K. (2005), Revised deformation history of the central Andes: Inferences from Cenozoic foredeep and intermontane basins of the Eastern Cordillera, Bolivia, Tectonics, v. 24, doi:10.1029/2003TC001619.

Horton, B. K., and P. G. DeCelles (1997), The modern foreland basin system adjacent to the Central Andes, Geology, v. 25, 895-898.

Horton, B. K., B. A. Hampton, B. N. Lareau, and E. Baldellon (2002), Tertiary provenance history of the northern and central Altiplano (Central Andes, Bolivia); a detrital record of plateau-margin tectonics, Journal of Sedimentary Research, v. 72, 711-726.

Horton, B. K., B. A. Hampton, and G. L. Waanders (2001), Paleogene synorogenic sedimentation in the Altiplano Plateau and implications for initial mountain building in the Central Andes, Geological Society of America Bulletin, v. 113, 1387-1400.

Hulka, C., K.-U. Grafe, B. Sames, C. E. Uba, and C. Heubeck (2006), Depositional setting of the Middle to Late Miocene Yecua Formation of the Chaco Foreland Basin, southern Bolivia, Journal of South American Earth Sciences, v. 21, 135-150.

Iaffaldano, G., H.-P. Bunge, and T. H. Dixon (2006), Feedback between mountain belt growth and plate convergence, Geology, v. 34, 893-896.

Instituto Geografico Militar (2000), Digital Atlas of Bolivia, La Paz, Bolivia, CDROM.

Isacks, B. L. (1988), Uplift of the Central Andean Plateau and bending of the Bolivian Orocline, Journal of Geophysical Research, v. 93, 3211-3231.

Jordan, T. E., J. H. Reynolds, III, and J. P. Erikson (1997), Variability in age of initial shortening and uplift in the Central Andes, in Tectonic uplift and climate change, W. F. Ruddiman (ed.), Plenum Press, New York, 41-61.

Kay, R. F., B. J. MacFadden, R. H. Madden, H. Sandeman, and F. Anaya (1998), Revised age of the Salla beds, Bolivia, and its bearing on the age of the Deseadan South American Land Mammal "Age", Journal of Vertebrate Paleontology, v. 18, 189-199.

Kennan, L., S. Lamb, and J. Rundle (1995), K-Ar dates from the Altiplano and Cordillera Oriental of Bolivia; implications for Cenozoic stratigraphy and tectonics, Journal of South American Earth Sciences, v. 8, 163-186.

Kennan, L., S. H. Lamb, and L. Hoke (1997), High-altitude palaeosurfaces in the Bolivian Andes; evidence for late Cenozoic surface uplift, in Palaeosurfaces; recognition, reconstruction and palaeoenvironmental interpretation, M. Widdowson (ed.), Special Publication of the Geological Society 120, London, 307-323.

Ketcham, R. A. (2003), Observations on the relationship between crystallographic orientation and biasing in apatite fission-track measurements, American Mineralogist, v. 88, 817-829.

Ketcham, R. A. (2005), Forward and inverse modeling of low-temperature thermochronometry data, in Low-Temperature Thermochronology: Techniques, Interpretations, and Applications, P. W. Reiners and T. A. Ehlers (ed.), Mineralogical Society of America, Chantilly, VA, 275-314.

Ketcham, R. A., R. A. Donelick, and W. D. Carlson (1999), Variability of apatite fission-track annealing kinetics; III, Extrapolation to geological time scales, American Mineralogist, v. 84, 1235-1255.

Ketcham, R. A., R. A. Donelick, and M. B. Donelick (2000), AFTSolve; a program for multi-kinetic modeling of apatite fission-track data, Geological Materials Research, v. 2, 1-32.

Kley, J. (1996), Transition from basement-involved to thin-skinned thrusting in the Cordillera Oriental of southern Bolivia, Tectonics, v. 15, 763-775.

Kley, J. (1999), Geologic and geometric constraints on a kinematic model of the Bolivian Orocline, Journal of South American Earth Sciences, v. 12, 221-235.

Kley, J., and C. R. Monaldi (1998), Tectonic shortening and crustal thickness in the Central Andes; how good is the correlation?, Geology, v. 26, 723-726.

Kley, J., C. R. Monaldi, and J. A. Salfity (1999), Along-strike segmentation of the Andean foreland; causes and consequences, Tectonophysics, v. 301, 75-94.

Kley, J., J. Mueller, S. Tawackoli, V. Jacobshagen, and E. Manutsoglu (1997), Pre-Andean and Andean-age deformation in the Eastern Cordillera of southern Bolivia, Journal of South American Earth Sciences, v. 10, 1-19.

Kley, J., and M. Reinhardt (1994), Geothermal and tectonic evolution of the Eastern Cordillera and the Subandean Ranges of southern Bolivia, in Tectonics of the southern central Andes: structure and evolution of an active continental margin, K. J. Reutter, E. Scheuber and P. J. Wigger (ed.), Springer-Verlag, Berlin, 155-170.

Lamb, S., and P. Davis (2003), Cenozoic climate change as a possible cause for the rise of the Andes, Nature, v. 425, 792-797.

Lamb, S., and L. Hoke (1997), Origin of the high plateau in the Central Andes, Bolivia, South America, Tectonics, v. 16, 623-649.

Masek, J. G., B. L. Isacks, T. L. Gubbels, and E. J. Fielding (1994), Erosion and tectonics at the margins of continental plateaus, Journal of Geophysical Research, v. 99, 13941-13956.

McFadden, B. J., K. E. Campbell, R. L. Ciffelli, O. Siles, N. M. Johnson, C. W. Naeser, and P. K. Zeitler (1985), Magnetic polarity stratigraphy and mammalian fauna of the Deseadan (late Oligocene-early Miocene) Salla beds of northern Bolivia, Journal of Geology, v. 93, 233-250.

McQuarrie, N. (2002), The kinematic history of the central Andean fold-thrust belt, Bolivia; implications for building a high plateau, Geological Society of America Bulletin, v. 114, 950-963.

McQuarrie, N., J. B. Barnes, and T. A. Ehlers (2008), Geometric, kinematic, and erosional history of the central Andean Plateau, Bolivia (15-17ºS), Tectonics, doi:10.1029/2006TC002054, in press.

McQuarrie, N., and G. H. Davis (2002), Crossing the several scales of strain-accomplishing mechanisms in the hinterland of the central Andean fold-thrust belt, Bolivia, Journal of Structural Geology, v. 24, 1587-1602.

McQuarrie, N., and P. G. DeCelles (2001), Geometry and structural evolution of the central Andean backthrust belt, Bolivia, Tectonics, v. 20, 669-692.

McQuarrie, N., B. K. Horton, G. Zandt, S. Beck, and P. G. DeCelles (2005), Lithospheric evolution of the Andean fold-thrust belt, Bolivia, and the origin of the central Andean plateau, Tectonophysics, v. 399, 15-37.

Molnar, P., P. England, and J. Martinod (1993), Mantle dynamics, uplift of the Tibetan Plateau, and the Indian monsoon, Reviews of Geophysics, v. 31, 357-396.

Montgomery, D. R., G. Balco, and S. D. Willett (2001), Climate, tectonics, and the morphology of the Andes, Geology, v. 29, 579-582.

Moretti, I., P. Baby, E. Mendez, and D. Zubieta (1996), Hydrocarbon generation in relation to thrusting in the Sub Andean Zone from 18 to 22ºS, Bolivia, Petroleum Geoscience, v. 2, 17-28.

Müller, J. P., J. Kley, and V. Jacobshagen (2002), Structure and Cenozoic kinematics of the Eastern Cordillera, southern Bolivia (21ºS), Tectonics, v. 21, doi: 10.1029/2001TC001340.

Oncken, O., D. Hindle, J. Kley, K. Elger, P. Victor, and K. Schemmann (2006), Deformation of the central Andean upper plate system - facts, fiction, and constraints for plateau models, in The Andes: Active Subduction Orogeny, O. Oncken, G. Chong, G. Franz, P. Giese, H.-J. Gotze, V. A. Ramos, M. R. Strecker and P. Wigger (ed.), Springer-Verlag, Berlin, 3-27.

Pardo-Casas, F., and P. Molnar (1987), Relative motion of the Nazca (Farallon) and South American plates since Late Cretaceous time, Tectonics, v. 6, 233-248.

Press, W. H., B. P. Flannery, S. A. Teukolsky, and W. T. Vetterling (1992), Numerical Recipes in C, 1020 pp., Cambridge University Press.

Ramos, V. A., T. Zapata, E. O. Cristallini, and A. Introcaso (2004), The Andean thrust system; latitudinal variations in structural styles and orogenic shortening, in Thrust Tectonics and Hydrocarbon Systems, K. R. McClay (ed.), American Association of Petroleum Geologists Memoir 82, 30-50.

Reiners, P. W., and M. T. Brandon (2006), Using Thermochronology to Understand Orogenic Erosion, Annual Reviews of Earth and Planetary Sciences, v. 34, 419-466.

Riera-Kilibarda, C., R. Roessling, and H. G. Mylius (1994), Geologia del Campo Volcanico Los Frailes-Kari Kari y la Franja Metalifera entre Potosi y Tupiza, edited by D. d. P.-. Bolivia, Boletin del Servicio Geologico de Bolivia, p. 2004.

Ring, U., M. T. Brandon, S. D. Willett, and G. S. Lister (1999), Exhumation processes, in Exhumation processes; Normal Faulting, Ductile Flow and Erosion, U. Ring, M. T. Brandon, G. S. Lister and S. D. Willett (ed.), Geological Society of London Special Publications, London, 1-27.

Roeder, D. (1988), Andean-age structure of Eastern Cordillera (Province of La Paz, Bolivia), Tectonics, v. 7, 23-39.

Roeder, D., and R. L. Chamberlain (1995), Structural geology of sub-Andean fold and thrust belt in northwestern Bolivia, in Petroleum basins of South America, A. J. Tankard, R. Suarez and H. J. Welsink (ed.), American Association of Petroleum Geologists Memoir 62, 459-479.

Royden, L. (1996), Coupling and decoupling of crust and mantle in convergent orogens; implications for strain partitioning in the crust, Journal of Geophysical Research, v. 101, 17679-17705.

Ruddiman, W. F., M. E. Raymo, W. L. Prell, and J. E. Kutzbach (1997), The uplift-climate connection; a synthesis, in Tectonic uplift and climate change, W. F. Ruddiman (ed.), Plenum Press, New York, 471-515.

Safran, E. B., A. Blythe, and D. Thomas (2006), Spatially variable exhumation rates in orogenic belts: An Andean example, Journal of Geology, v. 114, 665-681.

Scheuber, E., D. Mertmann, H. Ege, P. Silva-Gonzalez, C. Heubeck, K.-J. Reutter, and V. Jacobshagen (2006), Exhumation and basin development related to formation of the central Andean plateau, 21°S, in The Andes: Active Subduction Orogeny, O. Oncken, G. Chong, G. Franz, P. Giese, H.-J. Gotze, V. A. Ramos, M. R. Strecker and P. Wigger (ed.), Springer-Verlag, Berlin, 285-301.

Schildgen, T. F., K. V. Hodges, K. X. Whipple, P. W. Reiners, and M. S. Pringle (2007), Uplift of the western margin of the Andean Plateau revealed from canyon incision history, southern Peru, Geology, v. 35, 523-526.

Sempere, T. (1995), Phanerozoic evolution of Bolivia and adjacent regions, in Petroleum basins of South America, A. J. Tankard, R. Suarez and H. J. Welsink (ed.), American Association of Petroleum Geologists Memoir 62, 207-230.

Sempere, T., R. Butler, D. Richards, L. Marshall, W. Sharp, and C. Swisher (1997), Stratigraphy and chronology of Upper Cretaceous-lower Paleogene strata in Bolivia and Northwest Argentina, Geological Society of America Bulletin, v. 109, 709-727.

Sempere, T., G. Carlier, P. Soler, M. Fornari, V. Carlotto, J. Jacay, O. Arispe, D. Neraudeau, J. Cardenas, S. Rosas, and N. Jimenez (2002), Late Permian-Middle Jurassic lithospheric thinning in Peru and Bolivia, and its bearing on Andean-age tectonics, Tectonophysics, v. 345, 153-181.

Sempere, T., G. Herail, J. Oller, and M. G. Bonhomme (1990), Late Oligocene-early Miocene major tectonic crisis and related basins in Bolivia, Geology, v. 18, 946-949.

Sobel, E. R., G. E. Hilley, and M. R. Strecker (2003), Formation of internally drained contractional basins by aridity-limited bedrock incision, Journal of Geophysical Research, v. 108, doi:10.1029/2002JB001883.

Sobel, E. R., and M. R. Strecker (2003), Uplift, exhumation and precipitation: tectonic and climatic control of Late Cenozoic landscape evolution in the northern Sierras Pampeanas, Argentina, Basin Research, v. 15, 431-451.

Springer, M. (1999), Interpretation of heat-flow density in the Central Andes, Tectonophysics, v. 306, 377-395.

Springer, M., and A. Forster (1998), Heat-flow density across the Central Andean subduction zone, Tectonophysics, v. 291, 123-139.

Tagami, T., and P. B. O'Sullivan (2005), Fundamentals of Fission-Track Thermochronology, in Low-Temperature Thermochronology: Techniques, Interpretations, and Applications, P. W. Reiners and T. A. Ehlers (ed.), Mineralogical Society of America, 19-47.

Trumbull, R. B., R. Ulrich, O. Oncken, S. Ekkehard, K. Munier, and F. Hongn (2006), The time-space distribution of Cenozoic volcanism in the south-central Andes: a new data compilation and some tectonic implications, in The Andes: Active Subduction Orogeny, O. Oncken, G. Chong, G. Franz, P. Giese, H.-J. Gotze, V. A. Ramos, M. R. Strecker and P. Wigger (ed.), Springer-Verlag, Berlin, 29-43.

Uba, C. E., C. Heubeck, and C. Hulka (2006), Evolution of the late Cenozoic Chaco foreland basin, southern Bolivia, Basin Research, v. 18, 145-170.

Wdowinski, S., and Y. Bock (1994), The evolution of deformation and topography of high elevated plateaus 2. Application to the Central Andes, Journal of Geophysical Research, v. 99, 7121-7130.

Welsink, H. J., F. M. A., and G. C. Oviedo (1995), Andean and pre-Andean deformation, Boomerang Hills area, Bolivia, in Petroleum basins of South America, A. J. Tankard, R. Suarez and H. J. Welsink (ed.), American Association of Petroleum Geologists Memoir, 481-499.

Willett, S. D. (1992), Dynamic and kinematic growth and change of a Coulomb wedge, in Thrust Tectonics, K. McClay (ed.), Chapman & Hall, London, UK, 19-31.

Willett, S. D., and D. C. Pope (2004), Thermo-mechanical models of convergent orogenesis; thermal and rheologic dependence of crustal deformation, in

Rheology and deformation of the lithosphere at continental margins, G. D. Karner, B. Taylor, N. W. Driscoll and D. L. Kohlstedt (ed.), Columbia University Press, New York, NY., 179-222.

Chapter 4

Plio-Quaternary sediment budget between thrust belt erosion and foreland deposition in the central Andes, southern Bolivia[1]

Abstract

Estimates of the physical boundary conditions on sediment source and sink regions and the flux between them provide insights into the evolution of topography and associated sedimentary basins. We present a regional-scale, Plio-Quaternary to recent sediment budget analysis of the Grande, Parapeti, and Pilcomayo drainages of the central Andean fold-thrust belt and related deposits in the Chaco foreland of southern Bolivia (18-23°S). We constrain source-sink dimensions, fluxes and their errors with topographic maps, satellite imagery, a hydrologically-conditioned digital elevation model, reconstructions of the San Juan del Oro (SJDO) erosion surface, foreland sediment isopachs, and estimated denudation rates. Modern drainages range from 7,453 km^2 to 86,798 km^2 for a total source area of 153,632 km^2. Paleo-drainage areas range from 9,336-52,620 km^2 and total 100,706 km^2, suggesting basin source area growth of ~50% since ~10 Ma. About 2.4-3.1 x 10^4 km^3 were excavated from below the SJDO surface since ~3 Ma. The modern foredeep is 132,080 km^2 with fluvial megafan areas and

---

[1]**Official citation:**

Barnes, J. B. and W. A. Heins (2008), Plio-Quaternary sediment budget between thrust belt erosion and foreland deposition in the central Andes, southern Bolivia, Basin Research, in press.

volumes ranging from 6,142-22,511 km^2 and 1,511-3,332 km^3, respectively. Since Emborozú Formation deposition beginning 2.1 ± 0.2 Ma, the foreland has a fill of ~6.4 x 10^4 km^3. The volume and rate of deposition require that at least ~40-60% of additional sediment be supplied beyond that incised from below the SJDO. The data also place a lower limit of ≥ 0.2 mm/yr (perhaps ≥ 0.4 mm/yr) on the time- and space-averaged source area denudation rate since ~2-3 Ma. These rates are within the median range measured for the Neogene, but are up to 2 orders of magnitude higher than some observations, as well as analytic solutions for basin topography and stratigraphy using a 2D-mathematical model of foreland basin evolution. Source-to-sink sediment budget analyses and associated interpretations must explicitly and quantitatively reconcile all available area, volume, and rate observations because of their inherent imprecision and the potential for magnification when they are convolved.

Introduction

The sediment-routing system links sources to sinks, determining how mountains erode, how topography evolves, and how landscapes translate into the sedimentary record [Allen, 2008]. Sediment sources and sinks are coupled through various surface processes and their fluxes to the extent that mountain belt deformation can be influenced by deposition downstream [e.g. Flemings and Jordan, 1989; Beaumont et al., 2000; Simpson, 2006]. Unfortunately, questions remain about what combination of factors influence the volume and rate of sediment production, the spatial variability of sediment production within the source, and the rate of sediment delivery to the sink [Tucker and Slingerland, 1996; Stock et al., 2006; Phillips and Gomez, 2007]. Sediment delivery rates are a particularly important control on the dimensions and physical characteristics of basin-filling sediments [Hovius and Leeder, 1998]. If estimates of the volume and mass flux (among other things) from the source area are available, then

quantitative tools can be used to predict sedimentary architecture [Robinson and Slingerland, 1998a, b; Geslin et al., 2001; Geslin et al., 2002; Clevis et al., 2003; Clevis, 2003; Van Wagoner et al., 2003; Overeem et al., 2005; Robin et al., 2005] and reservoir quality [Lander and Walderhaug, 1999; Perez et al., 1999; Bray et al., 2000; Bonnell and Lander, 2003].

A mass balance approach has been used to quantify sediment budgets for the Alps, Appalachians, Himalayas, and Rocky Mountains by integrating river sediment loads, paleogeographic reconstructions, seismic data, and the stratigraphic record [Hay et al., 1992; Le Pichon et al., 1992; Curray, 1994; Einsele et al., 1996; Pazzaglia and Brandon, 1996; Kuhlemann et al., 2001; Schlunegger et al., 2001; Clift et al., 2002; Kuhlemann et al., 2002; Clift, 2006; McMillan et al., 2006]. These sediment budgets provide some of the best constraints for inferring mountain paleotopography and estimating denudation rates, but uncertainties are often large and/or not quantified because of the scales over which they are applied.

Active fold-thrust belts and their foreland basin systems are sources and sinks closely linked in space and time that possess a variety of evidence that can be used to constrain their sediment budget (Fig. 4.1) [DeCelles and Giles, 1996; Critelli, 1999; Critelli et al., 2003]. For example, many thrust belts have paleosurfaces, formed by periods of protracted erosion [Widdowson, 1997], that have been used as markers to (a) estimate uplift magnitudes [de Sitter, 1952; Epis and Chapin, 1975; Scott, 1975; Kennan, 2000; Barke and Lamb, 2006], (b) estimate exhumation magnitudes [Sobel and Strecker, 2003; Babault et al., 2005; McMillan et al., 2006], (c) reconstruct paleo-drainage networks [Kennan et al., 1997; Kennan, 2000], (d) constrain the deformation history [Gubbels et al., 1993; Clark et al., 2006], and (e) calculate the amount of material removed from below the surface by post-formation incision [Kennan et al., 1997; McMillan et al., 2006]. In the sink, flexure associated with the adjacent topographic load

creates a foreland basin consisting of wedgetop, foredeep, forebulge and backbulge depozones [DeCelles and Giles, 1996]. Fluvial megafans (typically 10^3–10^5 km^2, with low gradients of 0.01-0.1°) are easily discernable and can be dominant depositional features of some wedgetops and foredeeps [Gohain and Parkash, 1990; Gupta, 1997; DeCelles and Cavazza, 1999; Leier et al., 2005]. Additionally, isopach maps constructed from measured sections, geochronology, seismic data, and well logs provide constraints on the spatio-temporal distribution of the foreland-filling sediments [e.g. Uba et al., 2006].

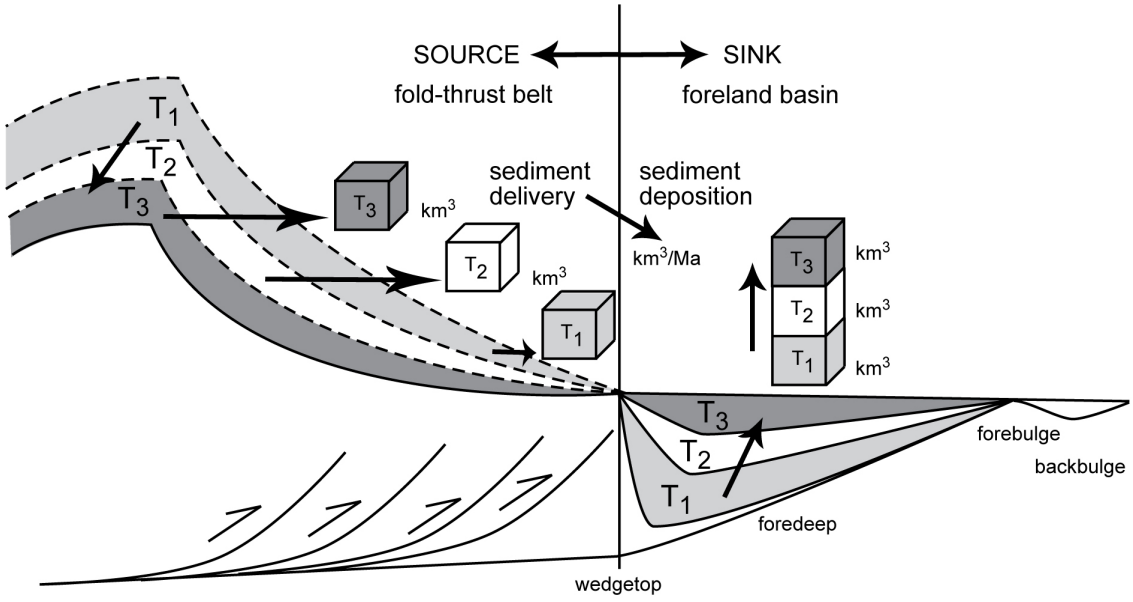

Figure 4.1. Schematic thrust belt-foreland basin system sediment budget in cross section. Eroded and deposited sediment volumes (gray to white shaded regions and boxes) for time slices T_1 – T_3 (increasing to the present) from a thrust belt hinterland source to an adjacent foredeep sink, respectively. The hinterland topographic evolution from ancient (dashed) to modern (solid) time and the equivalent sink foreland sedimentary evolution are also shown. In this ideal case, boxes T_1 – T_3 in the source are the same size as the equivalent boxes in the sink. For simplicity, no thrust belt propagation is shown.

This foreland sedimentary record is shaped by thrust belt topography, tectonics, climate, erosion, lithology, drainage patterns, and base level [Dickinson, 1974; Flemings and Jordan, 1989; Damanti, 1993; Devlin et al., 1993; Patterson et al., 1995; Van Wagoner, 1995; Burgess and Allen, 1996; Tucker and Slingerland, 1996; Schlunegger et al., 1997; Leeder et al., 1998; Geslin et al., 2002]. Although prior studies have characterized sediment source and sink dimensions and determined erosion rates, few attempts have been made to quantify regional-scale sediment budgets and associated uncertainties in thrust belt-foreland settings.

The goal of this paper is to quantify the sediment budget for the central Andean fold-thrust belt and foreland in southern Bolivia since the Plio-Quaternary (~ 3-0 Ma). We account for the area, volume and rates of sediment removed from the upland sources and deposited within the downstream sink, specifically fluvial megafans and the foredeep. The following logic governs our analysis. The amount of sediment produced must fall within limits imposed by the size of the drainage, the rate and duration of denudation, and the volume of deposited sediment. The amount of sediment generated must be at least as great as the amount of sediment deposited in the proximal foredeep. The generated sediment cannot be greater than the amount denuded from the present-day drainage at the maximum estimated rate of denudation over the longest possible denudation time. This lower sediment-production limit excludes some combinations of size, rate, and duration placing improved constraints on the large range of denudation rates estimated.

Why southern Bolivia?

The central Andean fold-thrust belt and Chaco foreland of southern Bolivia (18-23°S) is well-suited for quantifying a Plio-Quaternary sediment budget (Fig. 4.2). Fluvial megafans have been important foreland depositional features since the mid-Tertiary and

currently occupy most of the Chaco plain [Horton and DeCelles, 2001]. Isopachs quantify the spatial and temporal distribution of the Chaco sediments since the late Oligocene [Uba et al., 2006]. Reconstructions of the widespread late Miocene San Juan del Oro (SJDO) erosion surface provides an unusual constraint on timing and volume of thrust belt erosion [Servant et al., 1989; Gubbels, 1993; Gubbels et al., 1993; Kennan et al., 1997]. Finally, source region erosion rates have been estimated across multiple spatial and temporal scales [e.g. Barnes and Pelletier, 2006 and references therein].

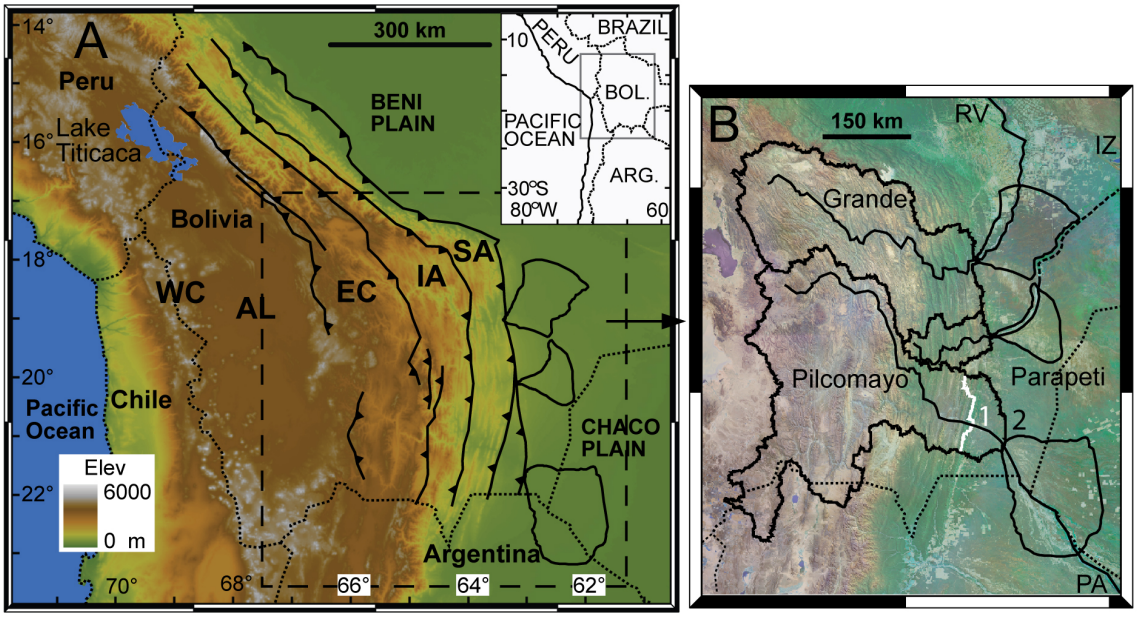

Figure 4.2. The central Andean fold-thrust belt and Chaco foreland in Bolivia. (A) Topography (GTOPO30 1 km) and major tectonic zones [modified from McQuarrie, 2002; Uba et al., 2006]: WC = Western Cordillera, AL = Altiplano, EC = Eastern Cordillera, IA = Interandean zone, SA = Subandes. Megafans are outlined in black. Inset shows location in west-central South America. (B) Satellite image of study area draped over topography (SRTM 90 m) showing the Rio Grande, Rio Parapeti, and Rio Pilcomayo channels (solid lines where perennial, dashed where ephemeral), their drainage areas, and megafans. RV = Rio Viejo area; IZ = Izogog swamp; PA = Patino swamp; 1 = white line representing the eastern basin edge of Pilcomayo 1 (Table 4.1); 2 = black line representing the eastern basin edge of Pilcomayo 2 (Table 4.1) at the megafan apex (see text and Appendix 4.1 for discussion).

Geologic setting

Crustal shortening associated with Cenozoic Andean mountain building has resulted in a retroarc plateau, fold-thrust belt, and foreland basin system in western Bolivia (Fig. 4.2) [Jordan and Alonso, 1987; Isacks, 1988; Jordan, 1995; Kley, 1996; Allmendinger et al., 1997; Horton and DeCelles, 1997; Jordan et al., 1997; Kley, 1999; McQuarrie, 2002; DeCelles and Horton, 2003; McQuarrie et al., 2005]. The dominantly east-vergent fold-thrust belt steps down in structural and topographic elevation from the Altiplano basin to the Eastern Cordillera, Interandean zone, Subandes and Beni/Chaco plains [Kley, 1996; McQuarrie, 2002]. Rocks involved in the deformation range from Paleozoic marine siliciclastics to Mesozoic non-marine clastics and Cenozoic synorogenic deposits [McQuarrie, 2002 and references therein]. In southern Bolivia, the fold-thrust belt is flanked on the west by the Altiplano plateau and on the east by the Chaco plain (Fig. 4.2). The Altiplano is a low-relief, internally drained, intermontane depression [e.g. Placzek et al., 2006]. The Chaco plain is a low-relief, low-elevation slope thought to be the aggradational surface of the wedge-top and foredeep depozones of the modern foreland [Horton and DeCelles, 1997]. The thrust belt is traversed by three large rivers, the Río Grande (or Guapay), Río Parapeti, and Río Pilcomayo, which form fluvial megafans in the Chaco (Fig. 4.2B) [Horton and DeCelles, 2001]. The relatively straight river courses across the Subandes suggests the rivers are antecedent from the late Miocene and hence the source drainages somewhat long-lived. Megafan apexes begin at the frontal-most Subandes structure implying a more recent origin (Fig. 4.2B) [Horton and DeCelles, 2001].

Timing of initial thrust belt deformation ranges from late Eocene to late Oligocene (~27-40 Ma) with deformation concentrated in the Subandes since the early to late Miocene (~10-20 Ma) [Elger et al., 2005; McQuarrie et al., 2005; Ege et al., 2007; Barnes et al., 2008; McQuarrie et al., 2008]. Sediment deposition in the Chaco foreland

commenced with the late Oligocene Petaca Formation and continues today with the Emborozú Formation [Uba et al., 2006]. Structural, stratigraphic, and geophysical data from southern Bolivia constrain the regional Neogene evolution, particularly in the Subandes [Baby et al., 1992; Baby et al., 1995; Dunn et al., 1995; Roeder and Chamberlain, 1995; Kley, 1996; Moretti et al., 1996; Kley, 1999; Müller et al., 2002; Uba et al., 2005] and Chaco [Marshall et al., 1993; Hulka et al., 2006; Uba et al., 2006].

San Juan del Oro (SJDO) surface

Here we summarize age constraints and reconstructions of the SJDO erosion surface that we adopt to quantify the paleo-drainage morphology and sediment volume removed from below the surface by Plio-Quaternary incision. The SJDO surface is identified by spatially correlative, remnant, low-relief surfaces at ca. 2000-3800 m elevations, which have been mapped throughout the Eastern Cordillera and Interandean zone of southern Bolivia (Fig. 4.3). The SJDO surface is a composite landform of (1) low-relief erosional uplands, (2) coalesced pediments, and (3) an unconformity beneath undeformed Tertiary sediments and ignimbrites that is the stratigraphic equivalent to surface types 1 and 2 [Servant et al., 1989; Gubbels et al., 1993; Kennan et al., 1995; Kennan et al., 1997; Barke and Lamb, 2006]. All surface types are subhorizontal, truncate deformed bedrock, decrease in elevation eastward, and are sometimes mantled by sediments up to 250 m thick with inter-bedded tuffs and fossiliferous layers [Gubbels et al., 1993; Kennan et al., 1995; Kennan et al., 1997]. Surveying the surfaces, $^{40}Ar/^{39}Ar$ dating of the tuffs, and ages of mammalian fossils bracketing the unconformity, show that the age of the SJDO is time-transgressive from ~12-3 Ma with incision beginning 3 ± 1.5 Ma [Gubbels, 1993; Gubbels et al., 1993; Kennan et al., 1995; Kennan et al., 1997; Barke and Lamb, 2006]. The lack of deformation and a dominantly ~10 Ma age for the SJDO surface suggests (a) cessation of deformation in the Eastern Cordillera and its

migration eastward into the Subandes, and (b) 1.1-2.5 km of surface uplift has occurred in the region since surface formation (Figs. 4.2 & 4.3) [Gubbels et al., 1993; Kennan et al., 1997; Barke and Lamb, 2006].

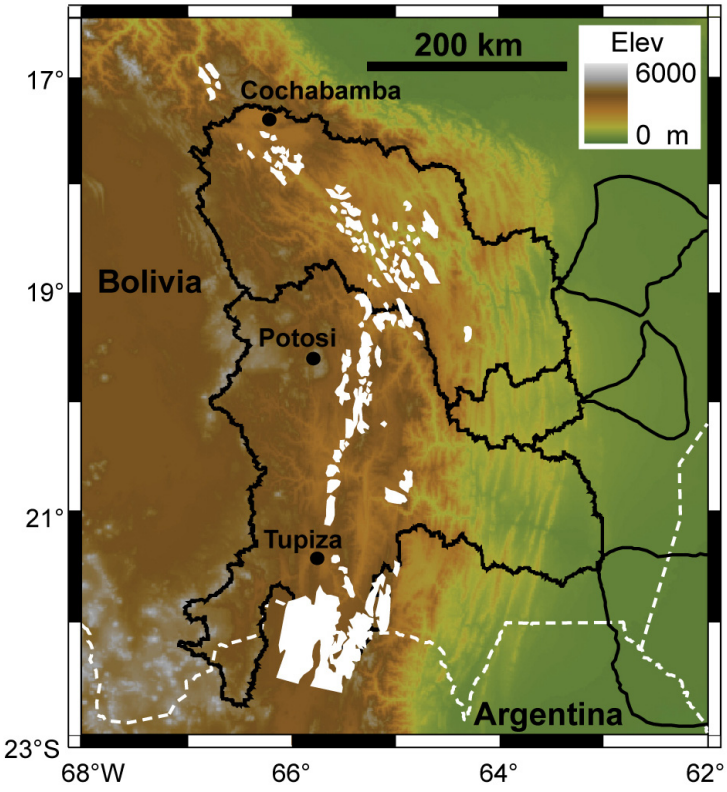

Figure 4.3. Preserved remnants of the San Juan del Oro surface in southern Bolivia. Remnant surfaces are mapped in white and simplified from Kennan et al. [1997] with the modern Grande, Parapeti, and Pilcomayo basins and megafans outlined in black for comparison.

Two different models for SJDO surface formation characterize it as a pediment and paleo-drainage base level, respectively. Gubbels and coworkers proposed a "cut and fill" model for the SJDO surface whereby as deformation ceased, aggradation and pediment development began (Fig. 4.4) [Gubbels, 1993; Gubbels et al., 1993]. Eventually, incision isolated the surface remnants. In this model, the SJDO surface

slopes down to the east from ~4.2 km elevation in the Eastern Cordillera to ~3 km in the Interandean zone over ~150 km [see Fig. 2.33 of Gubbels, 1993]. This model suggests a regional gradient of ~0.46° and implicitly allows that the SJDO pediment was not ubiquitous and that intervening highlands existed (Fig. 4.4). Kennan and coworkers

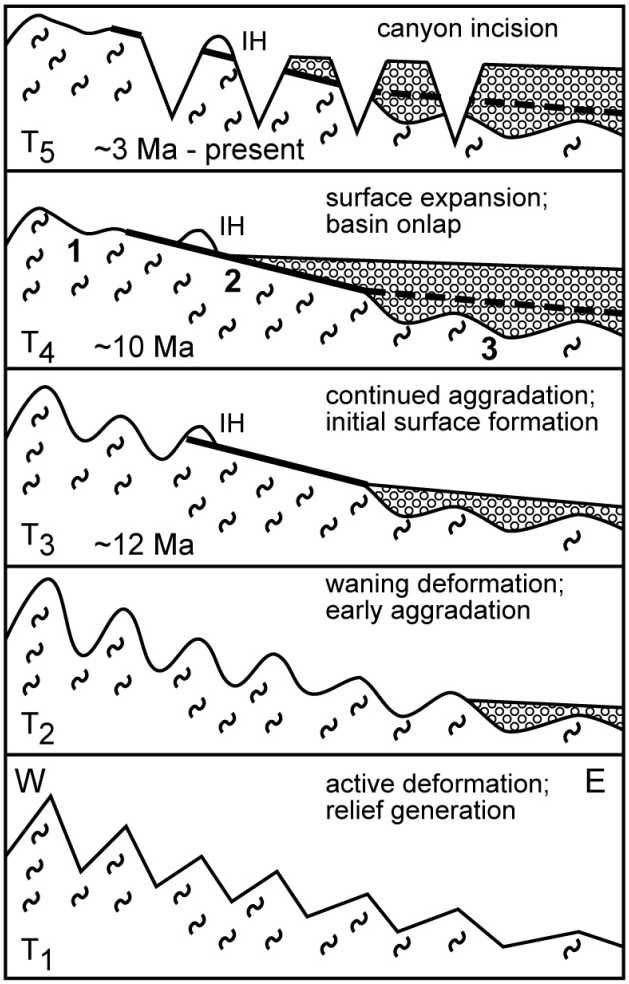

Figure 4.4. Schematic of the cut and fill model for San Juan del Oro surface evolution in cross section (modified from Fig. 4.1 of Gubbels [1993]). Five time steps are shown from pre-Miocene (T_1) to present (T_5) with absolute ages indicated where possible. Numbers 1 – 3 in T_4 indicate the three surface types as discussed in the text. IH = intervening highlands.

proposed that the SJDO surface represents the regional base-level associated with two paleo-drainage basins (Fig. 5.5A) [Kennan et al., 1997; Kennan, 2000]. This model suggests regional, upstream basin gradients of ~0.46° that decrease to ~0.23-0.27° in the downstream reaches. In both models, the preserved extent of the SJDO surface represents the minimum size of the drainage basin source area that supplied sediment to the foreland.

Key aspects of the SJDO surface relevant for quantifying a sediment budget include: (a) it formed ~10 Ma and (b) it experienced rapid incision at ~3 ± 1.5 Ma [Gubbels et al., 1993; Kennan et al., 1995; Kennan et al., 1997; Barke and Lamb, 2006]. Additionally, an estimated 1-2 x 10^4 km^3 of material was eroded from the pre-existing topography above the paleo-drainage base levels that together form the SJDO surface [Kennan et al., 1997]. All of this sediment was apparently transported out to the foreland (and possibly beyond) because neither (1) adequate local sinks exist in the EC or IA to store the estimated sediment nor (2) any major depositional hiatus exists in the Subandes source region between 12 and 3 Ma [Coudert et al., 1993; Kennan et al., 1997].

Foreland sediments

Isopachs constrain the spatio-temporal distribution of Oligocene to recent foredeep sediments in the Chaco plain [Uba et al., 2006]. The sedimentary unit most correlated with sediment exported from the thrust belt since the Plio-Quaternary is the Emborozú Formation [see Uba et al., 2006 their Fig. 15E]. The Emborozú Formation is the currently depositing, sedimentary unit characterized by fluvial megafan-dominated conglomerates interbedded with sandstone and mudstone [Uba et al., 2005]. A seismic N5 interval is equivalent to the Emborozú Formation which has a maximum thickness of ~1500 m at the mountain front and tapers rapidly eastward (Fig. 4.6) [Uba et al., 2006].

Beginning of Emborozú Formation deposition has been variously estimated at 3.3 Ma [Moretti et al., 1996], 2.1 ± 0.2 Ma [Hulka, 2005], and 1.8 Ma [Echavarria et al., 2003]. The basal age of 2.1 ± 0.2 Ma is preferred [Uba et al., 2006] because it agrees with the 1.8 Ma documented correlative strata in Argentina by Echavarria et al. [2003].

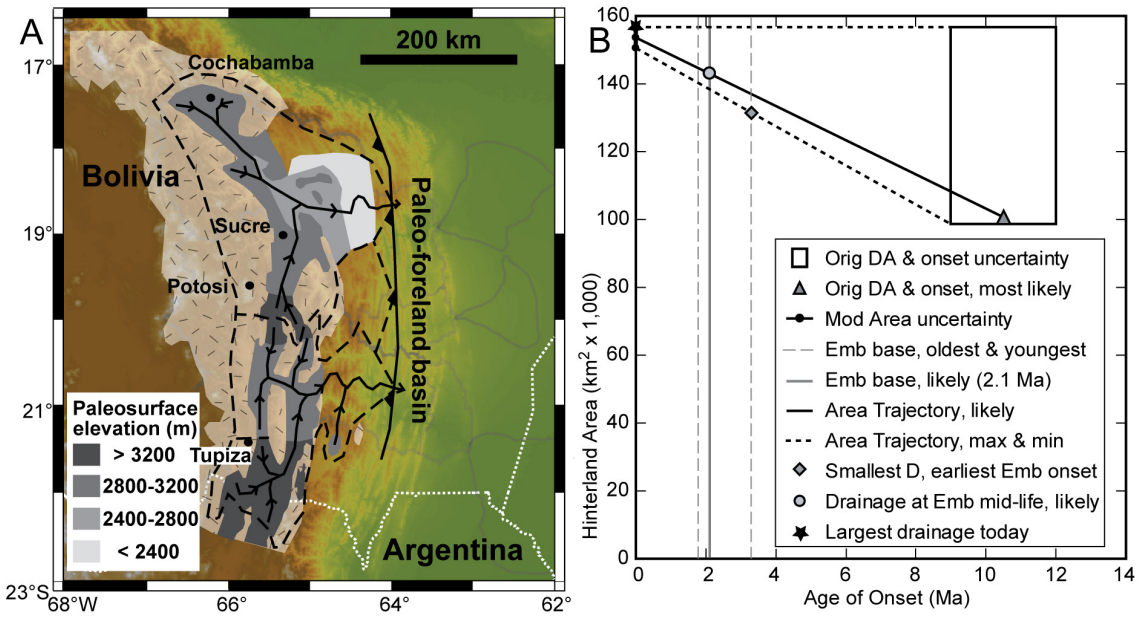

Figure 4.5. The late Miocene (~10 Ma) paleo-drainage model for San Juan del Oro surface evolution overlaying the modern topography. (A) Map of the paleo-drainage basins (dashed black lines = boundaries, shaded regions are distributions of SJDO surface elevations today) from Kennan et al. [1997] with minor modifications at the outlet convergence to mimic the modern basins. Other features include local highlands (jackstraw pattern), river networks (solid black lines with arrows), mountain front (thrust fault) and paleo-foreland basin (now occupied by the Subandes). Modern drainage basins and megafans (background gray lines) are shown for comparison. Two things to note; (1) the area between Potosi and Sucre used to be part of the paleo-Grande basin, but has been captured by the Rio Pilcomayo (compare with Fig. 1B), and (2) the SJDO surface elevation range suggests typical regional gradients of 0.4-0.8% [Kennan et al., 1997]. (B) Various potential evolutionary trajectories between the paleo- and modern drainages. Orig = original; DA = drainage area, Mod = modern, Emb = Emborozú Formation.

Methods

We account for the sediment budget in the Andean fold-thrust belt and Chaco foreland across a range of scales: spatially, from the drainage basin and megafan to entire hinterland drainage and proximal foredeep; and temporally, from recent to the late Miocene-Pliocene. Here we briefly outline the datasets and methods. Further details, particularly related to the definition and quantification of uncertainties, are available in Appendix 4.1.

We used ArcGIS™ 9.2 and the following datasets to estimate the modern morphology and area of the Río Grande, Río Parapeti, and Río Pilcomayo catchments and megafans: 1:250,000 topographic maps from the Instituto Geografico Militar (IGM) in Bolivia, 15 to 150 m LANDSAT TM-7 satellite imagery, a hydrologically-conditioned digital elevation model (HydroSHEDS: http://hydrosheds.cr.usgs.gov/), and digital topography derived from NASA's 2000 Shuttle Radar Topographic Mission (SRTM). All mapping and calculations reported were carried out in the Geographic and Universal Transverse Mercator (Zone 20 South) coordinate systems with the datum WGS84.

We defined and mapped megafan margins by one or several of the following criteria; (1) at the transition from foreland-convex to mountain-front parallel contours, (2) the boundary between (a) well-defined distributary channels and their flanking overbank areas (both of which can be clearly linked back to the fan apex) and (b) inter-megafan areas (with drainages originating from the frontal anticlinal ridge, not from the fan apex), (3) systematic changes in local slope aspects and their magnitudes, and (4) consistent contrasts in color, morphology, and texture from 15 m satellite images artificially enhanced by topographic shading from multiple sun angles (criteria 2 and 3 after Horton and DeCelles (2001); B. K. Horton, pers. comm. 2006).

We overlaid the paleotopography associated with the SJDO surface reconstructions of Gubbels (1993) and Kennan et al. (1997) onto the modern topography

in order to compare them. We created gridded surfaces corresponding to the reconstructed SJDO surfaces for both models to estimate the volume of material incised from below the surface by measuring the volume difference relative to the modern topography (Fig. 4.6). For the cut and fill model [Gubbels, 1993], we created a surface by interpolating between four N-S contours that span 66.5-64.4°W to 17-23°S. The contours have decreasing values from east to west of 4200, 3600, 3000, and 2400 m to replicate a regional gradient of 0.46°. This surface has a calculated mean slope of 0.46° ± 0.06 (1σ). For the paleo-drainage model [Kennan et al., 1997], we created a surface by interpolating between contours tracing the distribution of regional paleosurface elevations (compare Figs. 4.5 & 4.7B). Additional contours were added for this interpolation to properly recreate the paleotopographic highlands and intermediate paleosurface elevations. However, the spatial extent of the contours was limited to that estimated by the paleo-drainage reconstructions [Kennan et al., 1997]. The resultant surface slopes mimic the estimated values of 0.46-0.23°, but locally possess slopes of < 0.2° in the downstream regions and > 1° in very limited areas of the mid-to-upper reaches.

The nature and geometry of fluvial megafan basal surfaces have yet to be studied. Therefore, we calculated megafan volumes between the modern topographic surface and two alternate basal–surface geometries: (1) a horizontal, planar, basal surface equal in elevation to the minimum megafan surface elevation, and (2) a basal surface that is the mirror image of the fan surface about a horizontal plane of symmetry at the lowest elevation. Under assumption (1), the volume of the megafan is equal to (average elevation – lowest elevation) x surface area. Under assumption (2), the volume is just twice the value of assumption (1). Assumption (1) is a minimum estimate and assumption (2) is a more realistic estimate (see Appendix 4.1 for further discussion).

We created a gridded surface corresponding to the base of the N5 seismic interval defined by isopachs [Uba et al., 2006] in order to estimate the sediment volume in the foredeep. To encompass the entire study area, isopachs were extended parallel to the mountain front both north and south. We inferred the zero isopach to be parallel to the 500 m isopach and east of the Pilcomayo megafan margin because there are no data to constrain its location more specifically (Fig. 4.6).

Results

Modern drainage areas

Drainage basin area estimates for the Grande, Parapeti, and Pilcomayo are 59,381 ± 1,188, 7,453 ± 149, and 86,798 ± 1,736 km^2, respectively (Table 4.1). These estimates are within 7-15% of those previously reported [Horton and DeCelles, 2001; Leier et al., 2005] for reasons related to choice of basin outlet position and/or differences in map projection and datum (Table 4.1 & Appendix 4.1). For example, variation among area estimates using identical catchment boundaries, but different projections is ~10%. Minimum, maximum, and average elevations, as well as relief, are also summarized in Table 4.1.

Paleo-drainage areas

The paleo-Río Grande and Río Pilcomayo drainage basins, as defined by the SJDO surface, may have covered an area of > ~100,000 km^2 at ~10 Ma (Fig. 4.5A). Taking the paleo-drainage model of the SJDO surface at face value, we estimate the size of the paleo-Grande, Parapeti, and Pilcomayo drainage basins (Fig. 4.5) to be 52,620 km^2, 9,336 km^2, and 38,750 km^2, respectively (Table 4.1). Apparently, the paleo-Grande basin was larger than the paleo-Pilcomayo basin because the Potosi-Sucre area was subsequently captured by the Río Pilcomayo (compare Figs. 4.2B & 4.5A). In total,

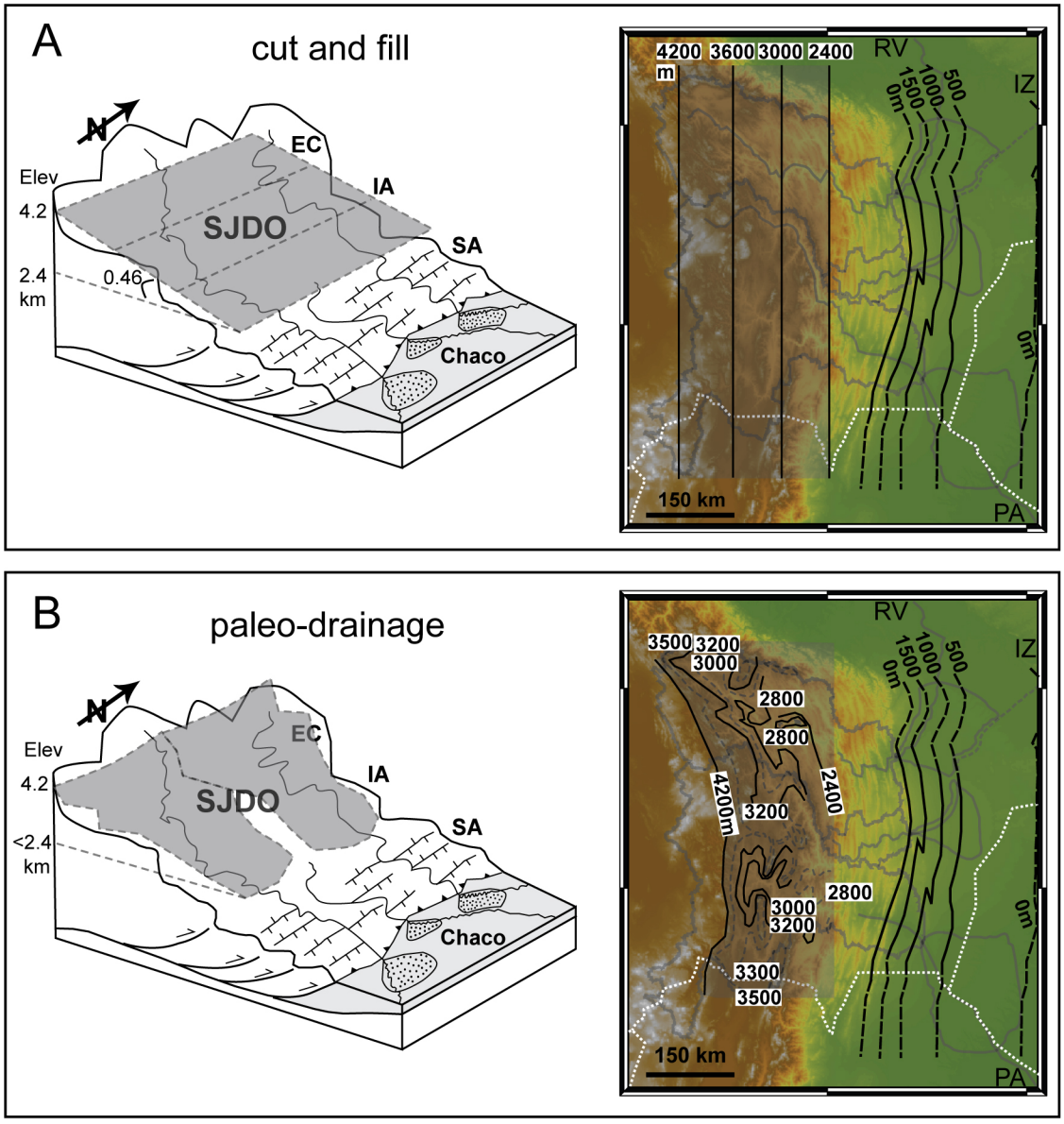

Figure 4.6. San Juan del Oro surface reconstructions and Chaco basin isopachs in southern Bolivia. Contours (solid lines; dashed where inferred) used to recreate the SJDO surface prior to Plio-Quaternary incision. Foreland isopachs (dashed where inferred in this study) are for the ~2.1-0 Ma Emborozú Formation (from Uba et al. [2006]; their Fig. 15E). Abbreviations are the same as in Figure 2. Schematic block diagrams of the idealized SJDO surface reconstructed (left) and the distribution of elevation contours used to create the gridded surface (right) on top of the modern topography for the cut and fill (A) and paleo-drainage (B) models. Idealized trellis drainage pattern shown for the Subandes. Grey-shaded region is the extent of the reconstructed SJDO surface in each model. Block diagram in B shows how basin slopes grade inward to the center and eastward to the foreland. Contours in B are from Figure 5 plus additional, inferred lines (grey dashed) where necessary.

Table 4.1. Source and sink physical dimensions in southern Bolivia.

	Grande	Parapeti	Pilcomayo (1)	Pilcomayo (2)	Total
Drainage Basin					
Maximum elevation (m)	4,988	3,303	5,741	5,741	
Minimum elevation (m)	442	631	389	320	
Relief (m)	4,546	2,672	5,352	5,421	
Average (m)	2,631	1,706	2,851	2,788	
Area (km^2)					
Horton & DeCelles (2001)	~70,000	~8,000	~81,300	--	
Leier *et al.* (2005)	59,000	~8,000	81,506	--	
this study	59,381	7,453	80,832	86,798	153,632
this study error (± 2%)	±1,188	±149	±1,617	±1,736	±3,073
~10 Ma	52,620	9,336	--	38,750	100,706
Basin outlet, fan apex					
Modern Long (°E)	63.4	63.19	63.47	63.01	
Modern Lat (°S)	18.91	20.02	21.27	21.56	
~10 Ma Long (°E)	~64	~64	--	~64	
~10 Ma Lat (°S)	~18.5	~20	--	~21	
Megafans					
Maximum elevation (m)	575	646	--	360	
Minimum elevation (m)	299	384	--	198	
Relief (m)	276	262	--	162	
Average (m)	423	507	--	272	
Area (km^2)					
Horton & DeCelles (2001)	~12,600	~5,800	--	~22,600	
Leier *et al.* (2005)	9,944	6,726	--	17,294	
this study	12,985	6,142	--	22,511	
this study error (± 20%)	±2,597	±1,228	--	±4,502	
(Average-Min) Elevation (km)	0.124	0.123	--	0.074	
Volume (km^3)					
Max (Areax1.2 x Av-Minx2)	3,864	1,813	--	3,998	9,675
Likely (Area x Av-Minx2)	3,220	1,511	--	3,332	8,063
Min (Areax0.8 x Av-Min)	1,288	604	--	1,333	3,225
Chaco Foredeep					
Area (km^2)					132,080
error (± 2%)					±2,642
Volume of Emborozú Fm (km^3)					63,772
error (± 20%)					±12,754

1 = pilcomayo basin boundary 1; 2 = pilcomayo basin boundary 2 (see Fig. 4.2)
Max = maximum area estimate and mirror-image basal-surface assumption
Likely = area estimate and mirror-image basal-surface assumption
Min = minimum area estimate and planar-basal-surface assumption

the preserved remnants of the SJDO surface delineate a minimum drainage area of 100,706 km^2, which is roughly two-thirds of the modern surface area of the three drainage basins (Table 4.1). The modern drainage (Fig. 4.2B) represents the maximum area that could have been covered by the SJDO surface. Figure 4.5B shows the range of uncertainty in paleo and modern area estimates and potential evolutionary trajectories between the two of them.

Volume excavated below the SJDO surface

We estimate 23,920 to 30,900 km^3 has been removed by incision from below the SJDO surface since 3 ± 1.5 Ma. Figure 4.7 shows regions that have experienced volume loss between the SJDO surface and the modern topography for both surface reconstruction models. The distribution of incision below both models is similar in the Pilcomayo basin. This reflects the fact that (1) the cut and fill model was based almost exclusively on remnants located in the Pilcomayo drainage [see Fig. 1 of Gubbels et al., 1993] and (2) most of the aerial extent of surface remnants is preserved there today (Fig. 4.3), providing most of the control for both models. Significantly less incision below the SJDO surface in the Grande basin is determined from the paleo-drainage model because this model predicts a lower local base level relative to the Pilcomayo basin (Fig. 4.5). The nature of the difference between the two models suggests the cut and fill surface represents an upper bound and the paleo-drainage surface represents a lower bound on the volume of material removed. The results are reported this way.

Megafan Areas

The fluvial megafans extend >150 km across the foredeep from their mountain-front apexes to their distal lobes. Total surface area of the megafans is ~42,000 km^2, whereas the total surface area of the proximal Chaco foredeep is ~132,000 km^2 (Table

4.1). We estimate the megafan surface areas to be 12,985 km^2, 6,142 km^2, and 22,511 km^2 ± 20% for the Grande, Parapeti, and Pilcomayo, receptively (Table 4.1 & Appendix 4.1). Our mapping criteria are sufficiently restrictive that the estimate of the Pilcomayo megafan is an order of magnitude less than the 210,000 km^2 reported by Iriondo [1993].

Megafan and foredeep basin fill volumes

Megafan volumes corresponding to the planar-basal-surface and mirror-image assumptions are reported in Table 4.1. The estimates range from 604 km^3 for the Parapeti megafan assuming a planar surface, to 3,332 km^3 for the Pilcomayo megafan assuming a mirror image between the fan surface and the basal surface. The foredeep volume of the Emborozú Formation is 63,772 km^3 ± 20% (Table 4.1 & Appendix 4.1).

Denudation-rate estimates

Barnes and Pelletier (2006) compiled denudation-rate estimates from a variety of methods for southern Bolivia. Estimates range from 0.04 to 1.6 mm/yr (= km/Ma) (Fig. 4.8). These estimates integrate sediment removal over temporal scales of 10^1 - 10^7 yrs and spatial scales from 10^0 to 10^5 km^2 (Fig. 4.9) (see Appendix 4.1 for further discussion).

The relevant denudation rate for our source-to-sink calculation is an idealized average over the whole hinterland (10^5 km^2) and the whole depositional history of the Emborozú Formation (10^6 yrs) (see Appendix 4.1 for additional discussion). Although observations span a range of values, the highest rates come from smaller spatial scales and larger temporal scales than the relevant analytic scale (Fig. 4.9). Observations that come from the relevant analytic scales (black oval in Fig. 4.9) fall into a much smaller range of 0.1 - 0.4 mm/yr. The only observation that matches the relevant analytic spatial and temporal scale is ~0.2 mm/yr (grey circle in Fig. 4.9).

Sediment production and deposition estimates

Boundary conditions. This source-to-sink sediment budget starts with today and integrates back to the Plio-Quaternary (~3 - 0 Ma). The chronologic boundary is either initial incision into the SJDO surface or initial deposition in the Emborozú Formation. In space, the budget starts with the modern landscape, bounded by the modern drainage divides of the Ríos Grande, Parapeti, and Pilcomayo on the source side and by the zero-isopach of the Emborozú Formation on the sink side. The spatial boundary is the pre-incision SJDO surface and bordering highlands and the basal surface of the Emborozú Formation.

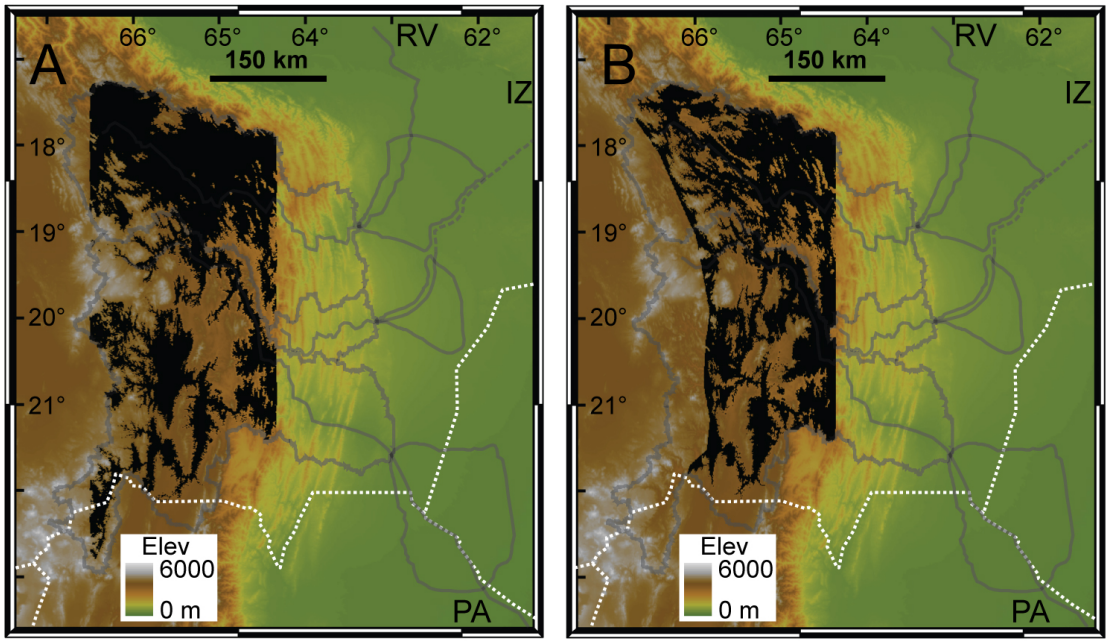

Figure 4.7. Spatial distribution of Plio-Quaternary (~3-0 Ma) incision for both San Juan del Oro surface models. Black areas indicate volume loss when comparing the reconstructed SJDO surfaces to the modern topography for the cut and fill (A) and paleo-drainage (B) models. Significantly less volume has been lost from the Grande basin in the paleo-drainage model.

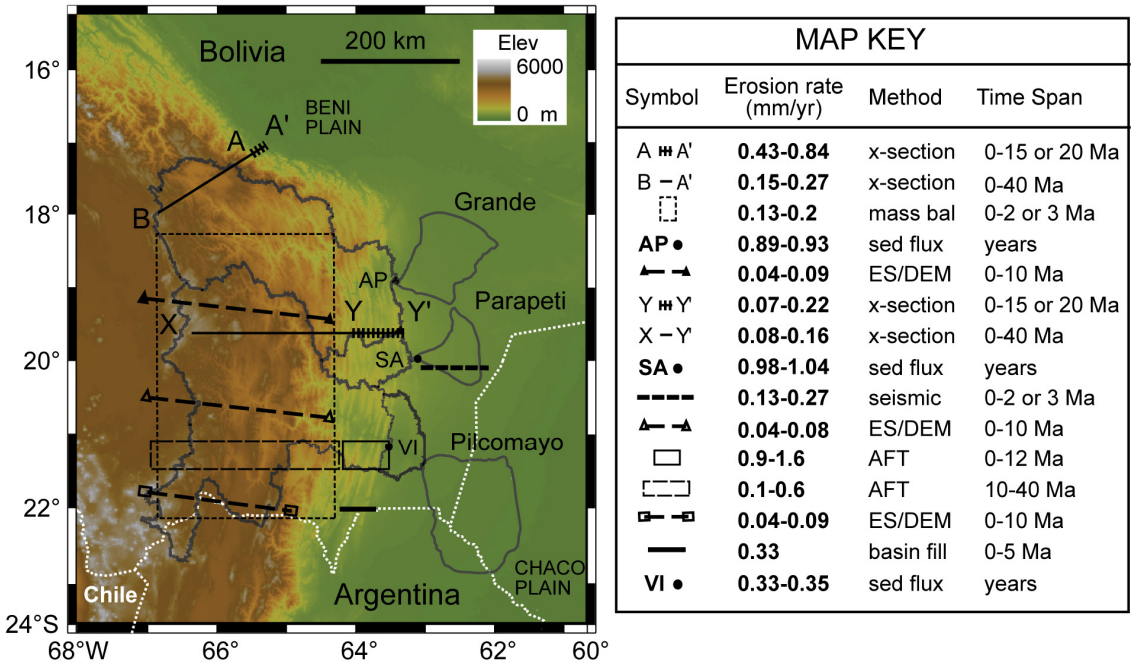

Figure 4.8. Map showing locations of erosion-rate estimates for the central Andean fold-thrust belt in southern Bolivia [modified from Barnes and Pelletier, 2006]. Method = method used for calculating the estimate; Time Span = time span over which the erosion rate is averaged; sed flux = sediment-flux data with range of published data from Aalto et al. [2006] and Barnes and Pelletier [2006]; AFT = apatite fission-track thermochronology; x-section = cross section; mass bal = mass balance; ES/DEM = erosion surface and DEM analysis; seismic = seismic cross-sectional area; basin fill = basin fill rate.

Volume balance. The source area sediment volume produced must be at least as large as the volume of sediment deposited in the Emborozú Formation. The maximum volume of sediments excavated from below the preserved area of the SJDO surface (~2.4 - 3.1 x 10^4 km^3) is smaller than the minimum volume of the Emborozú Formation (~5.1 x 10^4 km^3) (Table 4.1). Initiation of incision into the SJDO surface (4.5 - 1.5 Ma) overlaps with initial Emborozú Formation deposition (3.3 - 1.8 Ma) within error, but incision (most likely age 3.0 Ma) probably predates initial deposition (most likely age 2.1 Ma). The volume disparity between incision and deposition means that erosion from

the intervening highlands and the drainage regions beyond the SJDO surface extent (Fig. 4.7) contributed at least ~40-60% of the sediment to the Emborozú or ~2-2.7 x 10^4 km^3 by volume.

Treatment of ions and pores. Exposed source-area bedrock is mostly Mesozoic and Paleozoic siliciclastic sedimentary rock [e.g. McQuarrie, 2002]. These rocks have some preserved porosity. Some fraction of the rocks is also lost to dissolution during conversion of bedrock to transportable sediment. We estimate that the volume lost to dissolved ions (~1-15%) plus the original rock porosity (≤ 12%) is similar to the volume of void space among sedimentary particles deposited in the basin (16-32%) (see Appendix 4.1 for quantitative justification). Thus, we treat gross volumes of denuded and deposited material as equivalent because the solid/void ratio is similar between source and sink.

Estimates. There are two paths for estimating sediment-production rates from the source area based on the data in this paper. First, we divided the volume of sediment excavated from beneath the SJDO surface by the time incision began. Table 4.2 summarizes the range of sediment-production rates calculated from the estimated volumes and time. Sediment-production rates range from 5,316 to 20,600 km^3/Ma with a middle value of 9,137 km^3/Ma. Second, we integrated linear denudation rates over the hinterland area. Table 4.2 also summarizes the sediment-production rates calculated from a range of denudation rates and potential hinterland areas. Denudation rates were chosen to uniformly cover (on a $\log_2$ scale) the range reported in Figure 4.8. We picked areas from Figure 4.5B to represent the smallest, likely, and largest regions that could have been encompassed by the drainage from the earliest initiation of Emborozú deposition to today. These sediment-production rates show a much wider range, from 5,261 to 250,733 km^3/Ma with a middle value of 57,215 km^3/Ma.

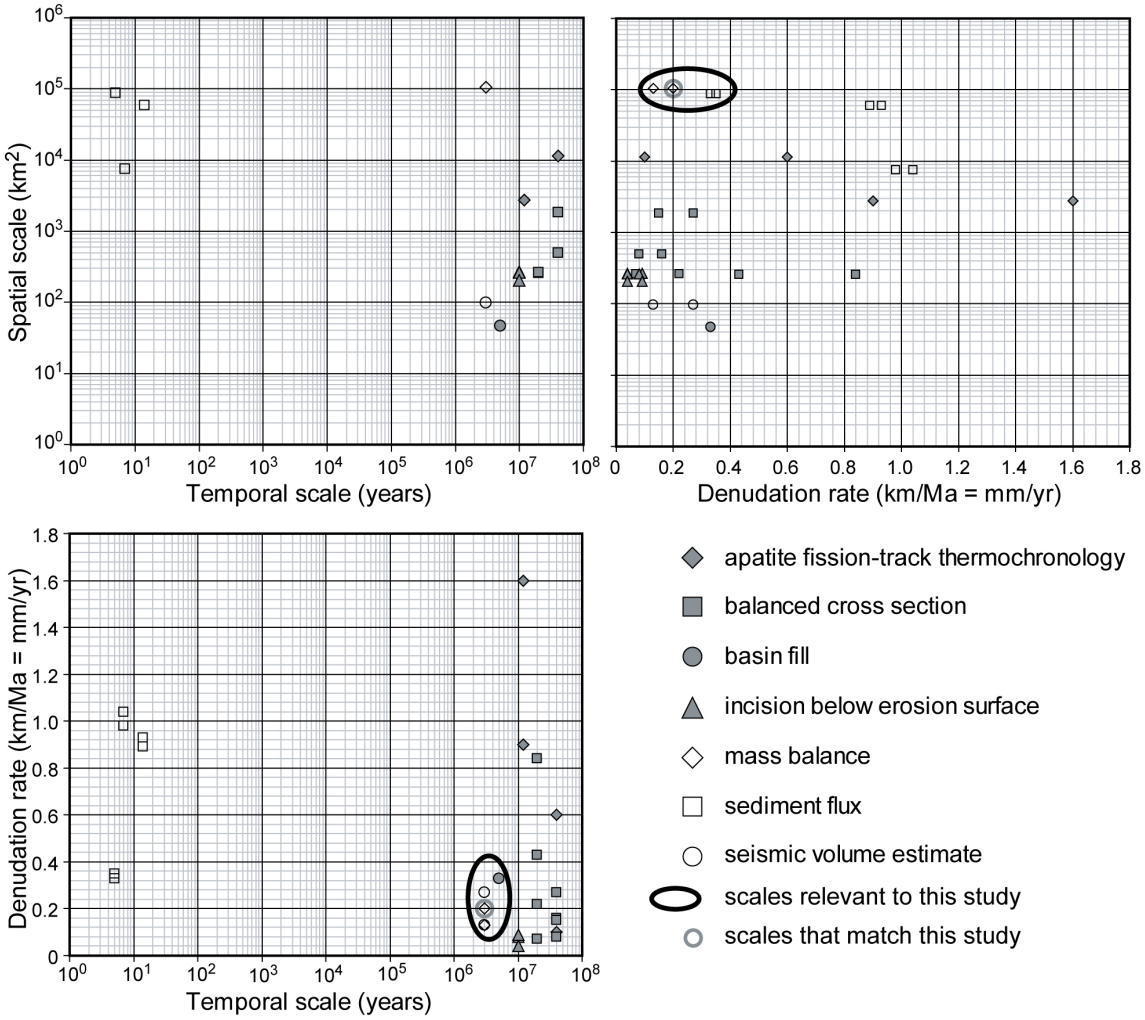

Figure 4.9. Erosion-rate estimates versus their integration in space and time for the central Andean fold-thrust belt in southern Bolivia [data from Barnes and Pelletier, 2006]. Ovals highlight values that are both relevant (black) and specifically match (gray) the scale of this study.

There is only one path to estimate sediment-deposition rates. We divided the Emborozú Formation sediment volume by the time since deposition began. Sediment-deposition rates calculated from a range of estimated volumes and times are in Table 4.2. Rates range from 22,182 to 42,515 km^3/Ma with a middle value of 30,368 km^3/Ma. The deposition duration of 3.3 Ma is included for completeness, but is considered unlikely (see discussion in Uba et al. (2005).

Reconciling the estimates. We calculated the minimum extra upland area required to produce the Emborozú sediment by subtracting the volume of SJDO surface excavation from the volume of the Emborozú then dividing by a linear denudation rate. The value is only a minimum because some SJDO surface-derived sediment might have been deposited elsewhere (e.g. in an older formation or bypassed downstream). Nevertheless, this exercise excludes denudation-rate estimates that are impossible for the relevant scale because they require more upland area than exists today. Table 4.3 summarizes the results within the ranges of rates, space, and time constrained by observations. Space limits encompass the smallest total paleo-drainage size (corresponding to the earliest onset of Emborozú deposition) to the largest possible modern drainage size (estimate plus error). Time limits were derived from the oldest potential onset of Emborozú deposition and the youngest possible onset of incision. Incision probably began earlier than the oldest onset of Emborozú deposition, but that case is not relevant to this calculation of minimum area. Table 4.3 rows are ordered by increasing mass flux required to fill the Emborozú. The results are shaded to indicate possibility: impossible (dark shading) because the combination of volumes and rates imply a hinterland area greater than the modern drainage, possible results (light shading) because they are within the range of potential hinterland areas, and certainly possible (no shading) results because they are smaller than the smallest drainage size.

Results indicate that any denudation rate < 0.1 km/Ma is impossible as the average is over the complete (time, space) that generated the Emborozú sediments (Table 4.3). Denudation rates < 0.2 km/Ma are impossible unless the volume of sediments in the Emborozú is near the low end of the likely range, and the onset of deposition is toward the old end of the likely range. Given the most likely volumes of SJDO surface excavation, Emborozú deposition and deposition duration, the average denudation rate should have been ≥ 0.2 km/Ma.

Modern sediment-production estimates

Boundary conditions. This source-to-sink sediment budget starts with today and integrates backward to the onset of modern megafan deposition. The budget starts with the modern landscape surface, bounded by the modern drainage divides of the Grande, Parapeti, and Pilcomayo rivers in the source, and bounded by the megafan extents in the sink.

Table 4.2. Potential Plio-Quaternary sediment production and deposition rates.

Sediment-production rates (km^3/Ma)				
		Excavation duration (Ma)		
Volume removed below SJDO (km^3)		1.5	3	4.5
Minimum	23,920	15,947	7,973	5,316
Likely	27,410	18,273	9,137	6,091
Maximum	30,900	20,600	10,300	6,867
		Potential hinterland area (km^2)		
Hinterland denudation rates (km/Ma)		131,517	143,037	156,708
highest	1.6	210,428	228,859	250,733
median sediment flux	1.0	131,517	143,037	156,708
median AFT, high balanced cross s	0.8	105,214	114,429	125,366
low sediment flux	0.4	52,607	57,215	62,683
median balanced cross section	0.2	26,303	28,607	31,342
low balanced cross section, AFT	0.1	13,152	14,304	15,671
lowest	0.04	5,261	5,721	6,268

Sediment-deposition rates (km^3/Ma) in the Emborozú Formation					
		Deposition duration (Ma)			
Volume deposited (km^3)		1.8	2.1	2.3	3.3*
Minimum	51,018	28,343	24,294	22,182	15,460
Likely	63,772	35,429	30,368	27,727	19,325
Maximum	76,526	42,515	36,441	33,272	23,190

middle values are shaded gray, see text for discussion

* values in this column unlikely, see text and Uba et al. [2005] for discussion

The megafan sediment volume is probably equal to, or slightly less than, the volume produced in the source area for the following reasons. Very little surface water escapes the Chaco foredeep because the Río Parapeti and Pilcomayo terminate into

swamps just downstream of their megafans and the Río Grande stalls as it bifurcates into small channels, drops sediments in the adjacent floodplains in the Río Viejo area beyond the megafan margin, and consequently severs its connection to the Río Paraguay (Fig. 4.2B) [Iriondo, 1984; Iriondo, 1993; Horton and DeCelles, 2001]. In particular, the Río Pilcomayo presently deposits such a sediment excess that it blocks its own channel, floods its levees, and spills into nearby swamps [Wilkinson et al., 2006]. Furthermore, tectonic depressions, vegetative-debris accumulations, and abandoned channels facilitate water and sediment ponding in lakes both on and around the megafans [Iriondo, 1993; Wilkinson et al., 2006]. Appendix 4.1 outlines observations that suggest the megafans themselves might not be entirely closed systems.

Sediment production. Integrating a linear denudation rate over the modern drainage area yields the modern sediment-production rate. Table 4.4 summarizes sediment-production rates calculated from a range of denudation rates and measured drainage areas. Denudation rates were chosen to cover the range reported with particular emphasis on rates estimated from the basin outlet on each of the rivers: 0.89-0.93 mm/yr for the Grande (point AP in Fig. 4.8), 0.98-1.04 mm/yr for the Parapeti (point SA in Fig. 4.8), and 0.33-0.35 mm/yr for the Pilcomayo (point VI in Fig. 4.8). The highest rate used represents the highest observed rate throughout the Neogene (apatite fission-track thermochronology) whereas the lowest rate is the lowest possible calculated in Table 4.3. For each river, the best sediment-production rate estimate (shading) is based on the most likely drainage size and the measured denudation rate for that drainage.

Age of megafan initiation. If all sediment produced in the drainages is deposited on the megafans, as observations documented above suggest, then onset of modern megafan deposition can be estimated by dividing the megafan sediment volume by the rate of sediment production. Table 4.5 summarizes the results of this calculation with

Table 4.3. Total hinterland area required (km^2) to supply deficient volume (Emborozu - excavation below SJDO)*.

	Excavated below SJDO (km^3)	Observed in Emborozu (km^3)	Extra volume required (km^3)	Excavation duration (Ma)	Production rate of extra volume (km^3/Ma)	Potential denudation rates (km/Ma = mm/yr)					
						highest	*median sediment flux*	*median AFT, high bal x-section*	*low sediment flux*	*median bal x-section*	*low bal x-section, AFT*
						1.6	1.0	0.8	0.4	0.2	0.1
	30,900	51,018	20,118	3.3	6,096	102,500	104,786	106,310	113,930	129,171	159,652
	27,410	51,018	23,608	3.3	7,154	103,161	105,843	107,632	116,574	134,459	170,228
	23,920	51,018	27,098	3.3	8,211	103,822	106,901	108,954	119,218	139,747	180,804
	30,900	51,018	20,118	2.1	9,580	104,677	108,269	110,664	122,639	146,589	194,488
	30,900	63,772	32,872	3.3	9,961	104,915	108,651	111,141	123,593	148,496	198,302
	27,410	63,772	36,362	3.3	11,019	105,576	109,708	112,463	126,237	153,784	208,878
	27,410	51,018	23,608	2.1	11,242	105,716	109,931	112,742	126,794	154,898	211,107
	23,920	63,772	39,852	3.3	12,076	106,237	110,766	113,785	128,881	159,071	219,453
	23,920	51,018	27,098	2.1	12,904	106,754	111,593	114,819	130,949	163,208	227,726
	30,900	51,018	20,118	1.5	13,412	107,072	112,101	115,454	132,219	165,748	232,807
	30,900	76,526	45,626	3.3	13,826	107,331	112,516	115,972	133,255	167,821	236,951
	27,410	76,526	49,116	3.3	14,884	107,992	113,573	117,294	135,899	173,108	247,527
	30,900	63,772	32,872	2.1	15,653	108,473	114,343	118,256	137,823	176,956	255,223
	27,410	51,018	23,608	1.5	15,738	108,526	114,428	118,363	138,036	177,382	256,074
	23,920	76,526	52,606	3.3	15,941	108,653	114,631	118,616	138,543	178,396	258,103
^	27,410	63,772	36,362	2.1	17,315	109,512	116,005	120,334	141,978	185,266	271,842
	23,920	51,018	27,098	1.5	18,065	109,980	116,755	121,271	143,852	189,015	279,340
	23,920	63,772	39,852	2.1	18,977	110,550	117,667	122,411	146,133	193,575	288,461
	30,900	76,526	45,626	2.1	21,727	112,269	120,417	125,848	153,007	207,324	315,958
	30,900	63,772	32,872	1.5	21,915	112,386	120,604	126,083	153,476	208,263	317,836
	27,410	76,526	49,116	2.1	23,389	113,308	122,078	127,926	157,162	215,633	332,577
	27,410	63,772	36,362	1.5	24,241	113,841	122,931	128,991	159,293	219,896	341,103
	23,920	76,526	52,606	2.1	25,051	114,346	123,740	130,003	161,316	223,943	349,196
	23,920	63,772	39,852	1.5	26,568	115,295	125,258	131,900	165,110	231,530	364,370
	30,900	76,526	45,626	1.5	30,418	117,701	129,107	136,712	174,734	250,778	402,866
	27,410	76,526	49,116	1.5	32,744	119,155	131,434	139,620	180,550	262,411	426,132
	23,920	76,526	52,606	1.5	35,071	120,609	133,761	142,528	186,367	274,044	449,399
Min	23,920	51,018	20,118	1.5							
Max	30,900	76,526	52,606	3.3		**Upper**			**Lower**		
Likely	27,410	63,772	36,362	2.1		**Limit =**	**156,708**	**km^2**	**Limit =**	**131,517**	**km^2**

*minimum area of preserved SJDO surface = 98,690 km^2; source areas required to supply deficit = extra vol production rate/denudation rate + 98,690

dark shading = impossible results; light shading = possible results; no shading = certainly possible results; see Figure 8 for abbreviations

^outlined row is most likely result based on best combination of time and amount of excavated sediment below the SJDO and observed in the Emborozú Formation

rate and volume ranges constrained by observation for each megafan and their aggregate.

For most likely values for drainage area, sediment delivery, and megafan volume, estimated age of megafan initiation varies considerably from 52-55 ka for the Grande, to 110-116 ka for the Pilcomayo, and 218-228 ka for the Parapeti (Table 4.5 & Appendix 4.1). It is possible that this result is correct and megafan initiation is diachronous. Alternatively, modern denudation rates may be inaccurate estimates of the average rate since the (common?) initiation time of the megafans because they are based on only a few years, compared to the 100's of ka over which the megafans must have been accumulating. If we apply the median denudation rate observed across the entire Neogene to the total volume of sediments in all megafans, onset of deposition would be ~66 ka. Table 4.5 essentially presents a series of hypotheses about the age of the modern Chaco megafans that can be tested by dating the actual basal surface. Radiocarbon or pollen ages from relatively shallow boreholes could provide the necessary information.

Discussion and implications

Sediment production volumes through time and space

Estimated sediment volumes have implications for erosion variability through time and the distribution of sediment production within the source region. The c. 1000 m relief between the SJDO surface and intervening highlands led Kennan et al. [1997] to estimate that ~1-2 x 10^4 km^3 was excavated from the original paleotopography to make the SJDO surface presumably prior to ~10 Ma. Since ~2-3 Ma, a minimum of ~5.1 x 10^4 km^3 has been deposited into the Emborozú Formation, of which at least ~40-60% (2.4 - 3.1 x 10^4 km^3) came from below the SJDO surface via incision. Although we cannot quantify the source area extent at any point prior to SJDO formation, we speculate

Table 4.4. Potential sediment-production rates from the modern landscape (km^3/Ma).

		Observed denudation rates (km/Ma = mm/yr)								
Drainage area (km^2)		*Neogene highest* 1.60	*Grande Highest* 1.04	*Grande Lowest* 0.98	*Parapeti Highest* 0.93	*Parapeti Lowest* 0.89	*Neogene median* 0.80	*Pilcomayo highest* 0.35	*Pilcomayo lowest* 0.33	*Neogene lowest* 0.20
Grande										
Maximum	60,569	96,910	62,991	59,357	56,329	53,906	48,455	21,199	19,988	12,114
Likely	59,381	95,010	61,756	58,193	55,224	52,849	47,505	20,783	19,596	11,876
Minimum	58,193	93,109	60,521	57,030	54,120	51,792	46,555	20,368	19,204	11,639
Parapeti										
Maximum	7,602	12,163	7,906	7,450	7,070	6,766	6,082	2,661	2,509	1,520
Likely	7,453	11,925	7,751	7,304	6,931	6,633	5,962	2,609	2,459	1,491
Minimum	7,304	11,686	7,596	7,158	6,793	6,501	5,843	2,556	2,410	1,461
Pilcomayo										
Maximum	88,534	141,654	92,075	86,763	82,337	78,795	70,827	30,987	29,216	17,707
Likely	86,798	138,877	90,270	85,062	80,722	77,250	69,438	30,379	28,643	17,360
Minimum	85,062	136,099	88,465	83,361	79,108	75,705	68,050	29,772	28,070	17,012
Total										
Maximum		250,727	162,973	153,571	145,735	139,467	125,364	54,847	51,713	31,341
Likely		245,811	159,777	150,559	142,878	136,732	122,906	53,771	50,699	30,726
Minimum		240,895	156,582	147,548	140,020	133,998	120,447	52,696	49,685	30,112

shading = best sediment-production rate estimate

relative denudation rates were low for some time period prior to ~10 Ma because the sediment volume produced was only ~20-40% of the volume deposited in the last 3 Myrs. This is already implied because most of the long-term (>10 Myr) averaged denudation rates are <0.4 mm/yr (Fig. 4.9) and we already demonstrated they were most likely ≥ 0.4 mm/yr during the Plio-Quaternary.

Comparison of estimated sediment volumes between source and sink over the last 2-3 Myrs shows at least ~40-60% came from incision into the SJDO surface. The remainder must have come from some combination of the intervening highlands and drainage areas outside the current SJDO surface extent. In map view (Fig. 4.7), the largest source areas not accounted for by SJDO incision are the modern Subandes and the intervening highlands. The Subandes probably contributed to the Emborozú Formation, but sediments probably can get trapped locally in the Tertiary piggyback basins prior to reaching the perennial Grande, Parapeti, and Pilcomayo trunk rivers. The best candidate source might be the intervening highlands because they extend over significant areas and exhibit the steepest slopes.

Plio-Quaternary to modern denudation rates

Measurements of denudation rates, drainage areas, and volumes of sediment produced or deposited are inherently imprecise. No singular observation, or even a range of observations on a single feature, can be considered accurate in isolation. Observations can only be evaluated based on their internal consistency. Our analysis demonstrates that estimates of denudation <0.1 km/Ma cannot (and estimates <0.2 km/Ma probably do not) characterize the entire Bolivian-Andes hinterland of the Chaco foreland over the Plio-Quaternary (last 2-3 Myrs) even though some observations demonstrate that such rates may be locally viable (Fig. 4.8). Modern estimates suggest the Pilcomayo basin erodes at a rate (0.34 mm/yr) near the minimum that characterized

the Plio-Quaternary. In contrast, both the Grande and Parapeti basin rates (0.91 and 1.01 mm/yr) are significantly higher (Fig. 4.8). This variation in erosion rates could be the result of the general southward aridification [e.g. Barnes and Pelletier, 2006], anthropogenic effects, and/or sediment discharge variations resulting from the type of dominant erosion process and precipitation storminess [e.g. Fuller et al., 2003].

Table 4.5. Potential age (Ma) of megafan initiation.

Megafan volume (km^3)		**Potential sediment production rates from the modern landscape (km^3/Ma)**			
		Absolute Highest	*High End of Likely*	*Low End of Likely*	*Absolute Lowest*
		96,910	61,756	58,193	11,639
Grande					
Maximum	3,864	0.040	0.063	0.066	0.332
Likely	3,220	0.033	0.052	0.055	0.277
Minimum	1,288	0.013	0.021	0.022	0.111
		Absolute Highest	*High End of Likely*	*Low End of Likely*	*Absolute Lowest*
		12,163	6,931	6,633	1,461
Parapeti					
Maximum	1,813	0.149	0.262	0.273	1.241
Likely	1,511	0.124	0.218	0.228	1.034
Minimum	604	0.050	0.087	0.091	0.414
		Absolute Highest	*High End of Likely*	*Low End of Likely*	*Absolute Lowest*
		141,654	30,379	28,643	17,012
Pilcomayo					
Maximum	3,998	0.028	0.132	0.140	0.235
Likely	3,332	0.024	0.110	0.116	0.196
Minimum	1,333	0.009	0.044	0.047	0.078
		Absolute Highest	*Neogene Median*		*Absolute Lowest*
		250,727	122,906		30,112
All megafans					
Maximum	9,675	0.039	0.079		0.321
Likely	8,063	0.032	0.066		0.268
Minimum	3,225	0.013	0.026		0.107

shading = best sediment-production rate estimate

Evolution of topography

Topographic evolution can be better understood by determining the amount and rate of morphologic change across different spatial and temporal scales. Here we use the physical dimensions determined in this study to comment on central Andean fold-thrust belt and Chaco foreland topographic variations over the late Miocene-Quaternary (last ~10 Myrs).

The Grande, Parapeti, and Pilcomayo basins collectively expanded by ~50% from ~100,000 to ~150,000 km^2 since ~10 Ma (Table 4.1). Migration of the drainage divide westward was ~100 km since ~10 Ma as was the migration of the drainage outlet eastward (Fig. 4.5). This migration rate of 10 mm/yr is similar to locally estimated rates of thrust belt propagation (6-8 mm/yr), shortening (~4-8 mm/yr), and foreland basin migration (~13 mm/yr) [McQuarrie et al., 2005; Barnes et al., 2008]. Westward, headward erosion, stream piracy, and eastward drainage expansion into the Subandes probably contributed to drainage basin growth. In particular, stream piracy by the Río Pilcomayo of the Sucre/Potosi region probably contributed the most to the Pilcomayo basin's growth of ~115% from ~40,000 to ~87,000 km^2 (Table 4.2). Despite the area lost to the Pilcomayo, the Grande basin still grew in overall size by almost 10%. Finally, the Parapeti basin actually decreased in size by ~15% probably via the encroachment of the two larger basins on either side of it. These data suggest that large (10^{4-5} km^2) drainages in (potentially protracted) semi-arid climates still evolve substantially over 10 Myr time frames.

The modern fluvial megafans are estimated to be up to ~228 kyrs old (Table 4.5). Unfortunately, to the best of our knowledge, no studies have estimated the age of any other modern megafans for comparison. Regardless, the ~228 kyr age suggests that large sediment bodies can be dispersed over distances of >200 km across low-sloped (mostly <0.35°) regions rather rapidly even in semi-arid climates. Furthermore, the

currently active megafans represent only a small portion (in either time or sediment volume) of the most recent seismically resolvable sedimentation history in the basin. In fact, sedimentary evidence suggests Subandes megafans have existed for the last ~8 Ma [Uba et al., 2007].

Thrust belt-foreland geodynamics

Thrust belt deformation and erosion are dynamically coupled to their associated foreland basin systems via deformation, foreland flexure, and erosion [e.g. DeCelles and DeCelles, 2001]. Models of this coupling predict that regions of reduced erosion are characterized by wedge growth, a wide, rapidly propagating thrust belt with dominantly wedgetop deposition and an underfilled foredeep, whereas regions of enhanced erosion are characterized by wedge recycling, a narrow thrust belt with more constant width, and dominantly foredeep deposition in a wide and largely filled foreland (Fig. 4.2) [Simpson, 2004, 2006]. These predictions are, to first-order, consistent with the central Andean fold-thrust belt where observations mentioned above suggest the dry, southern Chaco foredeep is basically underfilled and the wet, northern Beni foredeep is overfilled because ~50% of the sediment bypasses it and enters the Amazon [Horton, 1999; Aalto et al., 2006; Barnes and Pelletier, 2006]. Unfortunately, the models have only been developed for the general case. They could be tested by calibrating them to specific regions and constraining the surface process parameters with such datasets as those presented here. Figure 4.10 schematically illustrates the central Andean thrust belt-Chaco foreland basin system sediment budget presented here. Selected, important values derived throughout this study are indicated. Comparison of Figures 4.1 and 4.10 illustrates the contrast between the idealized and our applied thrust belt-foreland system sediment budget analysis.

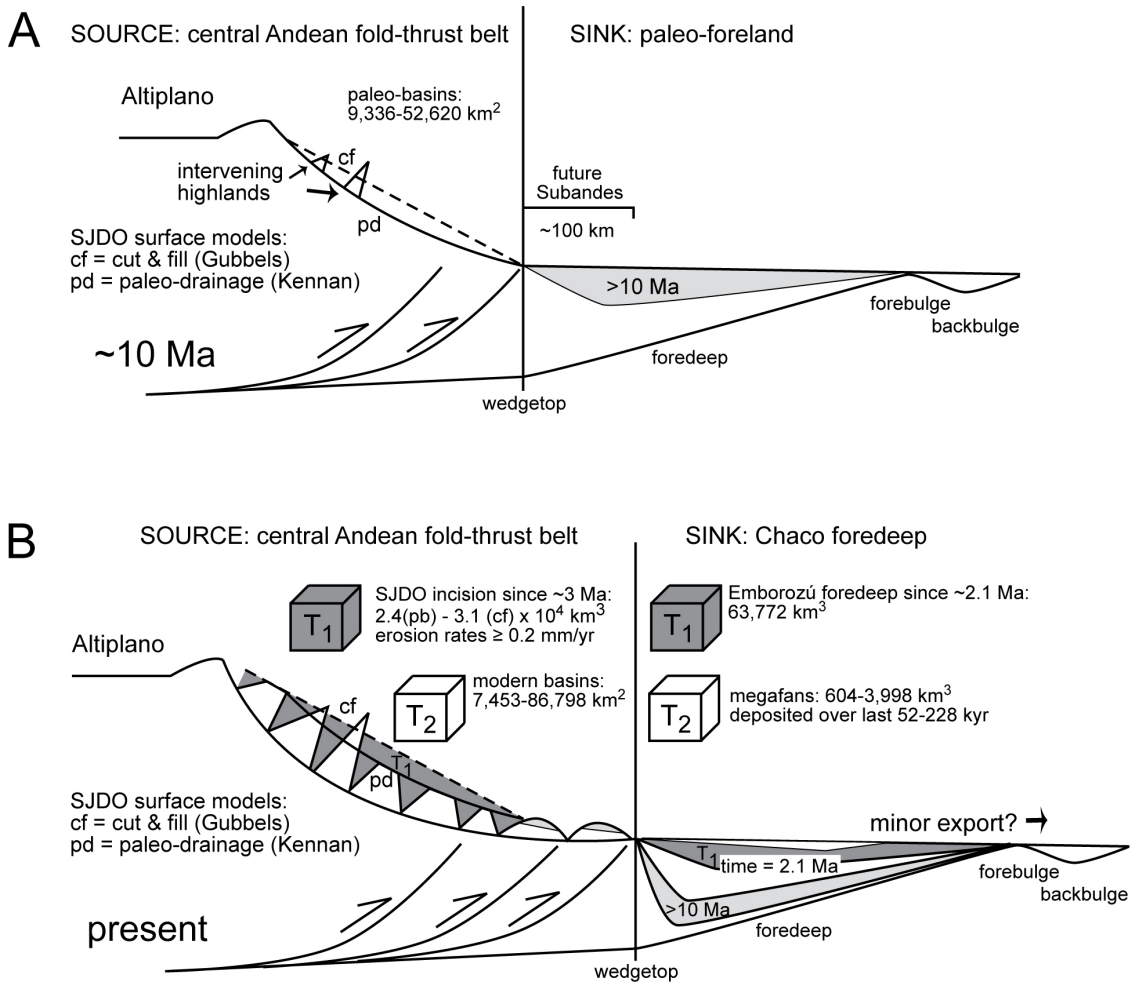

Figure 4.10. Schematic central Andean fold-thrust belt and Chaco foreland basin system sediment budget in cross section at ~20°S. cf = cut and fill model surface representation (dashed line in source), pd = paleo-drainage surface representation (solid concave up line in source). (A) Source and sink features during peak San Juan del Oro (SJDO) formation at ~10 Ma prior to incision. (B) Source and sink features after incision at present. Time slice T_1 is the Plio-Quaternary to recent (~2 or 3 – 0 Ma) represented by the volume eroded by incision into the SJDO surface in the source and deposited within the Emborozú Formation in the sink, respectively. Time slice T_2 is very recent time (~230 – 0 ka) represented by the modern drainage areas and the megafan volumes in the foreland, respectively. Additional source region solid lines represent the modern maximum (jagged line) and minimum (lowest line) topography.

Acknowledgements

Financial support was provided to J. Barnes by an ExxonMobil summer internship and NSF grant EAR 0409289 to T. A. Ehlers. We thank Bob Brovey for providing the enhanced satellite images. This paper benefited from early discussions with Brian Horton, Lorcan Kennan, and Peter DeCelles, and very thorough reviews by Kennan, an anonymous reviewer, and editor DeCelles.

Appendix 4.1. Elaboration on methods, uncertainties, and discussion

Overview

This Appendix elaborates on methodologies and reported uncertainties as well as provides further discussion on several items mentioned in the main text.

Method details

All mapping and calculations were performed in ArcGIS™ 9.2, primarily with the Functional Surface, Raster Surface, Extraction, Hydrology, Interpolation, and Surface modules within the 3D Analyst and Spatial Analyst extensions. All mapping was done using the Geographic Coordinate System WGS84 datum. Area calculations were made on maps projected to WGS84 UTM Zone 20 South.

Modern drainage area

The Grande, Parapeti, and Pilcomayo watershed boundaries were extracted by determining the area of contributing flow to the pixel of maximum flow accumulation located within the active channel at the mountain front. The contributing flow area was defined by the HydroSHEDS flow-accumulation grid using the “Watershed” function in ArcGIS Spatial Analyst. Although no internally drained basins occupy the Parapeti and

Grande drainage basins, three small (<20 km^2), internal basins within the Pilcomayo watershed were removed and assumed to contribute to the overall basin area for simplicity. We estimate ~200 m (or ~2 pixels) accuracy in outlet location determined by comparisons between the DEM and satellite images that translates to at most a 2% difference in estimated basin area. Therefore, we report at 2% error on our measured basin areas.

Our area estimate for the Grande drainage basin is very close to the estimate published by Leier et al. (2005), but ~15% smaller than the value reported by Horton and DeCelles (2001) (Table 4.1). Our estimates are within 7% of the values previously reported for the Parapeti drainage (Table 4.1). In the case of the Pilcomayo catchment, Horton and DeCelles (2001) and Leier et al. (2005) based their drainage-basin outline (white boundary in Fig. 4.2, corresponding to Pilcomayo 1 area estimates in Table 4.1), on the location of the nearest gauging station, which lies >50 km west of the megafan apex. If we use that definition, our estimate of the drainage basin area is virtually identical to the previous estimates (Table 4.1). However, we prefer to locate the drainage basin outlet at the megafan apex, because the extra ~6000 km^2 between the major mountain front and the megafan apex is certainly part of the source area contributing to megafan deposition.

It is important to note that map projections and datums are important when comparing area estimates from different sources. Using the same watershed boundary, area estimates for the Grande drainage varies from 53,864 km^2 (South America Lambert Conformal Conic projection) to 59,342 km^2 (Albers Equal Area projection). This magnitude of variation projections is ~10%, which is the same order of magnitude (~7-15%) as the deviation of our reported drainage areas from other published estimates.

Paleo-drainage area

The paleo-drainage area is conceptually bounded by the area of the preserved SJDO surface and the area of the modern drainage. The measurement uncertainty on these limits is the same as for the modern drainage, as discussed above.

Megafan areas

The upstream megafan margins were the easiest to delineate based primarily on criteria 1-3. We estimate the accuracy on these portions of the megafan margins to be ~1 km. The megafan terminations (eastern margins) were more difficult to define and were mostly distinguished by criteria 3 and 4 due to the more subtle topography. We estimate the accuracy on these portions of the megafans to be on the order of ~10 km. A 10 km radius extension of a symmetrical, double-cone-shaped megafan with an internal apex angle of 66°, 145 km radius, and 933 km^3 in volume (roughly the size of the Grande megafan) would result in a 14% increase in area.

In detail, the western and northern margins of the Pilcomayo megafan are well-defined, but the eastern margin accuracy is poor. For the Parapeti megafan, the northern margin is well-defined by the modern floodplain of the active channel, but the southeastern margin is poorly constrained due to the overprint of dunes. Finally, for the Grande megafan, the southeastern margin is well-constrained by the modern floodplain of the ephemeral portion of the Río Parapeti channel [see also Horton and DeCelles, 2001] and poorly constrained in its northwestern and southwestern margins by the overprint of agriculture and dunes, respectively.

The southern Bolivia megafans vary by an order of magnitude in size, but display relatively similar surface slopes and relief (Table 4.1). Most surface slopes are <0.35° (<~0.45%) with values as high as ~15° (~35%) localized along the active channel banks. The dominantly low relief and gradients on the megafan surfaces mean area calculations are most sensitive to the map-view outline of the megafan. The total variation among

the three megafan estimates, defined as (largest-smallest)/average, is 25.7% for the Grande, 14.9% for the Parapeti, and 25.5% for the Pilcomayo.

With the Geographic Coordinate System WGS84, our Grande megafan area estimate is 12,985 km^2 (Table 4.1). Using the same megafan boundary, area estimates using different projections vary from 11,796 km^2 (South America Lambert Conformal Conic projection) to 12,994 km^2 (Albers Equal Area projection). The magnitude of variation among area estimates obtained with different projections is 9%, which is similar to the uncertainty for megafan margin positions (~14%). We presume that some portion of the difference in our reported areas, compared to Horton and DeCelles (2001) or Leier et al. (2005), is due to differences in fan margin location, whereas the remaining difference is due to differences in the mechanics of area calculation. It is possible that these two sources of difference could work in opposite directions, making the apparent divergence in area estimates either smaller or larger than we have reported.

Megafan volumes

The planar base assumption probably represents an unrealistically small approximation of the fan volumes. Accommodation space created by thrust-loading of the basin margin commonly decreases basinward from the thrust front. Thus, a horizontal basal surface for the fan equal to the elevation of the most distal edge of the fan likely represents a lower bound for the megafan volume. Assumption (2) is directionally more realistic because it places the basal surface progressively deeper closer to the thrust front where the elevation of the fan surface is higher. Unfortunately, there is no clear evidence to test whether it over-estimates or under-estimates the true depth to the real basal surface. Seismic lines shot across the fans, or boreholes through the fans, would provide the only definitive observations to properly establish the proper geometry of the basal surface. In addition to uncertainty about the exact position of the

basal surface, errors associated with the map-view outline of the megafans propagate into the volume calculation.

Uncertainty in megafan area is a very small contribution to megafan volume uncertainty fan because the megafan is vanishingly thin at the position of the uncertain margins.

Foredeep basin fill volumes

Significant topography and islands of zero thickness only ~20 km east of the Parapeti megafan termination [Uba et al., 2006] suggest our reconstructed basal surface is too deep in places, implying that the volume estimates derived from this method may represent an upper limit, regardless of the uncertainties discussed below.

Uncertainties include: (a) how closely the N5 seismic-package lower boundary actually corresponds to the dated base of the Emborozú Formation; (b) how accurately the lower boundary of the N5 can be picked, given the limitations of the seismic-data coverage and quality; (c) how precisely time on the seismic section is converted to depth; and (d) how confidently we can extrapolate published contours to the north of the region where they have actually been mapped. The first two uncertainties (a and b) are likely to be small (a few 10s of meters) and non-systematic, so that their overall contribution to the uncertainty of the volume estimate can be neglected. The time-depth conversion uncertainty (c) cannot be answered directly from the published details [Uba et al., 2006]. There are at least a dozen wells that tie to their seismic, so errors might be as low as 3%. However, errors on the order of 12-20% are known from time-depth conversions calculated only from seismic moveout velocities (C. Lloyd, ExxonMobil Geophysical Applications Specialist for South America, pers. comm.). The northward extrapolation uncertainty (d) appears reasonable because the mapped isopachs parallel the mountain front, but remain speculative.

We take 20% as the integrated value of all these uncertainties based on the maximum uncertainty of time-depth conversion. Uncertainty in the vertical dimension of the basin fill is certainly larger than the uncertainty in the horizontal dimensions, and so should be the dominant factor in assessing overall uncertainty.

Denudation-rate estimates

At any scale, most denudation will occur in a relatively small fraction of the space or time over which the estimate is integrated. In space, feldspar mineral dissolution is localized on the mineral surface [Lüttge, 2005], disaggregation within rock is initially localized at fractures and microfractures [Heins, 1995], and landscape-scale erosion is focused by relief in rills, spurs, or valleys [Brandt and Thornes, 1987]. In time, mineral-surface dissolution is most significant during isolated periods of step-wave migration [Lasaga and Lüttge, 2001], hillslope sediment export is most rapid during episodic mass-wasting events [Crozier, 1986], and alluvial/fluvial sediment transport is most significant during episodic high-flow events [Kochel, 1988]. Every denudation observation integrates active with inactive (space, time). Every observation is an appropriate estimate for some relevant (time, space), but none of the observations are appropriate estimates for every (time, space).

Treatment of ions and pores

Assuming reasonable values for the hinterland provenance lithotypes of 20% Q-rich sand, 10% F-rich sand, 10% L-rich sand, 50% shale, and 10% meta-sandstone, no more than 1-15 wt% of the weathered rock should be lost to dissolved ions based on an equilibrium weathered mineral assemblage constrained by the aluminum content of the provenance lithotypes [Heins and Kairo, 2007]. Void space among deposited sedimentary particles depends on the degree of sorting within the deposit [Beard and

Weyl, 1973; Atkins and McBride, 1992], particle ductility, and their burial depth [Paxton et al., 2002]. For reasonable sediment properties: ductile:rigid = 4; Folk sorting = 0.7; matrix volume fraction = 0.1 and β = 0.06 MPa^{-1}, we would expect porosities in the Chaco foreland sediments to be on the order of 32% near the surface, declining to approximately 16% at maximum burial depth (1,500 m).

Modern sediment-production estimates

Geomorphic evidence suggests the megafans are not closed systems themselves. The megafans are not closed because (a) some suspended sediments bypass the megafans via the active channels that range from 10s m wide at the mountain front to 10s of km wide by the time they reach the megafan terminations [Iriondo, 1993], (b) stratigraphic and isotopic evidence suggest the Parapeti and Pilcomayo channels may have been stable over the last 1 - 35 kyrs [Iriondo, 1993; Geyh et al., 1998], (c) the Río Parapeti channel beyond the megafan appears to be both eroding into and being deflected by the Río Grande megafan as it sweeps northward towards the Izogog swamp (Fig. 4.2B), (d) small ephemeral channel headwaters originate within the megafans themselves [Horton and DeCelles, 2001], and (e) aeolian input on both seasonal and glacial time scales give rise to present (e.g. light areas on the south-to-southeast margins of the Grande and Parapeti megafans, Fig. 4.2B) and past dune fields, depositing loess up to 20 m thick in the Quaternary alone [Iriondo, 1997]. This collective evidence suggests our megafan volume calculations are minimums.

References

Aalto, R., T. Dunne, and J. L. Guyot (2006), Geomorphic controls on Andean denudation rates, Journal of Geology, v. 114, 85-99.

Allen, P. A. (2008), From landscapes into geological history, Nature, v. 451, 274-276.

Allmendinger, R. W., T. E. Jordan, S. M. Kay, and B. L. Isacks (1997), The evolution of the Altiplano-Puna Plateau of the Central Andes, Annual Review of Earth and Planetary Sciences, v. 25, 139-174.

Atkins, J. E., and E. F. McBride (1992), Porosity and packing of Holocene river, dune, and beach sands, American Association of Petroleum Geologists Bulletin, v. 76, 339-355.

Babault, J., J. van den Driessche, S. Bonnet, S. Castelltort, and A. Crave (2005), Origin of the highly elevated Pyrenean peneplain, Tectonics, v. 24, doi:10.1029/2004TC001697.

Baby, P., G. Herail, R. Salinas, and T. Sempere (1992), Geometry and kinematic evolution of passive roof duplexes deduced from cross section balancing; example from the foreland thrust system of the southern Bolivian subandean zone, Tectonics, v. 11, 523-536.

Baby, P., R. Limachi, I. Moretti, E. Mendez, J. Oller, B. Guiller, and M. Specht (1995), Petroleum system of the northern and central Bolivian sub-Andean zone, in Petroleum basins of South America, A. J. Tankard, R. Suarez and H. J. Welsink (ed.), American Association of Petroleum Geologists Memoir 62, 445-458.

Barke, R., and S. Lamb (2006), Late Cenozoic uplift of the Eastern Cordillera, Bolivian Andes, Earth and Planetary Science Letters, v. 249, 350-367.

Barnes, J. B., T. A. Ehlers, N. McQuarrie, P. B. O'Sullivan, and S. Tawackoli (2008), Thermochronometer record of central Andean Plateau growth, Bolivia (19.5ºS), Tectonics, doi:10.1029/2007TC002174, in press.

Barnes, J. B., and J. D. Pelletier (2006), Latitudinal variation of denudation in the evolution of the Bolivian Andes, American Journal of Science, v. 306, 1-31.

Beard, D. C., and P. K. Weyl (1973), Influence of Texture on Porosity and Permeability of Unconsolidated Sand, American Association of Petroleum Geologists Bulletin, v. 57, 349-369.

Beaumont, C., H. Kooi, and S. Willett (2000), Coupled tectonic-surface process models with applications to rifted margins and collisional orogens, in Geomorphology and global tectonics, M. Summerfield (ed.), John Wiley & Sons, Chichester, UK, 29-55.

Bonnell, L. M., and R. H. Lander (2003), Reservoir quality prediction in deep water to tight gas sandstones using a process/stochastic modeling approach, American

Association of Petroleum Geologists Bulletin, v. 87, AAPG Distinguished Lectures.

Brandt, C. J., and J. B. Thornes (1987), Erosional energetics, in Energetics of physical environment: energetic approaches to physical geography, K. J. Gregory (ed.), John Wiley & Sons, Chichester, 51-87.

Bray, A. A., R. H. Lander, C. A. Watkins, C. J. Lowrey, M. Owen, and Anonymous (2000), Characterisation and prediction of clastic reservoir quality; an integrated model for use in exploration, appraisal and production projects, paper presented at American Association of Petroleum Geologists Bulletin.

Burgess, P. M., and P. A. Allen (1996), A forward-modelling analysis of the controls on sequence stratigraphical geometries, Geological Society of London Special Publication, v. 103, 9-24.

Clark, M. K., L. H. Royden, K. X. Whipple, B. C. Burchfiel, X. Zhang, and W. Tang (2006), Use of a regional, relict landscape to measure vertical deformation of the eastern Tibetan Plateau, Journal of Geophysical Research, v. 111, doi:10.1029/2005JF000294.

Clevis, Q., P. de Boer, and M. Wachter (2003), Numerical modelling of drainage basin evolution and three-dimensional alluvial fan stratigraphy, Sedimentary Geology, v. 163, 85-110.

Clevis, Q. J. W. A. (2003), Three-dimensional modelling of thrust-controlled foreland basin stratigraphy, Doctoral thesis, Geologica Ultraiectina, v. 226, 135 pp, Universiteit Utrecht, Utrecht.

Clift, P., C. Gaedicke, R. Edwards, J. Lee, II, P. Hildebrand, S. Amjad, R. S. White, and H.-U. Schlueter (2002), The stratigraphic evolution of the Indus Fan and the history of sedimentation in the Arabian Sea, Marine Geophysical Researches, v. 23, 223-245.

Clift, P. D. (2006), Controls on the erosion of Cenozoic Asia and the flux of clastic sediment to the ocean, Earth and Planetary Science Letters, v. 241, 571-580.

Coudert, L., T. Sempere, M. Frappa, C. Viquier, and R. Arias (1993), Subsidence and crustal flexure evolution of the Neogene Chaco foreland basin, paper presented at Third International Symposium on Andean Geodynamics, Oxford, extended abstracts.

Critelli, S. (1999), The interplay of lithospheric flexure and thrust accommodation in forming stratigraphic sequences in the Southern Apennines foreland basin system, Italy, Atti della Accademia Nazionale dei Lincei. Rendiconti Lincei. Scienze Fisiche e Naturali, v. 9, 257-326.

Critelli, S., J. Arribas, E. Le Pera, A. Tortosa, K. M. Marsaglia, and K. K. Latter (2003), The recycled orogenic sand provenance from an uplifted thrust belt, Betic Cordillera, southern Spain, Journal of Sedimentary Research, v. 73, 72-81.

Crozier, M. J. (1986), Landslides: Causes, Consequences and Environment, 252 pp., Croom Helm, London.

Curray, J. R. (1994), Sediment volume and mass beneath the Bay of Bengal, Earth and Planetary Science Letters, v. 125, 371-383.

Damanti, J. F. (1993), Geomorphic and structural controls on facies patterns and sediment composition in a modern foreland basin, in Alluvial sedimentation, M. Marzo and C. Puigdefabregas (ed.), International Association of Sedimentologists Special Publication, 221-233.

de Sitter, L. U. (1952), Pliocene uplift of Tertiary mountain chains, American Journal of Science, v. 250, 297-307.

DeCelles, P. G., and W. Cavazza (1999), A comparison of fluvial megafans in the Cordilleran (Upper Cretaceous) and modern Himalayan foreland basin systems, Geological Society of America Bulletin, v. 111, 1315-1334.

DeCelles, P. G., and P. C. DeCelles (2001), Rates of shortening, propagation, underthrusting, and flexural wave migration in continental orogenic systems, Geology, v. 29, 135-138.

DeCelles, P. G., and K. A. Giles (1996), Foreland basin systems, Basin Research, v. 8, 105-123.

DeCelles, P. G., and B. K. Horton (2003), Early to middle Tertiary foreland basin development and the history of Andean crustal shortening in Bolivia, Geological Society of America Bulletin, v. 115, 58-77.

Devlin, W. J., K. W. Rudolph, C. A. Shaw, and K. D. Ehman (1993), The effect of tectonic and eustatic cycles on accommodation and sequence-stratigraphic framework in the Upper Cretaceous foreland basin of southwestern Wyoming, in Sequence stratigraphy and facies associations, H. W. Posamentier, C. P. Summerhayes, B. U. Haq and G. P. Allen (ed.), International Association of Sedimentologists Special Publication 18, 501-520.

Dickinson, W. R. (1974), Plate tectonics and sedimentation, in Tectonics and sedimentation, W. R. Dickinson (ed.), SEPM Special Publication 22, 1-27.

Dunn, J. F., K. G. Hartshorn, and P. W. Hartshorn (1995), Structural styles and hydrocarbon potential of the sub-Andean thrust belt of southern Bolivia, in Petroleum basins of South America, A. J. Tankard, R. Suarez and H. J. Welsink (ed.), American Association of Petroleum Geologists Memoir 62, 523-543.

Echavarria, L., R. Hernandez, R. Allmendinger, and J. Reynolds (2003), Subandean thrust and fold belt of northwestern Argentina; geometry and timing of the Andean evolution, American Association of Petroleum Geologists Bulletin, v. 87, 965-985.

Ege, H., E. R. Sobel, E. Scheuber, and V. Jacobshagen (2007), Exhumation history of the southern Altiplano plateau (southern Bolivia) constrained by apatite fission-track thermochronology, Tectonics, v. 26, doi:10.1029/2005TC001869.

Einsele, G., L. Ratschbacher, and A. Wetzel (1996), The Himalaya-Bengal Fan denudation-accumulation system during the past 20 Ma, Journal of Geology, v. 104, 163-184.

Elger, K., O. Oncken, and J. Glodny (2005), Plateau-style accumulation of deformation: Southern Altiplano, Tectonics, v. 24, doi:10/1029/2004TC001675.

Epis, R. C., and C. E. Chapin (1975), Geomorphic and tectonic implications of the post-Laramide, late Eocene erosion surface in the southern Rocky Mountains, in Cenozoic history of the southern Rocky Mountains, B. F. Curtis (ed.), Geological Society of America Memoir 144, 45-74.

Flemings, P. B., and T. E. Jordan (1989), A synthetic stratigraphic model of foreland basin development, Journal of Geophysical Research, v. 94, 3851-3866.

Fuller, C. W., S. D. Willett, N. Hovius, and R. Slingerland (2003), Erosion rates for Taiwan mountain basins: new determinations from suspended sediment records and a stochastic model of their temporal variation, Journal of Geology, v. 111, 71-87.

Geslin, J. K., T. M. Demko, P. A. Drzewiecki, H. R. Feldman, S. T. Hasiotis, G. G. McCrimmon, J. C. Van Wagoner, and R. W. Wellner (2001), Sediment flux, paleoclimate, and sequence stratigraphy; lessons learned from numerical modeling, paper presented at 7th International Conference on Fluvial sedimentology Proceedings, Open-File Report - University of Nebraska-Lincoln, Conservation and Survey Division, Report: OFR-60.

Geslin, J. K., T. M. Demko, P. A. Drzewiecki, H. R. Feldman, S. T. Hasiotis, G. G. McCrimmon, J. C. Van Wagoner, and R. W. Wellner (2002), Relative role of stream discharge, sediment flux, and baselevel change in stratal architecture of continental and nearshore sequences; results from forward numerical modeling, paper presented at AAPG Annual Meeting Expanded Abstracts.

Geyh, M. A., W. Kruck, R. Pasig, and L. Feldhaus (1998), Isotope hydrological study on the origin and age of deep groundwater in the semi-arid Chaco boreal, South America, paper presented at Isotope techniques in the study of environmental change: proceedings of an international symposium on isotope techniques in the study of past and current environmental changes in the hydrosphere and the atmosphere, International Atomic Energy Agency.

Gohain, K., and B. Parkash (1990), Morphology of the Kosi Megafan, in Alluvial fans: A field approach, A. H. Rachocki and M. Church (ed.), John Wiley & Sons, Chichester, 151-178.

Gubbels, T. L. (1993), Tectonics and geomorphology of the eastern flank of the central Andes, 18-23°S latitude, Doctoral thesis, 211 pp, Cornell University, Ithaca.

Gubbels, T. L., B. L. Isacks, and E. Farrar (1993), High-level surfaces, plateau uplift, and foreland development, Bolivian central Andes, Geology, v. 21, 695-698.

Gupta, S. (1997), Himalayan drainage patterns and the origin of fluvial megafans in the Ganges foreland basin, Geology, v. 25, 11-14.

Hay, W. W., C. N. Wold, and J. M. Herzog (1992), Preliminary mass-balanced 3-D reconstructions of the Alps and surrounding areas during the Miocene, in Computer graphics in geology, R. Pflug and J. W. Harbaugh (ed.), Lecture Notes in Earth Sciences 41, 99-110.

Heins, W. A. (1995), The use of mineral interfaces in sand-sized rock fragments to infer ancient climate, Geological Society of America Bulletin, v. 107, 113-125.

Heins, W. A., and S. Kairo (2007), Predicting sand character with integrated genetic analysis, in Sedimentary Provenance and Petrogenesis: Perspectives from Petrography and Geochemistry, M. J. Johnsson, S. Critelli and J. Arribas (ed.), Geological Society of America Special Paper 420, 345-379.

Horton, B. K. (1999), Erosional control on the geometry and kinematics of thrust belt development in the central Andes, Tectonics, v. 18, 1292-1304.

Horton, B. K., and P. G. DeCelles (1997), The modern foreland basin system adjacent to the Central Andes, Geology, v. 25, 895-898.

Horton, B. K., and P. G. DeCelles (2001), Modern and ancient fluvial megafans in the foreland basin system of the Central Andes, southern Bolivia; implications for drainage network evolution in fold-thrust belts, Basin Research, v. 13, 43-63.

Hovius, N., and M. Leeder (1998), Clastic sediment supply to basins, Basin Research, v. 10, 1-5.

Hulka, C. (2005), Sedimentary and tectonic evolution of the Cenozoic Chaco foreland basin, southern Bolivia, Doctoral thesis, Freie Universitat, Berlin.

Hulka, C., K.-U. Grafe, B. Sames, C. E. Uba, and C. Heubeck (2006), Depositional setting of the Middle to Late Miocene Yecua Formation of the Chaco Foreland Basin, southern Bolivia, Journal of South American Earth Sciences, v. 21, 135-150.

Iriondo, M. (1993), Geomorphology and late Quaternary of the Chaco (South America), Geomorphology, v. 7, 289-303.

Iriondo, M. H. (1984), The Quaternary of northeastern Argentina, in Quaternary of South America and Antarctic Peninsula, J. Rabassa (ed.), A.A. Balkema, 51-78.

Iriondo, M. H. (1997), Models of deposition of loess and loessoids in the upper Quaternary of South America, Journal of South American Earth Sciences, v. 10, 71-79.

Isacks, B. L. (1988), Uplift of the Central Andean Plateau and bending of the Bolivian Orocline, Journal of Geophysical Research, v. 93, 3211-3231.

Jordan, T. E. (1995), Retroarc foreland and related basins, in Tectonics of sedimentary basins, C. J. Busby and R. V. Ingersoll (ed.), Blackwell Science, Oxford, 331-362.

Jordan, T. E., and R. N. Alonso (1987), Cenozoic stratigraphy and basin tectonics of the Andes Mountains, 20°-28° south latitude, American Association of Petroleum Geologists Bulletin, v. 71, 49-64.

Jordan, T. E., J. H. Reynolds, III, and J. P. Erikson (1997), Variability in age of initial shortening and uplift in the Central Andes, in Tectonic uplift and climate change, W. F. Ruddiman (ed.), Plenum Press, New York, 41-61.

Kennan, L. (2000), Large-scale geomorphology of the Andes; interrelationships of tectonics, magmatism and climate, M. A. Summerfield (ed.), John Wiley & Sons, Chichester, 167-199.

Kennan, L., S. Lamb, and J. Rundle (1995), K-Ar dates from the Altiplano and Cordillera Oriental of Bolivia; implications for Cenozoic stratigraphy and tectonics, Journal of South American Earth Sciences, v. 8, 163-186.

Kennan, L., S. H. Lamb, and L. Hoke (1997), High-altitude palaeosurfaces in the Bolivian Andes; evidence for late Cenozoic surface uplift, in Palaeosurfaces; recognition, reconstruction and palaeoenvironmental interpretation, M. Widdowson (ed.), Special Publication of the Geological Society 120, London, 307-323.

Kley, J. (1996), Transition from basement-involved to thin-skinned thrusting in the Cordillera Oriental of southern Bolivia, Tectonics, v. 15, 763-775.

Kley, J. (1999), Geologic and geometric constraints on a kinematic model of the Bolivian Orocline, Journal of South American Earth Sciences, v. 12, 221-235.

Kochel, R. C. (1988), Geomorphic impact of large floods; review and new perspectives on magnitude and frequency, in Flood Geomorphology, V. R. Baker, R. C. Kochel and P. C. Patton (ed.), John Wiley & Sons, New York, 169-187.

Kuhlemann, J., W. Frisch, I. Dunkl, and B. Szekely (2001), Quantifying tectonic versus erosive denudation by the sediment budget; the Miocene core complexes of the Alps, Tectonophysics, v. 330, 1-23.

Kuhlemann, J., W. Frisch, B. Szekely, I. Dunkl, and M. Kazmer (2002), Post-collisional sediment budget history of the Alps; tectonic versus climatic control, International Journal of Earth Sciences, v. 91, 818-837.

Lander, R. H., and O. Walderhaug (1999), Predicting porosity through simulating sandstone compaction and quartz cementation, American Association of Petroleum Geologists Bulletin, v. 83, 433-449.

Lasaga, A. C., and A. Lüttge (2001), Variation of Crystal Dissolution Rate Based on a Dissolution Stepwave Model, Science, v. 291, 2400-2404.

Le Pichon, X., M. Fournier, and L. Jolivet (1992), Kinematics, topography, shortening, and extrusion in the India-Eurasia collision, Tectonics, v. 11, 1085-1098.

Leeder, M., T. Harris, and M. Kirkby (1998), Sediment supply and climate change; implications for basin stratigraphy, Basin Research, v. 10, 7-18.

Leier, A. L., P. G. DeCelles, and J. D. Pelletier (2005), Mountains, monsoons, and megafans, Geology, v. 33, 289-292.

Lüttge, A. (2005), Etch pit coalescence, surface area, and overall mineral dissolution rates, American Mineralogist, v. 90, 1776-1783.

Marshall, L. G., T. Sempere, and M. Gayet (1993), The Petaca (late Oligocene-middle Miocene) and Yecua (late Miocene) formations of the Subandean-Chaco Basin, Bolivia, and their tectonic significance, in Documents des Laboratoires de Geologie, Lyon, vol.125, M. Gayet (ed.), Universite Claude Bernard, Departement des Sciences de la Terre, 291-301.

McMillan, M. E., P. L. Heller, and S. L. Wing (2006), History and causes of post-Laramide relief in the Rocky Mountain orogenic plateau, Geological Society of America Bulletin, v. 118, 393-405.

McQuarrie, N. (2002), The kinematic history of the central Andean fold-thrust belt, Bolivia; implications for building a high plateau, Geological Society of America Bulletin, v. 114, 950-963.

McQuarrie, N., J. B. Barnes, and T. A. Ehlers (2008), Geometric, kinematic, and erosional history of the central Andean Plateau, Bolivia (15-17ºS), Tectonics, doi:10.1029/2006TC002054, in press.

McQuarrie, N., B. K. Horton, G. Zandt, S. Beck, and P. G. DeCelles (2005), Lithospheric evolution of the Andean fold-thrust belt, Bolivia, and the origin of the central Andean plateau, Tectonophysics, v. 399, 15-37.

Moretti, I., P. Baby, E. Mendez, and D. Zubieta (1996), Hydrocarbon generation in relation to thrusting in the Sub Andean Zone from 18 to 22ºS, Bolivia, Petroleum Geoscience, v. 2, 17-28.

Müller, J. P., J. Kley, and V. Jacobshagen (2002), Structure and Cenozoic kinematics of the Eastern Cordillera, southern Bolivia (21ºS), Tectonics, v. 21, doi: 10.1029/2001TC001340.

Overeem, I., J. P. M. Syvitski, E. W. H. Hutton, and A. J. Kettner (2005), Stratigraphic variability due to uncertainty in model boundary conditions; a case study of the New Jersey shelf over the last 40,000 years, Marine Geology, v. 224, 23-41.

Patterson, P. E., A. R. Sprague, R. E. Hill, K. M. McDonald, and Anonymous (1995), Sequence stratigraphy and fluvial facies architecture, Farrer and Tuscher

formations (Campanian), Tusher Canyon, Utah, paper presented at AAPG and SEPM Annual Meeting Abstracts 4.

Paxton, S. T., J. O. Szabo, and J. M. Ajdukiewicz (2002), Construction of an intergranular volume compaction curve for evaluating and predicting compaction and porosity loss in rigid-grain sandstone reservoirs, American Association of Petroleum Geologists Bulletin, v. 86, 2045-2065.

Pazzaglia, F. J., and M. T. Brandon (1996), Macrogeomorphic evolution of the post-Triassic Appalachian Mountains determined by deconvolution of the offshore based sedimentary record, Basin Research, v. 8, 255-278.

Perez, R., S. Ghosh, J.-Y. Chatellier, R. Lander, and Anonymous (1999), Application of sandstone diagenetic modeling to reservoir quality assesment of the Misoa Formation, Bachaquero Field, Maracaibo Basin, Venezuela, paper presented at AAPG Annual Meeting Expanded Abstracts.

Phillips, J. D., and B. Gomez (2007), Controls on sediment export from the Waipaoa River basin, New Zealand, Basin Research, v. 19, 241-252.

Placzek, C., J. Quade, and P. J. Patchett (2006), Geochronology and stratigraphy of late Pleistocene lake cycles on the southern Bolivian Altiplano; implications for causes of tropical climate change, Geological Society of America Bulletin, v. 118, 515-532.

Robin, C., D. Rouby, D. Granjeon, F. Guillocheau, P. Allemand, and S. Raillard (2005), Expression and modelling of stratigraphic sequence distortion, Sedimentary Geology, v. 178, 159-186.

Robinson, R. A. J., and R. L. Slingerland (1998a), Grain-size trends, basin subsidence and sediment supply in the Campanian Castlegate Sandstone and equivalent conglomerates of central Utah, Basin Research, v. 10, 109-127.

Robinson, R. A. J., and R. L. Slingerland (1998b), Origin of fluvial grain-size trends in a foreland basin; the Pocono Formation on the central Appalachian Basin, Journal of Sedimentary Research, v. 68, 473-486.

Roeder, D., and R. L. Chamberlain (1995), Structural geology of sub-Andean fold and thrust belt in northwestern Bolivia, in Petroleum basins of South America, A. J. Tankard, R. Suarez and H. J. Welsink (ed.), American Association of Petroleum Geologists Memoir 62, 459-479.

Schlunegger, F., T. E. Jordan, and E. M. Klaper (1997), Controls of erosional denudation in the orogen on foreland basin evolution; the Oligocene central Swiss Molasse Basin as an example, Tectonics, v. 16, 823-840.

Schlunegger, F., J. Melzer, and G. E. Tucker (2001), Climate, exposed source-rock lithologies, crustal uplift and surface erosion; a theoretical analysis calibrated with data from the Alps/North Alpine foreland basin system, International Journal of Earth Sciences, v. 90, 484-499.

Scott, G. R. (1975), Cenozoic surfaces and deposits in the southern Rocky Mountains, in Cenozoic history of the southern Rocky Mountains, B. F. Curtis (ed.), Geological Society of America Memoir 144, 227-248.

Servant, M., T. Sempere, J. Argollo, M. Bernat, G. Feraud, and P. Lo Bello (1989), Cenozoic morphogenesis and uplift of the Eastern Cordillera in the Bolivian Andes, Comptes Rendus de l'Academie des Sciences de Paris, v. 309, 416-422.

Simpson, G. (2004), Dynamic interactions between erosion, deposition, and three-dimensional deformation in compressional fold belt setting, Journal of Geophysical Research, v. 109, doi:10.1029/2003JF000111.

Simpson, G. (2006), Modelling interactions between fold–thrust belt deformation, foreland flexure and surface mass transport, Basin Research, v. 18, 125-143.

Sobel, E. R., and M. R. Strecker (2003), Uplift, exhumation and precipitation: tectonic and climatic control of Late Cenozoic landscape evolution in the northern Sierras Pampeanas, Argentina, Basin Research, v. 15, 431-451.

Stock, G. M., T. A. Ehlers, and K. A. Farley (2006), Where does sediment come from? Quantifying catchment erosion with detrital apatite (U-Th)/He thermochronometry, Geology, v. 34, 725-728.

Tucker, G. E., and R. L. Slingerland (1996), Predicting sediment flux from fold and thrust belts, Basin Research, v. 8, 329-349.

Uba, C. E., C. Heubeck, and C. Hulka (2005), Facies analysis and basin architecture of the Neogene Subandean synorogenic wedge, southern Bolivia, Sedimentary Geology, v. 180, 91-123.

Uba, C. E., C. Heubeck, and C. Hulka (2006), Evolution of the late Cenozoic Chaco foreland basin, southern Bolivia, Basin Research, v. 18, 145-170.

Uba, C. E., M. R. Strecker, and A. K. Schmitt (2007), Increased sediment accumulation rates and climatic forcing in the central Andes during the late Miocene, Geology, v. 35, 979-982.

Van Wagoner, J. C. (1995), Sequence stratigraphy and marine to nonmarine facies architecture of foreland basin strata, Book Cliffs, Utah, U.S.A, in Sequence stratigraphy of foreland basin deposits; outcrop and subsurface examples from the Cretaceous of North America, J. C. Van Wagoner and G. T. Bertram (ed.), American Association of Petroleum Geologists Memoir 64, 137-223.

Van Wagoner, J. C., R. T. Beaubouef, D. C. J. D. Hoyal, P. A. Dunn, N. L. Adair, V. L. D. Abreu, R. W. Wellner, D. N. Awwiller, T. Sun, M. Deffenbaugh, and H. C (2003), Energy dissipation and the fundamental shape of siliciclastic sedimentary bodies, paper presented at AAPG and SEPM Annual Meeting Extended Abstracts.

Widdowson, M. (1997), The geomorphological and geological importance of palaeosurfaces, in Palaeosurfaces: recognition, reconstruction and

palaeoenvironmental interpretation, M. Widdowson (ed.), Special Publication of the Geological Society 120, London, 1-12.

Wilkinson, M. J., L. G. Marshall, and J. G. Lundberg (2006), River behavior on megafans and potential influences on diversification and distribution of aquatic organisms, Journal of South American Earth Sciences, v. 21, 151-172.

Chapter 5

Cenozoic deformation, uplift, and evolution of the central Andean Plateau[1]

.

Abstract

We synthesize a wide range of geologic, geochemical, and geophysical observations to present a current description and evaluation of geologic and geodynamic models of central Andean Plateau (AP) development (14-28°S). We discuss consistencies and inconsistencies in studies of the history of deformation, sedimentation, exhumation and uplift as well as the structure of the lithosphere. We find that AP deformation began ~60-40 Ma and migrated eastward with variable shortening magnitudes (~530-150 km) and rates (~20-1 mm/yr) in space and time, respectively. Constraints on the resulting uplift history indicate a ~1.5 km elevation gain since ~10 Ma, but are equally consistent with a linear rise since ≥25 Ma as a rapid rise of ~2.7 km ~10-6 Ma within error. Widespread, substantial incision (2.5-1 km) occurred along the western AP flank since ~11-8 Ma associated with surface uplift or climate change. Geophysical and geodynamic investigations identify an isostatically-compensated thick crust (~80-65 km), elevated heat flow, zones of low and high velocity and attenuation in the crust and mantle, and stress the importance of weakened lithosphere, partial melt, and crustal flow or delamination for AP morphology. We conclude that significant upper-

[1]**Citation:**

Barnes, J. B., and T. A. Ehlers (in prep), Cenozoic deformation, uplift, and evolution of the central Andean Plateau.

plate deformation is an essential process in AP growth and that the history of shortening: (a) has taken significantly longer and (b) was more uniform over an along-strike distance of ~1500 km than previously thought. Finally, we suggest that late Miocene, rapid surface uplift models for the AP are not entirely consistent with observations used to support this interpretation and a more protracted Cenozoic uplift history is tenable.

Introduction

The plateaus of Tibet and the central Andes are the most prominent modern orogenic features on Earth. Despite this, the topographic, tectonic, and geodynamic evolution of orogenic plateaus is imprecisely known and the focus of much current research. These high elevation plateaus are thought to influence local-to-far-field lithospheric deformation, global sediment fluxes, ocean chemistry, atmospheric circulation, precipitation, and climate change [Richter et al., 1992; Molnar et al., 1993; Masek et al., 1994; Lenters and Cook, 1995; Royden, 1996; Ruddiman et al., 1997; Sobel et al., 2003]. A plethora of important processes has been invoked for facilitating plateau growth. These processes include: (1) magmatic addition [Thorpe et al., 1981; Kono et al., 1988], (2) distributed shortening [Dewey et al., 1988; Isacks, 1988; Tapponnier et al., 2001], (3) spatio-temporal variations in upper plate properties, plate interface, and subduction geometry [Jordan et al., 1983; Isacks, 1988; Gephart, 1994; Allmendinger and Gubbels, 1996; Kley et al., 1999; McQuarrie, 2002a; Lamb and Davis, 2003; Hoke and Lamb, 2007], (4) ablative subduction, crustal flow, and delamination [England and Houseman, 1989; Bird, 1991; Kay and Mahlburg Kay, 1993; Kay et al., 1994; Lamb and Hoke, 1997; Pope and Willett, 1998; Clark and Royden, 2000; Beaumont et al., 2001; Husson and Sempere, 2003; Garzione et al., 2006], (5) cratonic under-thrusting [Lamb and Hoke, 1997; Matte et al., 1997], (6) spatial erosion gradients [Masek et al., 1994; Horton, 1999; Beaumont et al., 2001; Montgomery et al., 2001], and

(7) gravitational collapse [Dewey, 1988; Molnar et al., 1993]. Although numerous studies have presented various data sets contributing valuable localized insights into these various processes, an updated and generalized view of plateau evolution is needed.

Previous plateau studies have resulted in a consensus that has eliminated processes like magmatic addition as important [e.g. Francis and Hawkesworth, 1994; Giese et al., 1999] and stressed the significance of shortening, thermal weakening, extrusion, and lithospheric thinning for plateau formation [e.g. Allmendinger et al., 1997; Hodges, 2000; Tapponnier et al., 2001; McQuarrie, 2002b; Clark et al., 2005]. However, controversy remains on other issues such as the history of plateau uplift [e.g. Molnar et al., 1993; Garzione et al., 2006; Rowley and Currie, 2006; Garzione et al., 2007; Hartley et al., 2007] and the structure and behavior of plateau lithosphere [e.g. Tapponnier et al., 2001; McQuarrie, 2002b; Müller et al., 2002; Beaumont et al., 2004; Bendick and Flesch, 2007]. Numerical models of orogenesis can reproduce realistic plateau morphologies when accounting for temperature-dependent viscosity variations in a thickening crust [Willett et al., 1993; Wdowinski and Bock, 1994b; Royden, 1996; Willett and Pope, 2004]. However, numerical modeling studies are often limited by inadequate knowledge of the kinematics, timing, and rates of plateau deformation and uplift as well as how variable they are along strike. This review addresses both the accepted and more tenuous existing hypotheses associated with Andean Plateau (AP) development and highlights possible directions for future research. The main purpose of this paper is to present an up-to-date, synoptic history of AP growth that can be used to (a) better evaluate conceptual geologic AP formation models and (b) calibrate and refine future numerical simulations of plateau evolution.

We identify plateau-wide trends from a diverse range of geologic observations that place constraints on the Cenozoic history of Andean Plateau development. More

specifically, we present a synthesis of (1) the structure and deformation history inferred from cross sections, sedimentary basins, and geo-thermochronology, (2) the deformation history estimated from rock exhumation, (3) the uplift history constrained by marine sedimentation, paleobotany, paleoclimate proxies, erosion surfaces, and stable isotopes, (4) the history of fluvial incision into the plateau margins quantified from geomorphic, stratigraphic, and thermochronologic analysis, and (5) the current lithospheric structure deduced from geophysical studies. Within each subject, we summarize the observations, highlight the key interpretations relevant to AP formation, and point out important caveats. Finally, we develop a single chronologic history for the Andean Plateau from the collective observations and interpretations and evaluate the implications it has for three current geologic models of AP formation. The most important conclusion is that substantial upper-plate deformation is essential to AP growth and it may have taken significantly longer and was more uniform along strike than previously appreciated.

Previous reviews

Several previous review papers have addressed the Cenozoic evolution of the central Andes. The most notable overview of the AP is by Isacks [1988] and the most recent review is by Allmendinger et al. [1997]. Individual papers addressing the entire Andes are rare [e.g. Kley et al., 1999; Montgomery et al., 2001], but regional-scale summaries with a particular geologic focus (e.g. shortening, erosion, uplift) are common [Megard, 1987; Noblet et al., 1996; Jordan et al., 1997; Gregory-Wodzicki, 2000; Kennan, 2000; Ramos et al., 2004; Barnes and Pelletier, 2006; Strecker et al., 2007]. Several papers focus on the upper-plate deformation and magmatism specifically associated with the AP [Isacks, 1988; Allmendinger et al., 1997; Riller and Oncken, 2003; Oncken et al., 2006b]. A few papers synthesize the local tectonic, sedimentary,

magmatic, and lithospheric structure and evolution of the central Andes in northern Chile and Bolivia [Lamb et al., 1997; McQuarrie et al., 2005]. The recent book *The Andes Active Subduction Orogeny* edited by Oncken et al. [2006a] contains chapters that present a database-oriented synthesis of specific geologic topics related to the southern-central Andes. An older book with a similar structure and theme is *Tectonics of the southern central Andes: structure and evolution of an active continental margin* edited by Reutter et al. [1994]. Finally, many papers simulate AP evolution with numerical models [e.g. Wdowinski and Bock, 1994b; Babeyko et al., 2002; Yang et al., 2003; Yanez and Cembrano, 2004; Vietor and Oncken, 2005].

This study builds upon previous work by including: (a) reference to the large amount of literature published in the last decade, and (b) a wide cross section of Earth Science sub-disciplines that are not all covered in the previous reviews. Finally, this study encompasses the entire AP region from southern Peru to northern Argentina (Fig. 5.1B). In this study, we focus on the well-cited, current, occasionally seminal, and thorough papers that often include regional compilations themselves. We generally exclude references to conference abstracts and less accessible journals.

Geologic overview and context

The central Andean (or Altiplano-Puna) Plateau (AP) is defined as the region >3 km in elevation in the core of the Andes at ~14-28°S in western South America (Fig. 5.1) [Isacks, 1988]. The AP spans ~1800 km north to south and ~200-450 km west to east. The AP overrides a normal, east-dipping (~30°) portion of the subducting Nazca Plate between zones of flat slab geometries. Cenozoic normal-to-oblique subduction in the central Andes has produced considerable magnitude and latitudinal variability in shortening (~530-150 km) that has both bent the Bolivian orocline and contributed to AP uplift [Isacks, 1988; McQuarrie, 2002a]. Neogene magmatism is distributed throughout

both flanks of the AP with Pliocene to recent volcanism concentrated only along its western flank and non-existent above the flat slab zones to the north and south [e.g. de Silva, 1989]. Crust and mantle thicknesses beneath the plateau range from ~50-75 km and 100-150 km, respectively [Beck et al., 1996; Whitman et al., 1996; Myers et al., 1998; Beck and Zandt, 2002]. The AP is morphologically divided into the northern Altiplano (~3700 m elevation, low relief) and the southern Puna (~4200 m elevation, higher relief) (Fig. 5.1C).

The AP region is divided into several tectonomorphic zones. From west to east these include: the Precordillera (PrC), the Western Cordillera (WC), the Altiplano-Puna basin (AL and PU), the Eastern Cordillera (EC), the Interandean zone (IA), and the Subandes (SA)/Santa Barbara Ranges (SB)/Sierras Pampeanas (SP) (Fig. 5.2). The Precordillera and Western Cordillera constitute the western AP flank, which is a faulted [Muñoz and Charrier, 1996; Victor et al., 2004], crustal-scale monocline of west-dipping late Oligocene to mid-Miocene sediments [Hoke et al., 2007]. The Precordillera includes the Atacama basin which forms a westward concave bend in the AP margin at ~23°S [Jordan et al., 2007]. The Western Cordillera is the modern volcanic arc marking the western drainage divide of the Altiplano-Puna basin. The Altiplano-Puna is a region of low-relief, closed depocenters filled with Tertiary sediments, evaporates, and volcanics [e.g. Sobel et al., 2003; Placzek et al., 2006; Strecker et al., 2007]. The eastern AP margin is occupied by the thick-to-thin skinned central Andean fold-thrust belt [e.g. McQuarrie, 2002b]. The Eastern Cordillera is the highest relief region consisting of deformed, predominantly Paleozoic sedimentary rocks with overlying Tertiary volcanism and is the eastern Altiplano-Puna drainage divide. North of ~23°S, the Interandean zone and Subandes step progressively downwards in topographic elevation and upwards in structural depth eastward exposing mostly Devonian and Carboniferous through Mesozoic and Tertiary rocks, respectively [e.g. Kley, 1996; McQuarrie, 2002b]. South of

Figure 5.1. The Andes of South America with particular focus on the Andean Plateau. (A) Topography is from the GTOPO30 1 km data set. Elev = elevation. Flat-slab regions marked with black bars. Central Andes present-day plate boundary (bold line) with shortening restored sequentially back to ~70 Ma (thin lines; values = km shortening) and plate convergence vectors and chronology from McQuarrie [2002b]. (B) Andean Plateau region topography is from the SRTM 90 m data set. Plateau extent is defined by the 3 km contour after Isacks [1988]. (C) 50 km swath-averaged S-N plateau topographic profile after Whitman et al. [1996]. Profile location is line in part B.

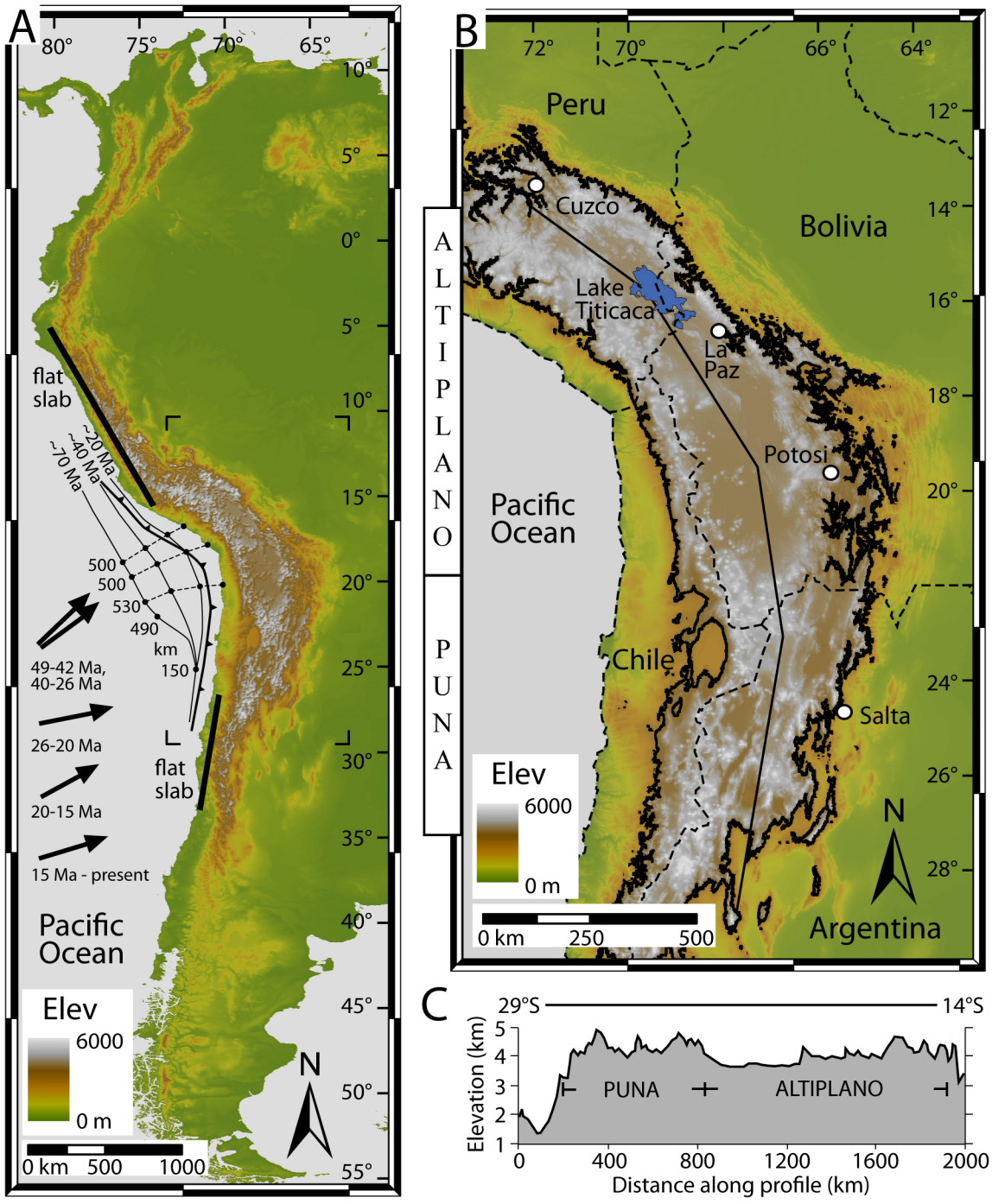
A
80°
75°
70°
65°
10°
5°
0°
5°
10°
15°
20°
25°
30°
35°
40°
45°
50°
55°
flat slab
~20 Ma
~40 Ma
~70 Ma
500
500
530
490
km
150
49-42 Ma, 40-26 Ma
26-20 Ma
20-15 Ma
15 Ma - present
flat slab
Pacific Ocean
Elev
6000
0 m
0 km 500 1000
N
B
72°
70°
66°
64°
12°
14°
16°
18°
20°
24°
26°
28°
Peru
Bolivia
Cuzco
Lake Titicaca
La Paz
Potosi
Salta
ALTIPLANO
PUNA
Pacific Ocean
Chile
Argentina
Elev
6000
0 m
0 km 250 500
N
C
29°S
14°S
Elevation (km)
1
2
3
4
5
PUNA
ALTIPLANO
0
400
800
1200
1600
2000
Distance along profile (km)

~23°S, the Interandean zone and Subandes transition into high angle, reverse-faulted ranges and basement-cored uplifts of the Santa Barbara Ranges [Kley and Monaldi, 2002] and Sierra Pampeanas [Schmidt et al., 1995; Ramos et al., 2002], respectively. The morphological and structural transition from Altiplano to Puna at ~23°S is related to Precambrian to Mesozoic paleogeography and changes in the lithospheric thickness and subduction geometry [Allmendinger et al., 1997 and references therein].

Three current geologic models of Andean Plateau (AP) development

There are three current and contrasting geologic models for AP development which provide an important framework for how the various data sets are synthesized in the following section. We outline the models here.

Model 1

Early characterization of Andean orogeny identified several major punctuated deformation events: the late Cretaceous Peruvian, the late Eocene Incaic, and the late Miocene Quechua phases [Megard, 1987; Sempere et al., 1990; Noblet et al., 1996]. The latter two deformation phases correlate with periods of rapid plate convergence reconstructed from seafloor magnetic anomalies and reconstructions of the western coastline (Fig. 5.1A) [Pardo-Casas and Molnar, 1987]. Isacks [1988] proposed a model consistent with these notions that has two distinct stages. Phase one (1) is pure shear, late Oligo-Miocene (~27-10 Ma) Quechua deformation and thickening in the Altiplano and Eastern Cordillera accompanied by lithospheric weakening due to lower-angle subduction relative to present. Phase two (2) is late Miocene to present (~10-0 Ma) simple shear deformation in the Subandes contemporaneous with lower crust thickening below the plateau [see also Gubbels et al., 1993; Allmendinger and Gubbels, 1996]. During phase 1, processes supposedly responsible for surface uplift include shortening

and lower crustal flow [Husson and Sempere, 2003]. During phase 2, uplift is related to under-plating of forearc material [Baby et al., 1997], lithospheric removal [e.g. Kay et al., 1994; Allmendinger et al., 1997], and under-thrusting of the Brazilian lithosphere below the foreland [e.g. Barke and Lamb, 2006].

Model 2

An alternative view of AP plateau formation is characterized by continuous simple shear deformation over a considerably longer time period [e.g. Noblet et al., 1996; McQuarrie et al., 2005]. This view is the result of recent estimates on the magnitudes, timing, and rates of shortening, exhumation, and foreland basin migration combined with kinematic reconstructions of the central Andean fold-thrust belt [McQuarrie, 2002b; DeCelles and Horton, 2003; Elger et al., 2005; Horton, 2005; Ege et al., 2007; Barnes et al., 2008; Carrapa and DeCelles, 2008; McQuarrie et al., 2008]. This model describes eastward-propagating deformation starting in the late Cretaceous-Paleocene (~70 Ma) in the Western Cordillera and jumping to the central Eastern Cordillera in the mid Eocene (~40 Ma). Deformation then became generally bi-vergent in the Eastern Cordillera and propagated into the Altiplano and Interandean zone during the Oligocene to mid-Miocene (~20-15 Ma). Deformation then moved farther east into the Subandes by the mid Miocene to present (~15-0 Ma). In this model, the massive shortening is controlled by large basement structures in the mid-upper crust [Kley, 1999; McQuarrie, 2002b]. This extended chronology, when combined with geodynamic models, has led to the suggestion that thickening and shortening facilitated removal of mantle lithosphere by ablative subduction and/or piecemeal-to-wholesale delamination [Pope and Willett, 1998; Beck and Zandt, 2002; McQuarrie et al., 2005; Garzione et al., 2006]. The associated surface uplift history ranges from a slow and steady rise since the Eocene to recent elevation gain of ~3.5-2.5 km during a delamination event ~10-6

Ma contemporaneous with migration of accelerated shortening into the Subandes [e.g. Garzione et al., 2006; Hartley et al., 2007; Ehlers and Poulsen, in prep].

Model 3

The most complex geologic model of AP formation involves the interplay between three key parameters: (1) differential motion between the subducting slab and upper plate (e.g. slab rollback), (2) high coupling of the plate interface due to low trench sedimentation, and (3) the lateral distribution of weakened zones in the upper plate [Oncken et al., 2006b]. This model highlights two main episodes determined from a quantitative analysis of spatio-temporal variations in deformation: (a) a period of higher sediment flux into the trench, which reduced the strength of the plate interface, decreased shortening, and enhanced slab rollback from 45-33 Ma, followed by (b) a period of reduced slab dip that accelerated shortening from 33-22 Ma. The focus and distribution of deformation is facilitated by inherited zones of structural weakness. Residency of the AP within the arid latitudinal zone is also important. In this model, recognition that deformation preceded magmatism and their time-space distribution vary independently [Trumbull et al., 2006] downplays the role of magmatism in preconditioning the lithosphere by thermal weakening, but supports delamination as a possible heat source. The associated uplift history is demonstrated by a simulated elevation history requiring 30 Myrs of thickening and isostasy with a transition from pure to simple shear at 10 Ma (without any redistributive mechanisms of crustal material). The simulated topography is similar to the Altiplano region, but not the Puna or Subandes.

Synthesis of observations

In the following, we organize, illustrate, and tabulate previous AP region studies into the following subsections: (1) structure, deformation, and the associated sedimentation, (2) spatial and temporal variations in exhumation, (3) surface and rock uplift histories, (4) fluvial incision along the plateau flanks, and (5) lithospheric structure derived from geophysical observations. In each subsection, we synthesize the observations, highlight key interpretations relevant to the formation of the AP, and briefly discuss associated caveats.

Structure, deformation, and associated sedimentation

Numerous studies have integrated sedimentology, stratigraphy, geo-thermochronology, reflection seismology, and structural data to constrain the chronology of Cenozoic upper-crustal deformation in the AP region. For example, (a) balanced sections and shortening estimates combined with chronologic information provide insight into the mode, style, and rate of deformation [e.g. Allmendinger et al., 1997; Kley and Monaldi, 1998; McQuarrie, 2002b], (b) dating growth strata with magnetostratigraphy or $^{40}Ar/^{39}Ar$ dating of interbedded tuffs provides time control on sedimentation synchronous with local deformation [e.g. Elger et al., 2005], and (c) dating sediments with palynology and detailing their provenance provides a proxy for the timing source region deformation uplift, and erosion [e.g. Horton et al., 2002]. In this compilation, we chose to exclude the literature of deformation magnitude and style that is devoid of chronologic constraints [e.g. Roeder, 1988; Sheffels, 1990; Baby et al., 1995; Dunn et al., 1995; Roeder and Chamberlain, 1995; Welsink et al., 1995].

Figure 5.2A shows the locations and timing of AP region deformation estimated from sedimentary and structural evidence by studies listed in Table 5.1. This synthesis shows deformation in the Precordillera/Western Cordillera region began in the Paleocene to mid-Eocene (~60-35 Ma). Deformation has been ongoing in these regions

since ~40-35 Ma. Deformation moved into the Eastern Cordillera in the mid-Eocene lasting until the late Miocene (~40-10 Ma). Deformation propagated both eastward and westward from the Eastern Cordillera since ~40 Ma in Bolivia. Eastward, deformation of the Interandean zone began in the early Miocene (~20 Ma) followed by the Subandes from late Miocene to today (9-0 Ma). Westward from the Eastern Cordillera, deformation of the Altiplano-Puna began in the earliest Oligocene (~30 Ma) and ceased in the Altiplano by late Miocene (~7 Ma), but remains active today in the Puna. In the Argentine Eastern Cordillera, both late Eocene (~40 Ma) and early Miocene to recent (~20-0 Ma) deformation is documented. Finally, paleomagnetic rotation data observe Cenozoic counterclockwise rotations (~10-30°) north of the Bolivian orocline and clockwise rotations (~10-60°) south of the orocline [see summaries in Lamb, 2001; Roperch et al., 2006; Barke et al., 2007].

There are several key interpretations relevant to AP development. The western plateau flank is a simple monoclinal structure that exhibits thrust deformation and has experienced associated uplift since ~60-40 Ma all along strike. Basement-involved structures kinematically link the Altiplano plateau to its eastern thrust belt margin. These basement structures have controlled the thrust belts' physiography, short-wavelength (1-10 km) deformation, and high magnitude shortening (~250-500 km; Fig. 5.1A) in a thick (8-15 km) sedimentary wedge [Kley, 1996; Kley and Monaldi, 1998; Kley, 1999; McQuarrie and DeCelles, 2001; McQuarrie, 2002b; McQuarrie et al., 2005]. However, controversy exists on how complicated the ramp-flat thrust sheet geometries are in the basement [e.g. compare McQuarrie, 2002b; Müller et al., 2002; Elger et al., 2005]. The sedimentary history and kinematic reconstructions of the Altiplano both suggest the modern width of the plateau was established by ~25-20 Ma after which most deformation ceased in the Eastern Cordillera [Horton et al., 2002; McQuarrie, 2002b; Horton, 2005]. Finally, estimated shortening rates for the Altiplano region average ~11-8 mm/yr, but

range in space and time from 16 to <1 mm/yr [Elger et al., 2005; McQuarrie et al., 2005; Oncken et al., 2006b; Barnes et al., 2008; McQuarrie et al., 2008].

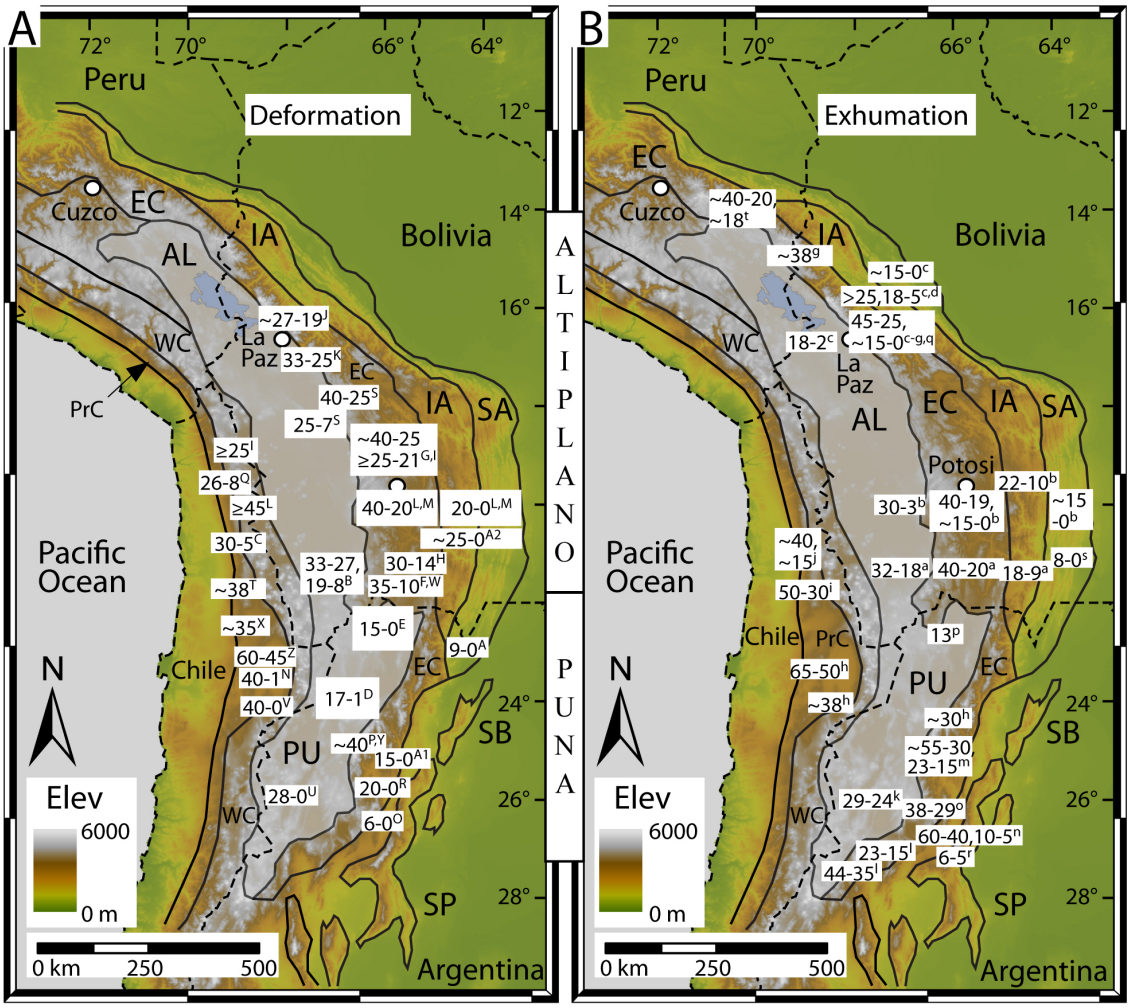

Figure 5.2. The deformation, sedimentation, and exhumation history of the Andean Plateau. Tectonomorphic zones are modified from Jordan et al. [1983], McQuarrie [2002], Roperch et al. [2006], and Insel et al. [in revision]: PrC = Precordillera, WC = Western Cordillera, AL = Altiplano, PU = Puna, EC = Eastern Cordillera, IA = Interandean zone, SA = Subandes, SB = Santa Barbara Ranges, SP = Sierras Pampeanas. (A) Timing (in Ma) of initiation and/or duration of deformation inferred from integrated sedimentation, geo-thermochronology, and structure data. Superscripted uppercase letters refer to rows in Table 5.1. (B) Timing (in Ma) of initiation and/or duration of deformation inferred from exhumation studies based on thermochronology data. Superscripted lowercase letters refer to rows in Table 5.2.

Table 5.1. Andean Plateau region deformation studies using sediments, geo-thermochronology, and structure.

Letter*	Methods	Age in Ma (Location)	Reference
A	magstrat., seismic, growth strata, bal. sections	9-0(SA)	Echavarria et al. 2003
B	K/Ar(b, fspar, glss) & Ar/Ar(b,hbl) of volcanoclastics, seismic, growth strata, bal. sections	33-27 & 19-8(AL: Khenayuni-Uyuni Fault Zone/Lipez basin)	Elger et al. 2005
C	Ar/Ar(hbl, b) of volcanoclastics, stratigraphy, seismic	30-5(PrC)	Victor et al. 2004
D	Ar/Ar(hbl, b, plag, wr) of volcanoclastics, kinematic data	17-1(PU)	Marrett et al. 1994
E	Ar/Ar(b) of volcanoclastics, kinematic data	15-0(PU/AL)	Cladoudos et al. 1994
F	K/Ar(b, wr) of volcanoclastics, kinematic data	29-10(EC: Tupiza area basins)	Herail et al. 1996
G	Ar/Ar(b, kspar) of volcanoclastics, basin stratigraphy	~40 & ≥25-21(EC)	Horton 2005
H	Ar/Ar(b) of tuffs, growth strata, stratigraphy	30-14(EC: Tupiza basins)	Horton 1998
I	Sediment provenance and stratigraphy	~40-23(AL basin seds)	Horton et al. 2002
J	Synthesized biochronology, K/Ar(b, m, kspar, wr), magstrat.	27-19(AL/EC)	Sempere 1990
K	Sediment provenance, growth strata	33-25(AL: Luribay & Salla beds)	Gillis et al. 2006
L	Sythesis of structural, stratigraphic, and thermchronologic data	≥45(WC), 40-20(EC), 20-0(IA & SA)	McQuarrie et al. 2005
M	Kinematic evolution linked to sediments, stratigraphy, and thermochronology	40-20(EC), 20-0(IA & SA)	McQuarrie 2002
N	Subsurface stratigraphy and correlation, structure, seismic	40-1(PrC: Atacama basin)	Jordan et al. 2007
O	Stratigraphy, seismic, structure, detrital FT(ap)	6-0(SP: El Cajon & Campo Arenal)	Mortimer et al. 2007
P	Structure, stratigraphy, growth strata, paleontology	~40(EC: Calchaqui Valley)	Hongn et al. 2007
Q	K/Ar(b, wr) & Ar/Ar(b, plag), stratigraphy, growth strata, structure	26-8(PrC: Aroma Region)	Farias et al. 2005
R	Structure, stratigraphy, detrital FT(ap), U-Pb(zr)	20-0(EC: Angastaco basin)	Coutand et al. 2006
S	K/Ar(b, fspar, hbl), stratigraphy	40-25(EC), 25-7(AL)	Kennan et al. 1995; Lamb & Hoke 1997
T	Ar/Ar(b, hbl) of volcanoclastics	~38(PrC)	Hammerschmidt et al. 1992
U	K/Ar & Ar/Ar(b, m, amph, kspar, wr, san, glss, fspar, plag) of volcanoclastics	~38? & 28-0(PU: Salar de Antofalla area)	Kraemer et al. 1999
V	Structure and synthesized chronostratigraphy	40-0(WC: SE Atacama margin)	Kuhn 2002
W	Ar/Ar(b, hbl) & K/Ar(b, fspar, glss) of volcanoclastics, kinematic data, bal. sections	40/30-10(EC: Atocha, Mochara, & Yunchara segments)	Muller et al. 2002
X	Structure, kinematic data, radiometric age data of volcanics, mylonites, mineral alteration	~35(PrC: Chuquicamata)	Reutter et al. 1996
Y	detrital FT(ap) & modeling, stratigraphy, sedimentology, provenance, detrital U-Pb(zr)	~40(PU: Salar de Pastos Grandes)	Carrapa & DeCelles 2008; DeCelles et al. 2007
Z	seismic, wells, stratigraphic correlation, growth strata	60-45(PrC: Atacama basin)	Arriagada et al. 2006
A1	magstrat, sediment provenance	15-0(EC/SB: Sierra de Gonzolaz)	Reynolds et al. 2000
A2	stratigraphy, seismic, well logs, biostratigraphy	25-0(SA: foreland deposits)	Uba et al. 2005, 2006; Hulka et al. 2006

* keyed to Figure 5.2; m = muscovite; b = biotite; fspar = feldspar; kspar = potassium feldspar; hbl = hornblende; wr = whole rock; plag = plagioclase; san = sanidine; glss = glass; K/Ar = 40K/39Ar; Ar/Ar = 40Ar/39Ar; magstrat. = magnetostratigraphy; bal. = balanced

location abbreviations same as in Figure 5.2.

The structure of the Argentine Puna is high-angle reverse fault-bounded, basement-cored ranges separated by intermontane basins characterized by long wavelength (10-30 km) deformation and lower magnitude shortening (~150 km; Fig. 5.1A) of a thin clastic wedge [Coutand et al., 2001; McQuarrie, 2002a]. Pre-existing Paleozoic and Mesozoic structures presumably exhibit the dominant control on the location of Puna deformation structures. Previous consensus was initial deformation and sedimentation began in the Puna (~20 Ma) significantly later than in the Altiplano [Allmendinger et al., 1997; Jordan et al., 1997; McQuarrie, 2002a]. However, we conclude from several studies that the Puna has experienced widespread and continuous deformation and sedimentation both internally and along its margins since ~40 Ma, perhaps even earlier along the western flank suggestive of deformation propagating eastward since the Paleocene (~60 Ma) (Table 5.1) [Marrett et al., 1994; Coutand et al., 2006; Hongn et al., 2007; Carrapa and DeCelles, 2008].

The paleomagnetic rotation data have been used to argue for [Kono et al., 1985; Isacks, 1988; Roperch et al., 2006; Barke et al., 2007] and against [Kley, 1999; Roperch et al., 2000] the Cenozoic bending of the Bolivian orocline with consensus developing around the former. This bending is believed to be accommodated by the observed shortening gradients [Lamb, 2001; Barke et al., 2007] and attests to the fact that the AP deformation has been fundamentally 3-dimensional in nature rather than 2-dinemsional as assumed by constructed cross sections. The distribution of outward rotations from the plateau center at the bend axis suggests that there is some element of extrusion of material outward along strike.

Spatial and temporal variations in exhumation

Various studies have used low-temperature thermochronology [Reiners and Ehlers, 2005] in bedrock to chronicle exhumation in the AP region. For example, apatite

fission-track thermochronology and inverse modeling of fission tracks can be used to quantify upper-crustal cooling of rock samples from temperatures of ~60-120°C [e.g. Deeken et al., 2006; Ege et al., 2007]. Combined analysis of multiple thermochronometer systems such as fission-track and $^{40}Ar/^{39}Ar$ thermochronology have been used to quantify AP exhumation histories sensitive to temperatures <~350°C [e.g. Gillis et al., 2006].

Figure 5.2B shows the locations and timing (in Ma) of rapid erosional exhumation estimated from AP region studies listed in Table 5.2 (for a plot of apatite fission-track ages throughout the southern-central AP see Figure 12.3 of Alonso et al. (2006)). This synthesis shows that the Precordillera/Western Cordillera region began exhumation first in the Paleocene to mid-Eocene (~60-40 Ma). Next, exhumation jumped into the Eastern Cordillera in the mid-Eocene and continued until the early Miocene (~45-40 to ~20 Ma). The exhumation front propagated both eastward and westward from the central Eastern Cordillera since ~40 Ma. Eastward, exhumation occurred in the Interandean zone from early to late Miocene (~20 to between 10-5 Ma) followed by the Subandes from mid-late Miocene to present (~15-0 Ma). In the south, the exhumation front migrated eastward into the Sierras Pampeanas in the late Miocene (10-5 Ma). Westward from the Eastern Cordillera, exhumation in the Altiplano-Puna began in the earliest Oligocene and continued into the Quaternary (~30-2 Ma), with some mid-Miocene (~15 Ma) exhumation also recorded in the Precordillera. It is important to note that the Eastern Cordillera experienced two distinct phases of exhumation; in Bolivia, localities record both late Eo-Oligocene (~40-20 Ma) and mid-late Miocene to recent (~15-0 Ma) exhumation, and in Argentina, sites record both mid Eo-Oligocene (~50-30 Ma) and early Miocene (23-15 Ma) exhumation (Fig. 5.2B).

Table 5.2. Andean Plateau region exhumation studies.

Letter*	Methods	Age in Ma (Location)	Reference
a	FT(ap) & modeling	32-18(AL), 40-20 (EC), 18-9 (IA)	Ege et al. 2007
b	FT(ap, zr) & modeling	30-3(AL), 36-19 & 16-11(EC), 22-10(IA), ~15-0(SA)	Barnes et al. 2008
c	FT(ap) & He(zr) & modeling	18-2(AL), ~40-25 & ~15-0(EC), 18-8(IA), ~15-0(SA)	Barnes et al. 2006
d	FT(ap, zr) & modeling	18-2(AL), 45-25 & ~15-0(EC), >25 & 18-5(IA)	McQuarrie et al. 2008
e	Ar/Ar(m, b, kspar), FT(ap,zr) & modeling	45-26 & 11-0(EC: Cordillera Real plutons)	Gillis et al. 2006
f	FT (ap, zr)	45-25 & 15-5(EC: Zongo & Huayna Potosi plutons)	Benjamin et al. 1987
g	K/Ar(m, b) & Ar/Ar(m, b)	~38(EC: Zongo-San Gaban zone)	Farrar et al. 1988
h	K/Ar(hbl, b) & FT(ap, zr, sph)	65-50(PrC), ~38(WC), ~30(EC)	Andriessen & Reutter 1994
i	FT(ap) & modeling	50-30(PrC: Domeyko Cordillera)	Maksaev & Zentilli 1999
j	FT(ap, zr)	~40 & ~15(PrC: Quebrada Choja)	Damm et al. 1990
k	FT(ap) & modeling	29-24(PU: Sierra de Calalaste)	Carrapa et al. 2005
l	FT(ap) & modeling	44-35 & 23-15(EC: Cerro Negro & Alto Grande)	Carrapa et al. 2006
m	FT(ap) & modeling	~55-30 & 23-15(EC: several ranges)	Deeken et al. 2006
n	FT(ap) & modeling	~60-40 & 10-5(SP: Sierra Aconquija)	Coughlin et al. 1998
o	FT(ap)	38-29(EC: Chango Real)	Coutand et al. 2001
p	FT(ap)	13(PU: Rinconada)	Cladoudos et al. 1994
q	K/Ar(b, m, hbl, kspar)	~39 (EC: Cordillera Real plutons)	McBride et al. 1987
r	FT(ap) & modeling	6-5(SP: Sierra Aconquija & Cumbres Calchaquies)	Sobel & Strecker 2003
s	FT(ap) & modeling	8-0(SA)	Scheuber et al. 2006
t	K/Ar & Ar/Ar(m, b, kspar), FT(ap)	~40-20 & ~18(EC plutons in southern Peru)	Kontak et al. 1990

* keyed to Figure 5.2

ap = apatite; zr = zircon; m = muscovite; b = biotite; kspar = potassium feldspar; hbl = hornblende; sph = sphene; FT = fission track; K/Ar = 40K/39Ar; Ar/Ar = 40Ar/39Ar; modeling = inverse thermal modeling &/or multi-diffusion domain modeling; PrC = Precordillera; Location abbreviations same as in Figure 5.2

The previous exhumation histories have been used to reconstruct AP evolution based on the assumption that rock cooling is a proxy for deformation. This assumption is generally valid in regions where cooling related to volcanism can be ruled out. In convergent orogens erosion is the primary mechanism of exhumation [Ring et al., 1999; Ehlers, 2005] and the onset of rapid erosional exhumation is a signature of deformation because it generates the topography and relief necessary to drive erosional processes [e.g. Coughlin et al., 1998; Carrapa et al., 2005; Barnes et al., 2006; Ege et al., 2007]. Some periods of recorded, rapid exhumation are considered the result of only enhanced erosion when combined with local geologic evidence [e.g. Gillis et al., 2006]. However, exhumation may not be recorded if the deformation magnitude is insufficient to cause rock cooling below the relevant thermochronometer system closure temperature (~40-70°C for apatite (U-Th)/He, ~60-130°C for apatite fission track, ~150-180°C for zircon (U-Th)/He, ~190-250°C for zircon fission track, and muscovite (400-345°C), biotite (325-280°C), and K-feldspar $^{40}Ar/^{39}Ar$ (150-250°C) [Reiners et al., 2005]).

Probably the most important interpretation that can be deduced from previous exhumation studies is that the modern width of the Altiplano plateau was established by ~15-20 Ma [Barnes et al., 2006; Ege et al., 2007; Barnes et al., 2008; McQuarrie et al., 2008]. In addition, the early episode of Eastern Cordillera exhumation (~50-20 Ma) is considered related to deformation all along strike [Gillis et al., 2006; Ege et al., 2007; Barnes et al., 2008; McQuarrie et al., 2008]. The later episode of Eastern Cordillera exhumation (23-0 Ma) is considered unrelated to major deformation and related to enhanced erosion in Bolivia [Horton, 2005; Gillis et al., 2006; Barnes et al., 2008], whereas it is related to deformation in Argentina [e.g. Deeken et al., 2006].

Constraints on the history of uplift

Many types of information have been used to reconstruct the uplift history of the AP. For example, (a) dated marine facies provide a paleoelevation constraint of near sea level [e.g. Sempere et al., 1997], (b) perched erosion surfaces are important for estimating rock uplift [e.g. Barke and Lamb, 2006], and (c) paleoaltimetry techniques such as fossil floras [Gregory-Wodzicki et al., 1998; Meyer, 2007] and stable isotopes [Quade et al., 2007] provide paleoelevation estimates. A previously compiled history of AP elevation suggested the AP had reached ~25-30% of its modern elevation by early-mid Miocene and ~50% by ~10 Ma [Gregory-Wodzicki, 2000; see also Hartley, 2003].

Figure 5.3 shows the locations and constraints on AP region uplift and elevation from marine facies, paleobotanical techniques, paleoclimate proxies, erosion surfaces, paleosol oxygen and clumped ^{13}C-^{18}O isotopes, and monocline tilting by studies listed in Table 5.3. Marine facies of the late Cretaceous El Molino Formation establishes the entire AP region at near sea level ~73-60 Ma [e.g. Sempere et al., 1997]. The remaining constraints generally support one of the following three simplified histories for the plateau: (1) significant (> ~1 km) uplift prior to 10 Ma, (2) minor uplift (≤ ~1 km) prior to 10 Ma with most gain (≥ ~3 km) post 10 Ma, and (3) significant uplift since ~25 to 20 Ma to present which equivocally could provide support for either history 1 or 2. We outline the constraints that support each simplified history here.

1. Significant pre-late Miocene (>10 Ma) uplift; Paleobotanical evidence using the nearest-living-neighbor method at the Corocoro and Potosi localities suggests 2-.2.4 km elevation prior to 11 Ma (5 and 6a in Table 5.3). Atacama Desert paleosols indicate a climate change to hyper-aridity 19-13 Ma implying >2 km elevation in the plateau region had induced a rain shadow by this time (9 in Table 5.3).

2. Mostly late Miocene to present (~10-0 Ma) uplift; Paleobotanical evidence using the nearest-living-neighbor method from the Chucal Formation suggests only 1 km elevation 25-19 Ma (4 in Table 5.3). Reinterpretation of the Potosi paleobotanical

evidence using the foliar-physiognomic method suggests ≤1320 m elevation was attained by 21-14 Ma (6b in Table 5.3). The Jakokkota site, also using the foliar-physiognomic method, suggests 600-1600 m elevation 11-10 Ma (7 in Table 5.3). 1.7 ± 0.7 km of rock uplift since 12-9 Ma was estimated from the San Juan del Oro surface in the Eastern Cordillera of southern Bolivia (12 in Table 5.3) and $\delta^{18}O$ and clumped ^{13}C-^{18}O isotopes from pedogenic carbonates suggest an elevation gain of ~2.7 ± 0.7 km 10.3-6.7 Ma (Fig. 5.3 and 13-18 in Table 5.3).

3. Most uplift since the latest Oligocene-early Miocene (~25 to 20 Ma to present); A 25 Myr-old abraded marine transgression surface in the Peruvian Precordillera suggests 1100 m of uplift since 25 Ma (1 in Table 5.3). Internal drainage development 24-14 Ma in the Puna implies uplifted regions of unknown elevation along both plateau flanks by this time (8 in Table 5.3). The elevated Altos de Camilaca surface suggests 1100-1300 m of rock uplift in southern Peru since 25-18? Ma (11 in Table 5.3) and monoclinal tilting and rock uplift of the western plateau flank escarpment suggest 1700-2500 m of uplift since 19 Ma (19 in Table 5.3).

When integrated together, the previous indicators of rock and surface uplift suggest that the high AP region was uplifted by ~1.5 km in elevation over the last ~10 Myrs (dashed lines in Fig. 5.3B). Estimates from perched erosion surfaces imply 1-3 km of rock uplift with as much as 2.4 km since 12-9 Ma. Within 1 sigma error, the paleoelevation data constrain the Altiplano elevation history as <~2 km elevation until ~11 Ma followed by a rapid rise from 0.5-2 km to the present elevation of ~3.8 km starting ~10 Ma (gray region in Fig. 5.3B). Within 2 sigma error, the paleoaltimetry data constrain the Altiplano elevation history as <~2.4 km elevation until ~18 Ma followed by either a rapid to steady rise from 0-2.4 km to the present elevation of ~3.8 km starting somewhere between ~18 and 10 Ma (dashed lines in Fig. 5.3B). We conservatively conclude that, within 2 sigma error, observations suggest anything from a slow and

steady rise of the Altiplano since ≥25 Ma to a recent and rapid rise from ~1 km 10.3 Ma to its modern height of 3.8 km ~6.7 Ma [Garzione et al., 2006; Ghosh et al., 2006].

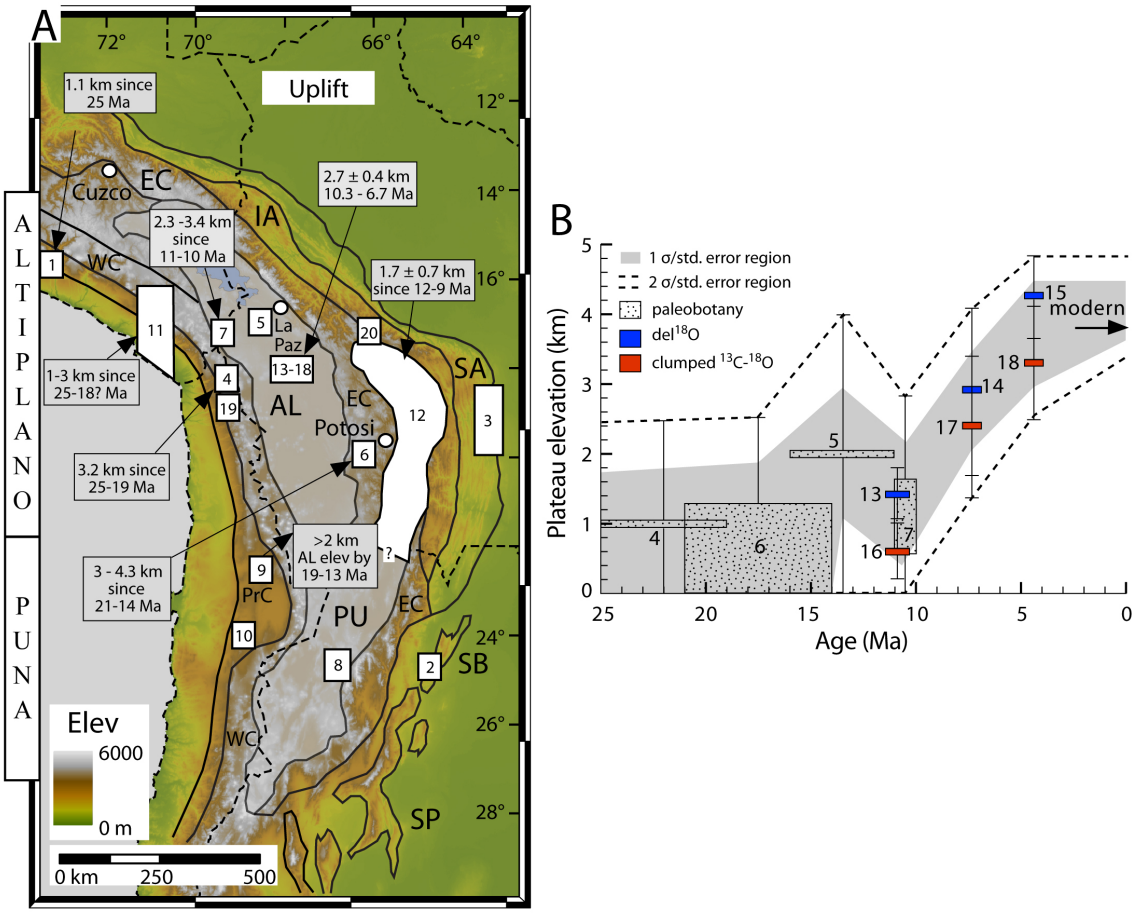

Figure 5.3. The uplift and elevation history of the Andean Plateau. (A) Study locations are shown with white polygons and labeled with letters that refer to rows in Table 5.3. Constraints are from sedimentary facies, paleobotany, paleoclimate, erosion surfaces, paleoaltimetry, and monocline tilting data. The quantity and timing of local surface uplift is highlighted for selected studies. See Figure 5.2 for tectonomorphic zones and their abbreviations. (B) Paleoelevation estimates of the high plateau region derived from paleobotany, oxygen isotopes, and clumped ^{13}C-^{18}O isotopes listed in Table 5.3. Errors bars shown are 2σ or standard (std.) error.

Table 5.3. Andean Plateau region uplift history studies and estimates (expanded from Gregory-Wodzicki 2000).

Type & Locality*	Uplift Type~	Age (Ma)	Elevation Paleo- (m)	Elevation Modern (m)	Elevation %Modern	Error# (m)	Reference
Marine facies							
El Molino Fm^	Rock	73-60	<0	4000	0	±200	Sempere et al. 1997
Moquegua Fm (1)	Rock	25	<0	1100	0	±200	Sebrier et al. 1988; Tosdal et al. 1984
Anta Fm (2)	Rock	14-15	<0	<1000	0	±100	Jordan & Alonso 1987
Yecua Fm (3)	Rock	14-7	<0	<1000	0	±100	Hulka et al. 2006; Hernandez et al. 2005; Marshall et al. 1993
Paleobotany							
Chucal Formation (4)	Surface	25-19	1000	4200	24	±1500	Munoz & Charrier 1996
Corocoro (5)	Surface	16-11	2000	4000	50	±2000	Singewald & Berry 1922
Potosi (6a)	Surface	21-14	2800	4300	65	±2000	Berry 1939
Potosi (6b)	Surface	21-14	0-1320	4300	0-31	±1200	Gregory-Wodzicki et al. 1998
Jakokkota (7)	Surface	11-10	590-1610	3940	15-41	±1200	Gregory-Wodzicki et al. 1998
Pislepampa (20)	Surface	7-6	1200-1400	3600	33-39	±1000	Graham et al. 2001
Paleo-climate							
Internal drainage (8)	Rock?	24-14	some	~3800	?	ND	Vandervoort et al. 1995; Alonso et al. 1991
Aridification (9)	Surface	19-13	>2000	2900-3500	>57-69	ND	Rech et al. 2006
Erosion rates (10)	R or S?	~15	1000-4500	~4500	0-25	ND	Alpers & Brimhall 1988; also Hartley & Rice 2005
Erosion Surfaces							
Altos de Camilaca (11)	Rock	25-18?	~0	1100-3000	0	±1000	Tosdal etal. 1984; Quang et al. 2005
San Juan del Oro (12)	Rock	12-9	~350-1880	~3250	11-58	±~700	Barke & Lamb 2006; also Kennan et al. 1997; Servant et al. 1989
Paleosols							
Oxygen Isotopes							
Corque syncline (13)	Surface	11.5-10.3	1419¤	3800-3900	36-37	±378¤	Ghosh et al. 2006 Table 1: del^{18}Osmow of water
Corque syncline (14)	Surface	7.6-6.8	2931¤	3800-3900	75-77	±1229¤	Ghosh et al. 2006 Table 1: del^{18}Osmow of water
Corque syncline (15)	Surface	6.8-5.6	4254¤	3800-3900	109-112	±567¤	Ghosh et al. 2006 Table 1: del^{18}Osmow of water
Clumped C-O Isotopes							
Corque syncline (16)	Surface	11.5-10.3	600	3800-3900	15-16	±400§	Quade et al. 2007; Ghosh et al. 2006
Corque syncline (17)	Surface	7.6-6.8	2400	3800-3900	62-63	±1000§	Quade et al. 2007; Ghosh et al. 2006
Corque syncline (18)	Surface	6.8-5.6	3300	3800-3900	85-87	±800§	Quade et al. 2007; Ghosh et al. 2006
Monocline Tilting							
Western Escarpment (19)	Rock	19-0	~0	1700-2500	0	ND	Worner et al. 2002

* numbers in parentheses keyed to Figure 5.3

standard error from specific reference or calculated by Gregory-Wodzicki (2000), ^ = relavent region is entire AL; ND = not determined; NA = not applicable

¤ calculated with paleoelev = -472.5*del18Osmow of water - 2645 after Garzione et al. 2007; Ghosh et al. 2006; § 2σ from Ghosh et al. 2006

~after England & Molnar (1990); R = Rock; S = Surface

There are several caveats associated with these uplift constraints. First, work done in the early 1900s is generally not accepted because so little was known about modern-to-ancient South American vegetation at that time (5 and 6 in Table 5.3) [Gregory-Wodzicki, 2000]. Second, paleoclimate proxies and erosion studies often invoke far-a-field causes, which may be non-unique. For example, Rech et al. [2006] infer plateau height of >2 km far from their study location in the northern Atacama as a mechanism for the onset of aridity (Fig. 5.3). In fact, the traditional view that hyper-aridity (related to rain shadow development) by 14 Ma induced supergene oxidation and enrichment of porphyry copper deposits throughout the AP western flank in Peru and Chile [Alpers and Brimhall, 1988; Stillitoe and McKee, 1996] has recently been called into question with periodic evidence of enrichment since the mid-Eocene (~44-0 Ma) [Hartley and Rice, 2005; Quang et al., 2005; Arancibia et al., 2006]. Third, rock uplift is not necessarily equivalent to surface uplift unless some correction is made for the isostatic response to erosion regionally (Table 5.3) [England and Molnar, 1990]. Finally, paleoelevation estimates from stable isotope data are based on modern relationships between fractionation in modern meteoric water, elevation, and surface temperatures [Quade et al., 2007], which may not be representative of the past. Climate and moisture sources change over time making the assumption that the modern meteoric fractionation relationship indicative of the past tenuous and the resultant $\delta^{18}O$ paleoelevation estimates potentially underestimates [Ehlers and Poulsen, in prep]. Clumped ^{13}C-^{18}O paleoaltimetry it is a nascent technique with large uncertainty (~±4°C) and compares the inferred paleo-surface temperature to modern lapse rates [Quade et al., 2007]. It is interesting to note that the oldest (~10 Ma) $\delta^{18}O$ and ^{13}C-^{18}O data are inconsistent with each other even at the 2 sigma uncertainty (Fig. 5.3B).

Constraints on the history of incision

Many studies have investigated the history of fluvial incision in the AP region which can be a proxy for uplift. For example, (U-Th)/He thermochronometry can constrain the timing of canyon incision [Schildgen et al., 2007] and degradation into erosion surfaces or stratigraphic markers of known age provides a measure of the amount and timing of incision [Sebrier et al., 1988; Kennan et al., 1997; Thouret et al., 2007].

Figure 5.4 shows the locations, timing, and estimates of incision magnitude from AP region studies listed in Table 5.4. The major observation is that substantial incision (1-2.5 km) has occurred along the western Altiplano plateau flank since 11-8 Ma (a-c, h-j in Table 5.4). Evidence exists for earlier incision of ≥400 m 16-11 Ma in southern Peru (g in Table 5.4) and tilting and incision of Atacama gravels starting ~15 Ma along the southern Puna (d in Table 5.4). Most recent evidence demonstrates <450 m of incision into the San Juan del Oro surface since ~3 Ma in the Bolivian Eastern Cordillera (e in Table 5.4).

There are several possible mechanisms for incision. Authors have suggested surface uplift [e.g. Sebrier et al., 1988; Servant et al., 1989; Gregory-Wodzicki, 2000; Schildgen et al., 2007] as the result of delamination [Garzione et al., 2006; Ghosh et al., 2006] or lower crustal flow [Schildgen et al., 2007; Thouret et al., 2007]. One key point is that even if surface uplift did trigger incision, the incision depth is not necessarily equal to the amount of uplift unless it has been corrected for the isostatic response to erosion [Molnar and England, 1990]. Climate change can also trigger incision (and result in regional uplift). Paleoclimate proxies of the western AP flank in Chile indicate both changes from semi-humid to arid conditions in the last 15 Myrs as well as contradictory conditions occurring simultaneously (e.g. both wet and dry climates) which suggests a climatic incision trigger is difficult to evaluate [e.g. Gaupp et al., 1999; Hartley, 2003].

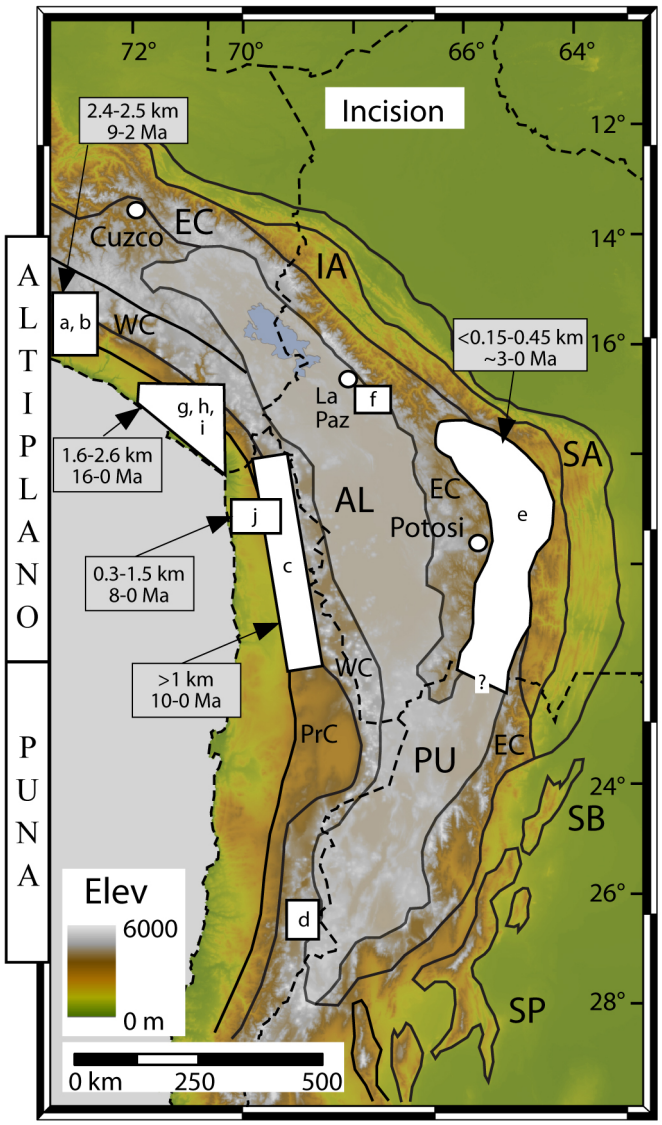

Figure 5.4. The incision history of the Andean Plateau. Study locations are shown with white polygons and labeled with letters that refer to rows in Table 5.4. Constraints are from geo-thermochronology, erosion surface and canyon incision, and topographic and river profile analysis data. The integrated quantity and timing of incision is highlighted for selected studies (see Table 5.4 for details). See Figure 5.2 for the tectonomorphic zones and their abbreviations.

Table 5.4. Andean Plateau region incision estimates.

Letter*	Methods	Age (Ma)	Amount (m)	Reference
a	Ar/Ar(b, fspar, gndmss) of volcanics	9-4	2000-2500	Thouret et al. 2007
b	Ar/Ar(fspar, san, gndmss) of volcanics & He(ap, zr)	9-5	1000	Schildgen et al. 2007
b	Ar/Ar(fspar, san, gndmss) of volcanics & He(ap, zr)	5-2	1400	Schildgen et al. 2007
c	erosion surfaces, stream profiles, U-Pb(zr), Ar/Ar(b)	10-0	>1000	Hoke et al. 2007
d	deposition, tilting, and incision of Atacama gravels	~15-0	?	Riquelme et al. 2003; Mortimer 1973
e	incision of San Juan del Oro surface	~3-0	<150-450	Kennan et al. 1997
f	Rio La Paz basin incision, FT(ap)	~5-0	~2000+	Barnes et al. 2006; McQuarrie et al. 2008
g	S1 flat paleotopography surface incision	16-11	≥400	Sebrier et al. 1988
h	S2 paleovalley fillings/Tamarugal pediplain incision	11-5	~1000	Sebrier et al. 1988
i	S3 aggradational pediplain incision	5-0	200-1000	Sebrier et al. 1988
j	river profiles, stratigraphy, sediment yields, cosmogenics	8-0	300-1500	Kober et al. 2006; Schlunegger et al. 2006

* = keyed to Figure 5.4

m = muscovite; b = biotite; fspar = feldspar; kspar = potassium feldspar; hbl = hornblende; wr = whole rock; plag = plagioclase; san = sanidine; glss = glass; gndmss = groundmass; K/Ar = $^{40}K/^{39}Ar$; Ar/Ar = $^{40}Ar/^{39}Ar$; He = (U-Th)/He

Lithospheric structure

Many types of geophysical studies have been conducted to gain insight into the lithospheric structure below the AP. For example, (a) earthquake locations and focal mechanism solutions provide constraints on the location of the subducting Nazca Plate [e.g. Cahill and Isacks, 1992], (b) seismic wave attenuation and tomography produce subsurface velocity variations that can be interpreted in terms of lithospheric structure [e.g. Dorbath et al., 1993; Whitman et al., 1996; Beck and Zandt, 2002], and (c) measured and modeled heat flow densities can provide approximations of the thermal structure of the lithosphere [e.g. Springer, 1999]. We chose not to include magnetotellurgic and electromagnetic studies [e.g. Swartz et al., 1994; Swartz and Kruger, 1997; Soyer and Brasse, 2001] in this compilation for brevity.

Figure 5.5 shows the locations of seismic stations and networks and highlights major features of the lithosphere below the AP with specific studies listed in Table 5.5. The Western Cordillera, Altiplano, and Eastern Cordillera regions exhibit a positive geoid height, a negative Bouguer gravity anomaly, and elevated heat flow with locally positive, isostatic residual gravity anomalies in the central Altiplano and Eastern Cordillera [Froidevaux and Isacks, 1984; Henry and Pollack, 1988; Gotze et al., 1994; Gotze and Kirchner, 1997; Springer and Forster, 1998; Scheuber and Giese, 1999; Springer, 1999]. Bouguer gravity combined with topography data have been used to determine strong flexural rigidity (effective elastic thickness, Te ~40 km) in the forearc and near the foreland in contrast to the high elevations which are characterized by the opposite (Fig. 5.5B) [Watts et al., 1995; Tassara, 2005; Perez-Gussinye et al., 2008]. The low gravity and high heat flow and topography are attributed to a thick crust (~65-80 km) that is isostatically compensated below the plateau, which sits above a hot asthenospheric wedge. The spatial variations in lithospheric strength are interpreted to be related to (a) the thermal structure and thickness of the felsic crust (Fig. 5.5B), (b) the age of the

Figure 5.5. The lithospheric structure of the Andean Plateau. Constraints are from geophysical studies. (A) Study locations and associated seismic stations and networks are shown with specific literature listed in Table 5.5. D93 = Dorbath et al. [1993], DG96 = Dorbath and Garnet [1996], W94 = Wigger et al. [1994], GA99 = Graeber and Asch [1999], CDP = common depth point reflection line [see Oncken et al., 2003], APVC = Altiplano Volcanic Complex. Upper mantle velocity (vel) zones and edge of Brazilian craton from Beck and Zandt [2002]. See Figure 5.2 for the tectonomorphic zones and their abbreviations. (B) Cross section of heat flow, thermal structure, and effective elastic thickness (Te) at ~20°S [modified from Tassara, 2005]. Moho discontinuity (thin short dashed line) is from Yuan et al. [2000]. Modeled isotherms and measured (thick solid lines above topography profile) mean heat flow densities are from Springer and Forster [1998] and Springer [1999]. Topography is exaggerated five times. (C) Along-strike variations in lithospheric structure (inferred from seismic attenuation) and depth to the Nazca Plate [modified from Whitman et al., 1996]. See Figure 5.2B for profile location. (D) Schematic lithospheric cross section modified from McQuarrie et al. [2005]. White stars are BANJO/SEDA stations in part A. Dark lithosphere reflects fast upper mantle P-wave velocities and white areas are slow (see also part A). White waves are crustal low velocity zones. Black/gray crustal low-velocity zones associated with partial melts are shown for the Western Cordillera and the Eastern Cordillera (Los Frailes ignimbrites). Upper-crustal structure is a balanced section from McQuarrie [2002] with basement in gray and cover rocks in white.

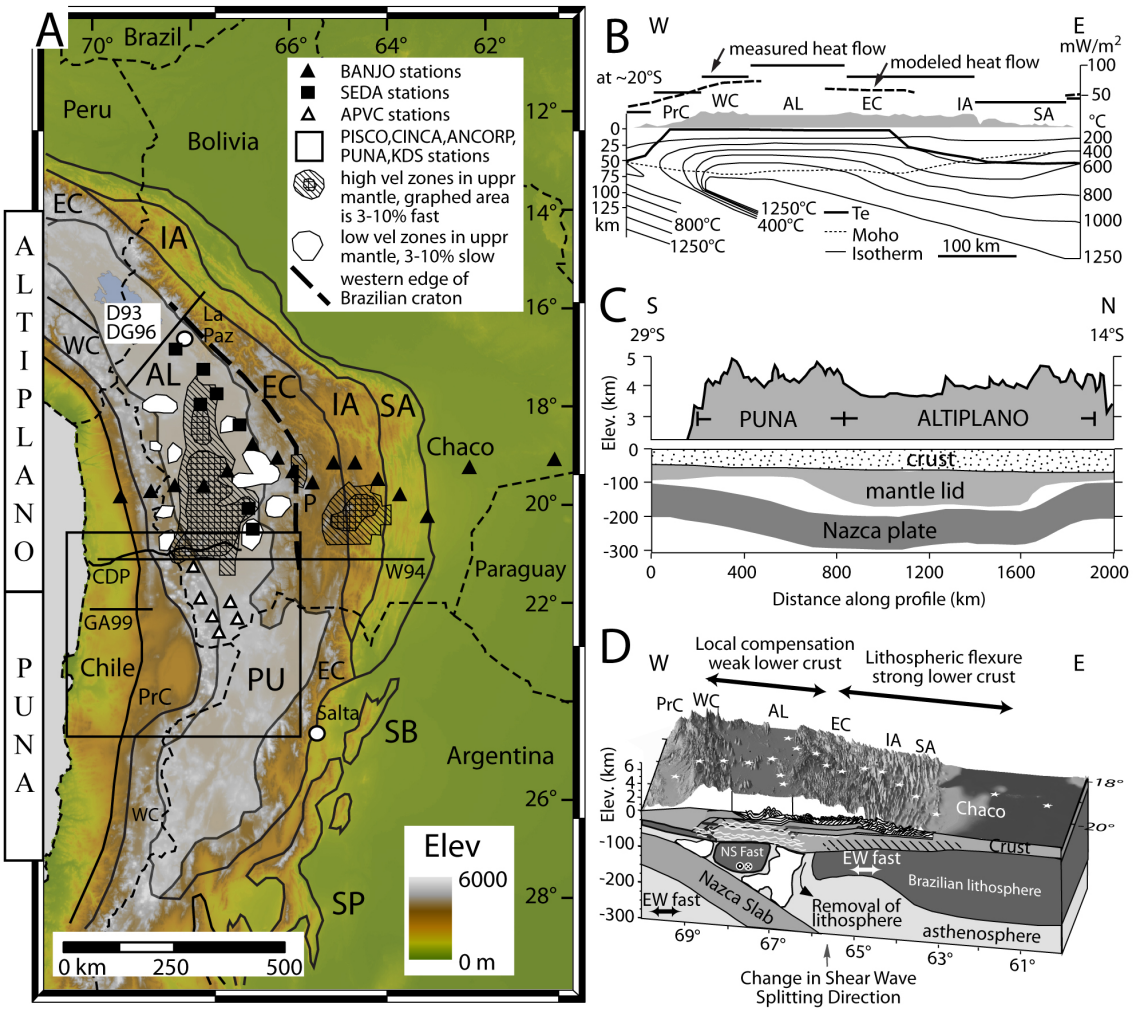
A
70°
Brazil
66°
64°
62°
Peru
Bolivia
12°
14°
16°
18°
20°
22°
26°
28°
ALTIPLANO
PUNA
EC
IA
WC
AL
SA
D93
DG96
La
Paz
P
W94
CDP
GA99
Chile
PrC
PU
Salta
SB
SP
Chaco
Paraguay
Argentina
BANJO stations
SEDA stations
APVC stations
PISCO,CINCA,ANCORP,
PUNA,KDS stations
high vel zones in uppr
mantle, graphed area
is 3-10% fast
low vel zones in uppr
mantle, 3-10% slow
western edge of
Brazilian craton
Elev
6000
0 m
0 km
250
500
B
W
E
mW/m2
measured heat flow
modeled heat flow
at ~20°S
PrC
WC
AL
EC
IA
SA
100
50
°C
200
400
600
800
1000
1250
0
25
50
75
100
125
km
800°C
1250°C
1250°C
400°C
Te
Moho
Isotherm
100 km
C
S
N
29°S
14°S
Elev. (km)
5
4
3
0
-100
-200
-300
PUNA
ALTIPLANO
crust
mantle lid
Nazca plate
0
400
800
1200
1600
2000
Distance along profile (km)
D
W
E
Local compensation
weak lower crust
Lithospheric flexure
strong lower crust
PrC
WC
AL
EC
IA
SA
Elev. (km)
6
4
2
0
-100
-200
-300
18°
20°
Chaco
Crust
NS Fast
EW fast
Brazilian lithosphere
Nazca Slab
EW fast
Removal of
lithosphere
asthenosphere
69°
67°
65°
63°
61°
Change in Shear Wave
Splitting Direction

Table 5.5. Andean Plateau region lithospheric structure constrained by geophysical studies.

Location	Methods	Results	Interpretations	Reference
4-22°S	terrestrial heat flow measurements	values range from 50-80 mW/m^2	high back arc heat flow	Henry & Pollack 1988
8-36°S	earthquake locations and focal solutions	depth to Wadati-Benioff zone	flat slab subduction Peru & south Chile/Arg.	Cahill & Isacks 1992
23-25°S	high-frequency mantle seismic wave attenuation	high Qp & Qs south of ~22°S, lower to north	mantle lithosphere in north, not in south	Whitman et al. 1992; 1996
15-18°S	teleseismic & local tomography	residual vel. increase at w. EC, Moho 66-50 km	Brazilian craton below western EC	Dorbath & other(s) 1993;1996
21-26°S	seismic refraction	crustal low vel. zones, 40-70 km crust	3 main crustal blocks; forearc, WC, and backarc	Wigger et al. 1994
21-23°S	tomography from 2 1993 EQs in southern Bolivia	vel. 5.9-8.4 km/s, 75-80 km crust	thick felsic crust over high vel. Mantle, no delam	Zandt et al. 1994
10-30°S	topgraphy, gravity, elastic plate flexure model	Te 0-50 km	Te variation due to Brazilian craton	Watts et al. 1995
20°S	teleseismic tomography	high vel zone zone dipping east down to 660 km	subducting Nazca plate slab	Dorbath et al. 1996
16-20°S	P to S wave conversions BANJO/SEDA	32-74 km crust, 60-65 km AL, 70-74 WC/EC	thick crust compensated by Airy isostasy	Beck et al. 1996
16-20°S	tomography & attenuation BANJO/SEDA	high vel., Qp, Qs in AL mantle, lwr in EC, low in WC	lithospheric mantle, partial melt in AL, delam	Myers et al. 1998
15-30°S	heat flow measurements, modeling	50-180 mW/m2 (WC/AL/EC), 40 mW/m2 (SA)	crustal doubling, mantle wedge	Springer (& other) 1998; 1999
21-25°S	local tomography PISCO	high vel. zone dipping east, high Vp/Vs mantle	Nazca slab, partially hydrated mantle	Graeber & Asch 1999
21-23°S	teles. & local P-S conversions	very low vel. zone at 19 km, 750-810 m thick	sill-like magma body below APVC	Chmielowsji et al. 1999
21-23°S	seismic refraction profiles PISCO	18-23 km uppr crust, 35-45 mid crust, 70 km Moho	old lwr crust, partial melt down to Moho	Schmitz et al. 1999
21°S	compilation of geologic & geophysical studies	well-imaged Nazca plate by EQs	WC melts 15-150 km depths	Scheuber & Giese 1999
15-25°S	compilation of geophysical studies	4-stage model of Andean subduction	variable subduction angle since Eocene	James & Sacks 1999
21-25°S	compilation of geophysical studies	Moho constraints, crustal balance estimates	root: 55% shortening, mantle hydration 20%, 25%?	Giese et al. 1999
16-26°S	P-S wave conversions of teleseismic & local EQs	mid-crust Altiplano Low Velocity Zone	ALVZ at 20-40 km - partial melt, 40-75 km Moho	Yuan et al. 2000
16-20°S	waveform modeling of 6 regional Eqs	AL 60-65 km crust, south: lower relative vel.	thick felsic crust, no high vel. lwr crust/partial melt	Swenson et al. 2000
16-23°S	surface wave phases & velocities	low vel. zones in AL uppr crust	partial melt - Los Frailes & AL, mantle lithosphere	Baumont et al. 2002
16-22°S	P-S conversions & surface waves BANJO/SEDA	74-30 km crust, mid-crustal low vel. zone	felsic crust/decoupled in AL, craton below EC, delam	Beck & Zandt 2002
17-25°S	teleseismic & local tomography	80-30 km crust, thickness-gravity correlation	100-<30 km lith. AL/Puna, felsic-mafic crust, delam	Yuan et al. 2002
20-22°S	attenuation tomography and electrical resistivity	low Qp mid-lwr crust, good conductor below AL	mid-lwr crust partial melt AL, no shallow asthen	Haberland et al. 2003
20-25°S	local EQ attenuation tomography	high Qp forearc, low Qp arc/backarc crust & mantle	fluid injection into mantle wedge, partial melt	Schurr et al. 2003
20-23°S	seismic reflection & various geophysics	east-dipping Nazca Reflector	Nazca dehydration, AL crust partial melt/decoupling	Oncken et al. 2003
14-33°S	topography, gravity, 2D flexural analysis	forearc/foreland rigidity, weak in high Andes	due to thermal structure, thick felsic crust, craton	Tassara et al. 2005
22-24°S	local EQ tomography & attenuation: Atacama basin	high Qp and P-wave velocity	high strength, cold lithospheric block	Schurr & Rietbrock 2004
20-25°S	local EQ tomography PISCO/ANCORP/PUNA	low vel. & high Qp WC/Puna, high Qp forearc/land	delam below Puna	Schurr et al. 2006
16-25°S	review of geophysics, petrophysics, & petrology	High Conductivity Zone, below WC/AL	partial melt below plateau, ~20% by vol in HCZ	Schilling et al. 2006
20-26°S	review of seismological studies	compiled from other studies	fluids & partial melt, delam below Puna	Asch et al. 2006
21°S	teleseismic tomography	Altiplano Low Velocity Zone and extension below EC	fluid migration, delam?, asthen wedge below	Heit et al. 2008

EQ = earthquake; Qp = P-wave attenuation; Qs = S-wave attenuation; vel. = velocity; lwr = lower; w. = western; Vp = P-wave velocity; Vs = S-wave velocity; uppr = upper; Te = effective elastic thickness; delam = delamination; asthen = asthenosphere;

subducting oceanic lithosphere, and (c) proximity to the under-plating Brazilian lithosphere.

In the early-mid 1990s, intermediate depth (>60 km) earthquakes and focal mechanisms were used to delineate a moderately dipping (30° to the east) Wadati-Benioff zone (representing the Nazca plate) below the plateau flanked by regions of flat slab subduction north of ~14°S in Peru and south of ~28°S in Argentina (Figs 5.1A & 5.5C) [Cahill and Isacks, 1992]. S and P waves generated from within the Nazca plate showed significant attenuation in the upper mantle below the plateau south of ~22°S relative to the north [Whitman et al., 1992]. The interpretation was the Altiplano had a thick mantle lithosphere whereas the Puna possessed a much thinner lithosphere perhaps due to delamination (Fig. 5.5C) [Whitman et al., 1996; see also Yuan et al., 2002]. Teleseismic and local tomography showed slow velocities below the Altiplano down to the Moho and recognized a upper mantle high velocity zone below the Eastern Cordillera and eastward [Dorbath et al., 1993; Dorbath and Granet, 1996]. Lower crustal velocity perturbations, seismic refraction, and tomography were also used to estimate crustal thicknesses of 32-80 km in Bolivia (70-74 km in the Western Cordillera, 65-80 km in the Altiplano, 50-74 km in the Eastern Cordillera, 43-47 in the Subandes, and 32-38 in the Chaco foreland) (Fig. 5.5) [Wigger et al., 1994; Zandt et al., 1994; Beck et al., 1996].

Many geophysical studies conducted since the mid-1990s have refined the structure of the Andean Plateau lithosphere. Earthquake locations, teleseismic and local earthquake tomography, attenuation, refraction surveys, and waveform modeling observe key features: (1) an east-dipping high velocity zone down to 660 km below the plateau [Dorbath and Granet, 1996; Graeber and Asch, 1999; Scheuber and Giese, 1999; Oncken et al., 2003; Asch et al., 2006], localized low and high velocity zones in the crust (2) and upper mantle (3) below the Western Cordillera, Altiplano, Puna, and Eastern Cordillera (Fig. 5.5A) [Myers et al., 1998; Chmielowski et al., 1999; Schmitz et

al., 1999; Yuan et al., 2000; Baumont et al., 2002; Beck and Zandt, 2002; Asch et al., 2006; Schurr et al., 2006; Heit et al., 2008], and (4) high attenuation (low Q_P) in the upper crust and mantle [Haberland et al., 2003; Schurr et al., 2003; Schurr and Rietbrock, 2004; Schilling et al., 2006]. These features are generally interpreted as the subducting Nazca slab (1), indications of high temperatures, fluids and partial melts (2 and 4), and intact mantle lithosphere to piecemeal-to-wholesale detached lithospheric mantle (3) below both the Altiplano and Puna (Fig. 5.5 & Table 5.5). Additional estimates of crustal thickness are similar to previous estimates (up to ~80 km below the center tapering to ~30 km in the foreland) and suggest a dominantly felsic to layered felsic-mafic composition [e.g. Beck and Zandt, 2002; Yuan et al., 2002]. Several studies infer that the Altiplano crust is decoupled [Beck and Zandt, 2002; Oncken et al., 2003]. The high velocity upper mantle down to 120 km below the western Eastern Cordillera is interpreted to be the western limit of the under-thrusted Brazilian craton (Fig. 5.5A) [e.g. Beck and Zandt, 2002]. Location of the Brazilian craton is further defined by an E-W fast direction in shear-wave splitting east of 66°W, which contrasts with a N-S fast direction directly below the Altiplano that is interpreted to be related to mantle flow [Bock et al., 1998; Polet et al., 2000]. Figure 5.5D is a schematic block diagram summarizing the interpreted lithospheric structure below the AP at ~20°S from many of the geophysical observations mentioned here.

There are caveats with the interpretations of lithospheric structure that stem from the geophysical data. In general, tomography depicts changes in relative seismic velocities and hence is less reliable at characterizing sharp boundaries especially for intra-crustal structures from teleseismic conversions. Resolution of tomographic images is usually dependable in the horizontal direction, but significantly less so in the vertical direction because that is parallel to the ray paths. For example, while the low and high mantle velocity regions below the Altiplano and Eastern Cordillera region are certainly

there, their vertical extent and any associated interpretation, such as lithospheric removal, is more tenuous (Fig. 5.5A&D). Furthermore, tomographic images are more reliable when they are constrained by local earthquakes rather than by teleseismic earthquakes. In either case, tomographic images are fundamentally limited by the frequency and spatial variability of earthquake sources.

Discussion

In this section, we integrate the observations summarized above into a synoptic chronology of AP evolution and then focus on consistencies and inconsistencies in the observations and interpretations. We then evaluate the synoptic history within the context of the three current geologic models described above.

Synoptic chronology of Andean Plateau (AP) evolution

Observations constraining the structure, deformation, sedimentation, and exhumation produce a chronology that is consistent throughout the entire AP from southern Peru to northern Argentina: (a) exhumation and deformation began along the entire western plateau flank ~60-40 Ma, (b) initial exhumation and deformation jumped into the central Eastern Cordillera ~40 Ma, (c) exhumation and deformation continued throughout the Eastern Cordillera until ~20 Ma, (d) the exhumation and deformation front propagated eastward into the Interandean zone contemporaneous with limited deformation in the Altiplano from ~20 to 10-5 Ma, and (e) finally, the exhumation and deformation front eventually migrated into the Subandes/Santa Barbara Ranges/Sierras Pampeanas ~15-10 Ma to present roughly contemporaneous with a second pulse of exhumation in the Eastern Cordillera (~23-15 Ma to present). One observation inconsistent with this chronology is a minor older phase of Oligocene (or older) exhumation recorded in the northern Interandean zone that is consistent with a recent

kinematic reconstruction that shows very limited local Eo-Oligocene deformation [McQuarrie et al., 2008]. The younger, mid-Miocene to recent (~15-0 Ma) phase of exhumation recorded in the Bolivian Eastern Cordillera is considered unassociated with significant deformation and probably the result of enhanced erosion [Barnes et al., 2006; Gillis et al., 2006; Barnes et al., 2008; McQuarrie et al., 2008]. In contrast, magnetostratigraphic, seismic, and detrital thermochronologic evidence shows mid-late Miocene to recent (~20-0 Ma) deformation in the Argentine Eastern Cordillera (Fig. 5.2) [Reynolds et al., 2000; Coutand et al., 2006; Mortimer et al., 2007].

The specific chronology of deformation and exhumation in the Altiplano-Puna is generally consistent, but differs in detail. Deformation is documented from ~30 Ma throughout the Altiplano-Puna, but ceased by ~8-7 Ma in the Altiplano and continues today in the Puna (Fig. 5.2) [Cladouhos et al., 1994; Marrett et al., 1994; Kennan et al., 1995; Lamb and Hoke, 1997; Kraemer et al., 1999; Elger et al., 2005]. Exhumation may have begun as recently as the Pliocene in parts of the Altiplano relative to older documented deformation (~3-2 vs. ~8-7 Ma) (Fig. 5.2) [Kennan et al., 1995; Lamb and Hoke, 1997; Elger et al., 2005; Barnes et al., 2006; Barnes et al., 2008]. The deformation and associated exhumation could either not be recorded if the magnitude was insufficient to reset the particular thermochronometer system or the exhumation could continue long after deformation has ceased via protracted erosion which could explain these discrepancies.

The most important observation of the integrated deformation, sedimentation, and exhumation history of the entire AP region is that it is uniform along strike and initiated as long ago as the Paleocene (~60-0 Ma) (Fig. 5.2). This idea challenges the previous consensus that deformation and sedimentation was ~5-10 Myrs younger in the Eastern Cordillera margin of the Puna compared to the Altiplano [e.g. Allmendinger et al., 1997; Jordan et al., 1997; McQuarrie, 2002a]. It is particularly interesting that (a) the

first pulse of exhumation in the Eastern Cordillera (~40 Ma) is synchronous and related to deformation related and (b) the younger pulse of Eastern Cordillera exhumation adjacent to the Puna is older (~23-15 Ma) and also related to deformation, while next to the Altiplano it is younger (~15-0 Ma) and probably only associated with enhanced erosion.

Inconsistency in upper-crustal structure of the Bolivian Altiplano

A major inconsistency in interpretations is the geometry of basement deformation below the Bolivian Eastern Cordillera and Altiplano inferred from the mapped surface geology. The basic issue is how the brittle upper-basement rocks accommodate the substantial shortening observed in the tightly folded and faulted Paleozoic and younger sedimentary cover rocks [e.g. McQuarrie et al., 2005]. One model treats the basement rocks as competent rocks above a weak detachment at the brittle-ductile transition zone itself [Hatcher, 2004] with ramp-flat-ramp geometries (called megathrusts) identical to those found in the cover-rock-cored thrusts sheets (upper-crustal structure in Fig. 5.5D) [McQuarrie and DeCelles, 2001; McQuarrie, 2002b; McQuarrie et al., 2005; McQuarrie et al., 2008]. The other model infers a more complicated pattern of basement-involved thrusts that shallow into the brittle-ductile transition zone [see Kley et al., 1996; Müller et al., 2002; Elger et al., 2005; Oncken et al., 2006b].

The most important point is that both models are more similar in overall outcome than is commonly appreciated. First, they both construct basement thrusts with similar aspect ratios (~1:10 – 1:15) and detachment depths (~15 and 25 km) and hence make similar assumptions about the depth to the brittle-ductile transition [McQuarrie et al., 2008]. Second, style of basement strain does not affect estimates of shortening magnitude, which are generally large in the central Andean fold-thrust belt (Altiplano to Chaco foreland in Bolivia: ~285-330 km) [McQuarrie et al., 2005]. The megathrust

model has also been tested to be viable (i.e. it has been sequentially restored to an undeformed state; see Elliot [1983]).

Inconsistency between history of deformation and uplift

The most significant and current debate about the AP is the inconsistency between the documented deformation and uplift history [Eiler et al., 2006; Garzione et al., 2006; Ghosh et al., 2006; Sempere et al., 2006; Garzione et al., 2007; Hartley et al., 2007]. A major premise is that since the dominant mode of Andean crustal thickening is shortening, the topographic/surface uplift history probably correlates in time and space with shortening and deformation [Jordan et al., 1997]. As outlined above, the geologic record attests to significant deformation, sedimentation, and exhumation throughout wide regions within and along the plateau and its margins ≥~10 Ma, which argues for substantial crustal thickness prior to the late Miocene (Fig. 5.2). Extensive ignimbrites as old as 25 Ma along both plateau margins [Worner et al., 2002; Barke et al., 2007] also indicate significant heat and crustal sources associated with a thickened crust were already in place (possibly with resulting isostatic uplift) by ~20 Ma [Babeyko et al., 2002; Hartley et al., 2007]. Yet, potentially 3.1-2.3 km of surface uplift (~80-60% of the total current elevation) did not occur until 10 million years later from ~10-6 Ma in the Altiplano (Fig. 5.3) [Quade et al., 2007]. The widespread and significant incision (2.5-1 km) of the plateaus' western flank since the late Miocene (11-8 Ma) is consistent with the recent rapid uplift hypothesis, but climate variations need to be ruled out as the trigger (Fig. 5.4 and Table 5.4). In fact, sediment accumulation rates on the eastern plateau flank in the Chaco foreland have been recently used to suggest significant climate change and monsoon intensification at ~8-6 Ma [Uba et al., 2007].

The rapid late Miocene surface uplift hypothesis makes several testable predictions. The hypothesis implies the following at ~10 Ma: (1) a decrease in the rate of

shortening across the Altiplano, (2) a shift in deformation eastward in the Subandes, and (3) a decrease in convergence rate between the Nazca and South American Plates [Garzione et al., 2006; Ghosh et al., 2006]. Although evidence exists to support these predictions [Garzione et al., 2006; Ghosh et al., 2006], several exhumation histories from the Bolivian Subandes are consistent with previous estimates that suggested deformation began as early as ~20 Ma (Fig. 5.2) and estimated shortening rates suggest either a relatively continuous rate since the Eocene to a decrease by half since the Miocene [McQuarrie et al., 2005; Barnes et al., 2006; Barnes et al., 2008; McQuarrie et al., 2008].

The most important conclusion is that the collective paleoaltimetry data, within 2 sigma error, are equally consistent with protracted, steady uplift since ≥25 Ma as implied by the deformation, sedimentation, exhumation constraints or recent surface uplift ~10-6 Ma inferred from the stable isotope data (Figs 5.2 & 5.3). This result certainly suggests more efforts are needed to better quantify the paleoelevation and uplift history of the AP.

Lithospheric structure interpretations

Observations of the lithospheric structure delimit similar zones of high/low velocity and attenuation in the crust and mantle below the AP, but there are inconsistencies in the interpretations (Table 5.5). Several studies stress the fact that the entire thick crust (~80-65 km) below the plateau is felsic [Zandt et al., 1994; Swenson et al., 2000; Beck and Zandt, 2002], but another study suggests the crust is layered: felsic down to 55-50 km and mafic below that [Yuan et al., 2002]. One study suggests there is no partial melt in the Altiplano crust [Swenson et al., 2000], but many suggest there is considerable partial melt [e.g. Schmitz et al., 1999; Yuan et al., 2000; Haberland et al., 2003; Schilling et al., 2006]. Although these studies are not in the exact same locations,

they emphasize variable observations and associated interpretations of the AP crust and imply that there are large lateral variations within it.

An interesting change in thinking since the mid-1990s is that delamination was only initially considered to be relevant to the Puna, now it is also interpreted for the Altiplano, albeit perhaps only in piecemeal form (Fig. 5.5C&D) [e.g. compare Whitman et al., 1996; Beck and Zandt, 2002]. Finally, even though direct observation is not possible, the history of plate vectors, their convergence rates, and magmatism have been combined to build a consensus that the geometry of subduction below the plateau used to be flat prior to changing to its current angle of ~30° [e.g. Isacks, 1988; James and Sacks, 1999].

A main conclusion is that consensus has identified the importance of weakened lithosphere in the evolution of the AP. Partial melting (perhaps via fluid injection into the mantle wedge), proximity above the asthenospheric wedge and adjacent to the arc, pre-existing stratigraphic and structural features, and foundering of the mantle root are some of the weakening mechanisms proposed [e.g. Isacks, 1988; Kley et al., 1999; Schurr et al., 2003; Asch et al., 2006; Oncken et al., 2006b; Schilling et al., 2006]. However, the relative roles of these mechanisms and the extent and nature of delaminated mantle lithosphere below the AP remain open questions.

Evaluation of geologic models of Andean Plateau (AP) development

Chronology is the main issue for evaluating the three current geologic models for Andean Plateau development (outlined above) in the context of the integrated observations. The chronology of Isacks' [1988] model of AP development since ~27 Ma needs to be pushed back to initiation ~60-40 Ma to be consistent with observations. Also, the switch in deformation mode from pure to simple shear could have happened anywhere between 20 and 8 Ma (as opposed to specifically at ~10 Ma) if it is best

represented by the onset of thin-skinned deformation in the Subandes. This shift also implies an equivalent shift in the slab geometry of flat subduction below the plateau. Isacks [1988] initially proposed flat slab subduction from ≥~12 Ma and its return to normal subduction ~10 Ma. Now, flat slab subduction must have been from ~35-25 Ma with its return to normal-angled subduction ~25-15 Ma [compare Isacks, 1988; James and Sacks, 1999]. However, the evidence for late Miocene onset of Altiplano western flank incision and rapid surface uplift makes a case that the switch in mode did occur at ~10 Ma. Both the long and continuous simple shear [e.g. McQuarrie et al., 2005] and the Oncken et al. (2006) models invoke deformation beginning ≥~45 Ma which is consistent with the observations, especially since neither model directly requires a particularly slow or rapid associated surface uplift history. Geophysical observations of the lithosphere structure and the suggestion that some form of mantle lithospheric thinning has occurred appear to be equally viable for all three models.

A distinction between the two long duration models of AP evolution is the temporal variation in shortening rates since deformation began in the Eocene. Oncken et al. (2006) exclusively used documented shortening-rate variations at ~21°S to highlight reduced shortening from 45-33 Ma followed by enhanced shortening from 33-20 Ma. In contrast, documented shortening rates along strike of the eastern Altiplano flank from 15-19.5°S estimate a consistent average rate of ~8-11 mm/yr since deformation began, potentially decreasing to ~3-4 mm/yr depending on the age of Subandes deformation (~20 vs. ~8 Ma) [McQuarrie et al., 2005; Barnes et al., 2008; McQuarrie et al., 2008]. However, in northern Bolivia, there is a pause to minor rates of shortening for 15-5 Myrs as inferred from a lack of a thermochronometer cooling signal from ~25 Ma until 20-8 Ma [McQuarrie et al., 2008].

Besides extending the chronology of deformation, the idea that the modal change in deformation from dominantly pure to simple shear with activation of Subandes

deformation appears to remain important today [Isacks, 1988; Allmendinger and Gubbels, 1996]. Unfortunately, temporally variable to near constant rates of shortening since the Eocene suggest anything from significant to no coupling of upper-plate deformation rate to changes in the magnitude and direction of plate convergence since that time [e.g. Pardo-Casas and Molnar, 1987; Oncken et al., 2006b].

Comparison of Andean observations with geodynamic models

Many studies have used numerical models of varying complexity to provide additional insights into AP formation processes. For example, (a) 1D models provide bounds on the feasibility of geodynamic processes such as mantle convection and delamination [Bird, 1979], (b) 2D thin sheet models with viscoplastic rheologies help determine important factors controlling deformation in the upper South American plate [e.g. Medvedev et al., 2006], and (c) 2D thermo-mechanical models with viscoplastic rheologies are used to determine the nature of coupling within and between the crust and mantle during orogenesis as well as explore conditions necessary to facilitate processes like lower crustal flow or delamination [e.g. Willett and Pope, 2004]. In this section, we include only a few relevant studies that focus on plateaus other than the AP for brevity.

Table 5.5 lists various geodynamic models relevant to the AP and outlines their type, major assumptions, key results, and important inferences. A few processes are consistently demonstrated to be important in plateau formation given reasonable boundary conditions, parameter values explored, and sometimes, poorly constrained, yet specific threshold rheological behavior values. For example, weakening of the AP lithosphere is paramount and related to partial melting, significant heat flux from the mantle, and thickening of the radiogenic and felsic crust which eventually reduces in viscosity and begins to flow [e.g. Royden, 1996; Beaumont et al., 2001; Willett and

Pope, 2004; Vietor and Oncken, 2005]. This weakened plateau lithosphere contrasts dramatically with the cold Brazilian craton to the east [e.g. Medvedev et al., 2006]. A few models show that delamination can occur provided some transition from gabbro to ecologite is implemented for the mid-lower crust [Sobolev and Babeyko, 2005; Sobolev et al., 2006; see also Molnar and Garzione, 2007].

These numerical models of AP development use constraints and produce results that are reasonably consistent with observations synthesized in this paper. Table 5.6 highlights comparisons between some AP model results and/or constraints and our generalized observations related to plateau region shortening, mean elevation, duration of deformation, crustal thickness, time needed to develop its modern width, and uplift history. Comparisons of modeled and observed heat flow values are not listed in Table 5.6, but are generally good [e.g. Pope and Willett, 1998]. While most models predict mean plateau elevation consistent with modern values, several chose substantially less shortening than the total inferred (~500 km) in the Altiplano as well as less than ~60-40 Myrs for the deformation duration. However, most of these models did prescribe the amount of shortening observed (~300-350 km). A few studies ran contrasting simulations of short and long (~25 and ~70 Myrs) deformation in which the longer duration result intuitively predicted more gradual rise from 2 km elevation ~25 Ma [Yang et al., 2003]. Two studies focused specifically on plateau evolution over only the last 10 Myrs [Babeyko et al., 2006; Iaffaldano et al., 2006]. Several models that include delamination predict a recent uplift history consistent with late Miocene rapid surface uplift. Finally, models predict both young (~10 Ma) and old (~15-20 Ma) establishment of the modern AP width, the latter consistent with interpretations of the documented structure, deformation, and exhumation.

Table 5.6. Geodynamic models of plateau development.

Reference	Model Type	Assumptions	Results	Comments
Bird 1979	1D viscous	t dependant, vertical conduit, low visc	mantle convection & delamination	Colorado Plateau; predicts basalt/granite magmatism
Wdowinski & Bock, 1994a, b	2D viscoplastic	t dependant, power-law rheology	AP topography from thermal perturbation	5+% thermal weakening since late Oligocene needed
Royden et al. 1996; 1997	3D viscoplate	d dependant visc, coupled/decoupled crust modes	decoupled crust like Tibetan Plateau	crust decoupling at arbitrary 55 km thickness
Pope & Willett 1998	2D viscoplastic	t depdendant & power-law rheology, ablative subduc	AP-like from high t, low visc lwr-crustal flow	crustal flow due to high heat prod uppr crust
Beaumont et al. 2001; 2004	2D viscoplastic	p dependant & power-law rheology, denudation	TP: coupled crustal flow & focused erosion	extra uppr crust "melt weakening" by factor of 10
Babeyko et al. 2002	2D viscoplastic	t & strain rate dependant power-law rheology	AP: additional mantle heat required for crustal melt	includes crustal magmatic intrusions
Husson & Sempere 2003	1D viscous	t dependant & power-law rheology	E-W directed lateral crustal flow thickens Altiplano	channel viscosity is crustal thickness dependant
Yang et al. 2003	3D viscous	elastic effects negligible, thermally weak crustal zone	AP: significant along-strike crustal flow	long vs. short time of shortening predicts variable uplift
Willett & Pope 2004	2D viscoplastic	t dependant visc, power-law rheology	plateau morph via ablation, mantle subduc/shear	plateau elev due to crustal strength, thickness, & t
Yanez & Cembrano 2004	2.5D viscoplate	t & strain rate dependant power-law rheology	reproduces AP shortening rates, crust thickness	intraplate coupling drives uppr plate deformation
Husson & Richard 2004	2D viscosheet	intraplate traction, basal drag, mass conservation	AP: stress magnitude unsufficient to explain elev	topography is only isostatic, neglects erosion/delam
Gerbault et al. 2005	2D viscoplastic	t dependant & power-law rheology	AP: south to north lower crustal flow	crustal flow does not produce surface deformation
Vietor & Oncken 2005	2D plastic	Coulomb behavior with strain-softening	AP: shear-stress decoupled crust gets plateau morph	implies lower crustal heating important for AP
Babeyko & Sobolev 2005	2D viscoplastic	t & strain rate dependant power-law rheology	AP: deformation modes due to failure of Paleoz seds	sedimentary failture reduces lith shortening force
Sobolev & Babeyko 2005	2D viscoplastic	t & strain rate dependant power-law rheology	AP: lots of shortening and delam of upper plate	slab geometry constant, fixed gabbro-ecologite trans.
Iaffaldano et al. 2006	2D viscoplate	t & strain rate dependant power-law rheology	predicted AP plate motions since 10 Ma	implies topography can control plate motion
Medvedev et al. 2006	2D viscoplate	tectonic thickening, gravity spreading, crustal flow	AP: crustal flow leads to flat topography	Andes lithosphere 5-15 xs weaker than Brazilian craton
Babeyko et al. 2006	2D viscoplastic	t & strain rate dependant power-law rheology	AP: 4 processes control uppr plate strength	internal weaking processes of uppr plate important
Sobolev et al. 2006	2D viscoplastic	t & strain rate dependant power-law rheology	westward drift of Nazca plate controls shortening	delam & foreland sed failure reduce uppr plate strength

t = temperature; d = depth; vert. = vertical; visc = viscosity; lith = lithosphere; AP = Andean Plateau; TP = Tibetan Plateau; morph = morphology; prod = production; lwr = lower; uppr = upper; trans. = transformation
sed = sediments; elev = elevation

Table 5.7. Andean Plateau model results and/or constraints compared to observations synthesized in this study.

Reference	Total Shortening		Topo (mean elev)		Deformation Time		Crustal Thickness		Plateau Width Time		Uplift History	
	Obs.* (km)	Model (km)	Obs. (km)	Model (km)	Obs. (Ma)	Model (Ma)	Obs. (km)	Model (km)	Obs. (Ma)	Model (Ma)	Obs. (Ma)	Model
Wdowinski & Bock, 1994b	530-150	NA	~4.5-3.7	~4	~60-40	30	55-80	NA	~20-15	~20	≥25-0	gradual from 30 Ma
Pope & Willett 1998	530-150	NA	~4.5-3.7	~4?	~60-40	30	55-80	~60	~20-15	NA	≥25-0	NA
Babeyko et al. 2002	530-150	NA	~4.5-3.7	NA	~60-40	70-25	55-80	~45	~20-15	NA	≥25-0	NA
Husson & Sempere 2003	530-150	NA	~4.5-3.7	~4	~60-40	60	55-80	>50-40	~20-15	NA	≥25-0	3 km post 10 Ma
Yang et al. 2003	530-150	530-150	~4.5-3.7	3.8-4.8	~60-40	70-25	55-80	65-60	~20-15	≥20	≥25-0	1-2 km pre 25 Ma
Willett & Pope 2004	530-150	~540?	~4.5-3.7	5-6	~60-40	30	55-80	~75	~20-15	NA	≥25-0	NA
Husson & Richard 2004	530-150	NA	~4.5-3.7	~4	~60-40	27	55-80	NA	~20-15	NA	≥25-0	NA
Gerbault et al. 2005	530-150	NA	~4.5-3.7	NA	~60-40	NA	55-80	~65	~20-15	NA	≥25-0	NA
Vietor & Oncken 2005	530-150	~175-275	~4.5-3.7	NA	~60-40	~27-25	55-80	NA	~20-15	NA	≥25-0	NA
Babeyko & Sobolev 2005	530-150	50	~4.5-3.7	NA	~60-40	10	55-80	45	~20-15	NA	≥25-0	NA
Sobolev & Babeyko 2005	530-150	300-350	~4.5-3.7	~4	~60-40	35-30	55-80	>45	~20-15	~10	≥25-0	3 km post 10 Ma
Iaffaldano et al. 2006	530-150	NA	~4.5-3.7	3.8	~60-40	10	55-80	NA	~20-15	NA	≥25-0	3 km post 10 Ma
Medvedev et al. 2006	530-150	NA	~4.5-3.7	≥3.5	~60-40	NA	55-80	>57-65	~20-15	NA	≥25-0	NA
Babeyko et al. 2006	530-150	70	~4.5-3.7	<5	~60-40	10	55-80	~45-60	~20-15	NA	≥25-0	NA
Sobolev et al. 2006	530-150	~350	~4.5-3.7	~4	~60-40	35	55-80	NA	~20-15	~10	≥25-0	3 km post 10 Ma

Obs. = observed; Topo = topography; NA = not available or applicable; * observed and inferred

It is important that in the context of observations synthesized in this paper, many numerical modeling studies of AP evolution under-simulated both the documented duration of deformation (≤~30 vs. ~60-40 Ma) and the maximum inferred magnitude of shortening (~530 vs. ~350 km) (Table 5.7). This may have a profound effect on the results and any associated interpretations, especially with results that are used to differentiate between the end-member uplift histories allowed by the paleoaltimetry data. Finally, many models also do not include erosion.

Future directions

There are several potentially fruitful lines of future research to better constrain Andean Plateau evolution in order to gain further insight into plateau formation. The synchronicity of deformation, sedimentation, and exhumation throughout the Bolivian Altiplano and the Argentina Puna implies a similar history for the northern portion of the AP in southern Peru, but observations do not yet exist (Fig. 5.2). Results from such studies, as well as balanced cross sections and kinematic reconstructions, along the northernmost Altiplano flanks could test the hypothesis that upper-crustal deformation in the AP is uniform along strike, determine how the flanking thrust belt is linked to the AP, and provide insight into how the structural and stratigraphic architecture varies northward. Shallow geophysical studies across the same regions as well as the Bolivian Altiplano may help solve the controversy surrounding the geometry of the basement-involved structures that link the AP to thrust belt deformation.

Another avenue of future research is better determination of the initial timing and duration of Subandes deformation and erosion throughout Bolivia and southern Peru. This pursuit could be used to test predictions of the model for AP formation that emphasizes substantial late Miocene surface uplift. Additionally, more oxygen and clumped ^{13}C-^{18}O isotope data need to be collected from various paleosols north and

south of the current location at 18°S (numbers 13-18 in Fig. 5.3) as well as in older (>10 Myr) sediments to better delimit the Eocene to recent plateau elevation history and reveal whether or not it is synchronous throughout the entire Altiplano as proposed. The uniform deformation, sedimentation, and exhumation history of the AP certainly begs the hypothesis of a complimentary uniform uplift history as well. However, mafic magmas in the Puna have been used to hypothesize delamination occurred only ~3 Ma [Kay and Mahlburg Kay, 1993]. Isotope paleoaltimetry data in the Puna could also test this hypothesis.

Additional avenues of future research include expanding the regional paleoclimate record back into the early Miocene, if not earlier. This would help with evaluating the reliability of the oxygen paleoaltimetry data and decipher which, if any, incision records may reflect a climatic change as opposed to some form of uplift. Expansion of geophysical studies to determine the lithospheric structure below the Puna, Argentine Eastern Cordillera, and northern Altiplano in Peru would go a long way towards along-strike substantiation or contradiction of the tomography-driven interpretations of piecemeal-to-wholesale mantle lithosphere delamination below the Altiplano. Finally, further numerical simulations constrained by the observations synthesized in this paper could be used to address questions such as: (1) What uplift histories are most consistent with the observed magnitudes, rates, and timing of deformation and shortening across the central Andean fold-thrust belt and Santa Barbara Ranges/Sierras Pampeanas? (2) How unique is the mechanism of mantle delamination to the possible late Miocene surface uplift history? (3) Has erosion limited thrust belt propagation (and effectively plateau width) as some have suggested? [e.g. Masek et al., 1994; Horton, 1999] and (4) Does any important plateau geodynamic process (i.e. crustal flow, delamination, eclogitization of the lower crust) produce any unique and identifiable evidence in the near surface that geoscientists can look for?

Conclusions

We conclude by listing a series of observations consistent across many investigations presented in our synthesis above. This list is presented to identify what can be said with confidence concerning the Cenozoic geologic evolution and structure of the Andean Plateau region and provide a litmus test for evaluating future geodynamic, erosion, and paleoclimate models of the orogen. More specifically, any model that attempts to explain Andean Plateau development must honor the following observations:

A. Initial deformation and exhumation began along the western flank ~60-40 Ma and then jumped into the central Eastern Cordillera ~40 Ma. Distributed Eastern Cordillera deformation continued from ~40-20 Ma with propagation of the deformation and exhumation front both eastward into the Interandean zone and westward in the Altiplano from ~20 Ma until 10-5 Ma. Finally, deformation and exhumation migrated further eastward into the Subandes/Santa Barbara Ranges/Sierras Pampeanas ~15-10 Ma where it continues today. A younger phase of early-mid Miocene to present (~23-0 Ma) exhumation in the Eastern Cordillera was probably the result of enhanced erosion along the northern Altiplano flank and related to deformation along the southern Puna flank. The 3-dimensional deformation field of the AP region is characterized by some rotation outward from the orocline axis.

B. The high AP region was uplifted by at least ~1.5 km in elevation since ~10 Ma. Paleoaltimetry and uplift constraints allow a wide variety in uplift history from a slow and steady rise since ≥25 Ma to a recent and rapid rise of most of its current elevation ~10-6 Ma.

C. Significant incision (2.5-1 km) of the Altiplano western flank has occurred since the late Miocene (11-8 Ma) with only minor incision prior to this time.

D. A central plateau region that is characterized by a positive geoid, a negative Bouguer gravity anomaly, low rigidity, high heat flow, and an isostatically compensated thick crust (~80-65 km). In contrast, the plateau margins are characterized by progressively thinner crust, reduced heat flow, and a more rigid lithosphere away from the plateau center.

E. A lithospheric structure that exhibits an east-dipping high velocity zone down to 660 km corresponding to the Nazca plate, plateau region low and high velocity zones and high attenuation in the crust and upper mantle, and a high velocity mantle beneath the Eastern Cordillera probably corresponding to the western margin of the under-thrusted Brazilian craton.

Acknowledgements

Financial support was provided to J. Barnes by a University of Michigan Rackham Graduate School Predoctoral Fellowship and to T. Ehlers by NSF grants EAR 0409289 and 0738822. We thank Jeroen Ritsema for discussions on caveats associated with geophysical data and Nadine McQuarrie and Brian Horton for discussions on the relationships between upper-crust structure, sedimentation, and exhumation in the Bolivian Altiplano and thrust belt. Chris Poulsen, Rob Van Der Voo, Larry Ruff, and Nadine McQuarrie reviewed an earlier version of this paper. This work would not have been possible without the extensive efforts by many on the central Andes; in particular, South American scientists and research groups and colleagues centered at Cornell University and University of Arizona in the US, Free University of

Berlin and University of Potsdam in Germany, University of Oxford in the UK, and the Institut de Recherche pour le Developpement, Laboratoire des Mecanismes et Transferts en Geologie in Toulouse, France.

References

Allmendinger, R. W., and T. L. Gubbels (1996), Pure and simple shear plateau uplift, Altiplano-Puna, Argentina and Bolivia, Tectonophysics, v. 259, 1-13.

Allmendinger, R. W., T. E. Jordan, S. M. Kay, and B. L. Isacks (1997), The evolution of the Altiplano-Puna Plateau of the Central Andes, Annual Review of Earth and Planetary Sciences, v. 25, 139-174.

Alonso, R. N., B. Bookhagen, B. Carrapa, I. Coutand, M. Haschke, G. E. Hilley, L. Schoenbohm, E. R. Sobel, M. R. Strecker, M. H. Trauth, and A. Villanueva (2006), Tectonics, climate, and landscape evolution of the southern central Andes: the Argentine Puna Plateau and adjacent regions between 22 and 30°S, in The Andes: Active Subduction Orogeny, O. Oncken, G. Chong, G. Franz, P. Giese, H.-J. Gotze, V. A. Ramos, M. R. Strecker and P. Wigger (ed.), Springer-Verlag, Berlin, 265-283.

Alonso, R. N., T. E. Jordan, K. T. Tabbutt, and D. S. Vandervoort (1991), Giant evaporite belts of the Neogene central Andes, Geology, v. 19, 401-404.

Alpers, C. N., and G. H. Brimhall (1988), Middle Miocene climatic change in the Atacama Desert, northern Chile; evidence from supergene mineralization at La Escondida, Geological Society of America Bulletin, v. 100, 1640-1656.

Andriessen, P. A. M., and K. J. Reutter (1994), K-Ar and fission track mineral age determinations of igneous rocks related to multiple magmatic arc systems along the 23 S latitude of Chile and NW Argentina, in Tectonics of the southern central Andes, K. J. Reutter, E. Scheuber and P. J. Wigger (ed.), Springer-Verlag, Berlin, 141-153.

Arancibia, G., S. J. Matthews, and C. Perez de Arce (2006), K-Ar and 40Ar/ 39Ar geochronology of supergene processes in the Atacama Desert, northern Chile; tectonic and climatic relations, Journal of the Geological Society of London, v. 163, 107-118.

Arriagada, C., P. R. Cobbold, and P. Roperch (2006), Salar de Atacama basin: A record of compressional tectonics in the central Andes since the mid-Cretaceous, Tectonics, v. 25, doi:10.1029/2004TC001770.

Asch, G., B. Schurr, M. Bohm, X. Yuan, C. Haberland, B. Heit, R. Kind, I. Woelbern, K. Bataille, D. Comte, M. Pardo, J. Viramonte, A. Rietbrock, and P. Giese (2006), Seismological studies of the central and southern Andes, in The Andes: Active Subduction Orogeny, O. Oncken, G. Chong, G. Franz, P. Giese, H.-J. Goetze, V. A. Ramos, M. R. Strecker and P. Wigger (ed.), Springer, Berlin, 443-457.

Babeyko, A. Y., and S. V. Sobolev (2005), Quantifying different modes of the late Cenozoic shortening in the Central Andes, Geology, v. 33, 621-624.

Babeyko, A. Y., S. V. Sobolev, R. B. Trumbull, O. Oncken, and L. L. Lavier (2002), Numerical models of crustal scale convection and partial melting beneath the Altiplano-Puna Plateau, Earth and Planetary Science Letters, v. 199, 373-388.

Babeyko, A. Y., S. V. Sobolev, T. Vietor, O. Oncken, and R. B. Trumbull (2006), Numerical study of weakening processes in the central Andean back-arc, in The Andes: Active Subduction Orogeny, O. Oncken, G. Chong, G. Franz, P. Giese, H.-J. Goetze, V. A. Ramos, M. R. Strecker and P. Wigger (ed.), Springer, Berlin, 495-512.

Baby, P., R. Limachi, I. Moretti, E. Mendez, J. Oller, B. Guiller, and M. Specht (1995), Petroleum system of the northern and central Bolivian sub-Andean zone, in Petroleum basins of South America, A. J. Tankard, R. Suarez and H. J. Welsink (ed.), American Association of Petroleum Geologists Memoir 62, 445-458.

Baby, P., P. Rochat, G. Mascle, and G. Herail (1997), Neogene shortening contribution to crustal thickening in the back arc of the Central Andes, Geology, v. 25, 883-886.

Barke, R., and S. Lamb (2006), Late Cenozoic uplift of the Eastern Cordillera, Bolivian Andes, Earth and Planetary Science Letters, v. 249, 350-367.

Barke, R., S. Lamb, and C. MacNiocaill (2007), Late Cenozoic bending of the Bolivian Andes: New paleomagnetic and kinematic constraints, Journal of Geophysical Research, v. 112, doi:10.1029/2006JB004372.

Barnes, J. B., T. A. Ehlers, N. McQuarrie, P. B. O'Sullivan, and J. D. Pelletier (2006), Variations in Eocene to recent erosion across the central Andean fold-thrust belt, northern Bolivia: Implications for plateau evolution, Earth and Planetary Science Letters, v. 248, 118-133.

Barnes, J. B., T. A. Ehlers, N. McQuarrie, P. B. O'Sullivan, and S. Tawackoli (2008), Thermochronometer record of central Andean Plateau growth, Bolivia (19.5ºS), Tectonics, doi:10.1029/2007TC002174, in press.

Barnes, J. B., and J. D. Pelletier (2006), Latitudinal variation of denudation in the evolution of the Bolivian Andes, American Journal of Science, v. 306, 1-31.

Baumont, D., A. Paul, G. Zandt, S. L. Beck, and H. Pedersen (2002), Lithospheric structure of the central Andes based on surface wave dispersion, Journal of Geophysical Research, v. 107, doi:10.1029/2001JB000345.

Beaumont, C., R. A. Jamieson, M. H. Nguyen, and B. Lee (2001), Himalayan tectonics explained by extrusion of a low-viscosity crustal channel coupled to focused surface denudation, Nature, v. 414, 738-742.

Beaumont, C., R. A. Jamieson, M. H. Nguyen, and S. Medvedev (2004), Crustal channel flows: 1. Numerical models with applications to the tectonics of the Himalayan-Tibetan orogen, Journal of Geophysical Research, v. 109, doi:10.1029/2003JB002809.

Beck, S. L., and G. Zandt (2002), The nature of orogenic crust in the central Andes, Journal of Geophysical Research, v. 107, doi:10.1029/2000JB000124.

Beck, S. L., G. Zandt, S. C. Myers, T. C. Wallace, P. G. Silver, and L. Drake (1996), Crustal-thickness variations in the central Andes, Geology, v. 24, 407-410.

Bendick, R., and L. Flesch (2007), Reconciling lithospheric deformation and lower crustal flow beneath central Tibet, Geology, v. 35, 895-898.

Benjamin, M. T., N. M. Johnson, and C. W. Naeser (1987), Recent rapid uplift in the Bolivian Andes; evidence from fission-track dating, Geology, v. 15, 680-683.

Berry, E. W. (1939), The fossil flora of Potosi, Bolivia, Johns Hopkins University Studies in Geology, v. 13, 1-67.

Bird, P. (1979), Continental delamination and the Colorado Plateau, Journal of Geophysical Research, v. 84, 7561-7571.

Bird, P. (1991), Lateral extrusion of lower crust from under high topography, in the isostatic limit, Journal of Geophysical Research, v. 96, 10275-10286.

Bock, G., R. Kind, A. Rudloff, and G. Asch (1998), Shear wave anisotropy in the upper mantle beneath the Nazca Plate in northern Chile, Journal of Geophysical Research, v. 103, 24333-24345.

Cahill, T. A., and B. L. Isacks (1992), Seismicity and shape of the subducted Nazca Plate, Journal of Geophysical Research, B, Solid Earth and Planets, v. 97, 17,503-517,529.

Carrapa, B., D. Adelmann, G. E. Hilley, E. Mortimer, E. R. Sobel, and M. R. Strecker (2005), Oligocene range uplift and development of plateau morphology in the southern central Andes, Tectonics, v. 24, doi:10.1029/2004TC001762.

Carrapa, B., and P. G. DeCelles (2008), Eocene exhumation and basin development in the Puna of northwestern Argentina, Tectonics, v. 27, doi:10.1029/2007TC002127.

Carrapa, B., M. R. Strecker, and E. R. Sobel (2006), Cenozoic orogenic growth in the Central Andes: Evidence from sedimentary rock provenance and apatite fission track thermochronology in the Fiambalá Basin, southernmost Puna Plateau margin (NW Argentina), Earth and Planetary Science Letters, v. 247, 82-100.

Chmielowski, J., G. Zandt, and C. Haberland (1999), The central Andean Altiplano-Puna magma body, Geophysical Research Letters, v. 26, 783-786.

Cladouhos, T. T., R. W. Allmendinger, B. Coira, and E. Farrar (1994), Late Cenozoic deformation in the Central Andes; fault kinematics from the northern Puna, northwestern Argentina and southwestern Bolivia, Journal of South American Earth Sciences, v. 7, 209-228.

Clark, M. K., J. W. M. Bush, and L. H. Royden (2005), Dynamic topography produced by lower crustal flow against rheological strength heterogeneities bordering the Tibetan Plateau, Geophysical Journal International, v. 162, 575-590.

Clark, M. K., and L. H. Royden (2000), Topographic ooze; building the eastern margin of Tibet by lower crustal flow, Geology, v. 28, 703-706.

Coughlin, T. J., P. B. O'Sullivan, B. P. Kohn, and R. J. Holcombe (1998), Apatite fission-track thermochronology of the Sierras Pampeanas, central western Argentina; implications for the mechanism of plateau uplift in the Andes, Geology, v. 26, 999-1002.

Coutand, I., B. Carrapa, A. Deeken, A. K. Schmitt, E. R. Sobel, and M. R. Strecker (2006), Propagation of orographic barriers along an active range front; insights from sandstone petrography and detrital apatite fission-track thermochronology in the intramontane Angastaco Basin, NW Argentina, Basin Research, v. 18, 1-26.

Coutand, I., P. Gautier, P. R. Cobbold, M. de Urreiztieta, A. Chauvin, D. Gapais, E. A. Rossello, and O. Lopez-Gammundi (2001), Style and history of Andean deformation, Puna Plateau, northwestern Argentina, Tectonics, v. 20, 210-234.

Damm, K.-W., S. Pichowiak, R. S. Harmon, W. Todt, S. Kelley, R. Omarini, and H. Niemeyer (1990), Pre-Mesozoic evolution of the central Andes; the basement revisited, in Plutonism from Antarctica to Alaska, S. M. Kay and C. W. Rapela (ed.), Geological Society of America Special Paper 241, 101-126.

de Silva, S. L. (1989), Altiplano-Puna volcanic complex of the Central Andes, Geology, v. 17, 1102-1106.

DeCelles, P. G., B. Carrapa, and G. E. Gehrels (2007), Detrital zircon U-Pb ages provide provenance and chronostratigraphic information from Eocene synorogenic deposits in northwestern Argentina, Geology, v. 35, 323-326.

DeCelles, P. G., and B. K. Horton (2003), Early to middle Tertiary foreland basin development and the history of Andean crustal shortening in Bolivia, Geological Society of America Bulletin, v. 115, 58-77.

Deeken, A., E. R. Sobel, I. Coutand, M. Haschke, U. Riller, and M. R. Strecker (2006), Development of the southern Eastern Cordillera, NW Argentina, constrained by apatite fission track thermochronology; from Early Cretaceous extension to middle Miocene shortening, Tectonics, v. 25, doi:10.1029/2005TC001894.

Dewey, J. F. (1988), Extensional collapse of orogens, Tectonics, v. 7, 1123-1139.

Dewey, J. F., R. M. Shackleton, C. Chang, Y. Sun, and J. Yin (1988), The tectonic evolution of the Tibetan Plateau, Philosophical Transactions of the Royal Society of London, Series A: Mathematical and Physical Sciences, v. 327, 379-413.

Dorbath, C., and M. Granet (1996), Local earthquake tomography of the Altiplano and the Eastern Cordillera of northern Bolivia, Tectonophysics, v. 259, 117-136.

Dorbath, C., M. Granet, G. Poupinet, and C. Martinez (1993), A Teleseismic Study of the Altiplano and the Eastern Cordillera in Northern Bolivia - New Constraints on a Lithospheric Model, Journal of Geophysical Research, v. 98, 9825-9844.

Dorbath, C., A. Paul, and TheLithosphereAndeanGroup (1996), Tomography of the Andean crust and mantle at 20°S: first results of the Lithoscope experiment, Physics of the Earth and Planetary Interiors, v. 97, 133-144.

Dunn, J. F., K. G. Hartshorn, and P. W. Hartshorn (1995), Structural styles and hydrocarbon potential of the sub-Andean thrust belt of southern Bolivia, in Petroleum basins of South America, A. J. Tankard, R. Suarez and H. J. Welsink (ed.), American Association of Petroleum Geologists Memoir 62, 523-543.

Echavarria, L., R. Hernandez, R. Allmendinger, and J. Reynolds (2003), Subandean thrust and fold belt of northwestern Argentina; geometry and timing of the Andean evolution, American Association of Petroleum Geologists Bulletin, v. 87, 965-985.

Ege, H., E. R. Sobel, E. Scheuber, and V. Jacobshagen (2007), Exhumation history of the southern Altiplano plateau (southern Bolivia) constrained by apatite fission-track thermochronology, Tectonics, v. 26, doi:10.1029/2005TC001869.

Ehlers, T. A. (2005), Crustal thermal processes and the interpretation of thermochronometer data, in Low-Temperature Thermochronology: Techniques, Interpretations, and Applications, P. W. Reiners and T. A. Ehlers (ed.), Mineralogical Society of America, Chantilly, VA, 315-350.

Ehlers, T. A., and C. J. Poulsen (in prep), A slow and steady rise of the Andean Plateau?, Earth and Planetary Science Letters.

Eiler, J., C. N. Garzione, and P. Ghosh (2006), Response to comment on “Rapid uplift of the Altiplano revealed through ^{13}C-^{18}O bonds in paleosol carbonates”, Science, v. 314, doi: 10.1126/science.1133131.

Elger, K., O. Oncken, and J. Glodny (2005), Plateau-style accumulation of deformation: Southern Altiplano, Tectonics, v. 24, doi:10/1029/2004TC001675.

Elliot, D. (1983), The construction of balanced cross-sections, Journal of Structural Geology, v. 5, 101.

England, P., and P. Molnar (1990), Surface uplift, uplift of rocks, and exhumation of rocks, Geology, v. 18, 1173-1177.

England, P. C., and G. Houseman (1989), Extension during continental convergence, with application to the Tibetan Plateau, Journal of Geophysical Research, v. 94, 17561-17579.

Farias, M., R. Charrier, D. Comte, J. Martinod, and G. Herail (2005), Late Cenozoic deformation and uplift of the western flank of the Altiplano: Evidence from the depositional, tectonic, and geomorphologic evolution and shallow seismic activity (northern Chile at 19°30'S), Tectonics, v. 24, doi:10.1029/2004TC001667.

Farrar, E., A. H. Clark, D. J. Kontak, and D. A. Archibald (1988), Zongo-San Gaban Zone; Eocene foreland boundary of the central Andean Orogen, Northwest Bolivia and Southeast Peru, Geology, v. 16, 55-58.

Francis, P. W., and C. J. Hawkesworth (1994), Late Cenozoic rates of magmatic activity in the Central Andes and their relationships to continental crust formation and thickening, Journal of the Geological Society of London, v. 151, 845-854.

Froidevaux, C., and B. L. Isacks (1984), The mechanical state of the lithosphere in the Altiplano-Puna segment of the Andes, Earth and Planetary Science Letters, v. 71, 305-314.

Garzione, C. N., P. Molnar, J. Libarkin, and B. MacFadden (2006), Rapid late Miocene rise of the Bolivian Altiplano: Evidence for removal of mantle lithosphere, Earth and Planetary Science Letters, v. 241, 543-556.

Garzione, C. N., P. Molnar, J. Libarkin, and B. MacFadden (2007), Reply to Comment on "Rapid late Miocene rise of the Bolivian Altiplano: Evidence for removal of mantle lithosphere" by Garzione et al. (2006), Earth Planet. Sci. Lett. 241 (2006) 543–556, Earth and Planetary Science Letters, v. 259, 630-633.

Gaupp, R., A. Kott, and G. Worner (1999), Palaeoclimatic implications of Mio–Pliocene sedimentation in the high-altitude intra-arc Lauca Basin of northern Chile, Palaeogeography, Palaeoclimatology, Palaeoecology, v. 151, 79-100.

Gephart, J. (1994), Topography and subduction geometry in the central Andes; clues to the mechanics of a noncollisional orogen, Journal of Geophysical Research, v. 99, 12279-12288.

Gerbault, M., J. Martinod, and G. Herail (2005), Possible orogeny-parallel lower crustal flow and thickening in the Central Andes, Tectonophysics, v. 399, 59-72.

Ghosh, P., C. N. Garzione, and J. M. Eiler (2006), Rapid uplift of the Altiplano revealed through ^{13}C-^{18}O bonds in paleosol carbonates, Science, v. 311, 511-515.

Giese, P., E. Scheuber, F. Schilling, M. Schmitz, and P. Wigger (1999), Crustal thickening processes in the Central Andes and the different natures of the Moho-discontinuity, in Central Andean deformation, K. J. Reutter (ed.), Pergamon, Oxford, 201-220.

Gillis, R. J., B. K. Horton, and M. Grove (2006), Thermochronology, geochronology, and upper crustal structure of the Cordillera Real: Implications for Cenozoic exhumation of the central Andean plateau, Tectonics, v. 25, doi:10.1029/2005TC001887.

Gotze, H.-J., and A. Kirchner (1997), Gravity field at the South American active margin (20° to 29°S), Journal of South American Earth Sciences, v. 10, 179-188.

Gotze, H.-J., B. Lahmeyer, S. Schmidt, and S. Strunk (1994), The lithospheric structure of the central Andes (20-26°S) as inferred from interpretation of regional gravity, in Tectonics of the southern Central Andes; structure and evolution of an active continental margin, K. J. Reutter, E. Scheuber and P. J. Wigger (ed.), Springer-Verlag, Berlin, 7-21.

Graeber, F. M., and G. Asch (1999), Three-dimensional models of P wave velocity and P-to-S velocity ratio in the southern central Andes by simultaneous inversion of local earthquake data, Journal of Geophysical Research, v. 104, 20237-20256.

Graham, A., K. M. Gregory-Wodzicki, and K. L. Wright (2001), A Mio-Pliocene palynoflora from the Eastern Cordillera, Bolivia: implications for the uplift history of the central Andes, American Journal of Botany, v. 88, 1545-1557.

Gregory-Wodzicki, K. M. (2000), Uplift history of the Central and Northern Andes; a review, Geological Society of America Bulletin, v. 112, 1091-1105.

Gregory-Wodzicki, K. M., W. C. McIntosh, and K. Velasquez (1998), Climatic and tectonic implications of the late Miocene Jakokkota Flora, Bolivian Altiplano, Journal of South American Earth Sciences, v. 11, 533-560.

Gubbels, T. L., B. L. Isacks, and E. Farrar (1993), High-level surfaces, plateau uplift, and foreland development, Bolivian central Andes, Geology, v. 21, 695-698.

Haberland, C., B. Schurr, A. Rietbrock, B. Schurr, and H. Brasse (2003), Coincident anomalies of seismic attenuation and electrical resistivity beneath the southern Bolivian Altiplano plateau, Geophysical Research Letters, v. 30, doi:10.1029/2003GL017492.

Hammerschmidt, K., R. Doebel, and H. Friedrichsen (1992), Implication of $^{40}Ar/^{39}Ar$ dating of early Tertiary volcanic rocks from the North-Chilean Precordillera, Tectonophysics, v. 202, 55-81.

Hartley, A. J. (2003), Andean uplift and climate change, Journal of the Geological Society of London, v. 160, 7-10.

Hartley, A. J., and C. M. Rice (2005), Controls on supergene enrichment of porphyry copper deposits in the Central Andes; a review and discussion, Mineralium Deposita, v. 40, 515-525.

Hartley, A. J., T. Sempere, and G. Worner (2007), A comment on “Rapid late Miocene rise of the Bolivian Altiplano: Evidence for removal of mantle lithosphere” by C.N. Garzione et al. [Earth Planet. Sci. Lett. 241 (2006) 543–556], Earth and Planetary Science Letters, v. 259, 625-629.

Hatcher, R. D. J. (2004), Properties of thrusts and upper bounds for the size of thrust sheets, in Thrust tectonics and hydrocarbon systems, K. R. McClay (ed.), American Association of Petroleum Geologists Memoir 82, 18-29.

Heit, B., I. Koulakov, G. Asch, X. Yuan, R. Kind, I. Alcocer-Rodriguez, S. Tawackoli, and H.-G. Wilke (2008), More constraints to determine the seismic structure beneath the Central Andes at 21°S using teleseismic tomography analysis, Journal of South American Earth Sciences, v. 25, 22-36.

Henry, S. G., and H. N. Pollack (1988), Terrestrial heat flow above the Andean subduction zone in Bolivia and Peru, Journal of Geophysical Research, v. 93, 15153-15162.

Herail, G., J. Oller, P. Baby, M. Bonhomme, and P. Soler (1996), Strike-slip faulting, thrusting and related basins in the Cenozoic evolution of the southern branch of the Bolivian Orocline, Tectonophysics, v. 259, 201-212.

Hernandez, R. M., T. E. Jordan, A. D. Farjat, L. Echavarria, B. D. Idleman, and J. H. Reynolds (2005), Age, distribution, tectonics, and eustatic controls of the Paranense and Caribbean marine transgressions in southern Bolivia and Argentina, Journal of South American Earth Sciences, v. 19, 495-512.

Hodges, K. (2000), Tectonics of the Himalaya and southern Tibet from two perspectives, Geological Society of America Bulletin, v. 112, 324-350.

Hoke, G. D., B. L. Isacks, T. E. Jordan, N. Blanco, A. J. Tomlinson, and J. Ramezani (2007), Geomorphic evidence for post-10 Ma uplift of the western flank of the central Andes 18°30'–22°S, Tectonics, v. 26, doi:10.1029/2006TC002082.

Hoke, L., and S. Lamb (2007), Cenozoic behind-arc volcanism in the Bolivian Andes, South America; implications for mantle melt generation and lithospheric structure, Journal of the Geological Society of London, v. 164, 795-814.

Hongn, F., C. del Papa, J. Powell, I. Petrinovic, R. Mon, and V. Deraco (2007), Middle Eocene deformation and sedimentation in the Puna-Eastern Cordillera transition (23°-26°S); control by preexisting heterogeneities on the pattern of initial Andean shortening, Geology, v. 35, 271-274.

Horton, B. K. (1998), Sediment accumulation on top of the Andean orogenic wedge; Oligocene to late Miocene basins of the Eastern Cordillera, southern Bolivia, Geological Society of America Bulletin, v. 110, 1174-1192.

Horton, B. K. (1999), Erosional control on the geometry and kinematics of thrust belt development in the central Andes, Tectonics, v. 18, 1292-1304.

Horton, B. K. (2005), Revised deformation history of the central Andes: Inferences from Cenozoic foredeep and intermontane basins of the Eastern Cordillera, Bolivia, Tectonics, v. 24, doi:10.1029/2003TC001619.

Horton, B. K., B. A. Hampton, B. N. Lareau, and E. Baldellon (2002), Tertiary provenance history of the northern and central Altiplano (Central Andes, Bolivia); a detrital record of plateau-margin tectonics, Journal of Sedimentary Research, v. 72, 711-726.

Hulka, C., K.-U. Grafe, B. Sames, C. E. Uba, and C. Heubeck (2006), Depositional setting of the Middle to Late Miocene Yecua Formation of the Chaco Foreland Basin, southern Bolivia, Journal of South American Earth Sciences, v. 21, 135-150.

Husson, L., and Y. Ricard (2004), Stress balance above subduction: application to the Andes, Earth and Planetary Science Letters, v. 222, 1037-1050.

Husson, L., and T. Sempere (2003), Thickening the Altiplano crust by gravity-driven crustal channel flow, Geophysical Research Letters, v. 30, doi:10.1029/2002GL016877.

Iaffaldano, G., H.-P. Bunge, and T. H. Dixon (2006), Feedback between mountain belt growth and plate convergence, Geology, v. 34, 893-896.

Insel, N., M. Haschke, M. Grove, A. Schmitt, M. R. Strecker, and O. Lovera (in revision), Pre-Neogene cooling and exhumation of the Puna plateau, NW-Argentina: Constraints from U-Pb zircon and $^{40}Ar/^{39}Ar$ K-feldspar thermochronology Tectonics.

Isacks, B. L. (1988), Uplift of the Central Andean Plateau and bending of the Bolivian Orocline, Journal of Geophysical Research, v. 93, 3211-3231.

James, D. E., and I. S. Sacks (1999), Cenozoic formation of the Central Andes: A Geophysical Perspective, in Geology and Ore Deposits of the Central Andes, B. J. Skinner (ed.), SEPM Special Publication, 1-25.

Jordan, T. E., and R. N. Alonso (1987), Cenozoic stratigraphy and basin tectonics of the Andes Mountains, 20°-28° south latitude, American Association of Petroleum Geologists Bulletin, v. 71, 49-64.

Jordan, T. E., B. L. Isacks, R. W. Allmendinger, J. A. Brewer, V. A. Ramos, and C. J. Ando (1983), Andean tectonics related to geometry of subducted Nazca Plate, Geological Society of America Bulletin, v. 94, 341-361.

Jordan, T. E., C. Mpodozis, N. Munoz, N. Blanco, P. Pananont, and M. Gardeweg (2007), Cenozoic subsurface stratigraphy and structure of the Salar de Atacama Basin, northern Chile, Journal of South American Earth Sciences, v. 23, 122-146.

Jordan, T. E., J. H. Reynolds, III, and J. P. Erikson (1997), Variability in age of initial shortening and uplift in the Central Andes, in Tectonic uplift and climate change, W. F. Ruddiman (ed.), Plenum Press, New York, 41-61.

Kay, R. W., and S. Mahlburg Kay (1993), Delamination and delamination magmatism, Tectonophysics, v. 219, 177-189.

Kay, S. M., B. Coira, and J. Viramonte (1994), Young mafic back arc volcanic rocks as indicators of continental lithospheric delamination beneath the Argentine Puna Plateau, Central Andes, Journal of Geophysical Research, v. 99, 24323-24339.

Kennan, L. (2000), Large-scale geomorphology of the Andes; interrelationships of tectonics, magmatism and climate, M. A. Summerfield (ed.), John Wiley & Sons, Chichester, 167-199.

Kennan, L., S. Lamb, and J. Rundle (1995), K-Ar dates from the Altiplano and Cordillera Oriental of Bolivia; implications for Cenozoic stratigraphy and tectonics, Journal of South American Earth Sciences, v. 8, 163-186.

Kennan, L., S. H. Lamb, and L. Hoke (1997), High-altitude palaeosurfaces in the Bolivian Andes; evidence for late Cenozoic surface uplift, in Palaeosurfaces; recognition, reconstruction and palaeoenvironmental interpretation, M. Widdowson (ed.), Special Publication of the Geological Society 120, London, 307-323.

Kley, J. (1996), Transition from basement-involved to thin-skinned thrusting in the Cordillera Oriental of southern Bolivia, Tectonics, v. 15, 763-775.

Kley, J. (1999), Geologic and geometric constraints on a kinematic model of the Bolivian Orocline, Journal of South American Earth Sciences, v. 12, 221-235.

Kley, J., A. H. Gangui, and D. Krueger (1996), Basement-involved blind thrusting in the eastern Cordillera Oriental, southern Bolivia; evidence from cross-sectional balancing, gravimetric and magnetotelluric data, in Geodynamics of the Andes, J. F. Dewey and S. H. Lamb (ed.), Elsevier, Amsterdam, 171-184.

Kley, J., and C. R. Monaldi (1998), Tectonic shortening and crustal thickness in the Central Andes; how good is the correlation?, Geology, v. 26, 723-726.

Kley, J., and C. R. Monaldi (2002), Tectonic inversion in the Santa Barbara System of the central Andean foreland thrust belt, northwestern Argentina, Tectonics, v. 21, doi:10.1029/2002TC902003.

Kley, J., C. R. Monaldi, and J. A. Salfity (1999), Along-strike segmentation of the Andean foreland; causes and consequences, Tectonophysics, v. 301, 75-94.

Kober, F., F. Schlunegger, G. Zeilinger, and H. Schneider (2006), Surface uplift and climate change; the geomorphic evolution of the western escarpment of the Andes of northern Chile between the Miocene and present, in Geological Society of America Special Paper 398, S. D. Willett, N. Hovius, M. T. Brandon and D. M. Fisher (ed.), 75-86.

Kono, M., Y. Fukao, and A. Yamamoto (1988), Mountain building in the Central Andes, in Rock magnetism and paleogeophysics, M. Kono (ed.), Rock Magnetism and Paleogeophysics Research Group in Japan, Tokyo, 73-80.

Kono, M., K. Heki, Y. Hamano, and D. B. Stone (1985), Paleomagnetic study of the Central Andes; counterclockwise rotation of the Peruvian Block, in Megaplates and microplates; proceedings, international symposium, Pergamon Press, Oxford - New York, 193-209.

Kontak, D. J., E. A. Farrar, A. H. Clark, and D. A. Archibald (1990), Eocene tectono-thermal rejuvenation of an upper Paleozoic-lower Mesozoic terrane in the Cordillera de Carabaya, Puno, southeastern Peru, revealed by K-Ar and $^{40}Ar/^{39}Ar$ dating, Journal of South American Earth Sciences, v. 3, 231-246.

Kraemer, B., D. Adelmann, M. Alten, W. Schnurr, K. Erpenstein, E. Kiefer, P. van den Bogaard, and K. Gorler (1999), Incorporation of the Paleogene foreland into the Neogene Puna plateau: The Salar de Antofalla area, NW Argentina, Journal of South American Earth Sciences, v. 12, 157-182.

Kuhn, D. (2002), Fold and thrust belt structures and strike-slip faulting at the SE margin of the Salar de Atacama basin, Chilean Andes, Tectonics, v. 21, doi: 10.1029/2001TC901042.

Lamb, S. (2001), Vertical axis rotation in the Bolivian Orocline, South America; 1, Paleomagnetic analysis of Cretaceous and Cenozoic rocks, Journal of Geophysical Research, v. 106, 26605-26632.

Lamb, S., and P. Davis (2003), Cenozoic climate change as a possible cause for the rise of the Andes, Nature, v. 425, 792-797.

Lamb, S., and L. Hoke (1997), Origin of the high plateau in the Central Andes, Bolivia, South America, Tectonics, v. 16, 623-649.

Lamb, S., L. Hoke, L. Kennan, and J. Dewey (1997), Cenozoic evolution of the Central Andes in Bolivia and northern Chile, Special Publication of the Geological Society 121, v., 237-264.

Lenters, J. D., and K. H. Cook (1995), Simulation and diagnosis of the regional summertime precipitation climatology of South America, Journal of Climate, v. 8, 2988-3005.

Maksaev, V., and M. Zentilli (1999), Fission track thermochronology of the Domeyko Cordillera, northern Chile; implications for Andean tectonics and porphyry copper metallogenesis, Exploration and Mining Geology, v. 8, 65-89.

Marrett, R. A., R. W. Allmendinger, R. N. Alonso, and R. E. Drake (1994), Late Cenozoic tectonic evolution of the Puna Plateau and adjacent foreland, northwestern Argentine Andes, Journal of South American Earth Sciences, v. 7, 179-207.

Marshall, L. G., T. Sempere, and M. Gayet (1993), The Petaca (late Oligocene-middle Miocene) and Yecua (late Miocene) formations of the Subandean-Chaco Basin, Bolivia, and their tectonic significance, in Documents des Laboratoires de Geologie, Lyon, vol.125, M. Gayet (ed.), Universite Claude Bernard, Departement des Sciences de la Terre, 291-301.

Masek, J. G., B. L. Isacks, T. L. Gubbels, and E. J. Fielding (1994), Erosion and tectonics at the margins of continental plateaus, Journal of Geophysical Research, v. 99, 13941-13956.

Matte, P., M. Mattauer, J. M. Olivet, and D. A. Griot (1997), Continental subductions beneath Tibet and the Himalayan Orogeny; a review, Terra Nova, v. 9, 264-270.

McBride, S. L., A. H. Clark, E. Farrar, and D. A. Archibald (1987), Delimitation of a cryptic Eocene tectono-thermal domain in the Eastern Cordillera of the Bolivian Andes through K-Ar dating and ^{40}Ar-^{39}Ar step-heating, Journal of the Geological Society of London, v. 144, 243-255.

McQuarrie, N. (2002a), Initial plate geometry, shortening variations, and evolution of the Bolivian Orocline, Geology, v. 30, 867-870.

McQuarrie, N. (2002b), The kinematic history of the central Andean fold-thrust belt, Bolivia; implications for building a high plateau, Geological Society of America Bulletin, v. 114, 950-963.

McQuarrie, N., J. B. Barnes, and T. A. Ehlers (2008), Geometric, kinematic, and erosional history of the central Andean Plateau, Bolivia (15-17ºS), Tectonics, doi:10.1029/2006TC002054, in press.

McQuarrie, N., and P. G. DeCelles (2001), Geometry and structural evolution of the central Andean backthrust belt, Bolivia, Tectonics, v. 20, 669-692.

McQuarrie, N., B. K. Horton, G. Zandt, S. Beck, and P. G. DeCelles (2005), Lithospheric evolution of the Andean fold-thrust belt, Bolivia, and the origin of the central Andean plateau, Tectonophysics, v. 399, 15-37.

Medvedev, S., Y. Podladchikov, M. R. Handy, and E. Scheuber (2006), Controls on the deformation of the central and southern Andes (10-35 degrees S); insight from thin-sheet numerical modeling, in The Andes: Active Subduction Orogeny, O. Oncken, G. Chong, G. Franz, P. Giese, H.-J. Goetze, V. A. Ramos, M. R. Strecker and P. Wigger (ed.), Springer, Berlin, 475-494.

Megard, F. (1987), Cordilleran Andes and marginal Andes; a review of Andean geology north of the Arica elbow (18 S), in Circum-Pacific orogenic belts and evolution of the Pacific Ocean basin, J. W. H. Monger and J. Francheteau (ed.), American Geophysical Union, 71-95.

Meyer, H. W. (2007), A review of paleotemperature-lapse rate methods for estimating paleoelevation from fossil floras, Reviews in Mineralogy and Geochemistry, v. 66, 155-171.

Molnar, P., P. England, and J. Martinod (1993), Mantle dynamics, uplift of the Tibetan Plateau, and the Indian monsoon, Reviews of Geophysics, v. 31, 357-396.

Molnar, P., and P. C. England (1990), Late Cenozoic uplift of mountain ranges and global climate change; chicken or egg?, Nature, v. 346, 29-34.

Molnar, P., and C. N. Garzione (2007), Bounds on the viscosity coefficient of continental lithosphere from removal of mantle lithosphere beneath the Altiplano and Eastern Cordillera, Tectonics, v. 26, doi: 10.1029/2006TC001964.

Montgomery, D. R., G. Balco, and S. D. Willett (2001), Climate, tectonics, and the morphology of the Andes, Geology, v. 29, 579-582.

Mortimer, C. (1973), The Cenozoic history of the southern Atacama Desert, Chile, Journal of the Geological Society of London, v. 129, 505-526.

Mortimer, E., B. Carrapa, I. Coutand, L. Schoenbohm, E. R. Sobel, J. Sosa Gomez, and M. R. Strecker (2007), Fragmentation of a foreland basin in response to out-of-sequence basement uplifts and structural reactivation; El Cajon-Campo del Arenal Basin, NW Argentina, Geological Society of America Bulletin, v. 119, 637-653.

Müller, J. P., J. Kley, and V. Jacobshagen (2002), Structure and Cenozoic kinematics of the Eastern Cordillera, southern Bolivia (21ºS), Tectonics, v. 21, doi: 10.1029/2001TC001340.

Muñoz, N., and R. Charrier (1996), Uplift of the western border of the Altiplano on a west-vergent thrust system, Northern Chile, Journal of South American Earth Sciences, v. 9, 171-181.

Myers, S. C., S. Beck, G. Zandt, and T. Wallace (1998), Lithospheric-scale structure across the Bolivian Andes from tomographic images of velocity and attentuation for P and S waves, Journal of Geophysical Research, v. 103, 21233-21252.

Noblet, C., A. Lavenu, and R. Marocco (1996), Concept of continuum as opposed to periodic tectonism in the Andes, Tectonophysics, v. 255, 65-78.

Oncken, O., G. Chong, G. Franz, P. Giese, H.-J. Gotze, V. A. Ramos, M. R. Strecker, and P. Wigger (ed.) (2006a), The Andes: Active Subduction Orogeny, 569 pp., Springer-Verlag, Berlin.

Oncken, O., D. Hindle, J. Kley, K. Elger, P. Victor, and K. Schemmann (2006b), Deformation of the central Andean upper plate system - facts, fiction, and constraints for plateau models, in The Andes: Active Subduction Orogeny, O. Oncken, G. Chong, G. Franz, P. Giese, H.-J. Gotze, V. A. Ramos, M. R. Strecker and P. Wigger (ed.), Springer-Verlag, Berlin, 3-27.

Oncken, O., S. Sobolev, M. Stiller, G. Asch, C. Haberland, J. Mechie, X. Yuan, E. Lueschen, P. Giese, P. Wigger, S. Lueth, E. Scheuber, J. Goetze, H. Brasse, S. Buske, M.-K. Yoon, S. Shapiro, A. Rietbrock, G. Chong, H.-G. Wilke, G. Gonzalez, P. Bravo, H. Vieytes, E. Martinez, R. Roessling, and E. Ricaldi (2003), Seismic imaging of a convergent continental margin and plateau in the central Andes (Andean Continental Research Project 1996 (ANCORP'96)), Journal of Geophysical Research, v. 108, doi:10.1029/2002JB001717.

Pardo-Casas, F., and P. Molnar (1987), Relative motion of the Nazca (Farallon) and South American plates since Late Cretaceous time, Tectonics, v. 6, 233-248.

Perez-Gussinye, M., A. R. Lowry, J. P. Morgan, and A. Tassara (2008), Effective elastic thickness variations along the Andean margin and their relationship to subduction geometry, Geochemistry, Geophysics, Geosystems, v. 9, doi: 10.1029/2007GC001786.

Placzek, C., J. Quade, and P. J. Patchett (2006), Geochronology and stratigraphy of late Pleistocene lake cycles on the southern Bolivian Altiplano; implications for causes of tropical climate change, Geological Society of America Bulletin, v. 118, 515-532.

Polet, J., P. G. Silver, S. Beck, T. Wallace, G. Xandt, S. Ruppert, R. Kind, and A. Rudloff (2000), Shear wave anisotropy beneath the Andes from the BANJO, SEDA, and PISCO experiments, Journal of Geophysical Research, v. 105, 6287-6304.

Pope, D. C., and S. D. Willett (1998), Thermal-mechanical model for crustal thickening in the central Andes driven by ablative subduction, Geology, v. 26, 511-514.

Quade, J., C. Garzione, and J. Eiler (2007), Paleoelevation reconstruction using pedogenic carbonates, Reviews in Mineralogy and Geochemistry, v. 66, 53-87.

Quang, C. X., A. H. Clark, J. K. Lee, and N. Hawkes (2005), Response of supergene processes to episodic Cenozoic uplift, pediment erosion, and ignimbrite eruption in the porphyry copper province of southern Peru, Economic Geology and the Bulletin of the Society of Economic Geologists, v. 100, 87-114.

Ramos, V. A., E. O. Cristallini, and D. J. Perez (2002), The Pampean flat-slab of the Central Andes, Journal of South American Earth Sciences, v. 15, 59-78.

Ramos, V. A., T. Zapata, E. O. Cristallini, and A. Introcaso (2004), The Andean thrust system; latitudinal variations in structural styles and orogenic shortening, in Thrust Tectonics and Hydrocarbon Systems, K. R. McClay (ed.), American Association of Petroleum Geologists Memoir 82, 30-50.

Rech, J. A., B. S. Currie, G. Michalski, and A. M. Cowan (2006), Neogene climate change and uplift in the Atacama Desert, Chile, Geology, v. 34, 761-764.

Reiners, P. W., and T. A. Ehlers (ed.) (2005), Low-temperature thermochronology: Techniques, Interpretations, and Applications, 622 pp., Mineralogical Society of America, Chantilly, VA.

Reiners, P. W., T. A. Ehlers, and P. K. Zeitler (2005), Past, Present, and Future of Thermochronology, in Low-temperature thermochronology : Techniques, Interpretations, and Applications, P. W. Reiners and T. A. Ehlers (ed.), Mineralogical Society of America, Chantilly, VA, 1-18.

Reutter, K. J., E. Scheuber, and G. Chong (1996), The Precordilleran fault system of Chuquicamata, Northern Chile: evidence for reversals along arc-parallel strike-slip faults, Tectonophysics, v. 259, 213-228.

Reutter, K. J., E. Scheuber, and P. Wigger (ed.) (1994), Tectonics of the southern central Andes; structure and evolution of an active continental margin 335 pp., Springer-Verlag, Berlin.

Reynolds, J. H., C. I. Galli, R. M. Hernandez, B. D. Idleman, J. M. Kotila, R. V. Hilliard, and C. W. Naeser (2000), Middle Miocene tectonic development of the transition zone, Salta Province, Northwest Argentina; magnetic stratigraphy from the Metan Subgroup, Sierra de Gonzalez, Geological Society of America Bulletin, v. 112, 1736-1751.

Richter, F. M., D. B. Rowley, and D. J. DePaolo (1992), Sr isotope evolution of seawater: The role of tectonics, Earth and Planetary Science Letters, v. 109, 11-23.

Riller, U., and O. Oncken (2003), Growth of the Central Andean Plateau by tectonic segmentation is controlled by the gradient in crustal shortening, Journal of Geology, v. 111, 367-384.

Ring, U., M. T. Brandon, S. D. Willett, and G. S. Lister (1999), Exhumation processes, in Exhumation processes; Normal Faulting, Ductile Flow and Erosion, U. Ring, M. T. Brandon, G. S. Lister and S. D. Willett (ed.), Geological Society of London Special Publications, London, 1-27.

Riquelme, R., J. Martinod, G. Herail, J. Darrozes, and R. Charrier (2003), A geomorphological approach to determining the Neogene to Recent tectonic deformation in the Coastal Cordillera of northern Chile (Atacama), Tectonophysics, v. 361, 255-275.

Roeder, D. (1988), Andean-age structure of Eastern Cordillera (Province of La Paz, Bolivia), Tectonics, v. 7, 23-39.

Roeder, D., and R. L. Chamberlain (1995), Structural geology of sub-Andean fold and thrust belt in northwestern Bolivia, in Petroleum basins of South America, A. J. Tankard, R. Suarez and H. J. Welsink (ed.), American Association of Petroleum Geologists Memoir 62, 459-479.

Roperch, P., M. Fornari, G. Herail, and G. V. Parraguez (2000), Tectonic rotations within the Bolivian Altiplano: Implications for the geodynamic evolution of the central Andes during the late Tertiary, Journal of Geophysical Research, v. 105, 795-820.

Roperch, P., P. Roperch, C. Arriagada, C. Tapia, T. Sempere, O. Macedo, M. Fornari, M. Garcia, and C. Laj (2006), Counterclockwise rotation of late Eocene-Oligocene fore-arc deposits in southern Peru and its significance for oroclinal bending in the central Andes, Tectonics, v. 25, doi:10.1029/2005TC001882.

Rowley, D. B., and B. S. Currie (2006), Palaeo-altimetry of the late Eocene to Miocene Lunpola basin, central Tibet, Nature, v. 439, 677-681.

Royden, L. (1996), Coupling and decoupling of crust and mantle in convergent orogens; implications for strain partitioning in the crust, Journal of Geophysical Research, v. 101, 17679-17705.

Royden, L., B. Burchfiel, R. King, E. Wang, Z. Chen, F. Shen, and Y. Liu (1997), Surface deformation and lower crustal flow in eastern Tibet, Science, v. 276, 788-790.

Ruddiman, W. F., M. E. Raymo, W. L. Prell, and J. E. Kutzbach (1997), The uplift-climate connection; a synthesis, in Tectonic uplift and climate change, W. F. Ruddiman (ed.), Plenum Press, New York, 471-515.

Scheuber, E., and P. Giese (1999), Architecture of the Central Andes; a compilation of geoscientific data along a transect at 21°S, Journal of South American Earth Sciences, v. 12, 103-107.

Scheuber, E., D. Mertmann, H. Ege, P. Silva-Gonzalez, C. Heubeck, K.-J. Reutter, and V. Jacobshagen (2006), Exhumation and basin development related to formation of the central Andean plateau, 21°S, in The Andes: Active Subduction Orogeny,

O. Oncken, G. Chong, G. Franz, P. Giese, H.-J. Gotze, V. A. Ramos, M. R. Strecker and P. Wigger (ed.), Springer-Verlag, Berlin, 285-301.

Schildgen, T. F., K. V. Hodges, K. X. Whipple, P. W. Reiners, and M. S. Pringle (2007), Uplift of the western margin of the Andean Plateau revealed from canyon incision history, southern Peru, Geology, v. 35, 523-526.

Schilling, F. R., R. B. Trumbull, H. Brasse, C. Haberland, G. Asch, D. Bruhn, K. Mai, V. Haak, P. Giese, M. Munoz, J. Ramelow, A. Rietbrock, E. Ricaldi, and T. Vietor (2006), Partial melting in the central Andean crust: a review of geophysical, petrophysical, and petrologic evidence, in The Andes: Active Subduction Orogeny, O. Oncken, G. Chong, G. Franz, P. Giese, H.-J. Goetze, V. A. Ramos, M. R. Strecker and P. Wigger (ed.), Springer, Berlin, 459-474.

Schlunegger, F., G. Zeilinger, A. Kounov, F. Kober, and B. Huesser (2006), Scale of relief growth in the forearc of the Andes of northern Chile (Arica latitude, 18°S), Terra Nova, v. 18, 217-223.

Schmidt, C. J., R. A. Astini, C. H. Costa, C. E. Gardini, and P. E. Kraemer (1995), Cretaceous rifting, alluvial fan sedimentation, and Neogene inversion, southern Sierras Pampeanas, Argentina, in Petroleum basins of South America, A. J. Tankard, R. Suarez and H. J. Welsink (ed.), American Association of Petroleum Geologists Memoir 62, 341-358.

Schmitz, M., K. Lessel, P. Giese, P. Wigger, M. Araneda, J. Bribach, F. Graeber, S. Grunewald, C. Haberland, S. Lueth, P. Roewer, T. Ryberg, and A. Schulze (1999), The crustal structure beneath the Central Andean forearc and magmatic arc as derived from seismic studies; the PISCO 94 experiment in northern Chile (21°-23°S), Journal of South American Earth Sciences, v. 12, 237-260.

Schurr, B., G. Asch, A. Rietbrock, R. Trumbull, and C. Haberland (2003), Complex patterns of fluid and melt transport in the central Andean subduction zone revealed by attenuation tomography, Earth and Planetary Science Letters, v. 215, 105-119.

Schurr, B., and A. Rietbrock (2004), Deep seismic structure of the Atacama Basin, northern Chile, Geophysical Research Letters, v. 31, L12601, doi:12610.11029/12004GL019796.

Schurr, B., A. Rietbrock, G. Asch, R. Kind, and O. Oncken (2006), Evidence for lithospheric detachment in the Central Andes from local earthquake tomography, Tectonophysics, v. 415, 203-223.

Sebrier, M., A. Lavenu, M. Fornari, and J. P. Soulas (1988), Tectonics and uplift in Central Andes (Peru, Bolivia and northern Chile) from Eocene to present, Geodynamique, v. 3, 85-106.

Sempere, T., R. Butler, D. Richards, L. Marshall, W. Sharp, and C. Swisher (1997), Stratigraphy and chronology of Upper Cretaceous-lower Paleogene strata in Bolivia and Northwest Argentina, Geological Society of America Bulletin, v. 109, 709-727.

Sempere, T., A. J. Hartley, and P. Roperch (2006), Comment on "Rapid uplift of the Altiplano revealed through ^{13}C-^{18}O Bonds in paleosol carbonates", Science, v. 314, doi: 10.1126/science.1132837.

Sempere, T., G. Herail, J. Oller, and M. G. Bonhomme (1990), Late Oligocene-early Miocene major tectonic crisis and related basins in Bolivia, Geology, v. 18, 946-949.

Servant, M., T. Sempere, J. Argollo, M. Bernat, G. Feraud, and P. Lo Bello (1989), Cenozoic morphogenesis and uplift of the Eastern Cordillera in the Bolivian Andes, Comptes Rendus de l'Academie des Sciences de Paris, v. 309, 416-422.

Sheffels, B. (1990), Lower bound on the amount of crustal shortening in the central Bolivian Andes, Geology, v. 18, 812-815.

Singewald, J. T., and E. W. Berry (1922), The geology of the Corocoro copper district of Bolivia, Johns Hopkins University Studies in Geology, v. 1, 1-117.

Sobel, E. R., G. E. Hilley, and M. R. Strecker (2003), Formation of internally drained contractional basins by aridity-limited bedrock incision, Journal of Geophysical Research, v. 108, doi:10.1029/2002JB001883.

Sobel, E. R., and M. R. Strecker (2003), Uplift, exhumation and precipitation: tectonic and climatic control of Late Cenozoic landscape evolution in the northern Sierras Pampeanas, Argentina, Basin Research, v. 15, 431-451.

Sobolev, S. V., and A. Y. Babeyko (2005), What drives orogeny in the Andes?, Geology, v. 33, 617-620.

Sobolev, S. V., A. Y. Babeyko, A. Y. Koulakov, and O. Oncken (2006), Mechanism of the Andean orogeny; insight from numerical modeling, in The Andes: Active Subduction Orogeny, O. Oncken, G. Chong, G. Franz, P. Giese, H.-J. Goetze, V. A. Ramos, M. R. Strecker and P. Wigger (ed.), Springer, Berlin, 513-535.

Soyer, W., and H. Brasse (2001), A magneto-variation array study in the central Andes of N Chile and SW Bolivia, Geophysical Research Letters, v. 28, 3023-3026.

Springer, M. (1999), Interpretation of heat-flow density in the Central Andes, Tectonophysics, v. 306, 377-395.

Springer, M., and A. Forster (1998), Heat-flow density across the Central Andean subduction zone, Tectonophysics, v. 291, 123-139.

Stillitoe, R., and H. McKee (1996), Age of supergene oxidation and enrichment in the Chilean porphyry copper province., Economic Geology, v. 91, 164-179.

Strecker, M. R., R. N. Alonso, B. Bookhagen, B. Carrapa, G. E. Hilley, E. R. Sobel, and M. H. Trauth (2007), Tectonics and Climate of the Southern Central Andes, Annual Review of Earth and Planetary Sciences, v. 35, 747-787.

Swartz, G., G. D. Chong, D. Kruger, E. Martinez, W. Massow, V. Rath, and J. Viramonte (1994), Crustal high conductivity zones in the Central Andes, in Tectonics of the Southern Central Andes, K. J. Reutter, E. Scheuber and P. Wigger (ed.), Springer-Verlag, Berlin, 219-231.

Swartz, G., and D. Kruger (1997), Resistivity cross section through the Southern Central Andean Crust as inferred from 3-D modelling of magnetotelluric and geomagnetic deep sounding measurements, Journal of Geophysical Research, v. 102, 11957-11978.

Swenson, J. L., S. L. Beck, and G. Zandt (2000), Crustal structure of the Altiplano from broadband regional waveform modeling; implications for the composition of thick continental crust, Journal of Geophysical Research, v. 105, 607-621.

Tapponnier, P., X. Zhiqin, F. Roger, B. Meyer, N. Arnaud, G. Wittlinger, and Y. Jingsui (2001), Oblique stepwise rise and growth of the Tibetan Plateau, Science, v. 294, 1671-1677.

Tassara, A. (2005), Interaction between the Nazca and South American plates and formation of the Altiplano-Puna plateau; review of a flexural analysis along the Andean margin (15°-34°S), Tectonophysics, v. 399, 39-57.

Thorpe, R. S., P. W. Francis, R. S. Harmon, and Anonymous (1981), Andean andesites and crustal growth, in Philosophical Transactions of the Royal Society of London, Series A: Mathematical and Physical Sciences, 305-320.

Thouret, J.-C., G. Worner, Y. Gunnell, B. Singer, X. Zhang, and T. Souriot (2007), Geochronologic and stratigraphic constraints on canyon incision and Miocene uplift of the Central Andes in Peru, Earth and Planetary Science Letters, v. 263, 151-166.

Tosdal, R. M., A. H. Clark, and E. Farrar (1984), Cenozoic polyphase landscape and tectonic evolution of the Cordillera Occidental, southernmost Peru, Geological Society of America Bulletin, v. 95, 1318-1332.

Trumbull, R. B., R. Ulrich, O. Oncken, S. Ekkehard, K. Munier, and F. Hongn (2006), The time-space distribution of Cenozoic volcanism in the south-central Andes: a new data compilation and some tectonic implications, in The Andes: Active Subduction Orogeny, O. Oncken, G. Chong, G. Franz, P. Giese, H.-J. Gotze, V. A. Ramos, M. R. Strecker and P. Wigger (ed.), Springer-Verlag, Berlin, 29-43.

Uba, C. E., C. Heubeck, and C. Hulka (2005), Facies analysis and basin architecture of the Neogene Subandean synorogenic wedge, southern Bolivia, Sedimentary Geology, v. 180, 91-123.

Uba, C. E., C. Heubeck, and C. Hulka (2006), Evolution of the late Cenozoic Chaco foreland basin, southern Bolivia, Basin Research, v. 18, 145-170.

Uba, C. E., M. R. Strecker, and A. K. Schmitt (2007), Increased sediment accumulation rates and climatic forcing in the central Andes during the late Miocene, Geology, v. 35, 979-982.

Vandervoort, D. S., T. E. Jordan, P. K. Zeitler, and R. N. Alonso (1995), Chronology of internal drainage development and uplift, southern Puna Plateau, Argentine Central Andes, Geology, v. 23, 145-148.

Victor, P., O. Oncken, and J. Glodny (2004), Uplift of the western Altiplano plateau: Evidence from the Precordillera between 20°and 21°S (northern Chile), Tectonics, v. 23, doi:10.1029/2003TC001519.

Vietor, T., and O. Oncken (2005), Controls on the shape and kinematics of the Central Andean plateau flanks; insights from numerical modeling, Earth and Planetary Science Letters, v. 236, 814-827.

Watts, A. B., S. H. Lamb, J. D. Fairhead, and J. F. Dewey (1995), Lithospheric flexure and bending of the Central Andes, Earth and Planetary Science Letters, v. 134, 9-21.

Wdowinski, S., and Y. Bock (1994a), The evolution of deformation and topography of high elevated plateaus 1. Model, numerical analysis, and general results, Journal of Geophysical Research, v. 99, 7103-7119.

Wdowinski, S., and Y. Bock (1994b), The evolution of deformation and topography of high elevated plateaus 2. Application to the Central Andes, Journal of Geophysical Research, v. 99, 7121-7130.

Welsink, H. J., F. M. A., and G. C. Oviedo (1995), Andean and pre-Andean deformation, Boomerang Hills area, Bolivia, in Petroleum basins of South America, A. J. Tankard, R. Suarez and H. J. Welsink (ed.), American Association of Petroleum Geologists Memoir, 481-499.

Whitman, D., B. L. Isacks, J.-L. Chatelain, J.-M. Chiu, and A. Perez (1992), Attenuation of high-frequency seismic waves beneath the central Andean Plateau, Journal of Geophysical Research, v. 97, 19929-19947.

Whitman, D., B. L. Isacks, and S. M. Kay (1996), Lithospheric structure and along-strike segmentation of the Central Andean Plateau; seismic Q, magmatism, flexure, topography and tectonics, in Geodynamics of the Andes, J. F. Dewey and S. H. Lamb (ed.), Elsevier, Amsterdam, 29-40.

Wigger, P. J., M. Schmitz, M. Araneda, G. Asch, S. Baldzuhn, P. Giese, W.-D. Heinsohn, E. Martinez, E. Ricaldi, P. Roewer, and J. Viramonte (1994), Variation in the crustal structure of the southern Central Andes deduced from seismic refraction investigations, in Tectonics of the southern Central Andes; structure and evolution of an active continental margin, K. J. Reutter, E. Scheuber and P. J. Wigger (ed.), Springer-Verlag, Berlin, 23-48.

Willett, S., C. Beaumont, and P. Fullsack (1993), Mechanical model for the tectonics of doubly vergent compressional orogens, Geology, v. 21, 371-374.

Willett, S. D., and D. C. Pope (2004), Thermo-mechanical models of convergent orogenesis; thermal and rheologic dependence of crustal deformation, in

Rheology and deformation of the lithosphere at continental margins, G. D. Karner, B. Taylor, N. W. Driscoll and D. L. Kohlstedt (ed.), Columbia University Press, New York, NY., 179-222.

Worner, G., D. Uhlig, I. Kohler, and H. Seyfried (2002), Evolution of the West Andean Escarpment at 18°S (N. Chile) during the last 25 Ma: uplift, erosion and collapse through time, Tectonophysics, v. 345, 183-198.

Yanez, G., and J. Cembrano (2004), Role of viscous plate coupling in the late Tertiary Andean tectonics, Journal of Geophysical Research, v. 109, doi:10.1029/2003JB002494.

Yang, Y., M. Liu, and S. Stein (2003), A 3-D geodynamic model of lateral crustal flow during Andean mountain building, Geophysical Research Letters, v. 30, doi:10.1029/2003GL018308.

Yuan, X., S. V. Sobolev, and R. Kind (2002), Moho topography in the Central Andes and its geodynamic implications, Earth and Planetary Science Letters, v. 199, 389-402.

Yuan, X., S. V. Sobolev, R. Kind, O. Oncken, G. Bock, G. Asch, B. Schurr, F. Graeber, A. Rudloff, W. Hanka, K. Wylegalla, R. Tibi, C. Haberland, A. Rietbrock, P. Giese, P. Wigger, P. Rower, G. Zandt, S. Beck, T. Wallace, M. Pardo, and D. Comte (2000), Subduction and collision processes in the Central Andes constrained by converted seismic phases, Nature, v. 408, 958-961.

Zandt, G., A. A. Valasco, and S. L. Beck (1994), Composition and thickness of the Southern Altiplano crust, Bolivia, Geology, v. 22, 1003-1006.

Chapter 6

Summary and conclusions

The principal goal of this dissertation is to constrain the deformation and erosion history of the Andean Plateau (results summarized in Fig. 6.1). Below, is a summary of the results of each dissertation chapter, some concluding remarks, and answers to the motivating questions about orogenic plateau evolution posed in chapter 1.

Results summary

Chapter 2 results from the eastern plateau margin in northern Bolivia at 15-17°S suggest (Fig. 6.1A&B): (1) Eo-Oligocene (~40–25 Ma) initial rapid exhumation in the Eastern Cordillera, (2) accelerated, distributed exhumation across the entire thrust belt since the early to mid-Miocene (~15-0 Ma), and (3) a reduction in the magnitude of erosion eastward from ~11-9 km in the Eastern Cordillera, to ~4 km in the Altiplano, ~6-4 km in the Interandean zone, and ~4 km in the Subandes. When compared to two end-member models of Andean evolution, this deformation and exhumation chronology favors the end-member that emphasizes long duration and large magnitude deformation controlled by sequentially-stacked basement structures. If this model is correct, this chronology implies early development of the Andean Plateau analogous to its modern width, but unknown elevation, by the early Miocene (~20 Ma). Associated work that integrates the local structural, kinematic, and exhumation history suggests exhumation rates of ~0.4-0.1 mm/yr in the Eastern Cordillera, ~0.9-0.3 mm/yr in the Interandean zone, and ~0.3-0.1 mm/yr or more in the Subandes as well as long-term shortening rates

of 8-4 mm/yr that imply a pause or deceleration in deformation rate and thrust-belt propagation between 25 and ~15 or 8 Ma [McQuarrie et al., 2008].

Chapter 3 results from the eastern plateau margin in southern Bolivia at ~19.5°S suggest (Fig. 6.1A&C): (1) Eo-Oligocene (36-27 Ma) initial rapid exhumation in the Eastern Cordillera, (2) continued, distributed Oligo-Miocene (25-19 Ma) exhumation in the Eastern Cordillera, (3) early Miocene (22-19 Ma) Interandean zone exhumation, (4) a third pulse of mid-Miocene (16-11 Ma) exhumation in the Eastern Cordillera backthrust belt and initial Miocene (20-8 Ma) cooling in the westernmost Subandes, (5) late Mio-Pliocene (8-2 Ma) exhumation in the central-to-eastern Subandes, (6) a reduction of exhumation magnitude from maximums of <8 km in the Eastern Cordillera, to ~3-2.5 km in the Altiplano, ~6-4 km in the Interandean zone, and ~3 km in the Subandes, (7) exhumation rates range from ~0.2-0.1 mm/yr in the Eastern Cordillera, to ~0.6-0.1 mm/yr in the Interandean zone, and ~0.4-0.1 mm/yr to locally 1.4 mm/yr or more in the eastern Subandes. Comparisons throughout Bolivia combined with constraints from sediments characterize Andean Plateau development by (A) distributed deformation throughout the Altiplano and Eastern Cordillera from ~40-20 Ma with minor deformation continuing until ~10 Ma, (B) contemporaneous cessation of most Eastern Cordillera deformation and exhumation of the Internadean zone ~20 Ma implying establishment of modern plateau width with significant, but unknown crustal thickness and elevation shortly thereafter by ~20-15 Ma, and (C) dominantly eastward propagation of deformation from the Interandean since ~20 Ma with minor out-of-sequence deformation in the central-eastern Subandes. Associated work suggests a difference of ~10% in shortening between the northern and southern Subandes is evidence that climate-driven erosion may be influencing thrust belt and plateau width since the Miocene, but not before [McQuarrie et al., in review].

Chapter 4 results from a quantified sediment budget of central Andean fold-thrust belt erosion and foreland sedimentation in southern Bolivia at ~18-22°S suggest: (1) Modern drainages range from 7,453-86,798 km^2 for a total source area of 153,632 km^2, (2) paleo-drainage areas range from 9,336-52,620 km^2 and total 100,706 km^2 which implies basin source area growth of ≤ 50% since ~10 Ma, (3) about 2.4-3.1 x 10^4 km^3 were excavated from below the San Juan del Oro (SJDO) erosion surface since ~3 Ma, (4) the modern foredeep is 132,080 km^2 with fluvial megafan areas and volumes ranging from 6,142-22,511 km^2 and 1,511-3,332 km^3, respectively, (5) the foreland has a fill of ~6.4 x 10^4 km^3 since Emborozú Formation deposition began 2.1 ± 0.2 Ma, and (6) volume and rate of deposition require that at least ~40-60% of additional sediment be supplied beyond that incised from below the SJDO surface and imply ≥ 0.2 mm/yr (perhaps ≥ 0.4 mm/yr) on the time- and space-averaged source area denudation rate since ~2-3 Ma.

Chapter five results from a synthesis of constraints on the structure, deformation, sedimentation, uplift, and fluvial incision history of the entire Andean Plateau from southern Peru to northern Argentina suggest: (1) deformation began ~60-40 Ma and propagated eastward with variable shortening magnitudes (~530-150 km) and rates (~20-1 mm/yr) in space and time, respectively, (2) surface and rock uplift data quantify a ~1.5 km elevation gain since ~10 Ma, but are equally consistent with a linear rise since ≥25 Ma to a rapid rise of ~2.7 km ~10-6 Ma within error, (3) widespread, substantial incision (2.5-1 km) is observed along the western Altiplano flank since ~11-8 Ma as the result of either surface uplift or climate change, (4) geophysical and geodynamic investigations identify an isostatically-compensated thick crust (~80-65 km), elevated heat flow, zones of low and high velocity and attenuation in the crust and mantle, and stress the importance of weakened lithosphere, partial melt, and crustal flow or delamination to AP morphology, and (5) the most important conclusion is Andean

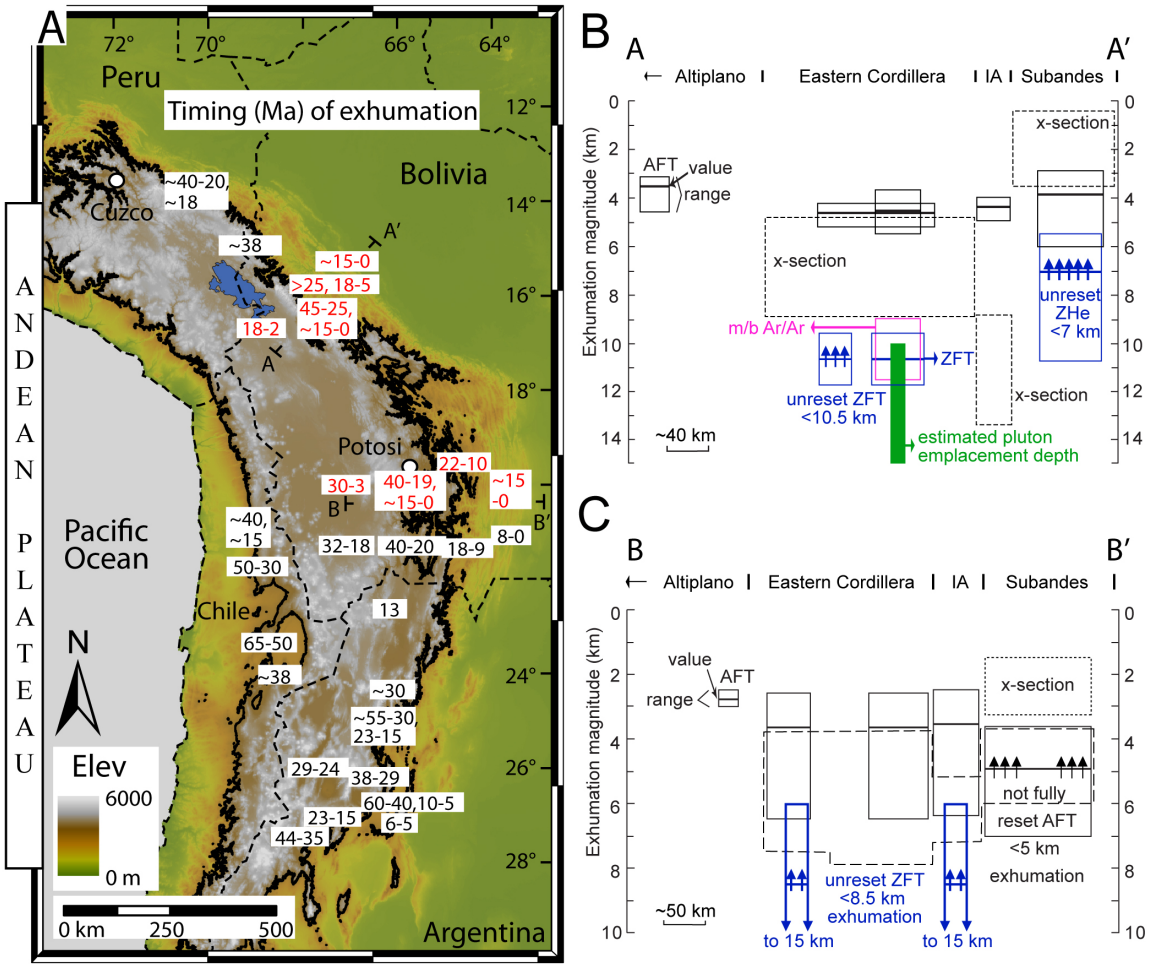

Figure 6.1. Thermochronologic constraints on the exhumation history across the entire Andean Plateau region. IA = Interandean zone. (A) Timing (in Ma) of initiation and/or duration of rapid exhumation from numerous studies based on thermochronology data (see chapter 5 for references). Red values are contributions from this dissertation (chapters 2 and 3). (B) Estimated exhumation magnitudes in northern Bolivia [simplified from McQuarrie et al., 2008]. Constraints from apatite fission-track (AFT) (solid black lines and boxes) data, zircon fission-track (ZFT) data (solid blue lines and boxes), and material removed from above the present-day topography of a balanced cross section (dashed black boxes; x-section). Vertical arrows indicate an upper limit due to not fully reset cooling ages. Muscovite and biotite $^{40}Ar/^{39}Ar$ (pink box; m/b Ar/Ar) data and estimated Eastern Cordillera pluton emplacement depth (green box) is from Gillis et al. [2006]. (C) Estimated exhumation magnitudes in southern Bolivia simplified from chapter 3. Constraints from apatite fission-track (AFT) (solid black lines and boxes) data, zircon fission-track (ZFT) data (solid blue lines and boxes), regional stratigraphy (long dashed polygon) and material removed from above the present-day topography of a balanced cross section (short dashed black boxes; x-section). Vertical arrows indicate an upper limit due to not fully reset cooling ages.

Plateau growth may have been significantly longer and more uniform along strike than previously thought.

Conclusions

Studies presented in, and associated with, this dissertation show that significant deformation and erosion has occurred as part of Andean Plateau growth particularly along its eastern margin throughout Bolivia since the late Eocene (Fig. 6.1). Any model that attempts to explain the development of the Andean Plateau must honor this observation.

This dissertation specifically demonstrates that deformation throughout the Andean Plateau started ~60-40 Ma along its western flank and began along its eastern flank ~40 Ma (Fig. 6.1A) (chapters 2-3 and 5). Although the chronology of plateau deformation is similar all along strike, deformation rates may have been variable. In northern Bolivia, shortening rates along the eastern flank were ~8-7 mm/yr during the late Eo-Oligocene (~40-25 Ma), potentially paused for ~15-10 Myrs, and then resumed at similar to reduced rates of 8-4 mm/yr depending on the age of the Subandes [McQuarrie et al., 2008]. In contrast, in southern Bolivia, shortening rates have been relative constant at ~11-8 mm/yr, potentially reducing to 4-3 mm/yr depending on the age of the Subandes (chapter 3).

This dissertation also specifically demonstrates that the eastern Andean Plateau flank has experienced significant magnitudes of exhumation and erosion since the late Eocene ranging from 11-7 km in the Eastern Cordillera to ~4-3 km in the Subandes (Fig. 6.1B&C) (chapters 2 and 3). In this case, the erosion magnitudes are variable along strike. Erosion magnitudes range from 11-9 km in the central Eastern Cordillera in northern Bolivia, but are limited to <~8 km in the Eastern Cordillera of southern Bolivia.

Erosion magnitudes are similar throughout the Interandean zone (~6-4 km) and are slightly higher in the northern Subandes by ~1 km (~4 vs. ~3 km).

Answers to motivating questions of plateau evolution

Below are brief answers to the motivating questions about orogenic plateau evolution posed in chapter 1 with specific focus on the Andean Plateau.

(1) What is the deformation history associated with plateau development?

The broadest view of the deformation and exhumation history of the Andean Plateau in Bolivia shows crustal shortening and thickening generally progressed at temporally variable rates of ~1-20 mm/yr from west to east since as early as the Paleocene (~60-40 Ma). Distributed deformation began in the Eastern Cordillera by the late Eocene (~40 Ma) and continued through the Oligocene into the early Miocene (~20 Ma) at which point it migrated eastward to the currently active Subandes. These observations, combined with results from Peru and Argentina, recommends that Andean Plateau deformation and growth was significantly longer and more uniform along strike than previously appreciated.

(2) What is the erosional response to plateau growth?

The erosional response of the eastern Andean Plateau flank in Bolivia has been significant with exhumation magnitudes up to 11-9 km and variable exhumation rates of ~0.1-≥1.4 mm/yr. The temporal distribution of greater erosion magnitude concentrated in the Eastern Cordillera and Subandes of northern Bolivia suggests that enhanced erosion has been important in the morphological development of the central Andean fold-thrust belt and plateau since the mid-late Miocene (~15 Ma). Since the mid-late

Miocene, a 10% reduction in shortening relative to the south implies increased erosion is regionally limiting plateau width [McQuarrie et al., in review]. The record of erosion and sedimentation since the Plio-Quaternary (~3-2 Ma to present) suggests variable erosion rates of ~1.0-0.1 mm/yr along the eastern plateau flank in southern Bolivia.

(3) What is the history of plateau elevation gain?

The history of Andean Plateau elevation gain remains controversial because of contrasting implications inferred from the histories of deformation, sedimentation, and exhumation and the paleoelevation and associated proxy data. Constraints quantify ~1.5 km of surface uplift since ~10 Ma, but within error, allow a range of hypotheses from a linear, slow and steady rise since ≥25 Ma to a recent, rapid rise of 2.7 km ~10-6 Ma. The late Eocene to present (~40-0 Ma) deformation and exhumation documented in this dissertation suggests the modern width of the plateau was established by ~20-15 Ma, presumably characterized by some significant amount of crustal thickness and associated isostatic uplift.

(4) Why are plateaus so broad and low relief?

The documented geometry and chronology of deformation suggests the Andean Plateau crust has been characterized by thrust sheets transporting material large distances at a constant structural elevation balanced by thrust deformation at the surface in smaller wavelengths since at least the late Eocene (~40 Ma). Particularly focused uplift and volcanism along the plateau margins as well as imbricate thrust-bound ranges throughout the AP helped create internal drainage, allowing a substantial amount of Tertiary sediments to pond and facilitate topographic smoothing. The significant and protracted crustal shortening and thickening eventually lead to the development of a weak lower crust that helps maintain the broad and flat morphology of the AP. In fact,

geodynamic simulations of plateau development show that plateaus develop because significantly shortened and thickened lithosphere eventually weakens and begins to flow at depth. A survey of current AP simulations suggests most are under-prescribing the documented duration and inferred magnitude of deformation, as well as neglecting erosion, which may be adversely influencing their results.

(5) What processes are important in plateau evolution?

There are many potentially important processes in plateau evolution. This dissertation demonstrates that sustained and substantial shortening and thickening of the AP crust since the Paleocene-Eocene (~60-40 Ma to present) is a particularly important part of plateau growth. Although significant along-strike erosion variability (Fig. 6.1; ~11-9 km in the northern Eastern Cordillera vs. <8-~6 km in the south) has been documented along the eastern AP flank, propagation of the plateau margin (and hence orogen growth) has been similar throughout Bolivia suggesting erosion has not been important. However, 10% greater shortening is documented in the Subandes suggesting that the enhanced erosion in the north has limited the thrust belt and plateau width since the mid-late Miocene (~15 Ma to present). This deformation and erosion has occurred within a hot lithosphere that is probably the result of partial melt, crustal flow, and/or delamination. Located in the core of this hot Andean orogen, crustal flow and/or delamination of mantle lithosphere have occurred probably following of the documented shortening and are also considered important processes responsible for Andean Plateau evolution.

References

Gillis, R. J., B. K. Horton, and M. Grove (2006). Thermochronology, geochronology, and upper crustral structure of the Cordillera Real: Implications for Cenozoic exhumation of the central Andean Plateau, Tectonics, v. 25, doi:10.1029/2005TC001887.

McQuarrie, N., **J. B. Barnes**, and T. A. Ehlers (2008), Geometric, kinematic, and erosional history of the central Andean Plateau, Bolivia (15-17ºS), Tectonics, doi:10.1029/2006TC002054, in press.

McQuarrie, N., T. A. Ehlers, **J. B. Barnes**, and B. J. Meade (in review), Temporal variation in climate and tectonic coupling in the central Andes. Geology.